Acid Gas Removal from Natural Gas Using Ionic Liquids

Heba Al-fnaish

Department of Chemical and Process Engineering

University of Strathclyde

A thesis submitted for the degree of

Doctor of Philosophy

6th December 2019

Declaration

This thesis is the result of the authors original research. It has been composed by the author and has not been previously submitted for examination which has led to the award of a degree. The copyright of this thesis belongs to the a uthor under the terms of the United Kingdom Copyright Acts as qualified by University of Strathclyde Regulation 3.50. Due acknowledgement must always be made of the use of any material contained in, or derived from, this thesis.

Dedication

I would like to dedicate this thesis to my parents, my husband and my son.

Acknowledgements

Abstract

The growth in demand for natural gas accounted for almost half the increase in global energy consumption in 2018 and is projected to increase by more than 10% over the next five years. This is due to its abundancy, efficiency and lower carbon content compared to oil and coal. However, raw gas contains undesirable components, such as hydrogen sulphide and carbon dioxide, which must be removed before its delivery to end users because of their toxicity, corrosivity, flammability and poor heating value. Various technologies have been used for acid gas removal. Amine-based absorption is the most widely used technique; however, they are corrosive, volatile, degrade at high temperatures and highly energy intensive to regenerate. This study aims to improve pre-existing amine processes by reducing their energy consumption and environmental impact through the use of ionic liquids (ILs) and their blend with other physical solvents as an alternative to amines. The consequences of replacing an amine with ILs or a blend of ILs with other physical solvent in an existing amine unit are examined and found to be promising. A thermodynamic description of the IL mixtures needed to be developed to examine their use to replace amine solutions. The perturbed chain statistical association fluid theory (PC-SAFT) is selected as the thermodynamic model to represent the vapour liquid equilibrium of acid gases-IL systems. The solubility of gases in ILs was successfully described without the need for empirical binary interaction parameters, as was required in previous studies. Up to 47% and 7% of the regeneration energy and the total annual cost, respectively, were saved by using IL instead of amine, while up to 40% and 27% of the regeneration energy and the total annual cost, respectively, were saved by using a blend of IL with other physical solvent.

Contents

List of Figures

List of Tables

Nomenclature

Greek Symbols

ε_i Strength of the dispersion interaction

$\varepsilon^{A_i B_i}$ Association energy between sites A and B

γ_i Activity coefficient of component i

μ_i Chemical potential of component i

ϕ_i Fugacity coefficient of component i

σ_i Segment diameter

ϵ_0 Vacuum permittivity in C^2/J/m

Superscripts

cal Calculated values

E Excess property

exp Experimental values

id Ideal state

res Residual property

Other Symbols

a_i Activity coefficient of component i

a^{assoc} Association contribution to the Helmholtz free energy

a^{disp} Dispersion-chain contribution to the Helmholtz free energy

a^{elec} Electrolyte contribution to Helmholtz free energy

a^{hc} Hard-chain contribution to the Helmholtz free energy

a^{polar} Polar contribution to the Helmholtz free energy

a^{res} Residual Helmholtz free energy

C_p Liquid heat capacity, J mol^{-1} K^{-1}

C_p^0 Ideal gas heat capacity, J mol^{-1} K^{-1}

D Dielectric constant of water

d Water density in kg/m^3

F Faraday's constant = 96485.33289 C/mol

G Gibbs free energy

g^{hs} Radial distribution function of hard-sphere fluid

a_i Activity of component i

f_i Fugacity of component i

k Boltzmann constant=1.38066×10^{-23} J/K

$K^{A_i B_i}$ Effective association volume

K_H Henry's law constant

K_i The equilibrium constant of component i

m Mean segment number in the mixture

m_i Number of segments per chain

N_A Avogadro's number = 46.022141×10^{23} mol^{-1}

R The universal gas constant

P_i^{sat} Saturation pressure of component i

T_r Reduced temperature

Z Compressibility factor

Acronyms

AARD   Average Absolute Relative Deviation

CIS   Commonwealth of Independent States

DEPG   Dimethyl Ethers of Polyethylene Glycol

DEA   Diethanolamine

IL   Ionic Liquid

MDEA   Methyldiethanolamine

PC-SAFT   Perturbed Chain-Statistical Associating Fluid Theory

PR EOS   Peng Robinson Equation of State

SRK EOS   Soave Redlich Kwong Equation of State

TAC   Total Annual Cost

VLE   Vapour Liquid Equilibrium

Chapter 1

Introduction

According to the International Energy Agency [1], natural gas demand increased by 4.6% in 2018, about half of the overall growth in the global energy demand. This rise is led by the fast-growing consumption of Asian economies and the continued development of the global gas trade. Natural gas consumption is projected to increase from 120.0 trillion cubic feet in 2012 to 203.0 trillion cubic feet in 2040 [2]. Due to its lower carbon content compared to other fuels such as oil and coal, natural gas is considered the most favoured type of fossil fuel from an environmental prospective. Carbon dioxide emitted by natural gas is estimated to be $56\,\text{kg}$ per GJ of energy produced. Carbon dioxide emitted by coal is 70% higher and that emitted by oil is 30% higher than that emitted by natural gas [3].

Carbon dioxide (CO_2) and hydrogen sulphide (H_2S) are among the undesirable impurities in raw natural gas. These gases must be removed from natural gas before it can be delivered to its end users. The process of H_2S and CO_2 removal is described as 'gas sweetening'. Because of their corrosive nature, H_2S and CO_2 can damage pipes and equipment. Moreover, H_2S is toxic and flammable, while CO_2 may freeze and cause a blockage of pipes when the gas is cooled for liquefaction [4]. In addition, CO_2 has poor heating value, and its removal can enhance the heating value of the gas [5]. Furthermore, the growing environmental concerns about CO_2 and H_2S emissions from the natural gas industry has led governments to impose strict regulations and policies on

acid gases disposal, which in turn, motivated engineers to develop more efficient technologies for emission minimisation and proper disposal of acid gases resulting from gas processing.

For the above-mentioned reasons, companies all over the world have specified limits for the H_2S and CO_2 content in the sales gas, which differ from one company to another according to the end user's requirement and local authorities regulations. Typical sales gas specifications for hydrogen sulphide are less than 4 PPM/V and from 2 to 5 mol% for carbon dioxide. However, for the liquefied natural gas (LNG) industry H_2S specifications are reduced to less than 2 PPM/V and CO_2 specifications to less than 50 PPM/V to prevent downstream corrosion and freezing complications [6].

Natural gas is referred to as sour if its hydrogen sulphide content is greater than 4 PPM/V H_2S [7]. Statistics from the International Energy Agency indicate that about 40% of the world's natural gas reserves are sour [4], 60% of the Middle Eastern natural gas reserves are sour, and 34% of Russia's reserves (the largest natural gas producer) are sour. The term sour gas can also be used to refer to any gas that is acidic alone or when combined with water such as H_2S and CO_2 [8]. In this thesis, the term sour gas is used to refer to natural gas with H_2S content greater than 4 PPM/V H_2S and CO_2 content greater than 2 to 5 mol%. The term acid gases is used to refer to H_2S and CO_2, as they form acids upon contact with water.

Various technologies have been used for the removal of acid gases from natural gas. Amine based chemical absorption is the most widely used technique, mainly due to the reactivity and availability of amines at low cost. However, amines are corrosive, volatile, degrade at high temperatures and their regeneration process is highly energy intensive. Therefore, research is ongoing to look for alternative techniques or solvents to overcome these drawbacks.

The aim of this study is to improve the pre-existing amine processes for sour gas treatment in order to reduce their energy cost and environmental impact. Our objective

is to investigate the use of ionic liquids and their blend with other physical solvents as an alternative solvent to the conventional amines for gas sweetening and modify the amine process configuration accordingly. The use of ILs for gas sweetening can reduce the solvent losses, thermal decomposition and the consequent environmental impact due to their negligible volatility and high thermal stability [9]. Furthermore, using ILs for gas sweetening can lead to an overall reduction in energy consumption because physical absorption takes place, rather than chemical absorption [9, 10]. In addition, the structure of ILs can be changed by using different anion-cation combinations to modify their properties, such as the viscosity the gas solubility and the selectivity. First, we aimed at selecting a proper thermodynamic model that is capable of describing IL-containing systems and validate it. The model can then be used for the design and simulation of an IL-based sweetening process. By analysing the simulation results and performing economic analysis, any issues associated with the use of ILs can be addressed. The feasibility of replacing amine with IL or IL blend with other physical solvent can also be investigated. The final objective is explore the potential of retrofitting an existing amine unit by replacing amine with the optimal composition IL-based solvent.

The remainder of the thesis is organised as follows. In Chapter 2, an overview of natural gas and acid gases is presented then the current methods for separating acid gases from raw natural gas are reviewed in order to assess and compare their relative performance with respect to their economics, energy consumption, and environmental impact. Thermodynamic models commonly used for describing the phase and chemical equilibrium for ideal and non ideal systems are presented in Chapter 3. The thermodynamic description of binary and multi-component systems involving ionic liquids, acid gases and methane is of central importance for evaluating the performance of the acid gases separation process and prove its effectiveness. Therefore, a review of the previous relevant thermodynamic models that have been used for describing such systems is performed in Chapter 3. The PC-SAFT model is selected and used in Chapter 4 to investigate the solubility of carbon dioxide (CO_2) and hydrogen sulphide (H_2S) in several methylimidazolium bis (tri-fluoro-methyl-sulfonyl) imide ionic liquids (ILs).

The PC-SAFT is then used in Chapter 5 for the simulation of an IL-based acid gas removal process. Two of the ILs investigated in Chapter 4 are examined with different concentrations to determine the optimal IL case. The IL-based process is compared to an existing amine-based sweetening process as the base case. In Chapter 6, the IL-based acid gas removal process is further optimised by blending the IL with other physical solvents to improve the process economy. Some retrofit options for an existing amine sweetening unit to replace the amine with a blend of an IL and a physical solvent are also presented in Chapter 6. Finally, our main findings and recommendations for future work are summarised in Chapter 7.

Chapter 2

Natural gas, acid gases and removal technologies

2.1 Introduction

Natural gas is a mixture of combustible hydrocarbon gases, including methane, ethane, propane, butane, etc., and non-hydrocarbon gases such as nitrogen, oxygen, carbon dioxide, hydrogen sulphide and rare gases such as argon and helium [11]. Methane, which has a huge potential as a fuel, accounts for 60–90% of natural gas composition [11]. Natural gas is regarded as the cleanest type of fossil fuel because it produces fewer carbon dioxide emissions per quantity of energy delivered, producing only 56 kg of CO_2 per GJ compared to 95 kg of CO_2 per GJ for coal and 73 kg of CO_2 per GJ for oil [3]. This is mainly due to its lower carbon content compared to other fossil fuels. Unfortunately, raw natural gas contains some unwanted impurities that must be removed before it can be used as a fuel. Carbon dioxide and hydrogen sulphide are among these impurities, and their removal from natural gas is the main focus of this study. These non-hydrocarbon gases are called acid gases as they form acids with water and become corrosive. They cause various complication in the transport and production of natural gas, as will be detailed later, therefore, they must be removed from natural gas.

There are many commercially available acid gas removal technologies. The most common of them are the amine based chemical absorption processes. Amines are characterised by their low cost and high acid gas absorption capacity. However, these technologies suffer from number of drawbacks, including amine losses, corrosion problems and high energy requirements for regeneration. Other removal technologies include physical absorption, adsorption, membranes and cryogenic distillation. Each technology has its own pros and cons and is suitable for certain applications as will be discussed later in this chapter.

This chapter is organised as follows. In section 2.2, we first provide an overview of the origin and historic formation, resources, composition and treatment of natural gas, then, we define its end users and discuss its reserves, production, consumption and market. Sour gas is then defined and the impact of the presence of acid gases on natural gas processing and their specified limits in the sales gas are presented in section 2.3. The major technologies for the removal of these acid gases, their advantages, limitations and the factors that affect the technology selection process are presented in section 2.4. Finally, once these gases are removed from natural gas their possible uses or proper disposal methods should be considered. A brief discussion on their uses and disposal is provided in section 2.5.

2.2   Natural Gas Overview

Natural gas is a fossil fuel formed by the break down of carbon bonds in the organic remains of plants, animals and microorganisms due to exposure to the high pressures and temperatures underneath the Earth [12]. The type of natural gas produced this way is called thermogenic. Another source of methane (the main component of natural gas) is animal manure, food waste, sewage and landfills. It is produced from the bacterial breakdown of the aforementioned wastes in absence of oxygen and is called biogenic or biogas [13]. A type of bacteria called methanogenic bacteria is responsible for this break down. They produce methane as a result of organic material decomposition during their energy metabolism [14]. Methane can then be captured and used for

electricity generation and heating.

Natural gas resources can be divided into two broad categories: Conventional and unconventional gas. Conventional gas is the natural gas produced using traditional extraction techniques, such as drilling, pumping and compression, and it can be non-associated or associated gas [15]. Non-associated gas is produced from geological formations that do not contain high amounts of hydrocarbons heavier than methane. Associated gas is produced during the oil extraction process and is associated with crude oil. It is released as a result of pressure reduction as the oil and gas mixture is transported to the surface [15, 16]. Associated gas is rich in natural gas liquids (NGLs), which include ethane, propane, butanes, pentanes and heavier hydrocarbons (C_6^+). Unconventional gas is more technologically difficult to produce than conventional gas [17]. Its extraction requires special recovery technologies, such as multiple fracturing. Examples of unconventional gas include: (i) tight gas found in reservoirs with law porosity and low permeability sediments, (ii) shale gas found in reservoirs with rocks of fine-grained and easily breakable into layers sedimentary, (iii) coal bed methane which is methane stored in coal deposits underground, and (iv) methane hydrates which is methane trapped in ice crystals found at or below freezing temperature area such as ocean floors and permafrost in polar regions.

The typical composition of natural gas before it is refined is given in Table 2.1 below [11]. These values vary from one well to another according to the source and type of the natural gas.

It is clear from Table 2.1 that methane is the major constituent of natural gas. It accounts for 60% to 90% of natural gas composition. The composition of light hydrocarbons, such as ethane, propane and butane, differs from one well to another, varying from 0 % to 20%. These NGLs and heavier hydrocarbons (C_6^+) are also valuable, however, they need to be removed to control the dew point of the natural gas to prevent condensation at high pressure and low temperature conditions. Once removed, each compound can be sold separately. Besides their use as fuel for cooking, heating and

Table 2.1: Typical Composition of Natural Gas, taken from Boehm and Saba [11].

Component	Composition vol%
Methane	60-90%
Ethane	
Propane	0-20%
Butane	
Carbon Dioxide	0-8%
Oxygen	0-0.2%
Nitrogen	0-5%
Hydrogen Sulphide	0-5%
Rare gases	trace

transportation, NGLs are used as a feedstock in petrochemical plants to produce chemicals, plastics, and rubber [18]. Other non-hydrocarbon gases such as carbon dioxide, hydrogen sulphide, oxygen, nitrogen and rare gases can also be found in natural gas in smaller amounts. These gases are considered as impurities in natural gas.

Natural gas must be treated to remove impurities other than methane and light hydrocarons before being delivered to end users. It should meet the pipeline quality standards specified by gas distribution companies (see Table 2.2). These standards require the natural gas to be within a specific range of heating value, be at or above a specified hydrocarbon dew point temperature to prevent pipeline damage due to condensation and formation of liquid slugs. Furthermore, to prevent methane hydrate formation problem in the processing facilities, in which a large amount of methane is trapped inside a solid crystal structure of water, natural gas should be dehydrated of water vapour. Natural gas should only contain traces of acid gases such as carbon dioxide and hydrogen sulphide as given in Table 2.2. Although the majority of sulphur in natural gas is present as H_2S, sulphur might be found in the form of organic compounds, such as mercaptans, sulphides, disulphides and thiophenes. These compounds are corrosive and have strong odour and most of them are highly toxic, thus their presence in natural gas is undesirable [19]. The total sulphur content of the sales gas, which include all organic and inorganic sulphur compounds should be limited to PPM levels as sulphur

leads to corrosion, catalyst poisoning and air pollution, besides their strong odour. Finally, natural gas should also be free of solid particles and contains undetectable levels of mercury to prevent equipment and pipelines damage and corrosion [20]. Table 2.2 provides some key typical pipeline quality specifications of natural gas.

Table 2.2: Typical pipeline quality specifications of natural gas [21].

Specification	Limits
Heating value	35-60 MJ.m^{-3}
Hydrocarbon dew point	-10°C - -5°C
Water vapour content	65 - 112 mg.m^{-3}
Carbon dioxide	2-3 mol%
Hydrogen sulphide	5.7-23 mg.m^{-3}
Total sulphur content	78.5–314 PPM/V(Parts per million by volume) [22]

The acid gases carbon dioxide and hydrogen sulphide are two of the major impurities in natural gas. They should be removed to meet the standard pipe line specifications, improve the heating value of the natural gas and avoid pipelines and equipment corrosion [5]. The removal of these gases is the main focus of this work.

Once natural gas is refined from impurities, it is then transported through a network of pipelines and delivered to its end users. The end users for natural gas are divided into three categories: the residential sector, the commercial sector and the industrial sector. The three sectors are defined by the U.S. Energy Information Administration (EIA) [23] as follows: The residential sector consumption represents gas used for heating, air-conditioning, cooking, water heating, and other household uses. The commercial sector consumption represents gas used by non-manufacturing establishments or agencies engaged in the sale of goods or services. Hotels, restaurants, wholesale and retail stores are also included. The industrial sector consumption represents gas used for heat, power, or chemical feedstock by manufacturing establishments, such as mining industry, agriculture, forestry, and fisheries. Generators that produce electricity to support the aforementioned industrial activities are also included in the industrial

sector consumption. Liquefied natural gas (LNG), imported from countries with large reserves, can also be used to meet part of the demand for natural gas in countries with low reserves. Natural gas in its liquid form can also be used as an alternative transportation fuel.

At the end of 2018, an estimate of 196.9 trillion cubic meter (tcm) of proven world natural gas reserves was reported in the BP Statistical Review of World Energy June, 2019 [24]. The world's largest reserves were recorded in Russia, Iran and Qatar. The global reserves in 2018 rose by 0.7 tcm due to the increased reserves in Azerbaijan. 2018 reserves are sufficient to meet 50.9 years of global production at 2018 levels, according to the BP statistics. The Middle East holds the largest proven reserves (75.5 tcm), accounting for 38.4% of the global reserves. The CIS (Commonwealth of Independent States) region represents the second largest contributor to the global reserves with 31.9% share or 62.8 tcm. The distribution of the world's proven natural gas reserves in 2018 on percentage basis is shown in Figure 2.1, taken from Ref. [24].

The world's natural gas consumption increased by 5.3% in 2018, the highest growth rate in 30 years [24]. The US demand growth was the main factor for this increase with 40% share of the global consumption growth. The increased US demand is mainly driven by the rising need for heating, cooling and power generation due to the severe weather conditions in both summer and winter. The US switch from coal to gas also contributed to the increased demand. Global natural gas production also increased by 5.2% in 2018, the fastest growth rate since 2010. Again, the growth in the US gas production was the leading factor for this increase followed by Russia, Iran and Australia. The production growth is a consequence of the rising consumption rates [24].

In 2018, natural gas prices rose in Europe, Asia and the US, yet remain below the 10-year average [24]. The increased need for liquefied natural gas, especially by China and Japan, is the main factor for this increase in gas prices. Figure 2.2 shows the fluctuation of natural gas prices over the period from 2001 to 2018. Prices are in $/GJ (gigajoules) and are determined based on different markets including: US Henry Hub,
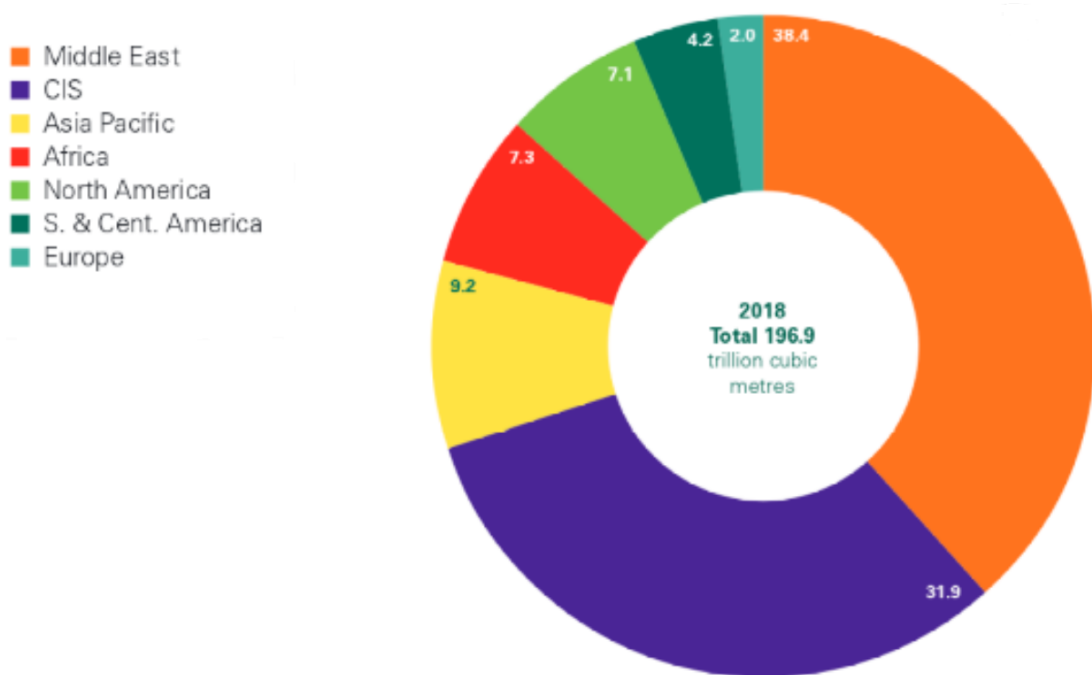
Figure 2.1: Distribution of the global natural gas proven reserves in 2018. Taken from Ref. [24]

Average German Import price, UK NBP, Netherlands TTF index, Japan LNG cif and Japan Korea Marker (JKM). Refer to the glossary in Appendix D for definitions of these market prices.

As the demand for natural gas increases, its prices soar accordingly, which motivates producers to improve their production and exploration capabilities. Natural gas prices are generally driven by the interaction of supply and demand. Demand is largely affected by three main factors: the relative prices of other fuels, economic growth, and weather, which drives heating demand in the winter and gas-fired generation demand for cooling in the summer [25]. In the following section, sour gas, its acidic components, the hazards associated with their presence in natural gas and their specified limits in the sales gas are presented.
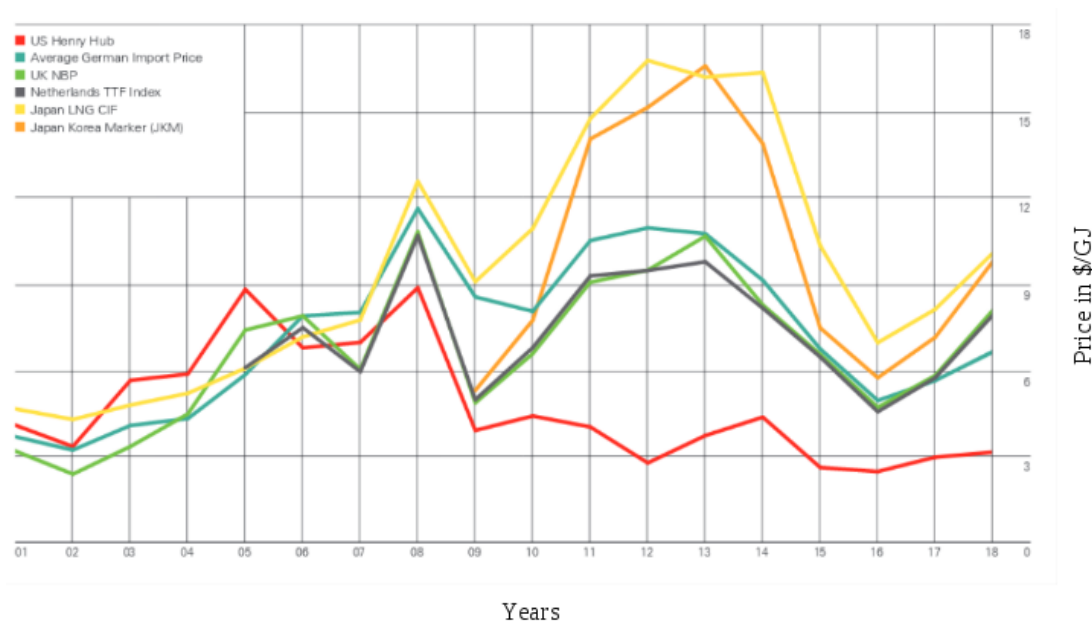
Figure 2.2: Natural gas prices in $/GJ. Taken from Ref. [24]

2.3 Sour Gas

The terms 'acid gas' and 'sour gas' are sometimes used interchangeably for the gas that contains significant amounts of acidic gases such as H_2S and CO_2. However, a sour gas is usually defined as any gas that specifically contains significant amounts of H_2S, whereas an acid gas is defined as any gas that contains significant amounts of acid gases such as CO_2 or H_2S. In this thesis, the term sour gas is used to refer to natural gas with H_2S and CO_2 content above the typical sales gas specifications of 5.7 mg per cubic meter of natural gas or 4 PPM/V for H_2S [7] and 2–5 mol% for CO_2 [6]. The term acid gas is used in this thesis to refer to gases of acidic nature such as H_2S and CO_2. The presence of these acid gases in natural gas causes many complications through the gas processing facilities due to their toxicity, corrosivity and low heating value. Consequently, they must be removed in an early stage in the gas treatment process. The process of H_2S and CO_2 removal is described as 'gas sweetening'.

Different companies have different sales gas specifications. TOTAL E&P UK ltd., for example, has specified the H_2S content as less than 2.3 PPM/V and the CO_2 content as less than 3.8 mol% for all gas entering the export pipeline [26], which are different to those shown in Table 2.2. The US Northern Natural Gas specified the H_2S content as less than or equal to 4 PPM/V and the CO_2 content as less than or equal to 2.0% by volume for all gas received into the Northern pipeline system [27]. Besides that, it has been reported in the Northern Natural Gas Company general terms and conditions sheet that " The gas shall be commercially free from objectionable odours, solid matter, dust, gums and gum-forming constituents, or any other substance which might interfere with the merchantability of the gas, or cause injury to or interference with proper operation of the lines, meters, regulators, or other appliances through which it flows " [27].

The presence of H_2S is undesirable due to its toxicity and corrosive nature. The US Occupational Safety and Health Administration (OSHA) reported that levels of H_2S gas at or above 100 PPM/V are immediately dangerous to life and health [28, 29]. Exposure to low levels of hydrogen sulphide causes eye, nose, and throat irritation. Moderate levels can cause headache, dizziness, nausea, vomiting, coughing and difficulty breathing. Higher levels can cause shock, convulsions, coma, and death [29]. As H_2S is one of natural gas industry by-products safety precautions should be considered by workers in gas fields and gas processing plants.

H_2S becomes corrosive in the presence of water because of acid formation which can lead to pipeline embrittlement [30]. HS^- ion produced from H_2S dissociation in water reacts with iron on a steel pipeline surface to form many types of iron sulphide, such as amorphous ferrous sulphide, cubic ferrous sulphide, smythite, greigte, pyrrhotite, troilite, pyrite and mackinawite [31]. Therefore, H_2S must be removed from natural gas prior to its transportation.

CO_2 is a gas with no calorific value; therefore, its presence in natural gas lowers the calorific value of the gas [32]. Moreover, CO_2 can cause severe corrosion to pipelines

and equipment upon water contact due to the formation of carbonic acid. In addition to that, CO_2 and water start to form a snow-like crystalline substance called hydrate at temperatures below 280 K (6.85°C), which is typical for many offshore pipelines [33]. For pipelines operating at temperatures higher than 280 K, hydrates may form during emergency blowdown as a result of temperature drops. Hydrate formation causes a blockage of pipe lines and equipment. In terms of its health effects, CO_2 at concentrations higher than 7 vol% "is likely to be instantly fatal" [34]. Consequently, CO_2 must also be removed to improve the heating value of the gas, prevent equipment corrosion and CO_2 crystallisation during liquefaction process.

Various technologies have been used for the removal of H_2S and CO_2 from the raw natural gas, including physical and chemical absorption, adsorption, membranes and cryogenics; each technology has its own benefits and drawbacks. No single process is suitable for all applications. The choice of the appropriate sweetening process depends on a variety of factors such as the impurities concentration in the feed gas, partial pressure of acid gases in the sour feed gas and the produced gas, the operating conditions and economic factors such as capital and operating cost [35]. These factors should be considered during the selection of a suitable method for sour gas processing.

Amine based chemical absorption is the most widely used technique for gas sweetening, mainly due to the reactivity and availability of amines at low cost [9]. However, due to some disadvantages associated with the amine processes, which will be detailed later, many alternative technologies have emerged, such as physical absorption, adsorption, cryogenics and membranes. The use of ionic liquids for natural gas cleaning applications is one of the emerging technologies that have attracted the attention of the research community in the recent decades [9, 36, 37, 38, 39, 40, 41, 42, 43, 44]. Ionic liquids are characterised by their negligible volatility, high thermal stability, high ionic conductivity, and structural tunability. They possess low melting points, which are much lower than the melting points of conventional ionic compounds, such as sodium chloride. Most of the gas solubility studies reported in literature focused on CO_2 solubility in ILs, and less attention has been paid to H_2S solubility. Simulations

of IL-based acid gas removal processes is not yet a mature area of research. Limited literature studies have been published on this subject [36, 39, 40, 41, 42, 43, 44]. This might be attributed to the sophisticated nature of IL molecules as opposed to conventional solvents and to the scarcity of the experimental data on the solubility of different gaseous species in ILs. Again, The majority of the studies were concerned with CO_2 capture and less attention have been paid to H_2S removal. The main focus of this thesis is to investigate further the option of using ionic liquids for H_2S and CO_2 removal from natural gas by studying the solubility of both gases in ILs and then exploring the potential use of ILs and their blend with other physical solvents as replacement to conventional amines in an existing process. In the following section, the different technologies of acid gas removal from the natural gas are presented.

2.4   Acid gas removal technologies

In this section, the available methods for acid gases removal from the raw natural gas are described and compared in terms of their economical, technical and environmental practicability. First, we introduce the most commonly used technology for acid gas separation (amine process) then provide an overview of the previous efforts made to improve these processes. Next we discuss amine process alternatives such as physical absorption including the use of ionic liquids, adsorption, membranes and cryogenic distillation. Finally, some established guidelines from the literature on the selection of the proper acid gas removal technology are presented. There are four major technologies for acid gas removal from natural gas. Absorption, adsorption, membranes and cryogenic separation. Below is a brief description of each of them.

2.4.1   Absorption

Absorption is one of the most widely used technologies for natural gas cleaning [9]. It is typically classified as chemical or physical absorption. In chemical absorption,

solvents react chemically with the acid gases, while in physical absorption, acid gases diffuse into the solvent and do not react chemically. Various chemical solvents have been used for acid gas absorption, such as aqueous ammonia (NH_3), amines, and hot potassium carbonate (K_2CO_3) [9, 45]. Many physical solvents have also been reported in the literature for the commercial use in acid gas separation; these include Selexol^{TM} (dimethyl ether of polyethylene glycol), Fluor^{TM} (propylene carbonate), Purisol$^®$ (N-methylpyrrolidone) and Rectisol$^®$ (methanol). In section 2.4.1.1, the amine processes will be detailed as an example of chemical absorption techniques and in section 2.4.1.3, ionic liquids will be introduced as an example for physical solvents absorption.

2.4.1.1 Chemical absorption: Amine processes

For many years, amines have been used for H_2S and CO_2 removal from sour natural gas. Alkanoamines are the most widely used solvents for sour gas sweetening. This is mainly because of their high selectivity to acid gases over hydrocarbons and ability to treat highly sour gases to meet the most strict sales specification [46], besides their availability at low cost as mentioned earlier. Different types of amines are available for different compositions and conditions of the sour gas to be treated. Alkanoamines are classified according to their structure into three categories: primary amines such as mono-ethanolamine (MEA) and di-glycolamine (DGA), secondary amines such as di-ethanolamine (DEA) and di-isopropanolamine (DIPA), tertiary amines such as tri-ethanolamine (TEA) and methyl-di-ethanolamine (MDEA) [47]. The chemical structure of an example of each category is shown in Figure 2.3 below.

All of them have been used for the separation of acid gases from natural gas. The type of amine used for treatment is specified according to the conditions and the requirements of each specific problem. MDEA, for instance, is preferred for treating gas streams with high H_2S content because of its higher affinity for H_2S over CO_2 [49]. However, MEA is preferred for CO_2 removal due to its high reactivity with it. It can be clearly seen from Table 2.3, that the value of the rate of reaction constant of MEA with CO_2 is 7600 $mol\,L^{-1}\,s^{-1}$ compared to only 1500 $mol\,L^{-1}\,s^{-1}$ for DEA, 16.8 $mol\,L^{-1}\,s^{-1}$ for TEA and 9.2 $mol\,L^{-1}\,s^{-1}$ for MDEA. The higher the rate con-

$$H$$
$$: N \longrightarrow CH_2CH_2OH$$
$$H$$

MEA

$$HOCH_2CH_2$$
$$: N \longrightarrow H$$
$$HOCH_2CH_2$$

DEA

$$HOCH_2CH_2$$
$$: N \longrightarrow CH_3$$
$$OHCH_2CH_2$$

MDEA

Figure 2.3: Chemical Structure of Primary (MEA), Secondary (DEA) and Tertiary (MDEA) Amines [48]

stant the faster the reaction, this implies that the reaction of MEA with CO_2 is the fastest compared to the reaction of other amines with CO_2. For this reason, MEA is favourable over other amines for CO_2 capture. Amines are typically mixed with water when used as solvents for gas sweetening.

Table 2.3: Heats of reaction, latent heats of vapourisation and rate constants for different amine solvents [50]

Solvent	Concentration (M)	Heat of reaction ($kJ\,mol^{-1}$ of CO_2)	Latent heat of vapourisation ($kJ\,kg^{-1}$)	Rate constant at 298 K ($mol\,L^{-1}\,s^{-1}$)
MEA	5 (30% wt)	72	826	7600
DEA	3.5 (36% wt)	65	670	1500
TEA	3.35 (50% wt)	62	535	16.8
MDEA	4.28 (50% wt)	53.2	550	9.2

Figure 2.4, shows the configuration of a typical amine unit. The absorption process of acid gases takes place in the absorber. The lean amine solution enters the top of the absorber where it captures the acid gases from the sour gas stream entering from the absorber bottom. The amine solution flows out of the absorber bottom is rich in acid gases and needs to be regenerated to remove the acid gases. The regeneration process takes place in the regenerator where the acid gases are flashed out of the amine solution by the effect of heat, and the lean amine solution is circulated back to the absorber to treat more gas.

17

Figure 2.4: Acid Gas Removal Unit, Taken from Lallemand et al. [51].

During the absorption process of acid gases in alkanolamines, CO_2 and H_2S react with the alkanolamine solution in the absorption tower through the following mechanism [52]:

$$2H_2O \rightleftharpoons H_3O^+ + OH^- \tag{2.1}$$

$$H_2O + H_2S \rightleftharpoons H_3O^+ + HS^- \tag{2.2}$$

$$H_2O + HS^- \rightleftharpoons H_3O^+ + S^{-2} \tag{2.3}$$

$$2H_2O + CO_2 \rightleftharpoons H_3O^+ + HCO_3^- \tag{2.4}$$

$$H_2O + HCO_3^- \rightleftharpoons H_3O^+ + CO_3^{-2} \tag{2.5}$$

$$H_2O + RR'R''NH^+ \rightleftharpoons H_3O^+ + RR'R''N \tag{2.6}$$
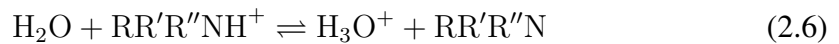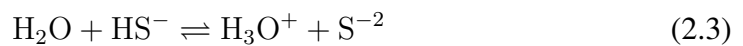
Equation (2.1) represents the ionisation of water to hydronium cation and hydroxide anion; in equation (2.2), H_2S dissociates in water producing bisulphide anion which is then dissociates in equation (2.3). CO_2 dissociation which is represented by equa-

tion (2.4); produces bicarbonate anion which dissociates to produce a carbonate anion as given by equation (2.5). Finally, equation (2.6) represents the dissociation of protonated alkanolamine where $RR'R''N$ is the chemical formula of alkanolamines and R refers to methyl group, R' refers to methanol group and R'' refers to hydrogen.

The rich solvent solution is then sent to the regeneration tower to be recovered by stripping through the addition of heat to break the chemical bonds and release the acid gases from the solution. In case of MEA and DEA, carbamate ions ($MEACOO^-$ and $DEACOO^-$) are formed as a result of their reaction with bicarbonate (HCO_3^-) which then dissociate according to the following reactions [53].

$$H_2O + MEACOO^- \rightleftharpoons HCO_3^- + MEA \qquad (2.7)$$
$$H_2O + DEACOO^- \rightleftharpoons HCO_3^- + DEA \qquad (2.8)$$
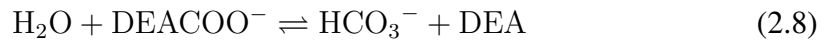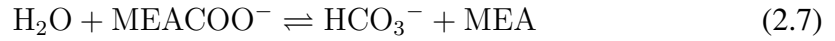
The above carbamate formation reaction is very energy intensive [54]. This reaction does not take place in case of MDEA since it is a tertiary amine; instead reaction 2.9 takes place. The energy use is the sum of the heat of desorption and the heat of vapourisation of water/amine solution in the stripper. Therefore, by using MDEA, energy saving can be achieved.

$$H_2O + MDEAH^+ \rightleftharpoons H_3O^+ + MDEA \qquad (2.9)$$
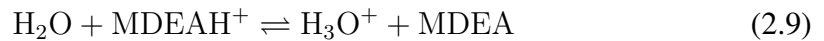
For this reason, tertiary amines such as (MDEA) have been used more extensively as they require less regeneration energy than primary and secondary amines [51]. The chemical equilibrium of CO_2 and H_2S in MDEA is described by Carey et al. [55] as follows:

$$H_2S(aq) + R_3N \rightleftharpoons HS^- + R_3NH^+ \tag{2.10}$$

$$CO_2(aq) + R_3N + H_2O \rightleftharpoons HCO_3^- + R_3NH^+ \tag{2.11}$$

$$HCO_3^- + OH^- \rightleftharpoons CO_3^{-2} + H_2O \tag{2.12}$$

$$R_3N + H_2O \rightleftharpoons R_3NH^+ + OH^- \tag{2.13}$$
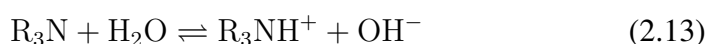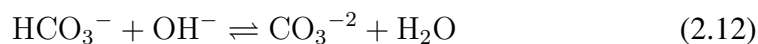
According to Chakma [50], the amount of solvent regeneration energy required can be measured by the sum of heat of reaction with the acid gas and latent heat of vapourisation of the solvent. Table 2.3 shows how the sum of heat of reaction of MDEA and CO_2 and the latent heat of vapourisation for MDEA solution is significantly smaller compared to primary and secondary amines.

Although amine solvents have proven their versatility and efficiency in acid gas removal down to the sales gas specifications, amine processes have several shortcomings including amine losses, corrosion issues, and high regeneration energy requirements [9].

According to Stewart and Lanning [56], there are five types of losses in amine-based treatment plants: (i) vapourisation, (ii) solubility, (iii) entrainment, (iv) degradation which can be chemical or thermal, and (v) mechanical losses. Vapourisation losses result from amine vapour pressure and increase at high temperature and low operating pressure. The solubility of amines in liquid hydrocarbons is another type of amine losses; it also increases as the temperature increases or the pressure decreases. Entrainment losses result from the formation of small droplets of amine which can be carried over by the treated gas stream to the top of the column. Degradation losses of amines can be due to chemical or thermal degradation. Chemical degradation involves the breakdown of amines to other compounds that can not remove acid gases or the formation of heat stable salts which accumulate and can cause corrosion problems [57]. Thermal degradation losses are a result of high operating temperatures, as all amines degrade at temperatures higher than 350°F (176.7°C) [56]. Finally, mechanical losses,

which represent the largest source of amine losses, result from the physical removal of amine solvent from the system through different areas such as pipe gasket connections, seal leaks or filter change outs. Amine losses problems have been addressed by Stewart and Lanning [56], where a systematic approach for solvent losses reduction in amine plants have been presented.

Corrosion problems in amine processes are not caused by amines as they are not corrosive, but some of the products of amine degradation are corrosive [57]. The choice of the proper material of construction in different parts of the amine unit is of a prime importance to alleviate corrosion problems [57].

The regeneration of amines is an energy intensive process, it accounts for 70% of the total operating cost of the capture process [9]. The energy consumption of a typical amine sweetening unit is on the order of 2.3 to 23 GJ/ton of acid gas removed [58, 59]. The process flow schemes of amine units can be efficiently improved to reduce the treatment cost and energy consumption of the process [51, 59]. In the following section, examples of some efforts made to improve the performance of amine processes are discussed.

2.4.1.2 Improving Amine Processes

This section discusses the recent research progress in the enhancement of amine processes. In an effort to improve the efficiency of the amine processes and overcome the economic and environmental challenges encountered in gas treatment process, many solutions have been presented by Lallemand et al. [51]. The solutions were proposed by Prosernat, and benefited from TOTAL's experience in sour gas processing [51].

One solution is the double-split flow process configuration shown in Figure 2.5, which was first presented in 1962 by Estep et al. [51]. It allows for much more severe gas specification with the same reboiler duty as the conventional amine process flow configuration when treating highly sour gases. In this configuration, a side stream of

the amine solution is withdrawn from the regenerator (stripper). This side stream is described as semi-lean amine and still has the ability to pick up some acid gases when its cooled and pumped back to the absorber. Another advantage of this configuration is the reduced regenerator reboiler duty due to the fact that the amine flow is reduced when part of it is withdrawn from the side stream.
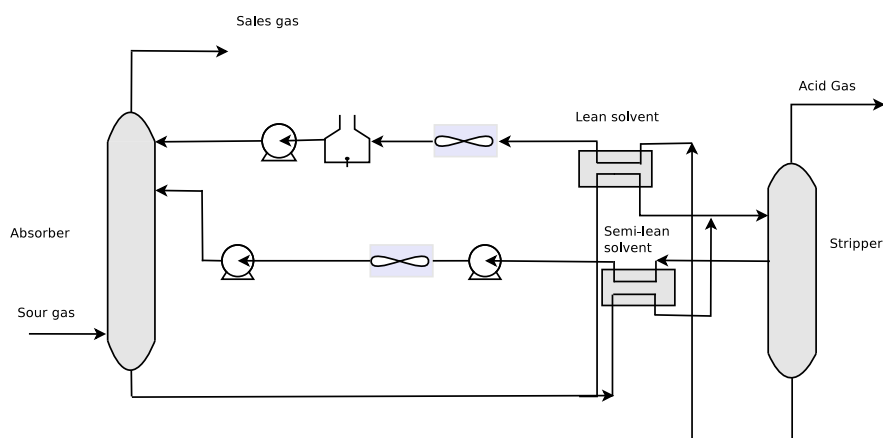
Figure 2.5: Conventional double-split flow configuration. Taken from Lallemand et al. [51]

Another approach to improve the performance of the amine process is to blend primary and secondary amines with tertiary amines [51, 60]. Generally, tertiary amines require less reboiler duty for regeneration than primary and secondary amines because the energy intensive carbamate formation reaction does not take place when they react with CO_2 unlike primary amines. However, the latter react fast with CO_2, thus by blending both of them, the solvent regeneration duty can be reduced [51]. The use of MDEA blended with primary and secondary amines is preferable in case of simultaneous removal of CO_2 and H_2S as the primary or secondary amine enhances the CO_2 capture through the carbamate formation reaction. A further reduction in the thermal regeneration energy can be achieved by the combination of the use of the MDEA blend with primary and secondary amines with the double-split flow process configuration described in Figure 2.5 [51].

An increase in the acid gas loading of the rich amine leaving the absorber can also contribute to the reduction in regeneration energy as lower solvent flow rate will need to be regenerated [61]. This is done by the installation of a liquid intercooler at an intermediate level of the absorber to lower the temperature of the amine solution in contact with the acid gases causing them to condense. However, thermodynamic equilibrium limitations and corrosion problems should be considered. The higher the acid gas partial pressure in the treated gas, the higher the amine loading at equilibrium, and high loading can only be achieved if the treated gas is very sour and at high pressure. Moreover, the rich amine pH is reduced with increasing its acid gas loading, leading to corrosion problems [61].

Therefore, amine processes can be optimised to treat highly sour gases, but they are still very costly in terms of the regeneration energy requirement. For example, a 30 w% MEA based solution has reported an energy requirement of 3.7 GJ/ton CO_2 [62] to 4.3 GJ/ton CO_2 [63] to be regenerated. Efforts are still continuous seeking more economic alternatives to amine processes. Ionic liquids have recently emerged as potential alternative physical solvents to chemical solvents for acid gas cleaning. They help to reduce the energy requirement of the acid gas removal process as will be detailed in the following section.

2.4.1.3   Physical absorption: Ionic Liquids

In physical absorption, acid gases are selectively absorbed from the treated gas stream by the solvent, no chemical reaction takes place. Physical absorption is favourable over chemical absorption when the partial pressure of acid gases is very high. The regeneration process of physical solvents usually involves pressure reduction only, and no addition of heat is needed as in chemical absorption [64]. Therefore, it is less energy intensive than chemical absorption regeneration process. Physical solvents are generally non-corrosive and more resistant to degradation [65]. However, it is more difficult to achieve very strict sales gas specifications with physical absorption, due

to the fact that acid gases are not strongly bound to the solvent; thus, they might travel to the treated gas from the lean solvent [65]. Many physical solvents have been commercially used for acid gas separation; these include Selexol^{TM} (dimethyl ether of polyethylene glycol), Fluor^{TM} (propylene carbonate), Purisol® (N-methylpyrrolidone), Rectisol® (methanol). Ionic liquids are new class of physical solvents, which have recently attracted the attention of the scientific community, and are introduced in the remainder of this section.

Ionic liquids (ILs) are organic molten salts with exceptional properties that make them a more economic alternative to the chemical alkanoamines for acid gas removal. They are characterised by their negligible volatility, acceptable thermal stability and structural tunability [66]. They are liquids over a wide range of temperatures, with low melting points ranging from ($-100°$C to $200°$C). Furthermore, due to the fact that ILs are physical solvents, physical absorption takes place rather than chemical absorption, thus less energy is required for solvent regeneration.

By replacing the volatile and possibly toxic organic solvents, ILs have the potential to contribute significantly to improving the safety, economy and environmental sustainability of acid gas removal processes [67]. Due to their negligible volatility and high thermal stability, the use of ILs for sweetening can reduce the solvent losses or the cost of solvent makeup, thermal decomposition and the consequent environmental impact. According to Kumar et al. [9], using ILs for the gas sweetening can lead to an overall reduction in energy consumption because physical absorption takes place, rather than chemical absorption. Furthermore, the tunable structure of ILs can be utilised to modify the absorption selectivity and capacity of the IL.

Over the past few years, a significant number of experimental and theoretical studies of ILs and their mixtures with gas species has been published. Most of the experimental studies reported in literature focused on CO_2 capture, and less attention has been paid to H_2S removal. Many studies provided experimental measurements for the solubility of CO_2 in different types of ILs [37, 68, 69, 70, 71]. Some research studies

provided measurements for H_2S solubility in different ILs with comparison to CO_2 and other gases solubility [72, 73, 74, 75]. A review of these studies is presented in Chapter 4.

In terms of the health and environmental impact of ILs, many research studies have been carried out in the past [76, 77, 78]. Research suggests that some ILs are toxic, have limited biodegradability and are soluble in water. However, the structure of ILs can be tuned to produce less harmful and more environmental friendly ILs [77]. Furthermore, aquatic media contamination with ILs can be alleviated by minimizing the IL discharge from the IL-based processes and a downstream separation stage should be considered at the end of these processes to remove the ILs from wastewater [76]. The need for more research on the nature and properties of ILs is of prime importance to accurately assess their environmental impact [9]. In Chapter 5, the use of ILs as an alternative solvent to amines in an existing amine unit is explored. Details on the investigated ILs for acid gas removal are presented in Chapter 4.

2.4.2 Adsorption

Adsorption is another common acid gas removal technology. It is defined as the spontaneous attraction of a molecule from a fluid phase to the surface of a solid, called adsorbent [79]. Adsorption can either be physical (physisorption) or chemical (chemisorption). In physisorption, adsorbed molecules (adsorbate) are held to the adsorbent surface via weak van der Waal's forces, while in chemisorption adsorbate molecules are held to the adsorbent surface via chemical bonds [80]. See Figure 2.6.

The driving force for separation in adsorption is the difference in affinity of the solid adsorbent material to different gaseous components in the gas mixture to be separated [81]. Adsorption is either controlled by manipulating the pressure of these gases and, in this case, called pressure swing adsorption (PSA) or by by manipulating the temperature and, in this case, called temperature swing adsorption (TSA) [81]. Adsorption capacity of different gases such as N_2, CH_4, CO_2 and H_2S in different physi-
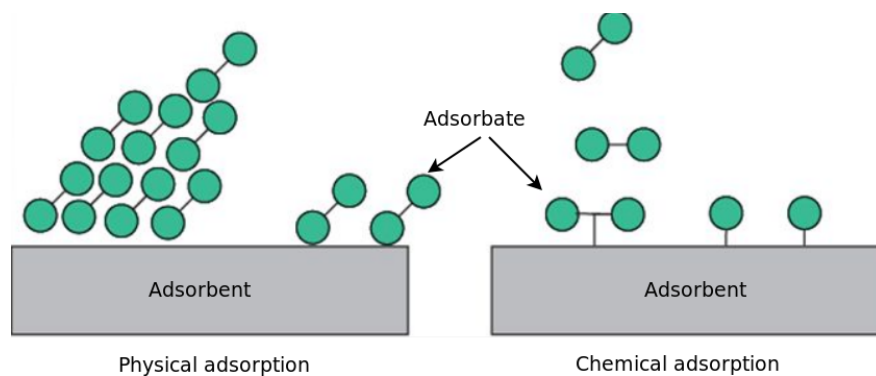
Figure 2.6: Physical versus chemical adsorption.

cal adsorbents such as zeolite, silica molecular sieve, sepiolite, silicalite, metal organic frameworks (MOFs), activated charcoal, iron sponge, zinc oxide, silica gel and alumina has been measured in several studies [9, 81, 82, 83, 84, 85, 86, 87, 88, 89, 90]. Chemical adsorbents investigated in the literature for CO_2 adsorption include amine functionalized materials such as ordered mesoporous supports (e.g., polyethyleneimine (PEI)-impregnated on silica) [91] and ordered microporous supports (eg.monoethanolamine (MEA) on zeolite) [92].

The main advantage of adsorption is its simplicity and lower energy requirement for regeneration of the adsorbent material compared to the liquid solvents such as amines [5, 81]. However, adsorption is not as commonly used as absorption for H_2S and CO_2 removal from natural gas. This can be attributed to its low product recovery, large compression requirement in case of PSA and large heating loads in case of TSA [5, 81]. Physical adsorbents such as zeolites, carbon-based materials and MOFs are hydrophilic, thus, adsorb water vapour over other gases and their CO_2 adsorption capacity is not sufficiently high at low pressure, thus, are more suitable for pre-combustion gas treatment rather than post-combustion gas treatment [93].

2.4.3 Membranes

Membrane separation technology is a pressure-driven process in which a mixture of gases to be separated is fed into the membrane under high pressure (between 10 to 200 bar). The difference in partial pressure of the gases in the feed mixture and permeate is the driving force for separation [94].

Membranes have been extensively used for carbon dioxide removal since 1980. Some examples of the plants using membranes for CO_2 removal were listed by Engelien [95], these include: Kadanwari plant in Pakistan; a two-stage unit for the treatment of 210 MMSCFD gas at 90 bars, the EOR facility in Mexico which processes 120 MMSCFD gas containing 70 % CO_2, the Slalm & Tarek plant in Egypt, a three-two-stage units each treating 100 MMSCFD natural gas at 65 bar and Texas, USA plant for treating 30 MMSCFD of gas containing 30% CO_2 at 42 bar. Figure 2.7 illustrates the mechanism of carbon dioxide separation from natural gas using membranes [95]. The process is based on the selective removal of fast permeating gases (CO_2) from slow permeating gases (CH_4).

Membranes are characterised by their simplicity, less environmental impact and lower energy requirement than other acid gas removal technologies [51]. Despite of these advantages, membranes have some limitations such as; the significant hydrocarbons loss (methane) [96], high pressure requirement [5], impurities plugging and membrane wetting [89]. Most membranes are very sensitive to hydrogen sulphide; however, they can be used for the co-removal of carbon dioxide and hydrogen sulphide in cases of low sulphur contents in the sour gas. Gases with high levels of H_2S can be handled with the use of polymeric membrane technologies such as that developed by UOP company in 2007 [97].

The integration of membranes with the existing amine units is usually the proper and more economical approach to meet the tight sales gas specification requirements. In case of membranes, permeation increases as the CO_2 partial pressure in the feed gas increases, making the membrane much more efficient at high concentration of CO_2.
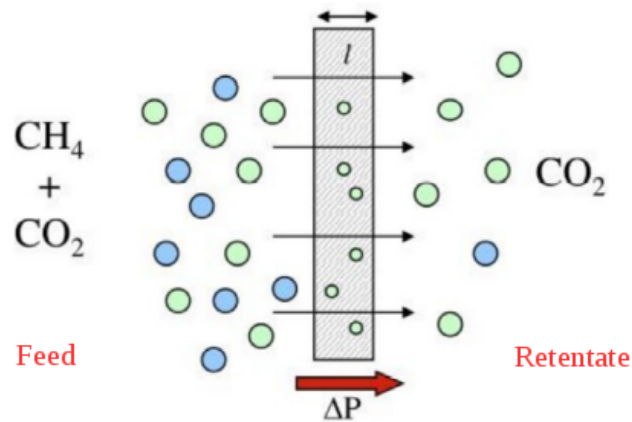
Figure 2.7: CO_2 separation using membranes, Taken from Ref. [95].

In contrast, for amine processes, as CO_2 partial pressures increases in the feed, the rich solvent loading increases to offset the increased demand for solvent. When the solvent approaches a maximum loading at high levels of CO_2, any further increase in CO_2 can only be removed by increasing the circulation rate. Amine processes however, can achieve low CO_2 product gas specification. Thus, by combining a membrane with an amine unit, the membrane works on the high CO_2 concentration in the feed, while amine works on achieving low CO_2 specification in the treated gas. Moreover, the presence of the membrane unit upstream the amine unit helps to reduce the reboiler duty of the amine regenerator, thus the operating cost [95, 97, 98, 99, 100, 101]. In West Texas, several combination of membranes and amines are used to recover CO_2 returned to the surface from the enhanced oil recovery wells and recover the valuable hydrocarbons in the gas [98]. Hybrid systems of a membrane followed by an amine unit are very good choice for treating a high pressure gas with a high CO_2 concentration to meet pipeline specification.

2.4.4 Cryogenic Distillation

Cryogenic distillation is a low temperature separation process in which acid gases are removed from natural gas as a liquid stream withdrawn from the bottom of a distillation column operated at certain conditions to avoid problems associated with CO_2 freezing out [102]. CO_2 changes its state from solid to gas or vice versa directly without intermediate formation of liquid in a process called sublimation [103]. At $-78.5°C$ and atmospheric pressure the gas and solid can co-exist and transform back and forth. At $-56°C$ and 5.187 bar (triple point) the three phases of CO_2 exist simultaneously [103]. CO_2 in its solid state is referred to as dry ice.

The formation of dry ice can cause a blockage of pipe lines and equipment in the processing facilities. To prevent the formation of CO_2 dry ice during cryogenic distillation different approaches have been pursued. Some are based on the addition of a heavier hydrocarbon to alter the solubility of components in the column [51, 104], others involve the division of the column into three zones as shown in Figure 2.8, the upper and the lower zones are the conventional rectification and stripping sections respectively, while the middle zone is where CO_2 freezing out is controlled by contact with a cold methane stream which freezes out the CO_2. The solid CO_2 then drops to a liquid layer on a tray in the lower section where it melt before passes through the downcomers of the melt tray [102, 105].

The combination of low temperature acid gas separation processes with existing amine units is another promising approach developed by Total and Prosernat for the bulk removal of CO_2 and H_2S [51]. This combination helps to reduce the refrigeration requirement compared to the stand alone cryogenic process and eliminates the need for gas dehydration and solvent addition to prevent ice formation, at the same time, the produced gas meets the strict sales gas specifications.

Cryogenic distillation technology plays a significant role in reducing the green house gas emissions and eliminating the need for undesired sulphur production in natural gas processing. Acid gases are recovered as high pressure liquids which elimi-
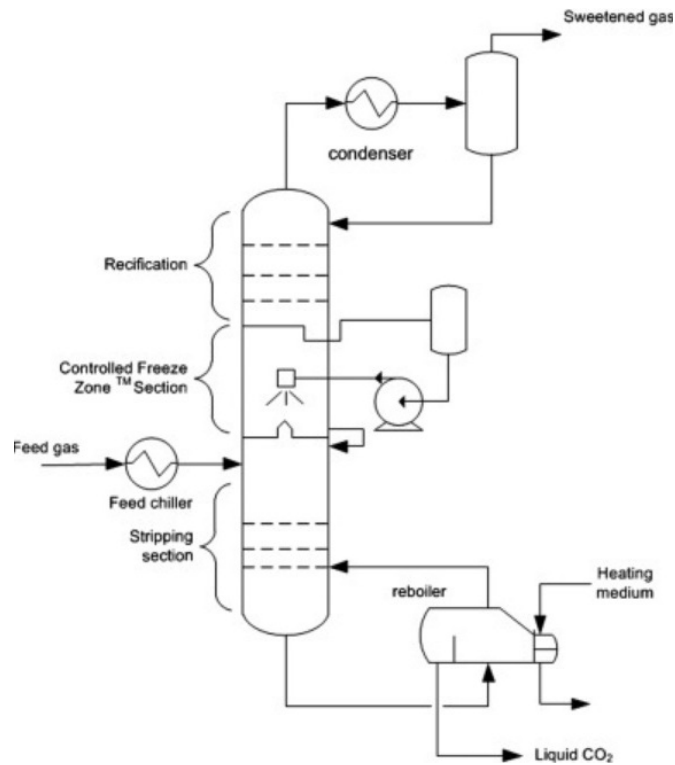
Figure 2.8: The Controlled Freeze Zone^{TM} process schematic, Taken from Ref. [106].

nates the need for the expensive gas compression operations. The acid gases can then be pumped and re-injected for enhanced oil recovery (EOR) or for geo-sequestration rather than venting them to the atmosphere or sending them to a sulphur recovery unit [102, 105].

Each of the four aforementioned technologies for gas sweetening has its own advantages and drawbacks. Table 2.4 provides a summary of the advantages and limitations of the different acid gas removal technologies. The following section provides some guidelines on the selection of the proper acid gas removal technology.

Table 2.4: Pros and cons of different acid gas removal technologies

Technology	Pros	Cons
Absorption	• Chemical absorption is a widely used technology for efficient removal of both CO_2 and H_2S • Physical solvents are less corrosive of chemical solvents (70% of the total operating cost) [9] • Chemical solvent such as amines are available at low cost (US \$1-2/kg) [108, 109]	• Low temperature (below ambient) and high partial pressure (3.4–4.1 bar) are usually needed while using physical solvents [107]. • High energy consumption for regeneration • Chemical solvents are volatile, thus, high solvent makeup rates are needed • Chemical solvents are corrosive
Adsorption	• Low energy requirement for regeneration compared to chemical absorption	• High pressure requirement in case of PSA (> 25 bar) [110] • Large heating loads in case of TSA (230°C–290°C) [111] • Complex design • Low product recovery • Low adsorption capacity at low pressure • Physical adsorbents are hydrophilic, thus, dehydration is needed
Membrane	• Simple structure thus, low capital and operating cost. • Minimum weight and space requirement • Stable at high pressure • Sensitive to hydrogen sulphide	• High pressure requirement up to 50 bar [112] • Impurities plugging and membrane wetting • Hydrocarbons loss • Moderate purity
Cryogenic	• Minimises greenhouse gases emissions • Acid gases can be used for EOR • No need for acid gases compression as they are recovered in the liquid state • High product recovery • High product purity	• Large refrigeration requirement (temperature $\leq$ -90°C) [113] • Feed gas dehydration is required • Addition of hydrocarbon solvents is needed to avoid CO_2 freezing

2.4.5 Acid gases removal technology selection

The selection of the appropriate technology for a certain application depends on several factors [64], these include, the type of acid gases and impurities to be removed (H_2S, CO_2, sulphur compounds) and their concentration in the feed gas, the acid gas specification requirement in the sales gas, the feed gas flow rate and conditions, the practicability of sulphur recovery, acid gas selectivity requirement, surrounding environment consideration and process economics. To illustrate how these factors affect the technology selection process, two examples are presented below.

For instance, adsorption or dry bed processes such as iron oxide sponge or zinc oxide process and molecular sieve beds are used when the sulphur content in the feed is low. Besides the sulphur found in the feed, some elemental sulphur is produced during the regeneration process of the bed [64]. This sulphur accumulates in the bed decreases its reactivity, therefore, the bed must be replaced after a certain number of

cycles [7].

Absorption using chemical or physical solvents (liquid phase processes) is selected when the feed gas contains large amounts of H_2S and CO_2, and physical solvents are preferred for the selective removal of H_2S and other sulphur compounds such as COS and CS_2t [64]. However, if both H_2S and CO_2 need to be removed, then chemical solvents such as amines can be used. For treatment of very high CO_2 concentration gas, membranes are efficient [64]. However, membranes are more feasible for natural gas sweetening than for flue gas treatment due to the high pressure requirement of membranes [114]. Cryogenic processes are used to extract light hydrocarbons such as ethane, propane, butane and pentane from natural gas with high recovery rates and product purity [7]. Once the acid gases are removed from the natural gas, they need to be properly disposed if not used. The following section discusses the possible uses and the proper disposal methods of acid gases.

2.5 Acid Gases Disposal and Uses

Due to the rising environmental concerns over emitted gases from natural gas processing, it becomes more important to search for more environmentally sound solutions for the proper disposal of acid gases removed from natural gas. One traditional solution to dispose of H_2S is the conversion of H_2S to elemental sulphur S in a process called Claus process developed by Carl Friedrich Claus in 1883 [115]. The process converts the toxic H_2S into sulphur according to the reaction 2.14. The produced sulphur can be used in the manufacture of fertilizers, rubber, cosmetics and pharmaceuticals.

$$2H_2S + O_2 \rightarrow 2S + 2H_2O \tag{2.14}$$

The re-injection of both separated gases (CO_2 and H_2S) and using them for en-

hanced oil recovery (EOR) or sending them for geo-sequestration rather than venting them to the atmosphere is another alternative solution [105]. H_2S re-injection provides a more economic alternative to the very expensive Claus process for an already saturated sulphur market [51].

Separation technologies that take in consideration the re-injection of acid gases rather than venting them to the ecosystem have more added-value than others. Cryogenic distillation processes, for example, recover CO_2 and H_2S as high pressure liquids which facilitates the re-injection process by replacing the energy-consuming compression stages with simple liquid phase pumps [102].

It has been reported by Meyer [116] that the oil and gas industry operates over 13,000 CO_2 EOR wells in the United States alone; which produces about 245,000 barrels of oil per day. CO_2 and H_2S produced form gas processing have also been safely re-injected for about 25 years in western Canada and about 41 depleted oil and gas reservoirs were used for this purpose as reported in 2008 by Bachu et al. [117].

Utilisation of acid gases produced from natural gas processing can also alleviate their undesired environmental impact. Besides their use in enhanced oil recovery; hydrogen sulphide and carbon dioxide have other useful applications. Hydrogen sulphide, for example has been used industrially in the production of sulphuric acid, in metallurgy to precipitate metals from ores, for coating of the walls of reactors operating at high temperatures in petroleum operations to prevent corrosion [118], for coal liquefaction as a hydrogen donor and a hydrocracking agent due to its ability to displace oxygen from oxygen-containing coal molecules [119]. Carbon dioxide is used in food industry for freezing of food products, in fire extinguishing systems, for carbonation of soft drinks and for alkaline water treatment [120].

It is worth mentioning that methane is also a greenhouse gas, which is a much more powerful than CO_2. Methane emissions from gas operations in 2018, were estimated to be about 40 (Mega tons) from wide variety of sources, almost the same amount emit-

ted from oil operations [121]. Despite of that, by switching to gas the total greenhouse gas emissions can be reduced by 50% when producing electricity and by 33% when providing heat [121].

2.6 Conclusions

Despite the fact that natural gas is the cleanest fossil fuel, it does contain some impurities that need to be removed such as acid gases (CO_2 and H_2S). These gases are corrosive, toxic, have low heating value and their presence causes several complications in the process facilities such as corrosion and pipeline blockage due to CO_2 dry ice formation. Several technologies are used in industry to clean natural gas from acid gases. Amine based chemical absorption is the most common process due to the high efficiency amines in acid gas removal and their availability at low cost. Amine processes, however, have some limitations such as amine losses, corrosion problems and high energy requirements for regeneration. Alternative processes to amine technology include physical absorption, adsorption, membranes and cryogenic distillation. Each technology has its own pros and cons and is suitable for a certain application. The selection of the proper process depends on several factors, either operational, economic or environmental factors. Physical absorption using ionic liquids is one of the recently emerging technologies for gas sweetening, which is considered in the following chapters.

Chapter 3

Thermodynamic modelling

3.1 Introduction

Understanding the equilibrium thermodynamic behaviour of acid gases in amines or any alternative solvent, is of immense importance for the assessment and the design of the acid gas removal process. Experimental data are often scarce, therefore, thermodynamic models are needed to estimate the properties of the systems of interest. The equilibrium behaviour of a system can be described by the thermodynamic potential functions such as, the internal energy, the Helmholtz free energy and the Gibbs free energy. These functions can be approximated using different thermodynamic models with different levels of accuracy. Ideal solution or gas systems behaviour, for example, can be described by simple models such as the ideal gas law and Raoult's Law. Non ideal systems can be described by more complex models such as equation of state and activity coefficient models. These models may also fail to describe systems with high intermolecular interactions such as hydrogen bonding, electrostatic interactions and dipole-dipole interactions. Therefore, many efforts of extension has been presented in literature [122, 123, 124]

In the recent decades, statistical mechanics based models called SAFT (statistical associating fluid theory) have gained considerable attention by the scientific community due to their greater predictive ability. These models account explicitly for the size

and the shape of the molecule as well as the intermolecular interactions in the system, thus provide better estimates of the pure and bulk properties of the system. The purpose of this chapter is to show how to derive all the thermodynamic properties of a system from the thermodynamic potential functions and their relation to the equation of state and activity coefficient models and phase equilibrium calculations.

In this chapter, first, the thermodynamic potential functions and their use to derive all the thermodynamic properties of a system are introduced in section 3.2. Then different equation of state (EOS) models for ideal and non ideal systems, which provide a mathematical approximation for the thermodynamic potential functions, are described in section 3.3. Activity coefficient models, as an alternative method to EOS to describe non-ideal solution behaviour, are then presented in section 3.4. The advantages and limitations of both model are highlighted. The phase equilibrium concept, conditions and its applications in VLE are explained in section 3.5. Finally, the main finding are summarised in section 3.6.

3.2 Thermodynamic potential

The thermodynamic behaviour of any system can be described using one of the many thermodynamic potential functions such as the internal energy U, the enthalpy H, the Helmholtz free energy A and the Gibbs free energy G [125]. These functions can be defined using the following pairs of independent variables: the temperature T and the entropy S or the pressure P and the volume V. Starting from the first and the second laws of thermodynamics, the relation between the thermodynamic potential functions and their independent variables can be defined. The first law of thermodynamics states that for a closed system, the change in the internal energy dU is equal to the amount of heat δQ supplied to the system minus the amount of work δW done by the system on its surroundings [126].

$$dU = \delta Q - \delta W \tag{3.1}$$

The second law of thermodynamics states that the total entropy of an isolated system can never decrease over time because it spontaneously evolves towards equilibrium. For actually possible (irreversible) process, the infinitesimal change in entropy dS should be greater than the infinitesimal transfer of heat δQ to the system divided by the temperature, i.e.

$$dS > \left(\frac{\delta Q}{T}\right)_{irrev.} \tag{3.2}$$

However, for a reversible process, the infinitesimal change in entropy dS of a closed system is equal to $\delta Q/T$ [126]. Thus

$$dS = \left(\frac{\delta Q}{T}\right)_{rev.} \tag{3.3}$$

Given that the work done by a body in an infinitesimal increase in volume dV against an opposite pressure P is PdV, then by substituting in Eq. (3.1) and combining the first and the second laws of thermodynamic we get

$$dU \leqslant TdS - PdV \tag{3.4}$$

For an open system, in which there is an exchange of matter with the surrounding; the mole numbers of each component in the system $(n_1, n_2, ..., n_m)$ should be considered as additional independent variables, where the subscript m refers to the number of components in the system. Therefore,

$$dU \leqslant \left(\frac{\partial U}{\partial S}\right)_{V,n_i} dS + \left(\frac{\partial U}{\partial V}\right)_{S,n_i} dV + \sum_i \left(\frac{\partial U}{\partial n_i}\right)_{S,V,n_{j\neq i}} dn_i \tag{3.5}$$

where

$$\left(\frac{\partial U}{\partial S}\right)_{V,n_i} = T \tag{3.6}$$

37

and

$$\left(\frac{\partial U}{\partial V}\right)_{S,n_i} = -P \tag{3.7}$$

n_i in Eq. (3.5) refers to all mole number and n_j refers to all mole numbers other than n_i. The partial differential of the internal energy with respect to the mole numbers at constant S, V and n_j is defined as the chemical potential μ_i.

$$\left(\frac{\partial U}{\partial n_i}\right)_{S,V,n_j} = \mu_i \tag{3.8}$$

then Eq. (3.5) can be written as

$$dU \leqslant TdS - PdV + \sum_i \mu_i dn_i \tag{3.9}$$

The internal energy is minimised when its natural variables are held constant because all spontaneous processes decrease the free energy, thus,

$$d(U)_{S,V,n_i} \leqslant 0 \tag{3.10}$$

and the system is said to be in equilibrium. The internal energy is therefore, a function of the three independent variables S, V and n_i. However, because the entropy S is hard to control, it is more useful to eliminate it and express the internal energy in terms of controllable variables such as temperature, volume and number of moles instead. For example, by subtracting the term $d(TS)$ from both sides of Eq. (3.9) we get

$$d(U - TS) \leqslant -SdT - PdV + \sum_i \mu_i dn_i \tag{3.11}$$

where the difference $U - TS$ is known as the *Helmholtz free energy* which is one of the thermodynamic potential functions and denoted by A

$$A = U - TS \tag{3.12}$$

substituting in Eqs. (3.11) gives

$$dA \leqslant -SdT - PdV + \sum_i \mu_i dn_i \tag{3.13}$$

thus, the Helmholtz free energy is also minimised when its natural variables (T, V and n_i) are held constant, i.e.

$$d(A)_{T,V,n_i} \leqslant 0 \tag{3.14}$$

in this case, the system has reached the equilibrium.

If the term $d(PV)$ is added to both sides of Eq. (3.9) we get

$$d(U + PV) \leqslant TdS + VdP + \sum_i \mu_i dn_i \tag{3.15}$$

where $U + PV$ is known as the *enthalpy*, another thermodynamic potential function denoted by H

$$H = U + PV \tag{3.16}$$

substituting in Eq. (3.15) gives

$$dH \leqslant TdS + VdP + \sum_i \mu_i dn_i \tag{3.17}$$

Again by subtracting the term $d(TS)$ from both sides of Eq. (3.17) we get

$$d(H - TS) \leqslant -SdT + VdP + \sum_i \mu_i dn_i \qquad (3.18)$$

where $H - TS$ is defined as the *Gibbs energy* and denoted by G, another important thermodynamic potential function.

$$G = H - TS \qquad (3.19)$$

then Eq. (3.18) can be rewritten as

$$dG \leqslant -SdT + VdP + \sum_i \mu_i dn_i \qquad (3.20)$$

thus, the Gibbs free energy is also minimised when its natural variables (T, P and n_i) are held constant, i.e.

$$d(G)_{T,P,n_i} \leqslant 0 \qquad (3.21)$$

and the system reaches the equilibrium.

Thus from Eqs. (3.9), (3.13), (3.17) and (3.20), the chemical potential can be expressed in terms of the partial derivative of fundamental thermodynamic potentials U, A, H or G with respect to the number of moles n_i as follows

$$\mu_i = \left(\frac{\partial U}{\partial n_i}\right)_{S,V,n_j} = \left(\frac{\partial A}{\partial n_i}\right)_{T,V,n_j} = \left(\frac{\partial H}{\partial n_i}\right)_{S,P,n_j} = \left(\frac{\partial G}{\partial n_i}\right)_{T,P,n_j} \qquad (3.22)$$

The pressure of the system can also be derived either from the Helmholtz or the internal free energies as follows

$$P = -\left(\frac{\partial A}{\partial V}\right)_{T,n_i} = -\left(\frac{\partial U}{\partial V}\right)_{s,n_i} \tag{3.23}$$

and the temperature can be derived from the internal energy as

$$T = -\left(\frac{\partial U}{\partial S}\right)_{V,n_i} \tag{3.24}$$

The entropy of the system can also be expressed in terms of the Helmholtz or the Gibbs free energies as

$$S = -\left(\frac{\partial A}{\partial T}\right)_{V,n_i} = -\left(\frac{\partial G}{\partial T}\right)_{P,n_i} \tag{3.25}$$

The heat capacity at constant pressure C_P and the heat capacity at constant volume C_V can also be obtained by taking the second derivative of Eq. (3.25) as follows

$$\left(\frac{\partial S}{\partial T}\right)_P = -\left(\frac{\partial^2 G}{\partial T^2}\right)_P = \frac{C_P}{T} \tag{3.26}$$

and

$$\left(\frac{\partial S}{\partial T}\right)_V = -\left(\frac{\partial^2 A}{\partial T^2}\right)_P = \frac{C_V}{T} \tag{3.27}$$

Therefore, if the free energy functions such as $U(S, V, n_i)$, $A(T, V, n_i)$ and $G(T, P, n_i)$ are known as functions of their natural variables, all thermodynamic properties of the system such as the chemical potential, the temperature, the pressure, the entropy and the heat capacities can be derived.

A mathematical approximation for the free energies is needed to describe the thermodynamic of a system. Equations of state (EOS) provide a mathematical expression

in terms of temperature, pressure, volume and composition, which can be used to approximate the free energy of a system. EOS are discussed in the following section.

3.3 Equations of state

Equations of state (EOS) are mathematical relations between temperature, pressure, volume and composition of a system [127]. These relations are used to provide approximate expressions for the free energies from which all thermodynamic properties, such as enthalpy, entropy and chemical potential can be derived. There are many different EOS reported in literature, and for space limitations, we provide a brief description of some of the most common EOSs. First, the ideal gas EOS and the mathematical expressions for the ideal gas free energies are presented in section 3.3.1, then other EOSs adjusted for non ideal gas systems are presented in section 3.3.2.

3.3.1 Ideal gas

Ideal gas is a hypothetical system consists of freely moving particles of negligible volume and negligible intermolecular forces [126]. In general, gases behave ideally at higher temperature and lower pressure as the intermolecular forces between particles becomes insignificant compared to their kinetic energy and their volume is negligible compared to the distance between them. Ideal gas is often used as a reference state for non ideal systems. Ideal gas obeys the equation of state,

$$PV = nRT \tag{3.28}$$

where n is the total number of moles and R is the universal gas constant.

The ideal gas law is commonly used to describe systems with pure ideal gas. The description can then be generalised for all systems [125]. By combining Eq. (3.20) at constant temperature and number of moles and low pressure with the ideal gas law given by

$$v_i^{ig} = \frac{RT}{P} \tag{3.29}$$

where v_i is the partial molar volume of pure i and is equal to V/n, we get

$$\left(\frac{\partial G^{ig}}{\partial P} \right)_{T,n_i} = v_i^{ig} = \frac{RT}{P} \tag{3.30}$$

and by integration at constant temperature,

$$G^{ig}(T, P) - G^{0,ig}(T, P^0) = RT \ln \frac{P}{P^0} \tag{3.31}$$

where the superscript 0 refers to the pure ideal gas as a reference state. P^0 is typically chosen to be 1 atm or 1 bar.

For ideal gas mixture, the total ideal gas Gibbs free energy G^{ig} of a system at temperature T and pressure P is defined by Smith and Van Ness [128] as

$$G^{ig} = \sum_k y_k G_k^{0,ig} + RT \sum_k y_k \ln y_k \tag{3.32}$$

where $G_k^{0,ig}$ is the is the ideal gas Gibbs free energy of species k at the system temperature and pressure and y_k is the mole fraction of species k.

The Helmholtz free energy can be obtained from the Gibbs free energy (Eq. (3.32)) given that

$$A = G - PV \tag{3.33}$$

and $PV = nRT$ therefore, the Helmholtz free energy of an ideal gas mixture is

$$A^{ig} = \sum_k y_k G_k^{ig} + RT \left[\sum_k y_k \ln y_k - n \right] \tag{3.34}$$

Refer to Ref. [128] for detailed derivation of the ideal gas mixture properties expressions.

In real life practical problems such as oil and gas processing plants, chemical plants and refineries, the pressure is high enough that the ideal gas law is not applicable. However, the ideal gas low provides a starting point for approximating the behaviour of real gas systems. Section 3.3.2 defines the non-ideal gas and explains how the ideal gas equation of state is adjusted for real gas system applications.

3.3.2 Non ideal gas

The assumptions mentioned in section 3.3.1 for ideal gas system are no longer applicable for high pressure and sometimes low temperature systems. Such systems behave non ideally where the intermolecular forces between particles and their volume become significant and should be considered. To account for system non-ideality, the compressibility factor Z is used where

$$Z = \frac{PV}{RT} \tag{3.35}$$

The compressibility factor can be obtained from the equations of state (EOS). These equations account for the deviation from ideality by introducing adjustable parameter into the ideal gas EOS can be represented. Virial EOS for instance, represents the volume deviation from ideality by power series as follows,

$$Z = \frac{PV}{RT} = 1 + B/V + C/V^2 + ... \tag{3.36}$$

where B and C are called the second and the third Virial coefficients, they depend on

the identity of the gas and the temperature [128].

Van der Waals equation (Eq. (3.37)) is another common EOS, it is a result of adjusting the pressure and the volume of the ideal gas EOS using the two adjustable parameters a and b.

$$\left(P + \frac{a}{V^2}\right)(V - b) = RT \tag{3.37}$$

where a/v^2 is defined as the internal pressure resulting from the attractive forces between particles and b is a volume correction parameter [126, 128].

Peng-Robinson (PR-EOS) [129] given by Eq. (3.38) and Soave Redlich Kwong (SRK-EOS) [130] given by Eq. (3.39) are also two of the most commonly known CEOSs. Both equations have similar formula and express the deviation from ideality using pressure and volume adjustable parameters a and b. Each equation has its own expression for the adjustable parameters with different constants. The constants can be evaluated by a fit to available PVT experimental data, and for simple cubic EOS, the critical temperature T_c and the critical pressure P_c can be used [128].

$$P = \frac{RT}{V - b} - \frac{a(T)}{V(V + b) + b(V - b)} \tag{3.38}$$

$$P = \frac{RT}{V - b} - \frac{a(T)}{V(V + b)} \tag{3.39}$$

Refer to Appendix A for more details on PR and SRK EOSs and their adjustable parameters, the compressibility factor and fugacity coefficient expressions derived from them.

To estimate the real gas properties, the ideal gas is used as a reference state and the deviation from that state is a measure of the system non-ideality. This is done

through the use of residual properties. The residual property X^{res} is defined as the difference between the real fluid property X and the ideal gas property X^{id} at the same temperature T, volume V and number of moles n:

$$X^{res}(T, V, n) = X(T, V, n) - X^{id}(T, V, n) \tag{3.40}$$

For example the residual Helmholtz free energy can be expressed as

$$A^{res}(T, V, n) = A(T, V, n) - A^{id}(T, V, n) \tag{3.41}$$

and given that

$$P = -\left(\frac{\partial A}{\partial V}\right)_{T,n} \tag{3.42}$$

Eq. (3.40) and Eq. (3.42) can be rewritten for the residual pressure as

$$P^{res}(T, V, n) = P(T, V, n) - P^{id}(T, V, n) \tag{3.43}$$

and

$$P^{res} = -\left(\frac{\partial A^{res}}{\partial V}\right)_{T,n} \tag{3.44}$$

The ideal gas pressure is $P^{id} = \rho RT$ and the real gas pressure can be defined using the compressibility factor Z as $P = Z\rho RT$, where Z acts as a correction factor to the ideal behaviour. Substituting for the pressures into Eq. (3.44) and taking the integral, the residual Helmholtz free energy can be obtained as follows

$$A^{res} = RT \int_0^\rho (Z - 1)\frac{d\rho}{\rho} \tag{3.45}$$

The compressibility factor Z can be obtained from any of the equations of state

described above. Once the Helmholtz free energy is obtained all other thermodynamic properties can be derived.

Cubic equations of state are commonly used for vapour pressures and equilibrium compositions calculation and produce accurate results against experimental data; however, they are known of their poor description of liquid phase properties [131]. Cubic equations of state rely on empirical mixing rules to provide approximate relationship to express their adjustable parameters in terms of composition. They have not always been successful in representing VLE of highly non-ideal liquid systems with multiple phases and associating components which tend to form hydrogen bonds such as water, alcohols, amines and acids [132]. In addition, for systems with polar components such as ketones, aldehydes, and ethers or electrolyte systems with charged species an explicit representation of the intermolecular forces such as dipole-dipole moment and electrostatic interactions is needed.

By accounting for different intermolecular forces in the system, a more accurate description of its thermodynamic properties can be achieved. Statistical mechanics theories have proved to be useful for this purpose to extend the use of EOSs for associating, polar and electrolyte systems. Many proposals for molecular-based EOSs, which account explicitly for the shape and the size of the molecule and the molecular interactions between molecules in the system such as association or hydrogen bonding interactions have been published in literature [123, 133, 134, 135, 136]. In 1990, the Statistical associating fluid theory-based EOSs or (SAFT) EOSs have emerged and gained a considerable attention [137, 138]. The following section provides a brief overview of the SAFT models.

3.3.3 Statistical associating fluid theory (SAFT) models

Equations of state have long been used to predict the thermodynamic properties and the phase equilibrium behaviour of simple fluid systems. However; complex fluid systems containing compounds of large molecules (chain like), such as polymers have only been recently considered. The application of statistical mechanics principles for

the equations of state has proven its success in developing rigorous models applicable for complex systems [139]. Statistical mechanics describes how macroscopic observations, such as temperature and pressure are related to the microscopic parameters and connects the thermodynamic quantities to the microscopic behaviour [140].

Beret and Prausnitz [141] and Donohue and Prausnitz [142] were first to develop an equation of state for chain molecules based on the perturbed hard-chain theory (PHCT). The thermodynamic properties of fluid mixtures with small and large molecules such as polymers can be calculated using (PHCT) model. This model accounts for the severe deviation from spherical shape in chain molecules [141].

Several modifications and extensions have been applied to PHCT equation to widen its range of applicability by accounting for polar and associating intermolecular forces exist in the system of interest [143, 144]. In 1990, Chapman et al. [137] and Huang and Radosz [138] developed an equation of state model called SAFT (Statistical Associating Fluid Theory). The model is applicable for both pure fluids and associating fluid mixtures.

In 1994, Banaszak et al. [145] and Johnson et al. [146] applied Wertheim's first-order thermodynamic perturbation theory (TPT1) [147], which is an expansion of the Helmholtz energy in a series of integrals of molecular distribution functions and the association potential, on the SAFT equation for freely-jointed Lennard-Jones Chain (LJC) model. The radial distribution function defines the probability of finding a particle at a certain distance from another particle [148]. It is strongly dependent on the type of matter thus vary for solids, gases and liquids. The Lennard-Jones fluid is the most widely used intermolecular interaction potential in simulation history to represent small spherical and nonpolar molecules based on the size of the molecules, the energy and the distance between them [149]. Banaszak et al. used Monte Carlo simulation to obtain values for the compressibility factor and the radial distribution function for Lennard-Jones spheres. The authors showed that the simulation results were in good agreement with Wertheim's first-order thermodynamic perturbation theory (TPTI) re-

sults determined using LJC simulations of Li and Chie [150]. Johnson et al. [146] presented an equation of state for chains of freely jointed Lennard-Jones spheres based on Wertheim's theory for associating fluids. Molecular dynamic simulations were also performed for different chain lengths at different temperatures. The pressure and the internal energy were predicted using the equation of state and the results were in good agreement with the molecular dynamics simulation results.

Gil-Villegas et al. [151] developed another version of SAFT EOS applicable for chain molecules of hard-core segments with attractive potentials of variable range; it was named SAFT-VR. This equation provided an additional parameter to characterize the range of the attractive part of the potential. Gross and Sadowski [139] applied the perturbation theory of chain molecules for the SAFT EOS to derive a dispersion term. The authors used a hard-chain fluid as a reference for the perturbation theory in their study; therefore their model was referred to as PC-SAFT (Perturbed Chain SAFT).

The PC-SAFT EOS was then used by many authors to calculate the equilibrium properties such as vapour pressure, saturated liquid density, heat of vapourisation and solubility of polymers and non-ideal solutions involved in natural gas treating such as aqueous ethanolamines [53, 152, 153]. The properties of polymers and ethanolamines as well as the vapour-liquid equilibrium of acid gas-aqueous ethanolamine solutions was successfully represented using PC-SAFT EOS over a wide range of conditions.As the PC-SAFT EOS was successful in representing such complex systems with long chain components such as polymers, and most ionic liquids consist of long chains, the PC-SAFT was chosen in this study as the thermodynamic model to be used for representing ionic liquid containing systems to investigate their use as an alternative solvent to amines for natural gas cleaning. In the following section, the PC-SAFT EOS is described in detail.

3.3.3.1 PC-SAFT EOS

PC-SAFT EOS represents the molecule as a chain of m_i spherical segments of diameter σ_i, as illustrated in Figure 3.1. For non-associating, neutral molecules, the molecules interact only through the excluded volume (inaccessible volume of a molecule because of the presence of another molecule) and the dispersion forces (van der Waals forces); therefore in this case, three molecular parameters are required to describe the molecules: m_i, σ_i, and the strength of the dispersion interaction ε_i.
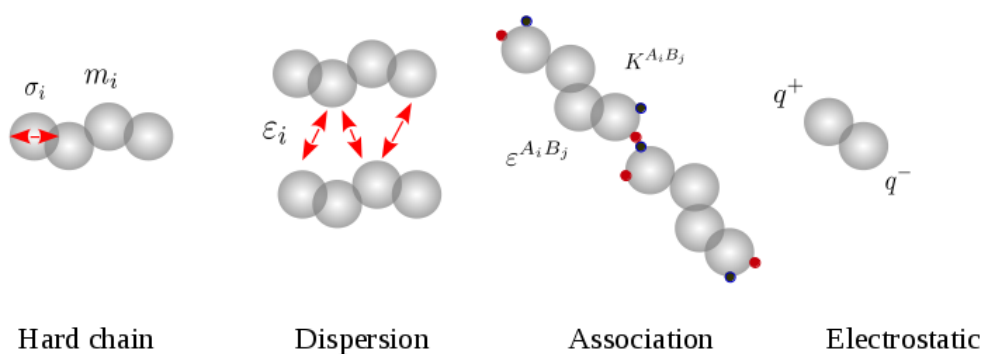
Figure 3.1: Illustration of PC-SAFT molecular parameters and the contributions to the Helmholtz free energy.

For associating molecules (e.g., molecules that tend to form hydrogen bonds), two more additional parameters are required: the association energy $\varepsilon^{A_iB_i}$ between sites A and B on molecule i and the effective association volume $K^{A_iB_i}$ between site A and B on the same molecule.

For charged ions or electrolytes, the Debye-Hückel term [154] is added to account for the long range Coulomb forces among ions in the system. In this case, the charge q of each ion is required as will be detailed later.

Within PC-SAFT, the Helmholtz free energy is expressed as a sum of separate contributions from different physical effects.

The residual Helmholtz free energy per molecules is given by

$$a^{res} = a^{hc} + a^{disp} + a^{assoc} + a^{elec} \tag{3.46}$$

where a^{hc} is the hard-chain reference contribution, a^{disp} is the dispersion contribution, a^{assoc} is the association contribution, and a^{elec} is the electrolyte contribution. The expressions for each of these terms will be summarized below, however, the reader is referred to Ref. [139] for details on the dispersion contribution, Ref. [137] for details on the association contribution, and Ref. [155] for details on the electrolyte contribution to Helmholtz free energy.

The hard-chain reference contribution is given by [139] as

$$a^{\text{hc}} = m a^{\text{hs}} - k_B T \sum_i x_i (m_i - 1) \ln g_{ii}^{hs} \tag{3.47}$$

where k_B is the Boltzmann constant, T is the absolute temperature of the system, x_i is the mole fraction of molecules of type i in the system, and $m = \sum_i x_i m_i$. The quantity g_{ii}^{hs} is the contact value of the radial distribution function, given as:

$$\begin{aligned}
g_{ij}^{hs} &= \frac{1}{(1 - \zeta_3)} + \left(\frac{d_i d_j}{d_i + d_j} \right) \frac{3\zeta_2}{(1 - \zeta_3)^2} \\
&+ \left(\frac{d_i d_j}{d_i + d_j} \right)^2 \frac{2\zeta_2^2}{(1 - \zeta_3)^3}.
\end{aligned} \tag{3.48}$$

where d_i is a temperature-dependent segment diameter of component i and defined as:

$$d_i = \sigma_i \left[1 - 0.12 \exp \left(-\frac{3\varepsilon_i}{k_B T} \right) \right], \tag{3.49}$$

ζ_n is given as:

$$\zeta_n = \frac{\pi}{6} \rho \sum_i x_i m_i d_i^n, \tag{3.50}$$

and ρ is the number density of molecules in the system.

The hard-sphere contribution to Helmholtz free energy is:

$$a^{hs} = \frac{k_B T}{\zeta_0} \left[\frac{3\zeta_1\zeta_2}{(1-\zeta_3)} + \frac{\zeta_2^3}{\zeta_3(1-\zeta_3)^2} + \left(\frac{\zeta_2^3}{\zeta_3^2} - \zeta_0 \right) \ln(1-\zeta_3) \right] \tag{3.51}$$

The dispersion contribution to the Helmholtz free energy is given by:

$$\frac{a^{disp}}{k_B T} = -2\pi\rho I_1(\zeta_3, m)\overline{m^2\varepsilon\sigma^3} \\ - \pi\rho m C_1 I_2(\zeta_3, m)\overline{m^2\varepsilon^2\sigma^3} \tag{3.52}$$

with

$$C_1 = \left(1 + Z^{hc} + \rho \frac{\partial Z^{hc}}{\partial \rho} \right)^{-1} \\ = \left(1 + m\frac{8\zeta_3 - 2\zeta_3^2}{(1-\zeta_3)^4} + (1-m)\frac{20\zeta_3 - 27\zeta_3^2 + 12\zeta_3^3 - 2\zeta_3^4}{[(1-\zeta_3)(2-\zeta_3)]^2} \right) \tag{3.53}$$

and

$$\overline{m^2\varepsilon\sigma^3} = \sum_{ij} x_i x_j m_i m_j \left(\frac{\varepsilon_{ij}}{k_B T} \right) \sigma_{ij}^3 \tag{3.54}$$

$$\overline{m^2\varepsilon^2\sigma^3} = \sum_{ij} x_i x_j m_i m_j \left(\frac{\varepsilon_{ij}}{k_B T} \right)^2 \sigma_{ij}^3 \tag{3.55}$$

The Lorentz-Berthelot mixing rules were employed to determine the parameters σ_{ij} and ε_{ij} between unlike segments:

$$\sigma_{ij} = \frac{1}{2}(\sigma_i + \sigma_j) \tag{3.56}$$

$$\varepsilon_{ij} = \sqrt{\varepsilon_i \varepsilon_j}(1 - k_{ij}) \tag{3.57}$$

The quantities $I_1(\zeta_3, m)$ and $I_2(\zeta_3, m)$ in Eq. (3.52) above are the integrals of the per-

turbation theory and are expressed as a power series in density as below

$$I_1(\zeta_3, m) = \sum_{i=0}^{6} a_i(m)\zeta_3^i \tag{3.58}$$

$$I_2(\zeta_3, m) = \sum_{i=0}^{6} b_i(m)\zeta_3^i \tag{3.59}$$

The coefficients of the power series are related to the segment number m as follows

$$a_i(m) = a_{0i} + \frac{m-1}{m}a_{1i} + \frac{m-1}{m}\frac{m-2}{m}a_{2i} \tag{3.60}$$

$$b_i(m) = b_{0i} + \frac{m-1}{m}b_{1i} + \frac{m-1}{m}\frac{m-2}{m}b_{2i} \tag{3.61}$$

where a_{0i}, a_{1i}, a_{2i}, b_{0i}, b_{1i}, and b_{2i} are the universal PC-SAFT constants, which can be found in Ref. [139] and are listed in Table B.1.

The association contribution to Helmholtz free energy is given by [137]

$$\frac{a^{\text{assoc}}}{k_B T} = \sum_i x_i \left[\sum_{A_i} \left(\ln X^{A_i} - \frac{X^{A_i}}{2} \right) + \frac{1}{2}M_i \right] \tag{3.62}$$

where X^{A_i} is the mole fraction of molecule i not bonded at site A, and M_i is the total number of association sites (both donor and acceptor sites) on molecule i. The quantities X^{A_i} can be determined by solving the equations:

$$X^{A_i} = \left[1 + N_{Av}\rho \sum_{j,B_j} x_j X^{B_j} \Delta^{A_i B_j} \right]^{-1} \tag{3.63}$$

where the index B_j runs over all association sites on molecule j, and $\Delta^{A_i B_j}$ is the association strength and is defined as

$$\Delta^{A_i B_j} = g_{ij}^{hs} \left[e^{\varepsilon^{A_i B_j}/(k_B T)} - 1 \right] \sigma_{ij}^3 K^{A_i B_j} \tag{3.64}$$

where $\varepsilon^{A_i B_j}$ and $K^{A_i B_j}$ are the association energy, and the effective association vol-

ume between a site A on molecule i and a site B on molecule j respectively.

For systems with charged components, the electrolyte term a^{elec}, as given by the Debye-Hückel theory [154], is added to contributions of Helmholtz free energy. Within the Debye-Hückel theory of electrolyte solutions, the ions are treated as spheres with charge q_i that can approach each other to within an effective ion diameter a_i and that are immersed in a background solvent characterized by a dielectric constant ϵ. The resulting expression for the molar Helmholtz free energy is

$$a^{elec} = -\frac{\kappa}{12\pi\epsilon} \sum_i x_i q_i^2 \chi_i \tag{3.65}$$

where the quantity χ_i is defined as

$$\chi_i = \frac{3}{(\kappa a_i)^3} \left[\frac{3}{2} + \ln(1 + \kappa a_i) - 2(1 + \kappa a_i) + \frac{1}{2}(1 + \kappa a_i)^2 \right], \tag{3.66}$$

where a_i is the ion diameter and κ is the inverse Debye screening length in $meter^{-1}$ and defined by Held et al. [155] as

$$\kappa = \sqrt{\frac{4\pi\rho}{\epsilon k_B T} \sum_i q_i^2 x_i}. \tag{3.67}$$

where q_i is the ion charge and x_i is the ion mole fraction. ϵ is the dielectric constant of the medium ($\epsilon = \epsilon_0 \epsilon_r$), where ϵ_0 is the vacuum permittivity and ϵ_r is the relative permittivity of the medium.

Once the all the contribution to Helmholtz free energy a^{hc}, a^{disp}, a^{assoc} and a^{elec} are calculated, the overall Helmholtz free energy can be obtained by adding the different contributions.

The dimensionless residual Helmholtz free energy a^{res} is defined as

$$a^{res} = \frac{A^{res}}{k_B T} \tag{3.68}$$

where A^{res} is the residual Helmholtz free energy per molecule, k_B is the Boltzmann constant, T is the absolute temperature of the system.

The compressibility factor $Z = P/\rho kT$ is defined as the derivative of the Helmholtz free energy with respect to the density at constant temperature and number of moles [156].

$$\left(\frac{\partial(A/NkT)}{\partial \rho}\right)_{(N_\alpha),T} = \frac{1}{\rho}Z \tag{3.69}$$

Obtaining the overall compressibility factor is analogous to obtaining the overall Helmholtz free energy. The different contributions to the compressibility factor, the hard chain Z^{hc}, the dispersion Z^{disp}, the association Z^{assoc} and the electrolyte Z^{elec} are added to get the overall compressibility factor. For example, the association contribution to the compressibility factor Z^{assoc} is given by

$$Z^{assoc} = \rho \sum_i x_i \sum_j x_j \sum_{A_j} \left[\left(\frac{1}{X^{A_j}} - \frac{1}{2}\right)\frac{\partial X^{A_j}}{\partial \rho_i}\right] \tag{3.70}$$

and the electrostatic contribution to the compressibility factor Z^{elec} is given by Eq. (3.71) below

$$Z^{elec} = \frac{P^{elec}}{\rho_N kT} = -\left(\frac{\partial a^{elec}/kT}{\rho_N \partial \upsilon}\right)_{T,N} = \frac{\kappa}{24\pi kT\epsilon}\sum_k x_k q_k^2 \sigma_k \tag{3.71}$$

where σ_k is given by Eq. (3.72)

$$\sigma_k = \left(\frac{\partial(\kappa\chi_k)}{\partial \kappa}\right)_{T,N} = -2\chi_k + \frac{3}{1 + \kappa a_k} \tag{3.72}$$

where ρ_N is the number density of the system and q_k is the ion charge. The overall

compressibility factor is then

$$Z^{res} = Z^{hc} + Z^{disp} + Z^{assoc} + Z^{elec} \tag{3.73}$$

Eq. (3.73) is analogous to Eq. (3.46).

A summary of equations used in this study for calculating the density, pressure, compressibility factor and the fugacity coefficient using PCSAFT EOS is provided in Appendix B. In the following section, an alternative approach for describing liquid solutions is presented, which is the activity coefficient approach. Besides the EOSs, activity coefficient models have also been used to describe non ideality in liquid solution systems, as will be detailed in section 3.4.

3.4   Activity coefficient models

Activity coefficient models provides an alternative approach to EOSs for describing liquid solution properties. These models are inherently different from EOS approach, they assume that the thermodynamic properties of the pure components are known and provide a description of properties change on mixing.

Before defining the activity coefficient, the concept of the *fugacity*, f needs to be introduced. Physically, the fugacity can be visualised as a partial pressure, which is a measurable variable. The ratio of the fugacity of component i in a solution at a given temperature, pressure and composition (f_i^l) to the standard state fugacity of that component at the same conditions (f_i^0) is defined as the activity a_i of component i at these conditions. It is a measure of the activity of component i in the solution relative to its standard state [125]. Thus

$$a_i = \frac{f_i^l}{f_i^0} \tag{3.74}$$

and the activity coefficient γ_i of component i is defined as the ratio of the activity a_i to the mole fraction x_i

$$\gamma_i = \frac{a_i}{x_i} \tag{3.75}$$

In section 3.4.1, we first define the ideal solution model, then show how the pure properties are used to estimate the ideal solution properties.

3.4.1 Ideal solution

Ideal solution is defined as the one in which all molecules are of the same size and all forces between molecules are equal [128]. In ideal solution, the fugacity of each component is proportional to its mole fraction at some constant temperature and pressure. Hence

$$f_i^l = K x_i \tag{3.76}$$

The proportionality constant $K = f_i^0$, where f_i^0 is the standard state fugacity of component i, then substituting Eq. (3.74) in (3.76) gives

$$a_i = x_i \tag{3.77}$$

In this case, the solution is called ideal. The activity coefficient is equal to unity and the difference of the ratio a_i/x_i from unity is a measure of the system non ideality.

Upon the formation of an ideal solution, it is assumed that no heat evolution or

absorption or volume change occur [125]. This can be expressed as

$$H^{id} = \sum_i x_i H_i \tag{3.78}$$

and

$$V^{id} = \sum_i x_i V_i \tag{3.79}$$

where H^{id} and V^{id} are the ideal solution enthalpy and volume, respectively, H_i and V_i are the pure species enthalpy and volume, respectively and x_i is the mole fraction of species i.

The Gibbs free energy of an ideal solution is defined as

$$G^{id} = \sum_i x_i G_i^0 + RT \sum_i x_i \ln x_i \tag{3.80}$$

thus, the ideal solution properties can be predicted using the properties of the pure species. All thermodynamic properties can be derived from the Gibbs free energy. The entropy S^{id} of an ideal solution, for example, can be derived as

$$S^{id} = -\left(\frac{\partial G^{id}}{\partial T}\right)_{P,n_i} \tag{3.81}$$

this gives

$$S^{id} = \sum_i x_i S_i - R \sum_i x_i \ln x_i \tag{3.82}$$

The second term on the right hand side of Eq. (3.82) is the entropy change of mixing.

The chemical potential of species can be derived from Gibbs free energy as

$$\mu_i^{id} = \left[\frac{\partial(nG^{id})}{\partial n_i}\right]_{P,T,n_j} \tag{3.83}$$

thus, the chemical potential of species i in an ideal solution μ_i^{id} is

$$\mu_i^{id} = G_i + RT \ln x_i \tag{3.84}$$

G_i is the pure species Gibbs free energy.

Most fluid mixtures however, deviate from ideality forming a non ideal solution. This will be defined in the following section.

3.4.2 Non ideal solution

Mixtures of real fluids deviate from the ideal behaviour and form non ideal solutions. Various intermolecular interaction forces act on real solutions, which makes it difficult to predict their properties. To relate the real solution properties to that of the ideal solution, the definition of the excess properties is required. The deviation of a real solution properties from the ideal solution behaviour at the same temperature, pressure and composition is defined by the *excess properties* [125, 126, 127]. The excess Gibbs energy for instance

$$G^E = G - G^{id} \tag{3.85}$$

The relations between excess thermodynamic properties H^E, G^E and A^E and their partial derivatives are the same as those given earlier in section 3.2 for the total properties. The excess Gibbs free energy is directly related to the activity coefficient. By replacing the pressure with fugacity in Eq.(3.31) we get

$$G = G^0 + RT \ln \frac{f_i}{f_i^0} \tag{3.86}$$

where the reference state Gibbs free energy G^0 is given by the summation of the pure species Gibbs free energy as

$$G^0 = \sum_i x_i G_i^0 \tag{3.87}$$

given that the ideal solution Gibbs free energy is

$$G^{id} = \sum_i x_i G_i^0 + RT \sum_i x_i \ln x_i \tag{3.88}$$

by subtracting Eq. (3.88) from Eq. (3.86) we get

$$G^E = RT \sum_i x_i \ln \gamma_i \tag{3.89}$$

and

$$\left[\frac{\partial(n G^E / RT)}{\partial n_i} \right]_{T,P,n_j} = \ln \gamma_i \tag{3.90}$$

Therefore, the activity coefficient of a species in a solution can be obtained by differentiating the excess Gibbs energy of the solution with respect to the number of moles at constant temperature and pressure.

The most common activity coefficient models are Van Laar, Margules, Wilson, non random two liquids or NRTL and universal quasi-chemical theory or UNIQUAC. Refer to Refs. [128] and [125] for the detailed mathematical expressions of these models.

Activity coefficient models provide a fairly accurate description of systems of non-ideal liquid mixtures as they express the system properties in terms of the molecular structure and the intermolecular forces. However, they sometimes fail to take into account strong vapour phase nonideality for systems with associating components [125].

SAFT EOS models described in section 3.3.3 perform better for such systems in both liquid and the vapour phases.

An analogous expression to the activity coefficient called the *fugacity coefficient* can be derived from the residual Gibbs free energy. Recalling that the chemical potential of a species in a solution is the partial molar Gibbs free energy, Thus, for an ideal gas we can write

$$\bar{G}_i^{ig} = G_i^{ig} + RT \ln y_i \tag{3.91}$$

where $\bar{G}_i^{ig}$ is the ideal gas partial molar Gibbs free energy, G_i^{ig} is the ideal gas Gibbs free energy of species i and y_i is the mole fraction. Differentiation at constant T and substituting for $dG^{ig} = RTd\ln P$ produces

$$d\bar{G}_i^{ig} = RTd\ln y_i P \tag{3.92}$$

and for a real solution we replace the pressure with the fugacity of species i in the solution f_i. Thus,

$$d\bar{G}_i = RTd\ln f_i \tag{3.93}$$

Subtracting Eq. (3.92) form Eq. (3.93) and applying the residual property definition results

$$d\bar{G}_i^{res} = RTd\ln \frac{f_i}{y_i P} \tag{3.94}$$

where the ratio $f_i/y_i P$ is the fugacity coefficient of species i in the solution and denoted as ϕ_i

$$\phi_i = \frac{f_i}{y_i P} \tag{3.95}$$

In situations where two or more phases brought into contact, the concept of phase equilibrium needs to be considered. The estimation of the activity coefficient and/or the fugacity coefficient is needed for solving phase equilibrium calculations. This will be detailed in the following section.

3.5 Phase equilibrium

Smith and Van Ness [128] defined the equilibrium as "a static condition in which no changes occur in the macroscopic properties of a system with time". For an isolated system consisting of fixed mount of species and liquid and vapour phases, there is no further tendency for change in temperature, pressure and composition of the system with time, they reach a fixed value. This state is called *phase equilibrium*. Solving the phase equilibrium problem involves the determination of the composition of each component in each phase and the temperature or the pressure of the system. Therefore, a relation between the composition of the components in different phases, the temperature or pressure is needed.

First, the criteria of phase equilibrium in terms of T, P and μ_i need to be introduced. At equilibrium, the internal energy U is a minimum and any variation in U at constant entropy S volume V and number of moles n_i vanishes [125]: i.e.

$$dU_{S,V,n_i} = 0 \tag{3.96}$$

Consider a system with m components splits into π phases, Eq. (3.9) can be written as

$$dU = \sum_{j=1}^{\pi} TdS - \sum_{j=1}^{\pi} PdV + \sum_{j=1}^{\pi} \sum_{i=1}^{m} \mu_i dn_i \tag{3.97}$$

By expanding Eq. (3.97) for two phase binary system for simplicity, we get

$$dU = T^{(1)}dS^{(1)} - P^{(1)}dV^{(1)} + \mu_1^{(1)}dn_1^{(1)} + \mu_2^{(1)}dn_2^{(1)}$$
$$+ T^{(2)}dS^{(2)} - P^{(2)}dV^{(2)} + \mu_1^{(2)}dn_1^{(2)} + \mu_2^{(2)}dn_2^{(2)} \tag{3.98}$$

and by applying the equilibrium condition of constant total entropy, constant total volume and constant total moles, we get

$$dS = dS^{(1)} + dS^{(2)} = 0 \tag{3.99}$$

$$dV = dV^{(1)} + dV^{(2)} = 0 \tag{3.100}$$

$$\sum_{j=1}^{2} dn_i = dn_1^{(1)} + dn_1^{(2)} + dn_2^{(1)} + dn_2^{(2)} = 0, \tag{3.101}$$

The above conditions can be used to eliminate some variables from Eq. (3.98). The elimination of $dS^{(1)}$, $dV^{(1)}$ and all $dn_i^{(1)}$ gives the following expression

$$dU = (T^{(2)} - T^{(1)})dS^{(2)} - (P^{(2)} - P^{(1)})dV^{(2)}$$
$$+ (\mu_1^{(2)} - \mu_1^{(1)})dn_1^{(2)} + (\mu_2^{(2)} - \mu_2^{(1)})dn_2^{(2)} \tag{3.102}$$

In Eq. (3.102) above, $dS^{(2)}$, $dV^{(2)}$ and all $dn_i^{(2)}$ are independent variable and by applying the equilibrium condition of Eq. (3.96), then

$$\frac{\partial U}{\partial S^{(2)}} = 0, \qquad \frac{\partial U}{\partial V^{(2)}} = 0, \qquad \frac{\partial U}{\partial n_1^{(2)}} = 0, \qquad \frac{\partial U}{\partial n_2^{(2)}} = 0 \tag{3.103}$$

This leads to the expression of uniform temperature, pressure and chemical potential of each component throughout the system at equilibrium as follows

$$T^{(1)} = T^{(2)} \tag{3.104}$$

$$P^{(1)} = P^{(2)} \tag{3.105}$$

$$\mu_1^{(1)} = \mu_1^{(2)}$$
$$\mu_2^{(1)} = \mu_2^{(2)} \tag{3.106}$$

The equilibrium criterion of uniform chemical potential given by Eq. (3.106) can be made more general and more physically meaningful if expressed in terms of fugasity instead of chemical potential. For two phases α and β in equilibrium, one can write,

$$\mu_i^{0\alpha} + RT \ln \frac{f_i^\alpha}{f_i^{0\alpha}} = \mu_i^{0\beta} + RT \ln \frac{f_i^\beta}{f_i^{0\beta}} \tag{3.107}$$

If the standard states are the same then,

$$\mu_i^{0\alpha} = \mu_i^{0\beta} \tag{3.108}$$
$$f_i^{0\alpha} = f_i^{0\beta} \tag{3.109}$$

this gives,

$$f_i^\alpha = f_i^\beta \tag{3.110}$$

Therefore, Eqs. (3.104), (3.105) and (3.110) are considered as the three fundamental equations of phase equilibrium [125].

To illustrate how the phase equilibrium problem is solved by relating the composition of different phases, we consider the following simple example of equilibrium in a two phase binary system with ideal behaviour. Assuming that the fugacity of a certain component in a certain phase at constant temperature and pressure is proportional to its mole fraction in that phase. If the two phases are vapour V and liquid L, then from Eq. (3.110) and by applying the above assumption we can write,

$$f_i^V = f_i^L \tag{3.111}$$

and

$$y_1 f_{pure1}^V = x_1 f_{pure1}^L \qquad (3.112)$$

Given that for a pure ideal gas the fugacity is equal to the pressure P and that the effect of pressure on the fugacity is negligible, then we can write,

$$y_1 P = x_1 P_1^{sat} \qquad (3.113)$$

where P_1^{sat} is the saturation pressure of the pure liquid 1 at temperature T. Eq. (3.113) is referred to as Raoult's law.

For real solutions, the relation between temperature, pressure and compositions can be obtained by means of equations of state or activity coefficient models described earlier in this chapter. From Eq.(3.74) and Eq.(3.95) we can write for species i in a real liquid solution

$$f_i^l = x_i \gamma_i f_i^0 \qquad (3.114)$$

and in a real gas mixture

$$f_i^v = y_i \phi_i P \qquad (3.115)$$

and at equilibrium we can write

$$y_i \phi_i P = x_i \gamma_i P_i^{sat} \qquad (3.116)$$

Fugacity coefficient is calculated using equation of state models such as PR, SRK or SAFT EOSs (see Appendix A and B) and activity coefficient is calculated using activity coefficient models such NRTL or UNIQUAC models [125, 128]. In phase equilibrium calculation, when the activity coefficient γ is used to account for liquid phase non ideality and the fugacity coefficient ϕ is used to account for vapour phase

non-ideality, the method is called γ-ϕ approach given by Eq. (3.116) above. However, when the fugacity coefficient is used to account for non-ideality in both phases, the method is called ϕ-ϕ approach given by Eq. (3.117) below.

$$y_i \phi_i^v = x_i \phi_i^l \tag{3.117}$$

Eq. (3.116) and Eq. (3.117) can be used to estimate the equilibrium composition using flash calculations described in Appendix A.

3.6 Conclusions

Understanding the use of different thermodynamic potential functions is of central importance. All thermodynamic properties of a given system can be determined from these functions. The fugacity coefficients and the activity coefficients can also be derived from the potential functions which can then be used for solving the VLE problem involved in any process for acid gas removal from natural gas. In general, VLE can either be solved by means of γ-ϕ approach or ϕ-ϕ approach. Different thermodynamic models have been used in literature for the calculation of the activity coefficient γ and the fugacity coefficient ϕ. These models can be divided into two broad categories: equations of state (EOS) models and activity coefficient models. Each model is applicable for certain systems and has its own advantages and limitations. Activity coefficient models can only be used to describe liquid phase non ideality. EOSs can be used to describe both phases, however, they are known of their poor prediction for liquid phase properties and poor representation of VLE of highly non-ideal systems with multiple phases and associating components such as water, alcohols, amines and acids. The more rigorous SAFT models have recently emerged and been successfully used to represent complex systems with large molecules such as polymers, associating and polar compounds. The PC-SAFT EOS, one of the SAFT models, will be used in the remainder of this thesis to represent the pure component properties of ionic liquids and VLE of ionic liquid containing systems.

Chapter 4

Ionic liquids as an alternative solvent to amines for gas sweetening

4.1 Introduction

Numerous technologies are available for acid gas removal from natural gas. Alkanolamine based chemical absorption is the most commercially utilized process, due to its versatility, efficiency, and low solvent cost. However, alkanolamines are volatile, corrosive, and their regeneration process is highly energy intensive, comprising 70% of the total operating costs [9, 58].

Ionic liquids (ILs), a relatively new class of materials, have emerged in the recent decades as an alternative solvent to alkanolamines for acid gas removal from natural gas [9]. Because ILs have negligible volatility, low melting points, high thermal stability, high ionic conductivity, and structural tunability, they offer a promising candidate as a solvent for acid gases in natural gas cleaning [58]. The solubility of acid gases in ILs needs to be properly modelled in order to understand the behaviour of acid gases to be removed in the selected ILs.

Most ILs consist of long chain organic cation and organic or inorganic anion. To represent systems with such complex molecules, a proper thermodynamic model

should be selected. The Perturbed Chain Statistical Association Fluid Theory (PC-SAFT) described in Chapter 3 is used in this chapter to investigate the solubility of carbon dioxide (CO_2) and hydrogen sulphide (H_2S) in several methylimidazolium bis (trifluoromethylsulfonyl) imide ionic liquids (ILs) or [$C_n$mim] [NTf_2] where $n = 2, 4, 6$, and 8. This is due to its success in representing the properties of complex systems with long chain components such as polymers and ethanolamines as well as the vapour-liquid equilibrium of acid gas-aqueous ethanolamine solutions over a wide range of conditions, given that most ionic liquids consist of long chains. Imidazolium-based ILs were selected in this study because of the availability of their experimental data due to their observed affinity towards CO_2 [58]. The CO_2 absorption capacity in imidazolium-based ILs and its interaction with the imidazolium groups have been widely studied in literature. Some research studies, which provide measurements for H_2S solubility in different ILs with comparison to CO_2 and other gases solubility are also available [72, 73, 74, 75].

The purpose of this chapter is to provide a solid thermodynamic basis for representing IL-containing systems involved in the IL-based acid gas removal process by validating the selected thermodynamic model for such systems to be used in the simulation of the IL-based process in the following chapters. This chapter is organized as follows, the following section gives a brief overview on the use of ILs as an alternative solvent to amines for acid gas removal, then the previous experimental and theoretical studies of IL properties and acid gases their solubility in them are summarised in section 4.3, then the thermodynamic models used in literature to represent IL-containing systems are reviewed in section 4.4. The rest of the chapter is focused on the use of the PC-SAFT model to represent acid gases-IL systems. The PC-SAFT model is validated for pure, binary and ternary systems of acid gases and methane in ILs in section 4.5. First, the pure component parameters for the acid gases and the studied ILs are determined and discussed. Second, the binary and the ternary solubility of acid gases in ILs is presented and analysed. Third, the solubility of methane in the studied ILs is discussed. Finally, the main findings are summarized in section 4.7.

4.2 Ionic liquids for acid gas removal

In the recent decades [9, 58], ionic liquids (ILs) have emerged as an alternative physical solvent for alkanolamines. ILs are organic salts characterized by their negligible volatility, high thermal stability, high ionic conductivity, and structural tunability. They are liquids over a wide range of temperatures; they can have melting points ranging from -100–$200°$C [9], which is much lower than the melting points of conventional ionic compounds, such as sodium chloride.

An IL consists of two types of ions: an organic cation, such as imidazolium, pyridinium or phosphonium ions and an inorganic anion, such as Cl^-, BF_4^-, PF_6^-, $CF_3SO_3^-$, NTf_2^-, or an organic anion such as carboxylate (RCO_2^-) [157], see Figure 4.1. ILs can be used in a variety of applications, including catalysis, gas storage and separation [158].

Due to the negligible volatility of ILs and their high thermal stability, the utilisation of ILs for gas sweetening can reduce the solvent losses, thus the cost of solvent makeup and the thermal decomposition and their consequent environmental impact. In addition, the use of ILs for the gas sweetening can lead to an overall reduction in energy consumption because physical absorption takes place, rather than chemical absorption. Furthermore, the tunable structure of ILs can be utilised to modify the absorption selectivity and capacity of the IL [9].

4.3 Experimental and theoretical studies of acid gases-IL systems

Over the past three decades, a significant number of experimental and theoretical studies of ILs and their mixtures with gas species has been published. Most of the experimental studies reported in literature focused on CO_2 capture, and less attention has been paid to H_2S removal. Many studies provided experimental measurements

Cations

Imidazolium   Phosphonium   Pyrrolidinium

Anions

Tetrafluoroborate   Hexafluorophosphate   Bis(trifluoromethanesulfonyl)amide
BF4   PF6   NTf2
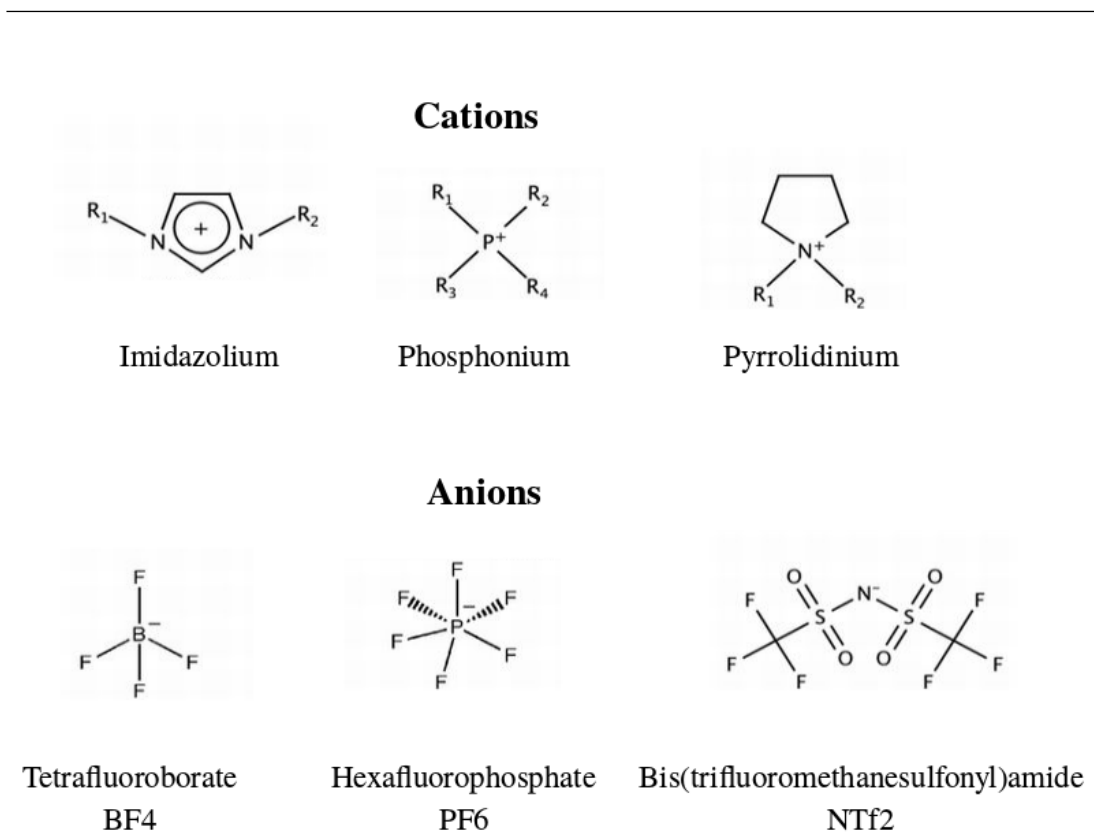
Figure 4.1: Common IL cations and anions. Taken from Ref. [159]

for the solubility of CO_2 in different types of ILs. The solubility is important because the more soluble the acid gas in the selected solvent, the more promising the solvent for acid gas removal; it is a measure of the solvent performance. The investigated ILs were either conventional ILs [68, 69, 70], task specific ILs (TSILs) for CO_2 capture [71] or functionalized ILs [37] with amine or hydroxyl group attached to the cation of the IL. Generally, both functionalized and TSILs showed comparable CO_2 solubility to traditional alkanolamine solvents. However, these ILs are highly viscous and their production require several synthetic and purification stages [71]. Camper et al. [38] presented an attractive method using amine-IL solutions as an alternative to the viscous and complex functionalized ILs and TSILs. The authors showed that an IL solutions containing 50 mol % of MEA are capable of capturing 1 mol of CO_2 per 2 moles of MEA to produce an insoluble MEA-carbamate precipitate that helps to drive

the capture reaction as opposed to traditional aqueous amine systems.

Some research studies provided measurements for H_2S solubility in different ILs with comparison to CO_2 and other gases solubility [72], [73], [74] and [75]. In all studies, H_2S showed higher solubility than CO_2 and other gases in ILs. Pomelli et al. [73] attributed that to the presence of specific interactions between H_2S and the ILs and used quantum chemical calculations to investigate the influence of these interactions on the H_2S solubility at the molecular level. As H_2S is more soluble than CO_2 in ILs, ILs can also be utilized for the separation of the two gases from each other.

Theoretically, molecular simulation and thermodynamic modelling have been used to describe the molecular structure, phase behaviour and thermodynamic properties of ILs and their mixtures. Molecular simulations have been used by many authors to study the microstructure of ILs and their microscopic properties [160, 161, 162, 163, 164, 165, 166, 167, 168]. They provide a tool for screening different ILs in terms of their structure and properties before using them for certain applications [169]. However, due to their computational expense, these methods have limited use in process simulation. An alternative approach for describing the behaviour of ILs and their mixtures theoretically is the thermodynamic modelling. This approach is presented in the following section.

4.4   Thermodynamic Models for IL-containing systems

Thermodynamic models used to describe the behaviour of ILs and their mixtures have been classified by Vega et al. [169] into four categories: cubic equations of state, activity coefficient methods, quantum mechanics-based methods, and statistical mechanics-based molecular approaches.

Shariati and Peters [170] and Shiflett and Yokozeki [171, 172, 173] used the classical cubic equations of state; Peng-Robinson [129] and Redlich Kwong [130], respectively, to model the phase behaviour and the solubility of the binary and ternary

systems of acid gases in IL. The systems were successfully described at the studied ranges of temperature and pressures however in both cases binary interaction parameters were used to adjust the model calculations to the experimental data.

Two activity coefficient models are used for the thermodynamic modelling of IL containing systems are the Non-Random Two-Liquid model (NRTL) [174] and the UNIversal QUAsi Chemical model (UNIQUAC) [175]. Both models were successfully used to describe the LLE and SLE data of different binary and ternary IL containing systems with superior results for the UNIQUAC model over the NRTL model [176] and [177].

Group contribution methods such as UNIFAC [178] and modified UNIFAC [179] have also been used to estimate several IL properties such as density, surface tension, viscosity, speed of sound, liquid heat capacity and transport properties [10, 180, 181, 182, 183]. The UNIFAC was able represent the pure IL experimental data and predict the properties of binary mixtures of ILs with reasonable accuracy (AAD% of less than 3.8% [181]). The phase equilibrium of IL binary and ternary systems containing alkanes, alkenes, aromatics, alcohols, ketones, acid gases and water have also been investigated using group contribution approach [10, 183, 184, 185]. In most cases the UNIFAC was found to be reliable for predicting phase equilibrium of mixtures containing ionic liquids.

The Conductor-like Screening Model for Real Solvents (COSMO-RS) developed by [186] is another approach used by some authors [187, 188, 189, 190] for the prediction of phase equilibria of IL systems and for the screening of suitable ionic liquids for certain separation and reaction problems. The model is a combination of a quantum chemical treatment of solutes and solvents with statistical thermodynamics procedure for the molecular surface interactions [186]. According to Klamt et al. [190], COSMO-RS gained a considerable attention in the field of ionic liquids since 2002, it provided reasonably accurate predictions for the activity coefficients of solutes in ionic liquids, without any adjustments or re-parameterization unlike other methods. Despite of that,

Klamt et al. [190] reported the limitations of COSMO-RS method, among them: the inaccuracy of the calculation of the chemical potentials, the restriction to incompressible liquids, the incapability of describing general electrolyte thermodynamics due to the neglect of long range ion-ion interactions and due to the extreme polarization charge densities appearing on small, highly charged ions, the restriction to fluid phase equilibrium properties where it cannot describe any dynamic, transport or structural properties of liquid systems.

In the recent decades, statistical mechanics-based molecular models have gained a considerable attention in modelling IL systems. These models account explicitly for the microscopic characteristics of IL mixtures. The original Statistical Associating Fluid Theory (SAFT) proposed by Chapman et al. [137] and Huang and Radosz [138] has been modified by many authors to produce different versions of the models for different systems. Some common versions include SAFT-VR for chain molecules of variable range potential [191], soft-SAFT for complex fluid mixtures [192], the group contribution SAFT-γ [193], and PC-PolarSAFT and truncated PC-PolarSAFT [194] for polar and associating fluid systems.

All of these models have been successfully used to represent the solubility of H_2S, CO_2, and other gases in some ILs and to estimate the thermodynamic properties of the IL-containing mixture [195, 196, 197, 198]. However, in most cases, binary interactions parameters, found by fitting to experimental data, have been used to enhance the accuracy of the VLE results; these parameters may be dependent or independent of temperature. Table 4.1 summarises some recent studies on the solubility of acid gases in ILs and Table 4.2 summarises some of the ILs studies based on SAFT models. The remainder of this chapter is focused on the use of the PC-SAFT model described in Chapter 3 as one of the SAFT models to represent the solubility of acid gases in alkyl imidazolium ILs.

Table 4.1: Summary of publications on the solubility of acid gases in ionic liquids

Experimental Studies	
Study	Ref.
CO$_2$ Solubility	
Designed a (TSIL) for CO$_2$ capture	[71]
Phase behaviour and solubility in imidazolium-based ILs	[68], [69] and [70]
Functionalized RTILs	[37]
Used amine-IL solutions	[38]
H$_2$S Solubility	
([C$_4$mim][PF$_6$]) IL	[72]
([C$_4$mim]$^+$) based ILs	[73]
Quaternary ammonium polyether IL	[74]
([C$_4$mim][BF$_4$]), ([C$_4$mim][Tf$_2$N]) and ([C$_2$mim][EtSO4])	[199] and [75]
Caprolactam tetrabutyl ammonium bromide ILs	[200]
Theoretical Studies	
Molecular Simulation Modelling	
To study the molecular structure of ILs and their properties	[160], [161], [201], [162], [163], [202], [164], [165], [166], [167], [168] and [203]
Thermodynamic Modelling	
PR EOS for the VLE of the binary system ([C$_2$mim]$^+$[PF$_6$]$^-$) IL and fluoroform	[170]
RK EOS for the VLE of the ternary system CO$_2$/H$_2$S/([C$_4$mim][PF$_6$])	[171]
NRTL EOS model for LLE and SLE of IL binary systems	[176]
UNIQUAC EoS for the ternary system IL+alcohol+alkane	[177]
UNIFAC group contribution methods	[204], [205], [206], [183], [184] and [10]
COSMO-RS method for the phase equilibria of IL containing systems	[187], [207], [188] and [189]
Statistical mechanics-based molecular models	[195], [208], [191], [194], [196], [197] and [198]

Table 4.2: Summary of publications on the solubility of acid gases in ILs based on SAFT modelling

Thermodynamic Modelling Studies			
SAFT Model	Acid Gas	Ionic Liquid	Ref.
PC-SAFT [139]	H$_2$S	Imidazolium-based	[195]
PC-SAFT [139]	CO$_2$	Imidazolium-based	[208]
SAFT-VR [191]	H$_2$S	Imidazolium-based	[195]
PC-polarSAFT [194]	CO$_2$	Imidazolium-based	[196]
tPC-PSAFT [194]	CO$_2$	Imidazolium-based	[196]
Soft-SAFT [192]	Various binary mixtures	Imidazolium-based	[197]
SAFT-γ [193]	CO$_2$	Imidazolium-based	[198]
Soft-SAFT [192]	CO$_2$	Pyridinium-based	[209]

4.4.1 PC-SAFT model for acid gases-IL systems

Here we aim to examine the ability of the PC-SAFT model developed by Gross and Sadowski [139] and described in Chapter 3 to represent the solubility of CO_2 and H_2S in several methylimidazolium bis (trifluoromethylsulfonyl) imide ILs as an alternative solvent to alkanolamines.

It is generally accepted that ILs cations and anions associate forming hydrogen bonds [210]. The typical hydrogen bond is defined as a bond formed between two molecules, one containing an electro-negative atom (possessing lone pairs of electrons) such as O, N, or F referred to as proton acceptor and another containing a covalent bond between hydrogen and an electronegative atom such as O, N or S referred to as proton donor [211]. However, covalent bonds with less electro-negative atoms such as C, Se and Si, are now recognized as proton donors as well [210].

Figure 4.2 provides an illustrative example for the hydrogen bonding between the anion and the cation of the studied ILs. The hydrogen bonds can be formed between any of the covalent C-H bonds on the methylimidazolium cation ring ($C_n$mim$^+$) as proton donors, circled in red in Figure 4.2 and any of the four oxygen atoms on the bis (trifluoromethylsulfonyl) imide anion (NTf$_2^-$) as proton acceptors, circled in blue in Figure 4.2. The central nitrogen (N) atom in NTf$_2^-$ anion is also electronegative and can form a hydrogen bond, however, according to Dong et al. [212], oxygen atoms are assumed to dominate the hydrogen bonding interactions between ion pairs in these ILs. The hydrogen bonding here could takes place between two IL molecules or between the cation and the anion of the same IL molecule. The effect of accounting for the IL cation-anion association interaction with different association schemes is examined here. To the best of our knowledge, the effect of changing the association scheme has not been examined yet.

Two strategies are adopted in this work to model the ILs. In the first strategy, ILs are modelled as neutral molecules and only the hard chain, the dispersion and the association contribution to Helmholtz free energy are considered. In the second
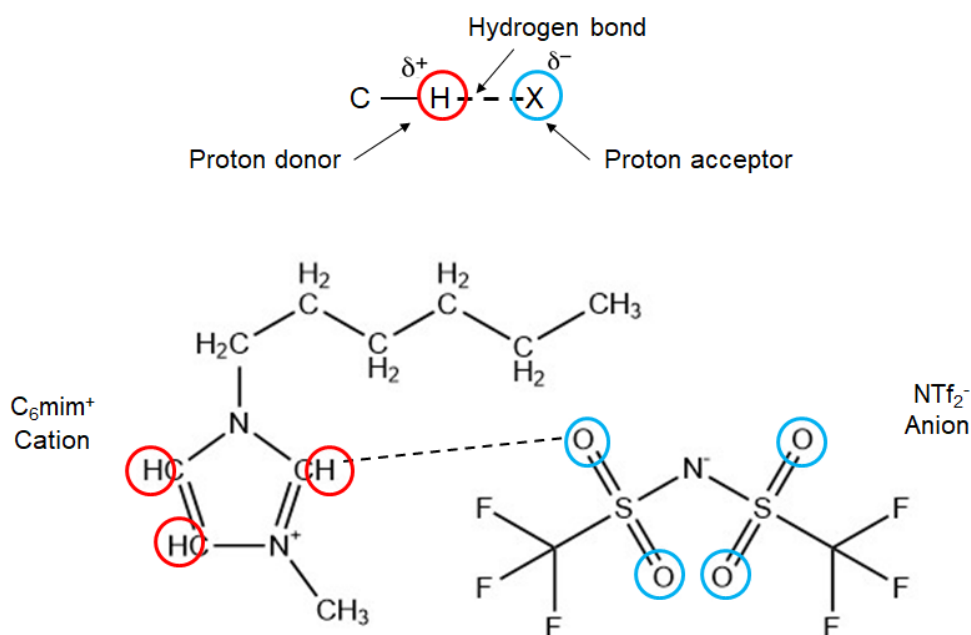
Figure 4.2: Illustrative example of hydrogen bonding between $[C_6mim]^+$ cation and $[NTf_2]^-$ anion in 1-hexyl-3-methylimidazolium bis (trifluoromethylsulfonyl) imide IL: Strategy 2, 2-site scheme (one donor and one acceptor).

strategy, ILs are modelled as two-part charged ions and the electrolyte contribution to Helmholtz free energy is also considered to account for the electrostatic attraction between charged ions. The charge of each ion is assumed to be localized within a segment, and, consequently, the ion diameter a_i is assumed to be equal to the segment diameter σ_i. The dielectric constant of the medium ϵ is set to unity in all cases, following Ji et al. [213]. The purpose of applying the second strategy is to enhance the predictive capability of the model by allowing the use of different IL cation-anion combinations in the future.

For the first time, four different association schemes for ILs are examined for both strategies: non-associating scheme, 2-sites scheme (one donor and one acceptor), 3-sites scheme (two donors and one acceptor) and 4-sites scheme (two donors and two acceptors). Our interest is mainly focused on finding the best strategy and association

scheme to represent the solubility of acid gases in ILs without the need for any binary interaction parameters to be used in modelling the acid gas removal problem that utilizes ILs as an alternative to alkanolamines. By eliminating the binary interaction parameters the model becomes predictive, i.e. it can be used to predict mixture properties with out the need for experimental data.

In this work, both acid gases are treated as non associating and non electrolyte components and cross association between acid gases and ILs is not considered. Self association refers to hydrogen bonds between molecules of the same components (e.g. self association between two same IL molecules), while cross association refers to hydrogen bonds between molecules of different components (e.g. cross association between H_2S and IL). The main focus here is to study the effect of IL association and electrolyte interactions on the solubility of acid gases in ILs.

In strategy 1, the association takes place between the neutral (uncharged) IL molecules where the proton donor is from one molecule and the acceptor from another molecule. In strategy 2, the association takes place between the cation and the anion of the same IL as illustrated by the connecting dashed line in Figure 4.2.

4.5 PC-SAFT model validation

4.5.1 PC-SAFT Pure Component Parameters

4.5.1.1 Acid Gases

Both acid gases, CO_2 and H_2S, are treated as non associating components, and the cross-association between the acid gases and the ILs is not considered in this work. Only three molecular parameters are required to describe each component within the PC-SAFT model: the number of segments m_i, the segment diameter σ_i, and the depth of square well potential ε_i. The parameter values for the acid gases are taken from Refs. [53] and [139] and are reported in Table 4.3 .

In order to validate these parameters, we used them to predict the vapour pres-

Table 4.3: PC-SAFT pure component parameters for acid gases used in this study.

| Component | MW | T range | m_i | σ_i | ε_i/k_B | Ref. |
	g mol^{-1}	K		Å	K	
H$_2$S	34.08	187–362	1.6686	3.0349	229	[53]
CO$_2$	44.01	216–304	2.0729	2.7852	169.21	[139]

sure for both acid gases using PC-SAFT. The calculations were able to successfully reproduce the experimentally measured vapour pressure data with reasonable accuracy (3.25% AARD (average absolute relative deviation) for CO_2 and 0.4% for H_2S). The vapour pressure curves are shown in Figure 4.3. The saturated liquid density of both gases is also calculated using the PC-SAFT parameters in Table 4.3 and compared to the experimental measurements from [214]. The saturated liquid density was satisfactorily represented using the same parameters with AARD of 1.75% for CO_2 and 1.13% for H_2S. At 298 K and 64.12 bar, the experimental saturated liquid density of CO_2 is 712.76 kg m^{-3} [214], the saturated liquid density of CO_2 calculated using PC-SAFT was 724.5 kg m^{-3}. The experimental saturated liquid density of H_2S at the same temperature and 20.11 bar is [214], and the calculated value using PC-SAFT was 783.8 kg m^{-3}.

4.5.1.2 Ionic Liquids

Four methylimidazolium bis (trifluoromethylsulfonyl) imide or [C$_n$mim][NTf$_2$] ILs with $n = 2$, 4, 6, and 8 are investigated in this work. The ILs are modelled using the two strategies described in the previous section.

The proton donor could be one of the three hydrogen atoms covalently bonded to the carbons on the imidazolium ring. The proton acceptor could be any of the four oxygen atoms or the central nitrogen on the NTf$_2^-$ anion. The possible donor and acceptor sites are highlighted in Figure 4.2. In this work, four association schemes are investigated for each strategy: a non-associating scheme (where association is neglected), a 2-site scheme (one donor and one acceptor), a 3-site scheme (two donors and one
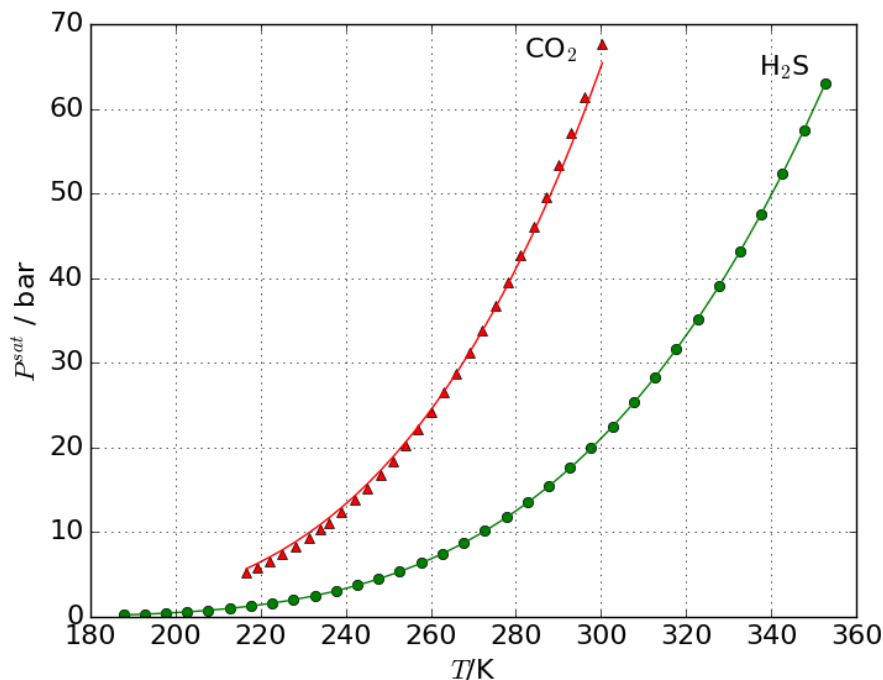
Figure 4.3: Vapour pressure of acid gases CO_2 (red lines and triangles) and H_2S (green lines and triangles). The symbols represent the experimental vapour pressure data taken from Ref. [214]). The lines are the vapour pressures calculated using PC-SAFT with the parameters given in Table 4.3.

acceptor), and a 4-site scheme (two donors and two acceptors).

Without association, only three molecular parameters are required to describe each IL using PC-SAFT: m, σ and ε. When self-association is included, two additional parameters are needed for each IL: the association energy $\varepsilon^{A_i B_i}$ between donor site A and acceptor site B on the molecule and the effective association volume $K^{A_i B_i}$ between sites A and B.

The values of the pure component parameters m_i, σ_i, ε_i, $\varepsilon^{A_i B_i}$ and $K^{A_i B_i}$ for the four studied ILs are determined by fitting to experimental density data recorded in

literature [215, 216, 217]. This is performed by using the Levenberg-Marquardt algorithm [218] within the LMFIT software package to minimize the following objective function OF:

$$OF = \sum_{i=1}^{n} \left(\rho_i^{exp} - \rho_i^{cal} \right)^2 \tag{4.1}$$

where n is the number of data points, ρ_i^{exp} is the experimental density at a particular temperature and ρ_i^{cal} is the density calculated using PC-SAFT EOS at the same temperature. The AARD between the calculated and the experimental data is calculated as:

$$AARD = \frac{1}{n} \sum_{i=1}^{n} \left| \frac{\rho_i^{exp} - \rho_i^{cal}}{\rho_i^{exp}} \right| \tag{4.2}$$

Density is used for parameter fitting here because it is the most important property for ILs as they are high density liquids and hardly volatile so the vapour pressure for example is not relevant. This approach has been followed by all previous studies. The $AARD$ of the calculated density at low pressure is in the range of 0.07%-0.38%. The results of the 4-site scheme for fitting the density of all ILs using strategy 1 are shown in Figure 4.4. There was no significant change in the predicted density between the different association schemes and between the two strategies at low pressure; therefore, only the results of the 4-site scheme of strategy 1 are shown in the figure. For C_6mimNTf$_2$ and C_8mimNTf$_2$ ILs, the experimental density data available in literature were limited to a narrow temperature range; therefore, their density is extrapolated using PC-SAFT EOS. It can be seen in Figure 4.4 that the extrapolated density follows the same trend as the available experimental density.

The densities of C_2mimNTf$_2$ and C_4mimNTf$_2$ at high pressures are shown in Figure 4.5 and Figure 4.6, respectively. At these pressures, strategy 2 provides a slightly better fit to the experimental density of the ILs; the AARD of [C_2mim][NTf$_2$] density at 500 bar is 0.48% for strategy 1 and 0.45% for strategy 2. For [C_4mim][NTf$_2$], the AARD for the density at 298.15 K and pressures ranging from 0–1500 bar is 0.59% for
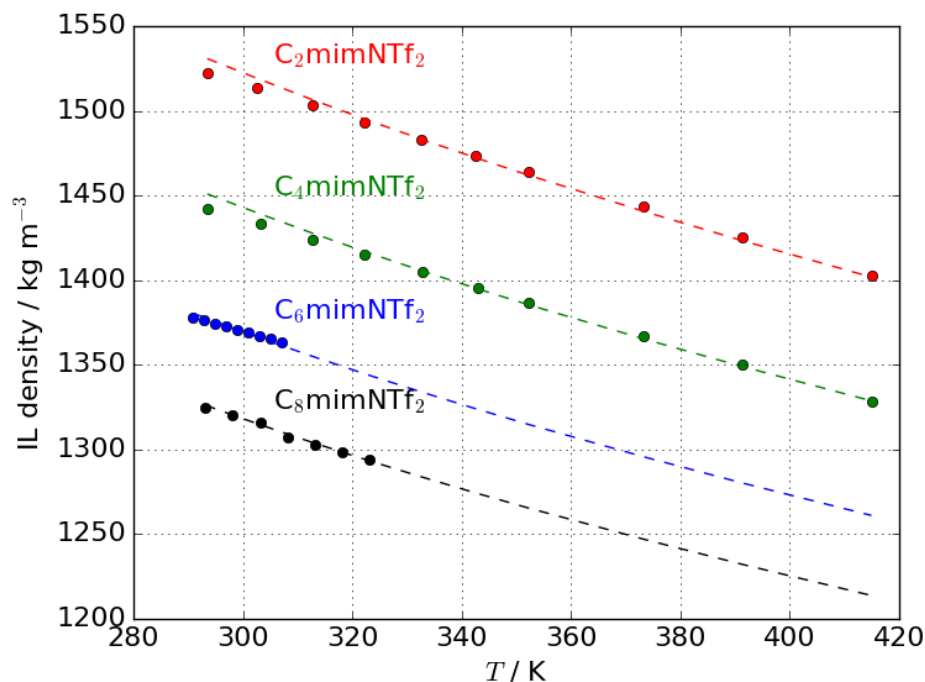
Figure 4.4: Density variation of the studied ILs with temperature at low pressure: (i) [C$_2$mim][NTf$_2$] (red), (ii) [C$_4$mim][NTf$_2$] (green), (iii) [C$_6$mim][NTf$_2$] (blue), and (iv) [C$_8$mim][NTf$_2$] (black). The symbols represent experimental data [215, 216, 217]. The lines are the predictions of PC-SAFT using strategy 1 with the 4-site association scheme.

strategy 1 and 0.27% for strategy 2.

Without association, the PC-SAFT predictions for the density of C$_2$mimNTf$_2$ at high pressure was better represented using strategy 1 with the AARD ranging from 0.3% at 51 bar to 0.5% at 900 bar. However, strategy 2 performs better when association is included, as compared to the non-associating scheme; the AARD ranges from 0.40% at 51 bar to 0.56% at 900 bar. For C$_4$mimNTf$_2$ at high pressure, including association improves the results for both strategies, with the AARD ranging from 0.2% to 0.9% for pressures up to 2500 bar.
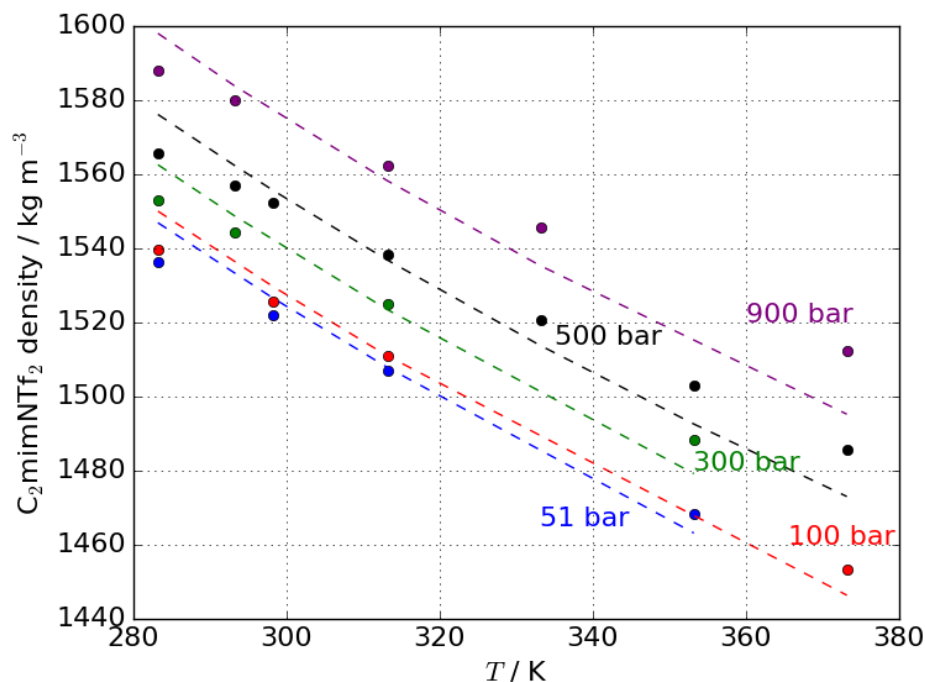
Figure 4.5: Density of [C$_2$mim][NTf$_2$] at high pressures. The symbols represent experimental data [219]. The lines are the calculations of PC-SAFT using strategy 1 with the 4-site association scheme.

The PC-SAFT provided a satisfactory description of the investigated IL densities at the given conditions with AARD ranging from 0.07 to 0.9%, compared to, for example, the cubic EOS model combination with the Group contribution method approach used by Gadamsetty et al. [220] to predict the density of ILs, who achieved 4.4% AARD.

In the following section, the PC-SAFT is validated for binary systems of acid gases-ILs. The binary solubility is calculated using PC-SAFT and compared to the experimental literature data.
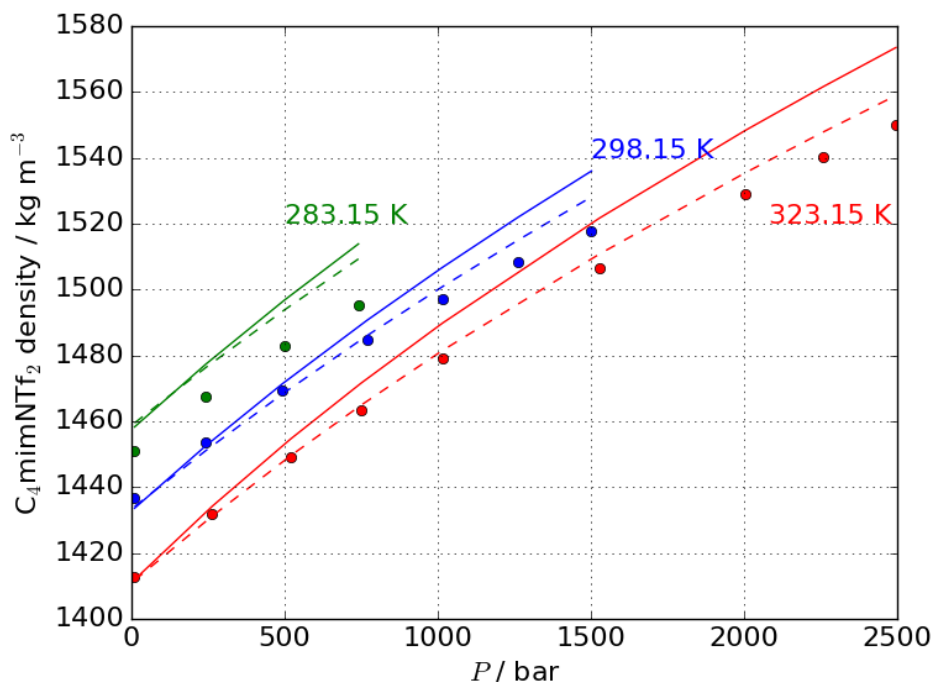
Figure 4.6: Density of [C$_4$mim][NTf$_2$] at high pressure and at different temperatures. The symbols represent experimental data [221]. The dashed lines are the calculations of PC-SAFT using strategy 2 with the 4-site association scheme. The solid lines are calculations using strategy 2 with the non-associating scheme.

4.5.2 Binary solubility of acid gases in ionic liquids

The solubility of acid gases in the studied ILs was calculated using PC-SAFT EOS. Phase equilibrium calculations were carried out by equating the fugacities of the acid gas in the vapour and liquid phases. The vapour pressure of the ILs was considered negligible due to their low volatility.

The optimized PC-SAFT pure component parameters obtained form the experimental density fitting are used to check the binary solubility of single acid gas in IL and adjusted to minimize the solubility AARD. The optimum values are that produce the minimum AARD for both the pure IL density and binary solubility of both acid

gases in IL. Note, however, no cross association between the acid gas and the ILs was included, and no binary interaction parameters were introduced. The optimum PC-SAFT pure component parameters obtained for the studied ILs for the first strategy with different association schemes are recorded in Table 4.4 and in Table 4.5 for the second strategy.

Table 4.4: Optimized PC-SAFT parameters of the studied ILs with different association schemes (ILs as neutral molecules: Strategy 1).

IL	T range	Association	σ_i	ε_i/k_B	m_i	$\varepsilon^{A_iB_i}/k_B$	$K^{A_iB_i}$	AARD	ρ_i^{exp}
	K	Scheme	Å	K		K		%	Ref.
[C$_2$mim][NTf$_2$]	293.49 – 414.92	Non	3.700	380	7.850			0.16	[215]
		2(1:1)	3.580	378	8.694	1350	0.00225	0.18	
		3(2:1)	3.556	378	8.880	1170	0.00225	0.18	
		4(2:2)	3.520	378	9.170	1020	0.00225	0.19	
[C$_4$mim][NTf$_2$]	293.49 – 414.92	Non	3.780	383	8.360			0.15	[215]
		2(1:1)	3.660	383	9.260	1350	0.00225	0.18	
		3(2:1)	3.640	382	9.410	1170	0.00225	0.18	
		4(2:2)	3.600	382	9.740	1020	0.00225	0.18	
[C$_6$mim][NTf$_2$]	290.95 – 307.05	Non	3.830	385	9.069			0.08	[216]
		2(1:1)	3.700	383	10.100	1350	0.00225	0.09	
		3(2:1)	3.680	382	10.262	1170	0.00225	0.09	
		4(2:2)	3.635	381	10.660	1020	0.00225	0.09	
[C$_8$mim][NTf$_2$]	293.15 – 323.15	Non	3.930	387	9.290			0.07	[217]
		2(1:1)	3.790	385	10.400	1350	0.00225	0.07	
		3(2:1)	3.760	384	10.655	1170	0.00225	0.07	
		4(2:2)	3.721	383	11.000	1020	0.00225	0.07	

A summary of the binary solubility results of both acid gases in the four studied ILs for both strategies with the best association scheme (4-site scheme) and at low pressure (up to 15 bar) is provided in Figure 4.7. Table 4.6 summarizes the AARD of all of the investigated systems in this study using both strategies with the 4(2:2) association scheme and the reference of experimental data.

Chen et al. [208] and Li and co-workers [213, 227] studied the same binary systems. The first strategy is the same as that used by Chen et al. [208] and [213]; however, in their study, only one association scheme was considered for the IL (the 2-site scheme), and despite using binary interaction parameters to improve the solubility fit, high values of AARD for CO$_2$-IL system were reported (5.845%–14.825%).

Table 4.5: Optimized PC-SAFT parameters of the studied ILs as dissociated ions with the electrolyte term included (ILs as charged ions: Strategy 2).

IL ion	MW g mol^{-1}	valency	T range K	Association	σ_i Å	ε_i/k_B K	m_i	$\varepsilon^{A_iB_i}/k_B$ K	$K^{A_iB_i}$	AARD %	ρ_i^{exp} Ref.
C$_2$mim$^+$	111.168	+1	293.49 – 414.92	Non	3.070	220.00	2.330			0.30	[215]
				2(1:1)	2.900	220.00	2.800	1480	0.00225	0.36	
				3(2:1)	2.795	220.00	3.170	1420	0.00225	0.36	
				4(2:2)	2.664	220.00	3.785	1360	0.00225	0.36	
C$_4$mim$^+$	139.221	+1	293.49 – 414.92	Non	3.400	227.00	2.920			0.36	[215]
				2(1:1)	3.220	227.00	3.470	1480	0.00225	0.38	
				3(2:1)	3.120	227.00	3.850	1420	0.00225	0.37	
				4(2:2)	2.970	227.00	4.520	1360	0.00225	0.37	
C$_6$mim$^+$	167.215	+1	290.95 – 307.05	Non	3.530	230.00	3.794			0.07	[216]
				2(1:1)	3.325	230.00	4.580	1480	0.00225	0.08	
				3(2:1)	3.230	230.00	5.025	1420	0.00225	0.08	
				4(2:2)	3.080	230.00	5.850	1360	0.00225	0.09	
C$_8$mim$^+$	195.335	+1	293.15 – 323.15	Non	3.830	242.00	3.860			0.07	[217]
				2(1:1)	3.620	242.00	4.600	1480	0.00225	0.07	
				3(2:1)	3.500	242.00	5.110	1420	0.00225	0.07	
				4(2:2)	3.340	242.00	5.920	1360	0.00225	0.07	
NTf$_2^-$	280.145	−1			3.720	375.65	5.960				

The second strategy treats the IL as two charged ions: a cation and an anion; therefore, the electrolyte contribution is also taken into consideration in this strategy. The same model was used by Ji et al. [213], referred to as strategy 6 in their work; however, they did not account for the association in this strategy and did not consider H$_2$S solubility in their study. Ji et al. studied H$_2$S solubility in Ref. [227] and only by introducing binary interaction parameters was the e-PC-SAFT able to reliably describe the H$_2$S solubility. The results of both strategies are plotted and compared to the experimental solubility data reported in literature (see Figure 4.8 and Figure 4.9).

The solubility of CO$_2$ in [C$_2$mim][NTf$_2$] and [C$_8$mim][NTf$_2$] at high pressure is also represented using the same set of parameters given in Table 4.4 and Table 4.5 for the 4-site scheme and for both strategies. The experimental data was reproduced with reasonable accuracy. No additional binary interaction parameters are needed. The results are shown in Figure 4.10, Figure 4.11 and Figure 4.12 and are detailed later.

PC-SAFT provides a better fit to the solubility of acid gases in ILs at low pressures
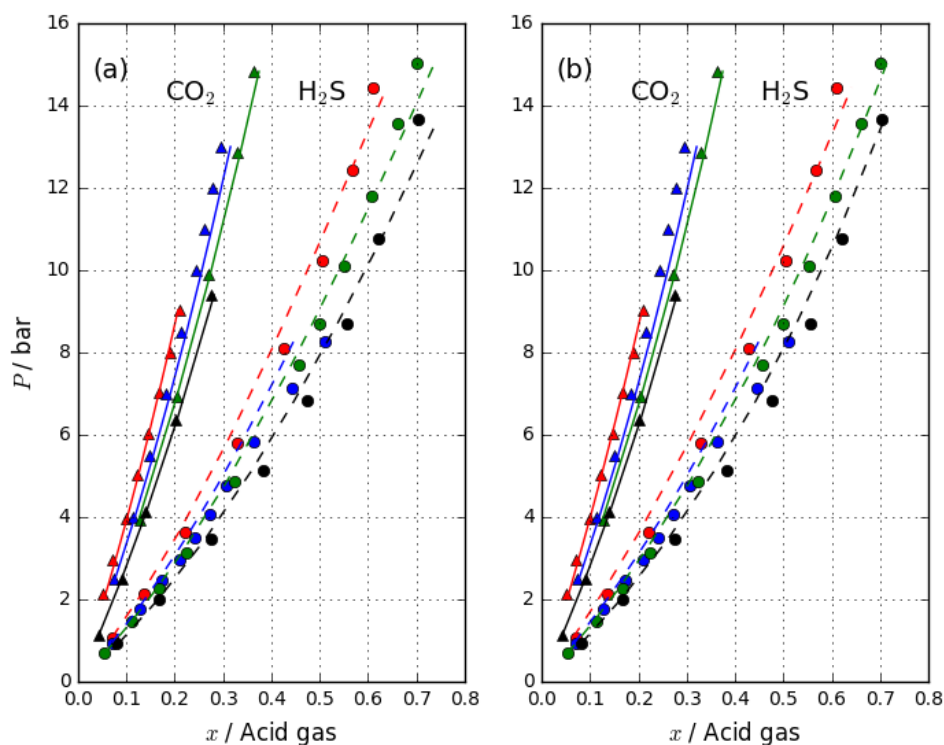
Figure 4.7: Solubility of acid gases in the studied ILs: (i) [C$_2$mim][NTf$_2$] (red), CO$_2$ at 298.15 K (solid) and H$_2$S at 303.15 K (dashed) (ii) [C$_4$mim][NTf$_2$] (blue), CO$_2$ at 298.15 K (solid) and H$_2$S at 303.15 K (dashed), (iii) [C$_6$mim][NTf$_2$] (green), CO$_2$ at 297.30 K (solid) and H$_2$S at 303.15 K (dashed) and (iv) [C$_8$mim][NTf$_2$] (black), CO$_2$ at 303.15 K (solid) and H$_2$S at 303.15 K (dashed). Symbols represent experimental data. Lines represent the predictions of PC-SAFT with the 4-site association scheme for (a) strategy 1 and (b) strategy 2 for CO$_2$ (solid) and H$_2$S (dashed).

than at high pressures. For the non-associating scheme, PC-SAFT over-estimates the solubility at high pressures. This might be attributed to the fact that the association contribution becomes more important at high pressure. Moreover, H$_2$S is about twice more soluble in the ILs than CO$_2$. The solubility of both acid gases in [C$_8$mim][NTf$_2$] is higher than that in [C$_6$mim][NTf$_2$] than in [C$_4$mim][NTf$_2$] than in [C$_2$mim][NTf$_2$], which is in agreement with conclusions obtained in previous studies [69, 158]; the sol-
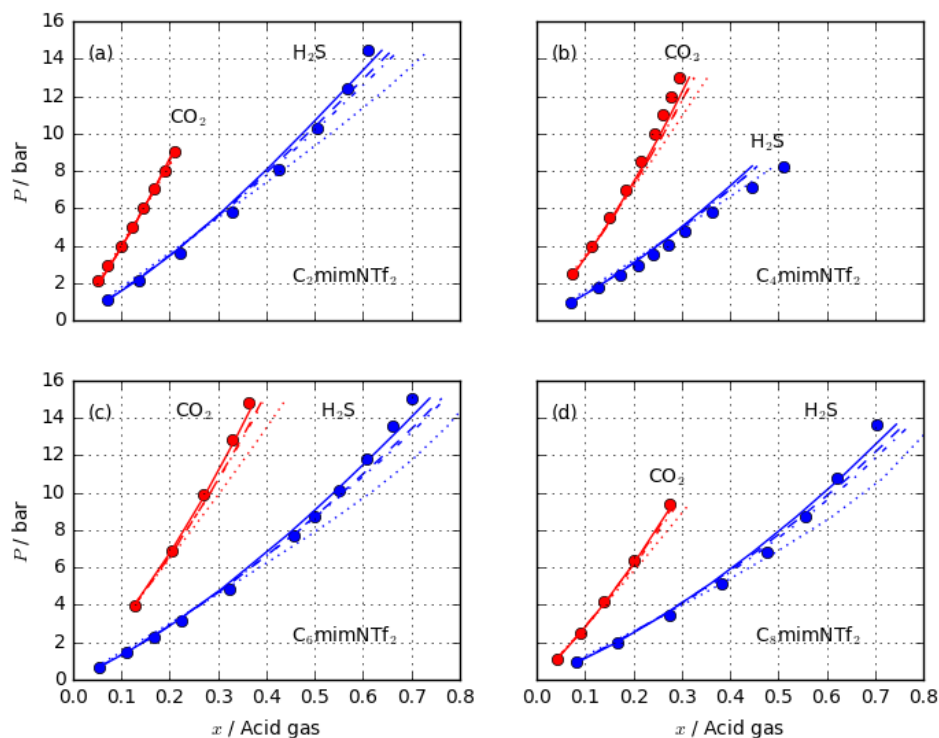
Figure 4.8: Binary solubility of CO_2 (red) and H_2S (blue) in the ILs (a) C_2mimNTf$_2$, CO_2 at 298.15 K and H_2S at 303.15 K, (b) C_4mimNTf$_2$, CO_2 at 298.15 K and H_2S at 303.15 K, (c) C_6mimNTf$_2$, CO_2 at 297.30 K and H_2S at 303.15 K and (d) C_8mimNTf$_2$, CO_2 at 303.15 K and H_2S at 303.15 K. The symbols represent experimental data. The lines represent the calculated solubilities using PC-SAFT with the ILs modelled in strategy 1 with (i) no association (dotted lines), (ii) 2-site association scheme (dashed-dotted lines), (iii) 3-site association scheme (dashed lines), and (iv) 4-site association scheme (solid lines).
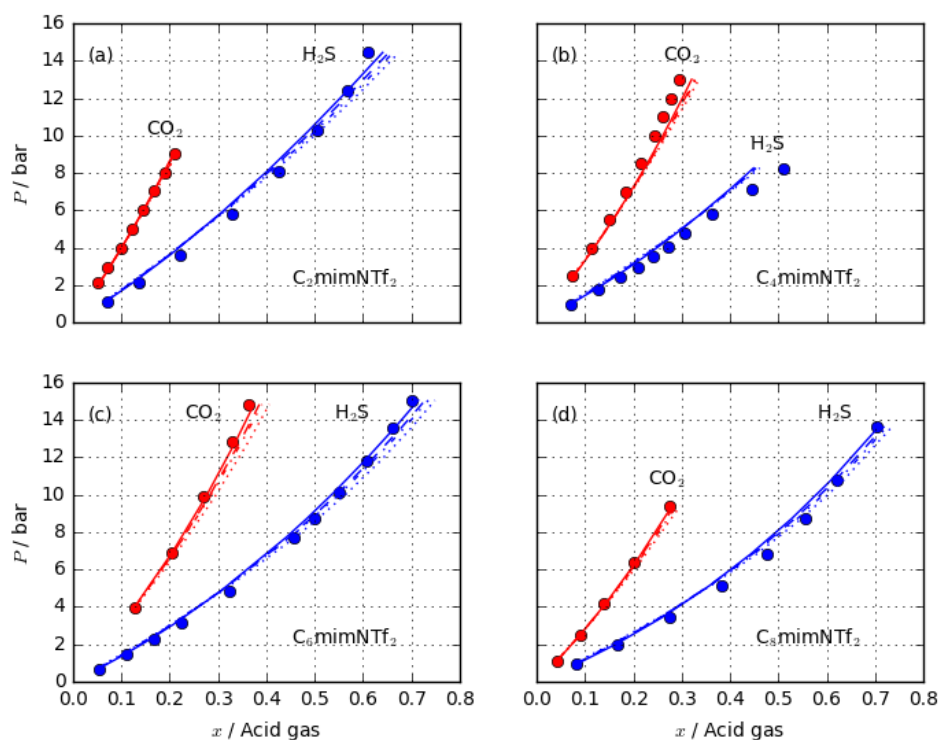
Figure 4.9: Binary solubility of CO_2 (red) and H_2S (blue) in the ILs (a) $C_2mimNTf_2$, CO_2 at 298.15 K and H_2S at 303.15 K, (b) $C_4mimNTf_2$, CO_2 at 298.15 K and H_2S at 303.15 K, (c) $C_6mimNTf_2$, CO_2 at 297.30 K and H_2S at 303.15 K and (d) $C_8mimNTf_2$, CO_2 at 303.15 K and H_2S at 303.15 K. The symbols represent experimental data. The lines represent the calculated solubilities using PC-SAFT with the ILs modelled in strategy 2 with (i) no association (dotted lines), (ii) 2-site association scheme (dashed-dotted lines), (iii) 3-site association scheme (dashed lines) (iv) 4-site association scheme (solid lines).

Table 4.6: Solubility AARD for systems investigated in this study with the 4(2:2) association scheme and both strategies.

System	T	P	Strategy 1 AARD	Strategy 2 AARD	Ref.
	K	bar	%	%	
CO_2–[C_2mim][NTf$_2$]	298.15 – 450.5	2.00 – 337.29	7.20	5.00	[222], [223]
H_2S–[C_2mim][NTf$_2$]	303.15	1.08 – 14.44	3.73	5.66	[224]
CO_2–[C_4mim][NTf$_2$]	298.15	2.50 – 13.00	4.98	6.51	[225]
	333.3	18.12 – 130.19	9.80	6.70	[69]
H_2S–[C_4mim][NTf$_2$]	303.15	0.94 – 8.26	6.62	7.48	[199]
CO_2–[C_6mim][NTf$_2$]	297.30	3.94 – 14.83	1.54	1.82	[172]
H_2S–[C_6mim][NTf$_2$]	303.15	0.68 – 15.04	2.76	3.13	[158]
CO_2–[C_8mim][NTf$_2$]	303.15	1.12 – 9.40	1.77	1.45	[158]
	345	16.00 – 231.00	7.80	6.65	[226]
H_2S–[C_8mim][NTf$_2$]	303.15 – 323.15	0.93 – 17.39	5.05	14.56	[158]
	303.15	1.72 – 9.60	H_2S: 6.24 CO$_2$: 7.99	H_2S:11.63 CO$_2$:9.10	[158]
CO_2–H_2S–[C_8mim][NTf$_2$]	323.15	2.04 – 10.90	H_2S: 12.57 CO$_2$: 2.56	H_2S: 31.69 CO$_2$: 20.59	[158]
	343.15	2.24 – 12.08	H_2S: 15.37 CO$_2$: 6.67	H_2S: 34.69 CO$_2$: 25.48	[158]

ubility of the acid gases in the IL increases with increasing alkyl chain length of the methylimidazolium cation. The increase in the alkyl chain length results in an increase in the volume available for acid gases interaction.

The solubility fit improves by accounting for the association contribution which can be noticed in Figure 4.8 and Figure 4.9. In most cases, the 4-sites association scheme provides the most accurate predictions for the solubility of both acid gases in the studied ILs without the need for any binary interaction parameters for fitting with an AARD of 2.76%–6.62% for H_2S-ILs systems and 1.54%–4.98% for CO_2-IL systems.

By adding association sites, the segment diameter σ_i of the IL decreases and the number of segments increases accordingly to keep the density of the IL fixed (see Table 4.4 and Table 4.5). Consequently, the reduced density (packing fraction) of the IL increases leaving no space for the acid gas to penetrate into the IL causing the solubility of the acid gas to decrease. This can be seen in Figure 4.8 and Figure 4.9. For this reason accounting for the association helped to improve the over estimated solubility

of the non-associating scheme.

In strategy 2, the difference between different association schemes is found to be smaller compared to that of strategy 1 which can be noticed by comparing Figure 4.8 and Figure 4.9. This indicates that the electrolyte term plays a similar role to the association term in improving the solubility fit. At low pressures no significant improvement has been achieved by treating the IL as electrolytes in strategy 2. However, at high pressures both the density and solubility fits are improved when strategy 2 is used. The model predictive capability is also enhanced by allowing the examination of different ILs anion-cation combinations in the future. Although this has not been applied in this study, it is considered as a starting point for a possible future work.

The solubility of CO_2 in ILs at high pressure is calculated using the same set of parameters without any additional binary parameters for both strategies. The experimental data are reproduced with reasonable accuracy. The results of CO_2 solubility in [C_2mim][NTf$_2$] for both strategies are shown in Figure 4.10 and Figure 4.11 and Table 4.6. In the temperature range of 298.15–450.5 K and pressure range of 2–337.29 bar, strategy 2 (AARD 5.0%) provides a better description than strategy 1 (AARD 7.2%) of the measured CO_2 solubility in [C_2mim][NTf$_2$].

The high pressure solubility of CO_2 in [C_8mim][NTf$_2$] at 345 K is represented using both strategies. It can be noticed from Figure 4.12 that the low pressure solubility is more accurately represented using strategy 1, while strategy 2 slightly underestimates it. However, at pressures above 50 bar the solubility is more accurately represented using strategy 2. In strategy 2 the IL is represented more explicitly as two part ions unlike in strategy 1 where the IL is represented as one neutral molecule. At high pressure stronger interactions between the cation and the anion are expected, which can not be represented if the IL was modelled as one neutral molecule.

The solubility of H_2S in [C_8mim][NTf$_2$] is also represented using the same set of parameters given in Table 4.4 for the 4-site scheme using strategy 1 at different
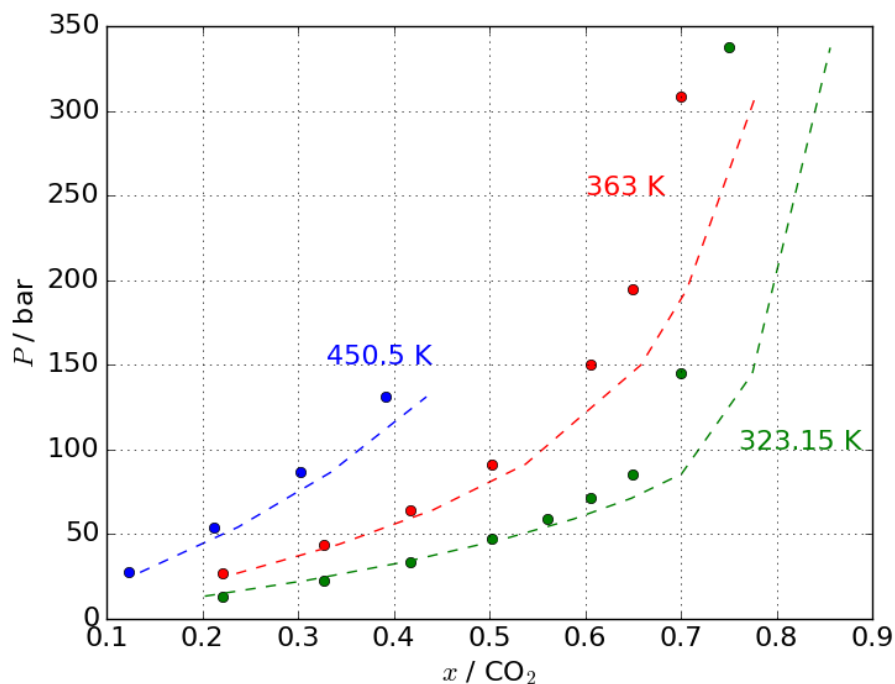
Figure 4.10: Solubility of CO_2 in [C_2mim][NTf_2] at different temperatures and high pressures. The symbols represent experimental data [222] and [223]. The lines are the calculations of PC-SAFT using strategy 1 with the 4-site association scheme.

temperatures. The experimental data from Jalili et al. [158] were reproduced with reasonable accuracy with AARD of 3.74% at 303.15 K, 5.1% at 313.5 K and 6.3% at 323.15 K (see Figure 4.13). No additional binary interaction parameters were used. At this range of low pressures (0.935 bar – 17.395 bar), strategy 1 results in a significantly more accurate representation (AARD 5.0%) of this system than strategy 2 (AARD 14.59%). This leads to conclusion that the molecule-based strategy 1 is preferable at low pressures (approximately from 0.9bar to 17 bar) in representing the solubility of acid gases in ILs, while at high pressure (approximately from 17 bar to 337 bar) the ion-based strategy 2 is preferable.

In the following section, the PC-SAFT is validated for the ternary system of CO_2-
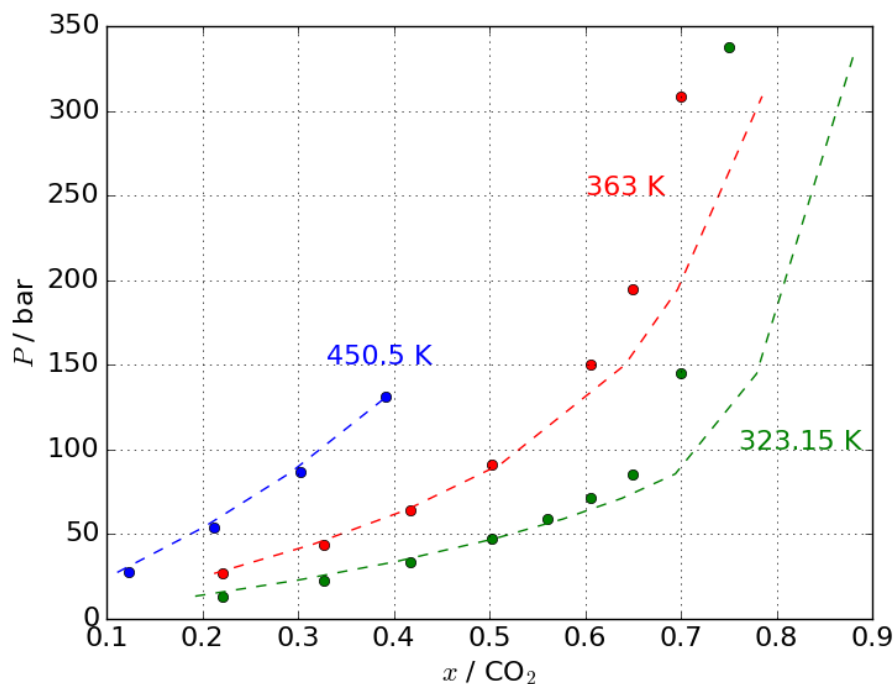
Figure 4.11: Solubility of CO_2 in [C_2mim][NTf_2] at different temperatures and high pressures: The symbols represent experimental data [222] and [223]. The lines are the calculations of PC-SAFT using strategy 2 with the 4-site association scheme.

H_2S-C_8mimNTf$_2$ IL. The ternary solubility is predicted using the PC-SAFT parameter obtained in the previous sections and the results are compared to the experimental literature data.

4.5.3 Ternary mixture of CO_2-H_2S-C_8mimNTf$_2$

In this section, the optimum parameters obtained from the experimental density and binary solubility fit for the 4-sites association scheme of strategy 1 are used to predict the solubility of the ternary system CO_2-H_2S-C_8mimNTf$_2$ at three different temperatures. The results are shown in Figure 4.14, Figure 4.15, and Figure 4.16. The experimental
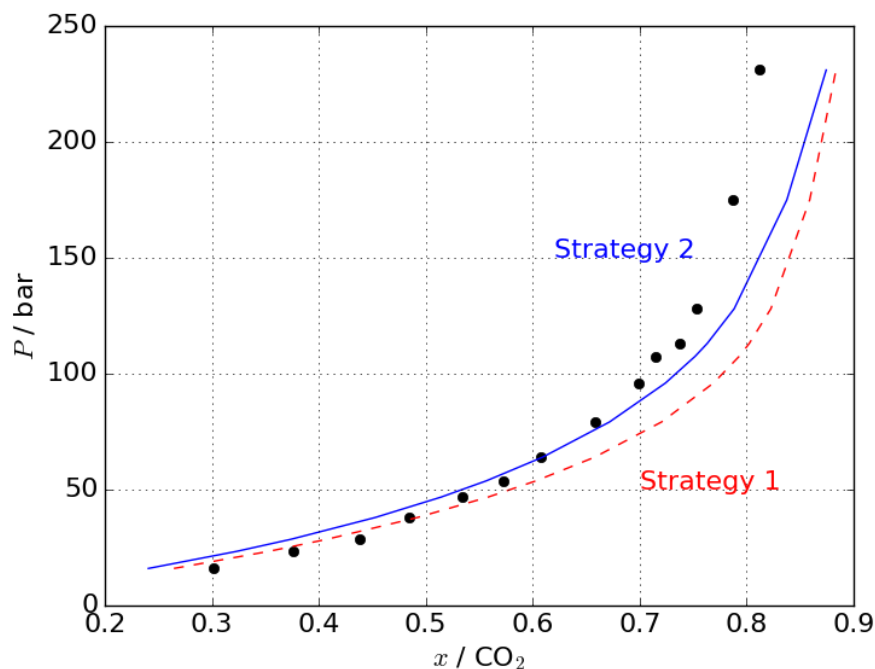
Figure 4.12: Solubility of CO_2 in [C_8mim][NTf$_2$] at 345 K and high pressures with the 4-site association scheme: The symbols represent experimental data [226].The dashed red line represents the calculations of PC-SAFT using strategy 1 and the solid blue line represents strategy 2.

data from Ref. [158] are reproduced with an AARD of 6.24% for H_2S and 7.99% for CO_2 at 303.15 K, 2.59% for CO_2 and 12.57% for H_2S at 323.15 K and 6.67% for CO_2 and 15.37 % for H_2S at 343.15 K without the need for binary interaction parameters.

Strategy 1 with the 4-site scheme parameters provided the best results for the ternary system. For example, the AARD of strategy 2 was found to be 9.1% for CO_2 and 11.63% for H_2S for the 4-site scheme at 303.15 K. Furthermore, the associating schemes provides better results than the non-associating schemes for both strategies. For instance, the AARD of the non-associating scheme of strategy 1 was found to be 14.6% for CO_2 and 8.90% for H_2S at 303.15 K. This was also the case for strategy 2 (see Table 4.6). For the ternary system, only low pressure data were available
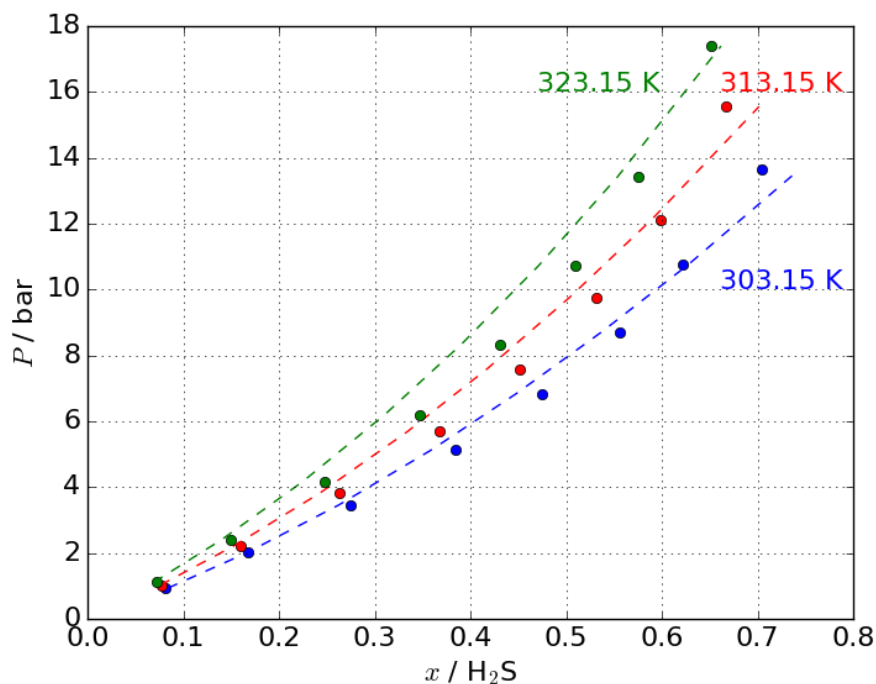
Figure 4.13: Solubility of H$_2$S in [C$_8$mim][NTf$_2$] at different temperatures: (i) 303.15 K (blue), (ii) 313.15 K (red) and (iii) 323.15 K (green). The symbols represent experimental data [158]. The dashed lines are the calculations of PC-SAFT using strategy 1 with the 4-site association scheme.

(1.72–12.08 bar) and at this range of pressures, strategy 1 provided significantly better results than strategy 2. This is consistent with the binary system results obtained in section 4.5.2. The following section discusses the solubility of methane in ILs.
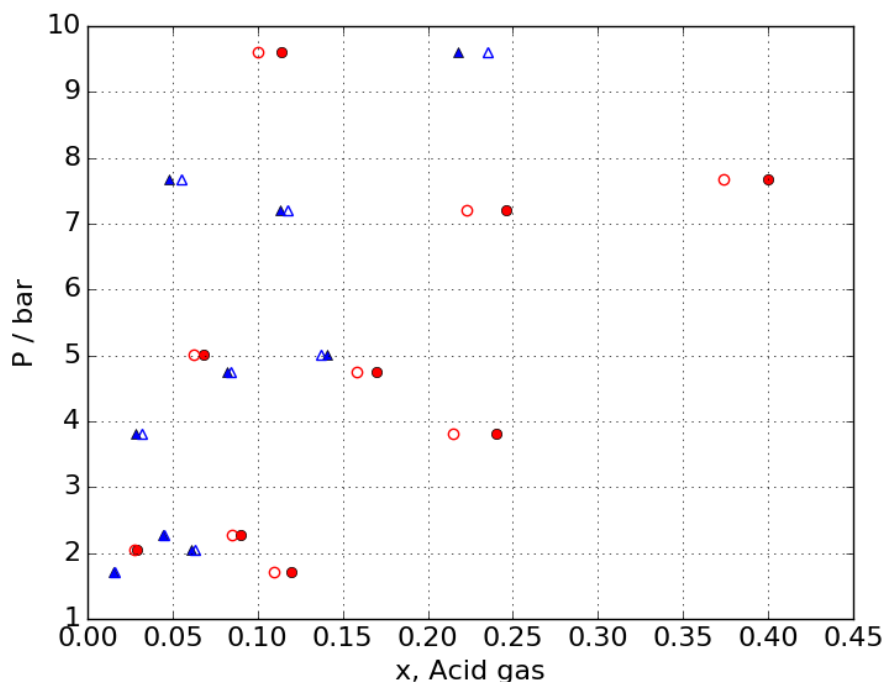
Figure 4.14: Ternary mixtures of CO_2-H_2S-$C_8mimNTf_2$ at 303.15 K with the 4-site association scheme (strategy 1). Open triangles represent the predicted CO_2 solubility using PC-SAFT, open circles represent the predicted H_2S solubility, and filled symbols represent experimental data [158].

4.5.4 Solubility of methane (CH_4) in ionic liquids

Methane is the main constituent of natural gas (70–90%). Therefore, the determination of its solubility in ILs is of crucial importance. The solubility of CH_4 in two of the studied ILs ($C_4mimNTf_2$ and $C_6mimNTf_2$) for which experimental data are available is represented using PC-SAFT. ILs are modelled as neutral molecules with the 4(2:2) association scheme, and the PC-SAFT parameters presented in Table 4.4. CH_4 is modelled as a non associating molecule with PC-SAFT parameters taken from Gross and Sadowski [139]. Binary interaction parameters of -0.148 for $C_4mimNTf_2$ and -0.185 for $C_6mimNTf_2$ are needed to fit the PC-SAFT calculations to the experimental solubility data taken from Raeissi and Peters [228] for $C_4mimNTf_2$ and from Kumelan et
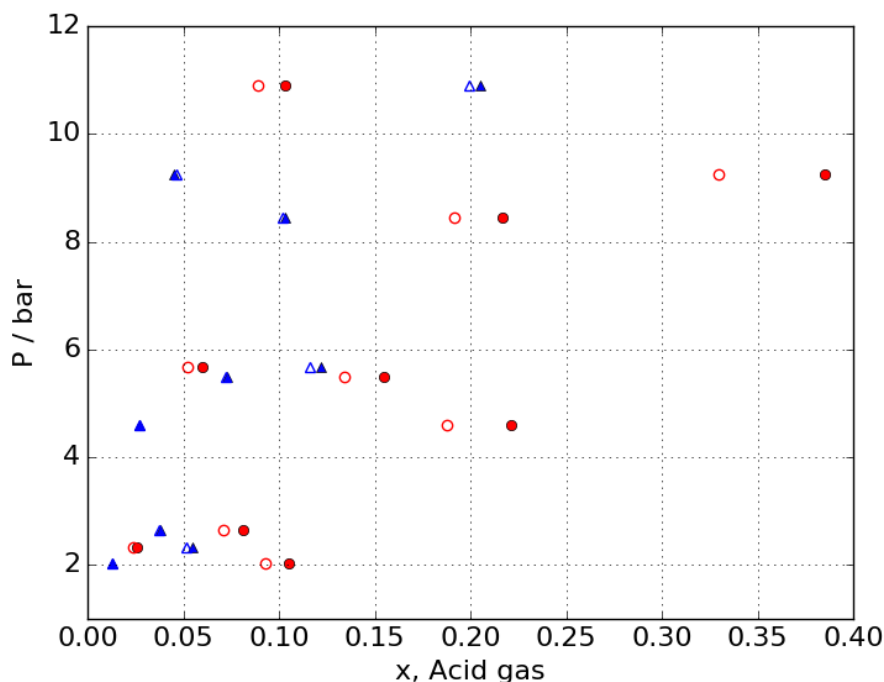
Figure 4.15: Ternary mixtures of CO_2-H_2S-$C_8mimNTf_2$ at 323.15 K with the 4-site association scheme (strategy 1). Open triangles represent the predicted CO_2 solubility using PC-SAFT, open circles represent the predicted H_2S solubility, and filled symbols represent experimental data [158].

al. [229] for $C_6mimNTf_2$. The results are shown below.

It can be seen from Figure 4.17 that the PC-SAFT underpredicts the solubility of CH_4 in ILs, where the model deviates by 79.8% from the experimental data for $C_4mimNTf_2$ (solid blue line) and by 88.1% for $C_6mimNTf_2$ (solid red line). This can be attributed to the polarity of ILs [230]. The PC-SAFT polar term is not considered in this work, and its effect is accounted for by using binary interaction parameters. The effect of polar interactions of ILs should be considered in future work. By including the aforementioned interaction parameters the model was able to fit to the experimental data with 4.5% AARD for $C_4mimNTf_2$ and 3.7% for $C_6mimNTf_2$. Further experimen-
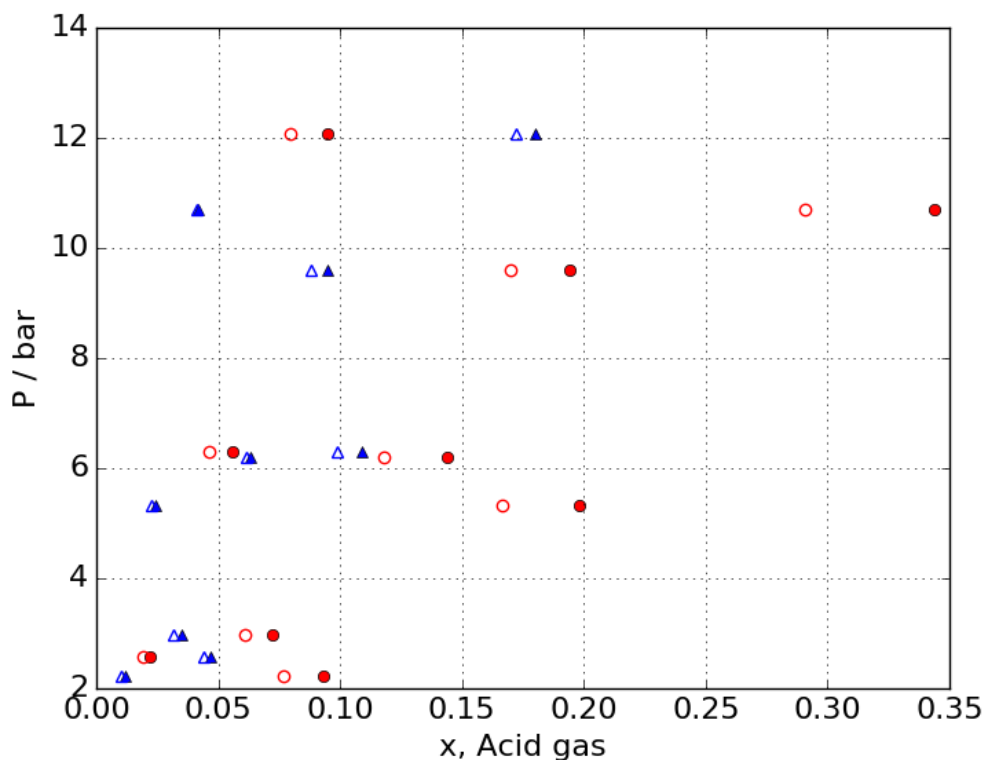
Figure 4.16: Ternary mixtures of CO_2-H_2S-$C_8mimNTf_2$ at 343.15 K with the 4-site association scheme (strategy 1). Open triangles represent the predicted CO_2 solubility using PC-SAFT, open circles represent the predicted H_2S solubility, and filled symbols represent experimental data [158].

tal measurement for the solubility of methane in this class of ILs are needed for more accurate model validation.

By comparing Figure 4.7 and Figure 4.17, it can be seen that the solubility of CH_4 in ILs is significantly lower than that of acid gases in ILs. Thus it can be efficiently used for the separation of these gases from CH_4. This explains why ILs are promising candidates for natural gas cleaning applications.

The mole fraction solubility of CH_4 in ILs is in the range of 0.03 and 0.2 on mole
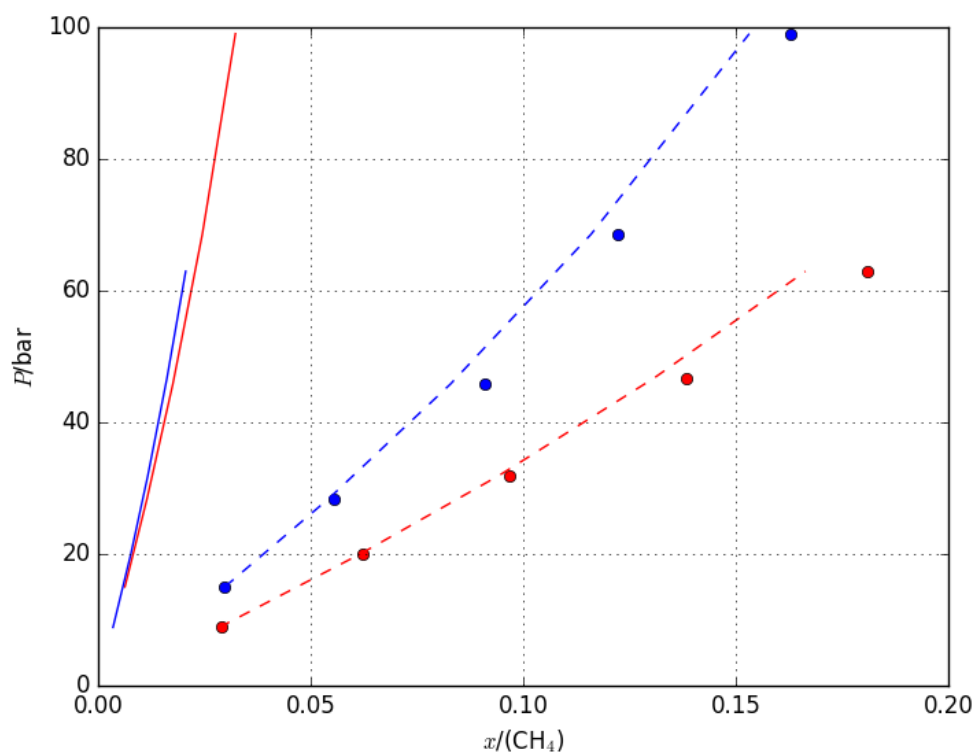
Figure 4.17: Solubility of CH_4 in ILs. Symbols represent experimental data taken from Raeissi and Peters [228] and Kumelan et al. [229], solid lines represent the predicted CH_4 solubility with PC-SAFT ($k_{ij} = 0.0$), dashed lines represent the fitted solubility with binary interaction parameters for (i) C_4mimNTf$_2$ (blue) at 313.15 K, ($k_{ij} = -0.148$) (ii) C_6mimNTf$_2$ (red) at 293.3 K, ($k_{ij} = -0.185$).

fraction basis [228, 229]. This is considered higher than the solubility of CH_4 in amines such as MDEA with CH_4 solubility ranging from 0.00059 to 0.08 on mole fraction basis [231]. This is one of the drawbacks of ILs over amines as the valuable methane dissolved in ILs will need to be recovered as will be addressed in the following chapter.

Water-ionic liquid pair is also one of the systems that need to be considered if an IL-based acid gas removal is to be implemented. The following section, the behaviour of such system and the assumptions adopted in our study for this system are discussed.

4.6   Water-ionic liquid systems

Water is one of the components of raw natural gas and is also used as a solvent to dissolve amines when the latter are used for gas sweetening as chemical absorbents. Water works as a proton donor in the chemical reactions taking place in the amine-based gas treatment processes, therefore, its presence is of essential importance. In this study, where ILs are used as an alternative solvent to amines, water is added to the IL to reduce the IL viscosity and cost, consequently, reducing the required pumping power and material cost.

Widegren and Magee [232] showed that the addition of 1% by mass of water to C_6mimNTf$_2$ decreases the kinematic viscosity by 47%, where the kinematic viscosity is the ratio of the dynamic viscosity to the density. At 298.15 K the kinematic viscosity decreases by 29% when the water mass fraction increased from 1×10^{-5} in the dried ionic liquid to 8.19×10^{-3} in the water-ionic liquid mixture. Widegren and Magee [232] also found that at 298.15 K the density of the dried C_6mimNTf$_2$ (with water mass fraction of 1×10^{-5}) decreases by 5 kg m^{-3} with the addition of water, i.e. by 0.37%.

According to Toh et al. [233], the class of ionic liquids investigated in this thesis ($C_n$mimNTf$_2$) are hydrophobic, thus are immiscible with water and form two phases. Nevertheless, the solubility of water into the IL and dissolution of the IL into water is not negligible. For C_6mimNTf$_2$, for example, Widegren and Magee [232] reported a

water mass fraction of about 0.01 in the saturated C_6mimNTf$_2$-H$_2$O mixture at 298.15 K. This figure is in agreement with the value reported by Klähn et al. [234], who also reported the values of water mass fraction in C_2mimNTf$_2$-H$_2$O mixture as 0.02, in C_4mimNTf$_2$-H$_2$O mixture as 0.01 and in C_8mimNTf$_2$-H$_2$O mixture as 0.009. It has also been found that the dissolution of ions from water-immiscible ILs in water is 1 to 4 orders of magnitude smaller than the solubility of water in ILs [234, 235, 236].

Santos et al. [237] presented experimental liquid-liquid equilibrium measurements for water with C_4mimNTf$_2$ and C_8mimNTf$_2$ ILs, the solubility of water in them and the solubility of both ILs in water at a temperature range from 293.2 K to 313.2 K. C_8mimNTf$_2$ IL is found to be more hydrophobic than C_4mimNTf$_2$. The larger the molecular size of the IL, the lower its solubility in water [237]. The authors found that the miscibility of both phases increased with temperature for all of the studied ILs. The miscibility region and the two phase mixture properties have not been clearly defined in this study.

Freire et al. [235] studied the liquid-liquid equilibria between water and $C_n$mimNTf$_2$ ILs, for ($n = 2$–8). The mutual solubilities for IL and water were measured at the temperature range of 288.15–318.15 K and atmospheric pressure. The temperature and pressure conditions involved in the acid gas removal process are higher than those considered by Freire et al., therefore, the liquid-liquid equilibria data provided by Freire et al. is not sufficient to model the interactions in the two-phase liquid mixture of IL-water used as a solvent for acid gas removal from natural gas.
Experimental phase equilibrium data and mutual solubilities of ILs with water reported literature are scarce.

Densities and viscosities of six pure ionic liquids, including [C_2mim][NTf$_2$] and [C_4mim][NTf$_2$] ILs as a function of temperature were measured by Jacquemin et al. [238]. The effect of the presence of water on the measured values for the pure ILs was then examined by comparing the densities and viscosities of dried and water-saturated samples. It was concluded that the presence of water slightly decreased the

density of the sample, while the viscosity was significantly dropped, roughly halved.

As for the experimental heat capacity data for the aqueous solutions of the class of ILs investigated in this study, no literature data are available. Troncoso [239] presented a review of the available literature data for heat capacity of aqueous solutions room temperature ILs. Aqueous $C_n$mimNTf$_2$ ILs are not among the systems that have been listed in this review.

Due to the lack of experimental data for the two liquid phase aqueous solution of the class of ILs investigated in this study, it was assumed that the IL and water are completely miscible and no second phase is formed. However, this assumption may have implications for the acid gas removal process from natural gas, which need to be considered in future for further investigations. Davies et al. [240] found that foaming is one possible implication of the presence of two liquid phases on the operation of a trayed columns. They reported that the foaming tendency of a two liquid phase system is greater than that of a similar system with one liquid phase, therefore, the former must be operated at lower vapour rates. Furthermore, the addition of anti-foaming agents should be considered to prevent foaming.

According to Cordeiro et al. [241], the formation of two liquid phases in a distillation column leads to a decrease in the distillate flow rate. Consequently, the energy consumption is reduced compared to that of the single liquid phase column. This implies that by assuming a single phase in the separation equipment higher energy is required, thus reduced energy consumption figures would be expected if two liquid phases were considered in the column. The separation efficiency however, would be less for the two phase system due to the reduced distillate flow rate which leads to a reduction in the reflux flow rate [241].

SAFT models have been used in the literature by some researchers to model liquid-liquid equilibria of binary and ternary systems containing IL and water. Paduszynski Domanska [242] attempted to model the liquid-liquid equilibria, among other thermo-

dynamic properties, of some binary systems of IL and organic solvent or water using PC-SAFT with the classical combining rules. The model was unable to predict phase splitting in the systems studied, thus, temperature-dependent binary interaction parameters were required to satisfactory describe the experimental data available.

Another attempt for modelling the liquid-liquid equilibria of systems containing water and ILs using PC-SAFT was presented by Alexander et al. [243], who studied the ternary system of 1-butanol-water-ionic liquid. The binary interaction parameters for both 1-butanol-water and water-IL pairs were obtained by fitting to binary experimental liquid–liquid equilibria data. No binary interaction parameters for 1-butanol-IL pairs were used. The liquid-liquid equilibria of the ternary 1-butanol-water-IL mixtures was then predicted without the need for any further parameters.

The electrolyte PC-SAFT (ePC-SAFT) with a concentration-dependent dielectric constant in the electrolyte contribution to the residual Helmholtz energy was used by Bulow et al. [244] to model liquid-liquid equilibria of systems containing ILs. This approach showed significant improvement in the prediction and correlation of liquid-liquid equilibria of such systems as compared to the ePC-SAFT without a concentration-dependent dielectric constant.

Further experimental measurements of the liquid-liquid equilibria of water-ionic liquid systems and the thermodynamic properties, such as solubility, heat capacity, density and viscosity of each component in each phase over a wide range of temperature and pressure conditions are needed to validate the PC-SAFT model for such systems. Due to the lack of experimental data of water-ionic liquid systems, it was assumed that water and the investigated ILs are completely miscible forming one liquid phase in our simulation in the chapters to follow.

4.7 Conclusions

In this chapter, we explored the use of PC-SAFT to quantitatively describe the thermodynamics of acid-gases in several methylimidazolium bis (trifluoromethylsulfonyl) imide ionic liquids. Firstly, we examined the use of treating the IL as either a system of neutral molecules or as separate cations and anions, where an electrolyte term is added to the free energy model. The inclusion of the electrolyte term improves the high pressure density and solubility fit, whereas its effect is insignificant at low pressures. The predictive capability is enhanced by allowing the description of different ILs anion-cation combinations without the need for additional experimental data. In addition, we examined the effect of using different self-association schemes for the ILs. By selecting the proper association scheme, the solubility of acid gases in ILs can be accurately described using PC-SAFT with AARD ranging from 1.54% to 6.62%. This yields a significant improvement to the accuracy of PC-SAFT for these systems without the need to include empirical binary interaction parameters, as was required in previous studies. Further experimental measurement for the solubility of methane in the class of ILs investigated here and for the water-IL miscibility are needed for more accurate model validation. The results obtained in this chapter for pure ILs and binary and ternary systems will be used in the following chapter for the simulation of an IL-based acid gas removal plant.

Chapter 5

Simulation of an IL-based acid gas removal process

5.1 Introduction

The use of alkyl imidazolium ionic liquids (ILs) as an alternative to methyl di-ethanol amine (MDEA) for CO_2 and H_2S removal from natural gas based on an existing processing site is investigated in this chapter. The main motivation for the conversion to ILs is to improve upon the existing MDEA based acid gas removal unit by reducing the regeneration energy requirement, thus reducing the CO_2 emissions, eliminating the need for solvent makeup due to the non-volatility of ILs and hence reducing the environmental impact.

The PC-SAFT model validated in Chapter 4 for pure, binary and ternary acid gas-IL systems are used in this chapter for the simulation of an IL-based gas sweetening process in Aspen Plus V9. The use of ILs as a replacement to MDEA in an existing sweetening process is explored in this chapter.

First in this chapter, an existing MDEA based gas sweetening process is selected and described in section 5.2 and then the base case study to be improved is defined and presented in section 5.3. Second, MDEA is replaced with IL as a solvent in the existing

process in section 5.4. The required structural and operational changes to the process, are then described and the process is simulated in Aspen Plus V9. Two of the alkyl imidazolium ILs explored in the previous chapter, 1-hexyl 3-methylimidazolium bis (trifluoromethylsulfonyl) imide and 1-octyl 3-methylimidazolium bis (trifluoromethyl-sulfonyl) imide with different IL-water solution compositions were tested to find the optimum composition that provides the minimum energy and overall cost. Therefore, different case studies with different compositions for each IL were generated. Equipment sizing and cost estimation of the IL process are then presented in sections 5.5 and 5.6. Finally, the main findings are summarised in section 5.7.

5.2 North Caroline plant amine unit

The North Caroline plant for gas processing located in Canada shown in Figure 5.1 was built in 1980, where the feed gas gathered from different wells passes through a standard refrigeration plant to extract liquids after being compressed and then sent to an amine unit for sweetening to meet the sales gas specifications of 2 mol% CO_2 and 4 PPM/V H_2S [245].
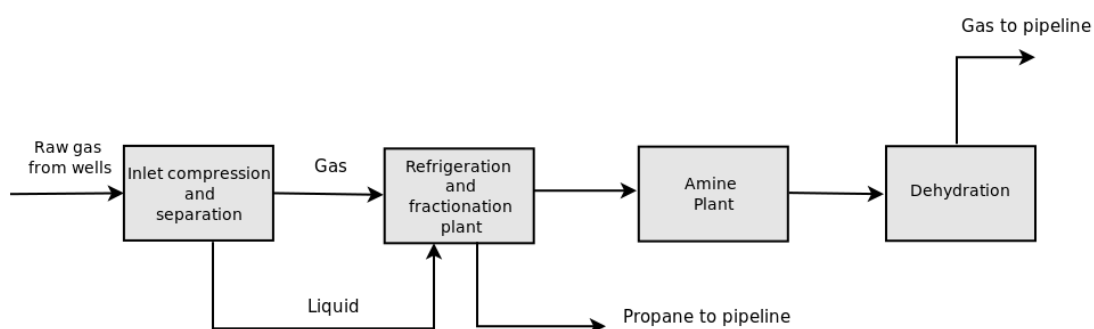
Figure 5.1: North Caroline Plant Schematic. Taken from Ref. [245]

The amine unit in the North Caroline plant was originally designed to process 47 MMSCFD (47 million standard cubic feet per day) which is equivalent to 1.33 million standard cubic meter per day (MSCMD) at 15°C of gas containing 2.65 mol% CO_2 and 100 PPM/V H_2S with 33 wt% of diethanolamine (DEA) solution as a solvent.

However, due to the completion of several new wells after the plant was built, new gas lines were brought onstream. As a result of the new gas lines, the CO_2 concentration in the amine unit increased while the H_2S concentration did not change notably. The new feed gas composition to the amine unit is given in Table 5.1. The existing DEA based amine unit could no longer handle this increase in CO_2 concentration. Moreover, the unit became unstable and any further increase in H_2S concentration would bring the sales gas off specification. Therefore, the plant capacity had to be reduced from 47 MMSCFD to 35 MMSCFD [245].

The plant was debottlenecked by Dome Petroleum Limited by converting the amine unit from DEA to methyldiethanolamine (MDEA). Dome found that with this change, the amine plant performed smoothly without the need for modification to the existing equipment.

The successful replacement of DEA to MDEA can be attributed to the higher selectivity of H_2S over CO_2 of MDEA than DEA, as it is harder to meet H_2S specification than CO_2 specification. Other advantages of MDEA over primary and secondary amines include, lower vapour pressure, lower heats of reaction, higher resistance to degradation and fewer corrosion problems [246].

5.3 Base case study

The North Caroline plant amine unit can be found in Aspen Plus V9 as an incomplete example for acid gas removal using MDEA [247], where only the absorber column is built and simulated. The inlet gas components flow rate and conditions for this case are given in Table 5.1 [247].

The Aspen Plus amine unit was first completed to match the existing North Caroline amine unit. The complete amine unit of North Caroline plant process flow diagram is shown in Figure 5.2, and the streams summary is provided in Table 5.2. A 33 wt% MDEA in water solution was used as a solvent. This was used as the base case to be

Table 5.1: Inlet sour gas stream to the amine unit of North Caroline plant. Taken from Ref. [247]

Component	Flow rate, kg/h
CH_4	25409.1
H_2S	3.1 (50 PPM/V)
CO_2	2508.0 (3.5 mol%)
H_2O	25.9
Total	27946.1
Temperature/ K	305.37
Pressure/ bar	55.158

improved by replacing the MDEA solvent with ILs in an effort to reduce its regeneration energy consumption and the overall cost.
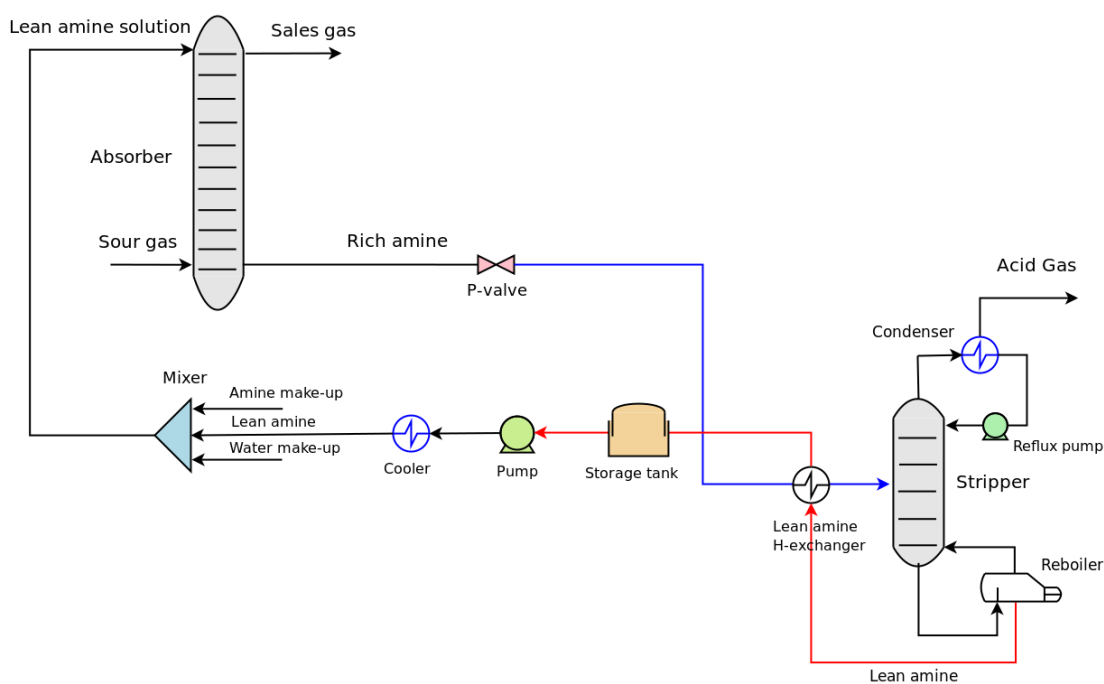
Figure 5.2: North Caroline plant amine unit PFD. Taken from [245].

Table 5.2: Base case stream table.

Stream	Acid gas	Sour gas	Water make up	Lean amine solution	Lean amine	Amine make up	Rich amine	Sales gas
Phase	Vapour	Vapour	Liquid	Liquid	Liquid	Liquid	Liquid	Vapour
Temperature, K	333.8	305.4	317.00	317.04	385.8	317.04	329.4	332.70
Pressure, bar	1.4	55.2	55	55	1.45	55	55	55
Total mass flow, kg/h	2400	27950	292.2	37403	37106	46.9	39506	25848
MDEA, kg/h	8.61E-12	0.00	0.00	12327	12281	46.92	6525	6.06E-02
H_2O , kg/h	164.4	25.9	292.2	25036	24744	0.0	24043	148.1
CO_2 , kg/h	2199	2508	0.00	22.7	1.59E-02	0.00	82.4	319.5
H_2S , kg/h	2.87	3.14	0.00	0.00	6.96E-05	0.00	0.19	0.20
H_3O^+ , kg/h	0.00	0.00	0.00	1.12E-02	1.70E-07	0.00	6.90E-06	0.00
OH^- , kg/h	0.00	0.00	0.00	2.66E-06	1.007	0.00	3.48E-03	0.00
HCO_3^- , kg/h	0.00	0.00	0.00	5.41	18.88	0.00	2942.41	0.00
CO_3^{-2} , kg/h	0.00	0.00	0.00	1.36E-05	3.32	0.00	14.28	0.00
HS^- , kg/h	0.00	0.00	0.00	0.00	6.53E-02	0.00	2.67	0.00
S^{-2} , kg/h	0.00	0.00	0.00	0.00	2.16E-08	0.00	6.38E-09	0.00
$MDEAH^+$, kg/h	0.00	0.00	0.00	10.58	57.84	0.00	5861	0.00
CH_4 , kg/h	33.6	25413	0.00	0.00	1.13E-18	0.00	33.6	25380

In this unit, an absorber with 21 trays has been used. The absorption column is operating at 317.04 K and 55 bar. In this column, the sour gas enters the bottom and comes into contact with the lean amine solution entering from the top to pick up the acid gases. The lean gas exits the top of the absorber, and the rich amine exits the bottom. The rich amine is then sent to a stripping column for regeneration. A regenerator (stripper) with 6 trays (estimated using Fenske-Underwood-Gilliland short cut method [248]), is added to recover the solvent (MDEA) and recycle it back to the absorber. Although the mixture is highly non-ideal in this system, FUG short cut method provided a good estimate for the number of trays, where the required sales gas specifications were meet with the estimated number of trays. The rich MDEA from the absorber bottom is at high pressure (55 bar), while the stripper works at 1.4 bar, therefore, a pressure let down valve is added to reduce the pressure of the rich MDEA stream from 55 to 2 bar. The stream is then preheated before being sent to the stripper where the acid gases are separated from the MDEA solution, and the lean MDEA that flows from the stripper bottom is then cooled and pumped back to the absorber. The water and MDEA lost during the process is compensated for by adding water and MDEA make-up streams. A stream table for the base case study of the North Caroline plant amine unit is provided in Table 5.2.

The MDEA case, which is the base case in this study, has been modelled in Aspen Plus V9 using the Electrolyte Non-Random Two-Liquid (Electrolyte NRTL) model for the liquid phase properties and the Redlich-Kwong equation of state for vapour phase properties. These models have been used in literature for the thermodynamic modelling of amine processes [52, 249, 250, 251] and proved to be successful.

The current MDEA unit consumes 6 MW in the stripper for regeneration, most of it, is to break the chemical bonds formed between MDEA and acid gases, and requires 47 kg/day of MDEA for makeup to process about 28 t/h of sour gas. In order to reduce the energy consumption of the MDEA unit, reduce or eliminate the cost associated with the solvent make up and hence the environmental impact of the unit, we propose to convert the North Caroline MDEA based unit from the volatile MDEA chemical absorption to the nonvolatile ionic liquid (IL) physical absorption. In the following sections, we describe the North Caroline plant gas sweetening unit with IL as an alternative to MDEA.

5.4   North Carolina plant gas sweetening unit with IL

The 33 wt% MDEA solution in the above plant is replaced by IL-water solutions with different concentrations from 5 to 20 mol% IL. Both 1-hexyl-3-methylimidazolium bis (trifluoromethylsulfonyl) imide ($C_6mimNTf_2$) and 1-octyl-3-methylimidazolium bis(trifluoromethylsulfonyl) imide ($C_8mimNTf_2$) ILs are examined for this purpose. These two ILs were selected due to their higher acid gas solubility compared to shorter ILs studied in Chapter 4.

Imidazolium-based ILs were selected in this study over other types of ILs because of the availability of their experimental data. Most experimental studies related to CO_2 capture using ILs focused on the ILs with imidazolium-based cations. This is due to their observed affinity towards CO_2 [58]. This high affinity was first observed by Blanchard et al. [252], who also observed that the product is not contaminated with the IL as the the ionic liquid is insoluble in CO_2 [253]. Furthermore, the CO_2 absorption ca-

pacity in imidazolium-based ILs and its interaction with the imidazolium groups have been widely studied in literature [58].

Some research studies provided measurements for H_2S solubility in different ILs with comparison to CO_2 and other gases solubility [72, 73, 74, 75]. In all studies, H_2S showed higher solubility than CO_2 and other gases in ILs. Pomelli et al. [73] attributed that to the presence of specific interactions between H_2S and the ILs and used quantum chemical calculations to investigate the influence of these interactions on the H_2S solubility at the molecular level.

According to Hert et al. [254], the solubility of carbon dioxide in C_6mimNTf$_2$ is significantly higher than that of methane in the same IL. Therefore, this IL can be used for the separation of the two gases from each other. However, Hert et al. [254] found that the solubility of CH_4 in C_6mimNTf$_2$ increases in the presence of CO_2, which is the case in the natural gas mixture. This is a drawback for using ILs for CO_2 removal from natural gas, as the methane dissolved in the IL needs to be recovered. The issue of high methane solubility is considered later in details in Chapter 6.

In this section, first the thermodynamic property packages used in the simulation and the component properties of interest are presented, then the IL gas sweetening process flowsheet with its different unit operations is described and finally, the process simulation procedures are explained.

5.4.1 Property input

Prior to building the flow sheet and simulating the process in Aspen Plus V9, all the pure component properties and binary interaction parameters have to be defined. Only then, we can move on to the simulation environment and start building the flow sheet. The PC-SAFT model described in Chapter 4 is used as the thermodynamic property method in Aspen Plus for all IL cases. All pure components other than the ILs exist in the Aspen Plus V9 library, hence, their properties can be retrieved from different databanks available in Aspen Plus. The IL properties have to be defined by the user, as

they are not library components.

First, the components involved in the process are selected from the library and added. Here, water, methane, carbon dioxide and hydrogen sulphide can already be found in the Aspen Plus V9 library, while ILs were defined by the user as conventional components. The properties of library components retrieved from Aspen Plus V9 databanks are listed in Appendix C.

Then, the thermodynamic property method to be used is selected. For IL cases, the PC-SAFT property method was chosen as the base method for the thermodynamic property calculations. The following pure component parameters were then defined for ILs, while other components were retrieved from different databases in Aspen Plus V9:

- Molecular weight, boiling point and critical properties:
  Values used in Aspen Plus V9 and their references are recorded in Table 5.3

Table 5.3: ILs molecular weight, boiling point and critical properties

IL	MW g/mol	T_b K	T_c K	P_c bar	V_c cc/mol	ω	Ref.
$C_6mimNTf_2$	447.36	908	1293.0	23.6	1104.59	0.372912	[208], [255]
$C_8mimNTf_2$	475.48	954	1317.8	21.0	1218.60	0.322219	[256]

- PC-SAFT EOS structural parameters:
  The PC-SAFT structural parameters obtained in Chapter 4, Table 4.4, for both ILs were used in Aspen Plus V9. The parameters are also given in Table 5.4

  The binary interaction parameter between methane and $C_6mimNTf_2$ was estimated from the experimental data taken from Kumelan et al. [229] as -0.185, see Figure 4.17. For the solubility of methane in $C_8mimNTf_2$ IL, no experimental data were found in literature, therefore, the binary interaction parameter between methane and $C_8mimNTf_2$ was extrapolated from the binary interaction parameters of $C_4mimNTf_2$ and $C_6mimNTf_2$, see Figure 4.17. Water and ILs

111

Table 5.4: PC-SAFT Parameters of the studied ILs used in Aspen Plus V9 (ILs as neutral molecules: Strategy 1)

IL	T range	Association	σ_i	ε_i/k_B	m_i	$\varepsilon^{A_iB_i}/k_B$	$K^{A_iB_i}$
	K	Scheme	Å	K		K	
C_6mimNTf$_2$	290.95 – 307.05	4(2:2)	3.635	381	10.660	1020	0.00225
C_8mimNTf$_2$	293.15 – 323.15	4(2:2)	3.721	383	11.000	1020	0.00225

were assumed as completely miscible due to the lack of experimental data for the studied ILs at a wide range of temperature and pressure conditions as detailed in section 4.6.

- Liquid heat capacity:

  The liquid heat capacity of both ILs was estimated by fitting to experimental heat capacity data from Ref. [257] using second order polynomials. The parameters of the polynomials are given in Table 5.5

Table 5.5: ILs heat capacity fit parameters, $C_p = AT^2 + BT + C$

IL	T range, K	A	B	C	C_p^{exp} Ref.
C_6mimNTf$_2$	293–358	0.003	-1.557	870.575	[257]
C_8mimNTf$_2$	293–358	-1.511E-03	2.528	1.134E+02	[257]

- Ideal gas heat capacity:

  The ideal gas heat capacity of both ILs was calculated using the following equation [257]

$$\frac{C_p - C_p^0}{R} = 1.586 + \frac{0.49}{1 - T_r} + \omega \left[4.2775 + \frac{6.3(1 - T_r)^{1/3}}{T_r} + \frac{0.4355}{1 - T_r} \right] \quad (5.1)$$

where C_p is the liquid heat capacity estimated by fitting to experimental data, C_p^0 is the ideal gas heat capacity of the IL in J mol^{-1} K^{-1} at the same temperature and zero pressure, R is the universal gas constant (8.314 J mol^{-1} K^{-1}), T_r is the reduced temperature ($T_r = T/T_c$) and ω is the acentric factor given in Table 5.3.

For ionic liquids, it is much more useful to consider liquid heat capacities than ideal gas capacities as they are hardly volatile. The ideal gas heat capacity is a reference state and is needed in Aspen Plus. It is not possible to run a column in Aspen Plus without identifying the ideal gas heat capacity of all components, for library components the C_p^0 is retrieved from the library database but for the user defined components, such as ILs, the C_p^0 has to be defined by the user.

The calculated values of ideal gas heat capacity were fitted to a second order polynomial, and its parameters were used in Aspen Plus V9. Figure 5.3 provides the plot of the calculated ideal gas heat capacities of both ILs fitted to experimental data [257] along with the polynomials coefficients.
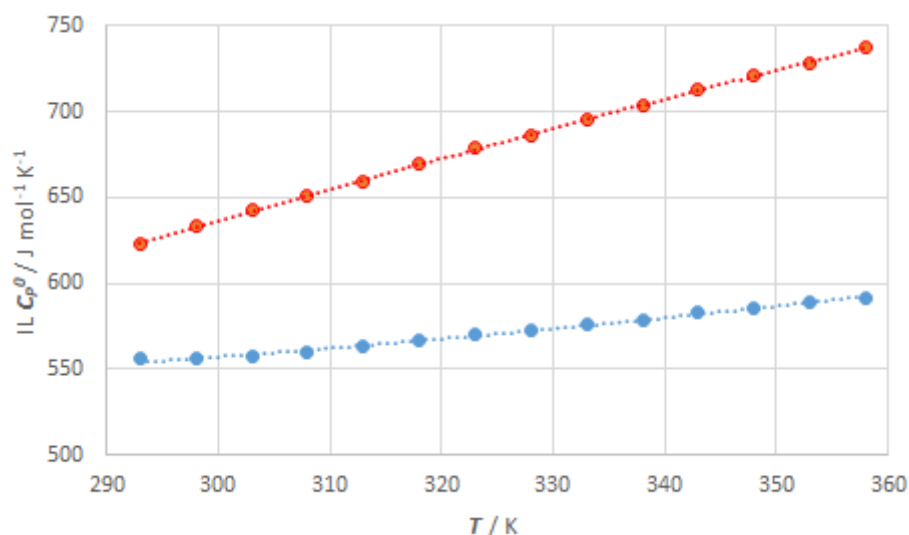
Figure 5.3: ILs ideal gas heat capacity, C_6mimNTf$_2$ (blue) and C_8mimNTf$_2$ (red). The symbols represent the experimental ideal gas heat capacity taken from Ref. [257]. The lines are the polynomials fit.

- Liquid viscosity:
  The liquid viscosity of both ILs was estimated by fitting experimental data for

C_6mimNTf$_2$ [258] and for C_8mimNTf$_2$ [259] with a third order polynomial. The viscosity is needed for the calculation of the towers efficiency as will be detailed in section 5.5.4. The parameters of the polynomial were then used in Aspen Plus V9. The polynomials fit and their coefficients are provided in Figure 5.4 and Table 5.6.

Table 5.6: ILs viscosity fit parameters, $\mu = AT^3 + BT^2 + CT + D$

IL	T range, K	A	B	C	D	Ref.
C_6mimNTf$_2$	288.15–433.15	-1E-07	0.0001	-0.0438	5.6502	[258]
C_8mimNTf$_2$	278–358	-1E-06	0.0014	-0.4806	53.568	[259]
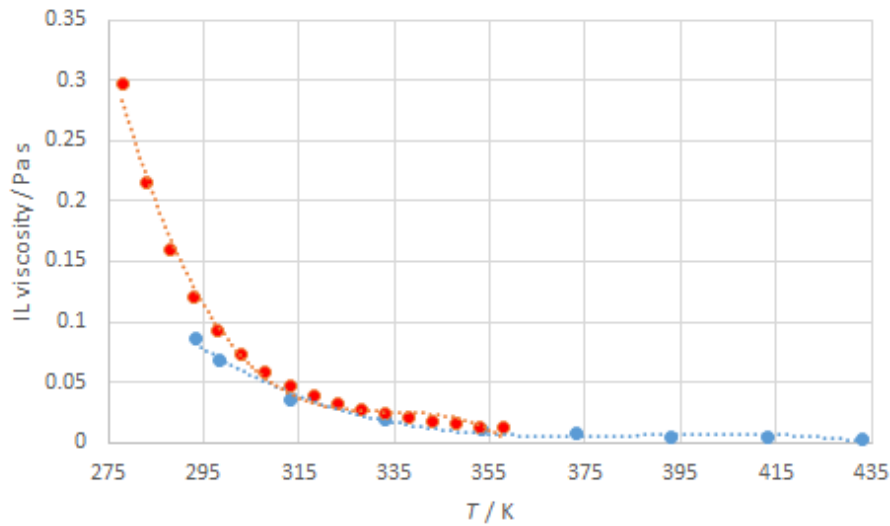
Figure 5.4: ILs viscosity, C_6mimNTf$_2$ (blue) and C_8mimNTf$_2$ (red). The symbols represent the experimental viscosity taken from Refs. [258] and [259]. The lines are the polynomials fit.

- Vapour pressure: Due to the negligible volatility of ILs [9, 10], the vapour pressure of both ILs was set to a very small number in Aspen Plus V9.

The following section provides a detailed description of the IL-based sweetening unit. The purpose of each unit operation in the process, including towers, flash tanks

and compressors is explained and a summary of the steam flow rates and conditions is presented.

5.4.2 Flowsheet description

The flowsheet for the IL gas sweetening unit is shown in Figure 5.5. Here, the same inlet sour gas and MDEA stream conditions given in section 5.3 for the base case are used. Furthermore, the same base case absorber is used for the IL-based sweetening unit in an effort to keep the same existing facilities and minimise the amount of retrofit.
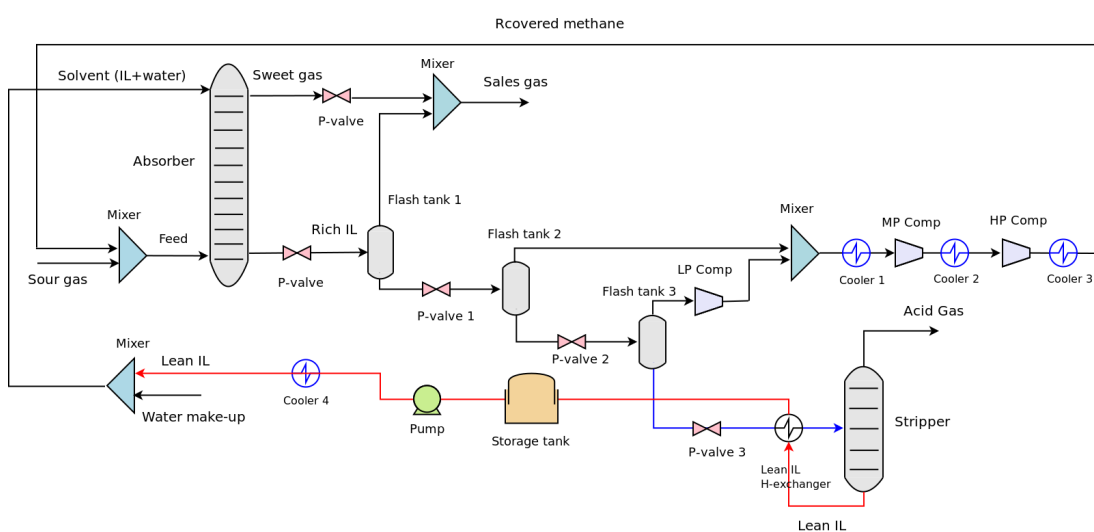
Figure 5.5: North Caroline plant gas sweetening unit with IL as a solvent.

In the absorber, the IL solution comes into contact with the sour gas and absorbs the acid gases (CO_2 and H_2S). However, no chemical reactions occur in the case of the ILs. The IL plant also consists of a regenerator to recover the IL, like in the MDEA case. Due to the fact that CH_4 is more soluble in ILs than in MDEA, multi-stage flashing and compression are needed in the IL plant to recover the valuable methane absorbed by the ILs. A detailed description of the unit operations in the IL unit is provided below.

115

5.4.2.1 Absorber

The sour gas stream enters the bottom tray of the absorber while the lean IL enters from the top tray. The same MDEA unit absorber with 21 trays is used for the IL cases in an effort to reduce the required plant modifications if retrofit is to be implemented to the existing MDEA unit. The absorption efficiency, however, would be less for IL cases due to the higher viscosity of ILs. The IL absorbs CO_2 and H_2S, as well as some CH_4, and flows out from the absorber bottom as rich IL, which needs to be regenerated. No chemical reaction takes place in the IL-based absorption. The sweet gas exits the top of the absorber and is considered sales gas once it meets the specifications of 2 mole % for CO_2 and 4 PPM/V for H_2S.

5.4.2.2 Flash tanks

Due to the fact that methane is also soluble in ILs, about 4 – 11 % of the inlet methane was observed in the IL stream from the absorber bottom. This stream needs to be flashed out using a multi-stage flashing process to recover the valuable methane. Three flash tanks were used for this purpose. In the first stage, the rich IL stream pressure of 55 bar is reduced using a valve to 45 bar to help flash out some of the methane. As the pressure is still high, the amount of CO_2 and H_2S flashed out with the methane is very low and will not affect the sales gas specification if the flashed gas is mixed with sweet gas stream from the top of the absorber (see Figure 5.5).

In the second flash stage, the pressure of the bottom stream that flows out of the first flash tank is reduced from 45 bar to 20 bar to flash more methane. However, some CO_2 and H_2S are also flashed with the methane, which does not allow the flashed gas to be mixed with the sweet gas stream. The gas from the second flash tank then needs to be compressed and recycled back to the absorber for further sweetening. In the third flash stage, the pressure of the bottom stream flows out of the second flash tank is further reduced from 20 bar to 5 bar to flash more methane. The flashed gas from the third tank also needs to be compressed and mixed with the flashed gas from the second flash tank then recycled back to the absorber for further sweetening. The pressure of

bottom stream flows out of the third flash tank is reduced to 3 bar and preheated before being sent to the stripper.

5.4.2.3 Compressors

In order for the flashed gas streams from the second and the third flash tanks to be recycled back to the absorber, they have to be compressed and cooled to bring them to the sour gas feed conditions of 305.37 K and 55 bar. In this case, we can mix the recovered methane with the sour gas feed (see Figure 5.5).

The flashed gas from the third tank is compressed from 5 bar to 20 bar to mix it with the flashed gas from the second flash tank. The mixed stream is then cooled and further compressed in two stages with inter-cooling following each stage to keep the compressor discharge temperature below the specified limit of 175°C for reciprocating compressors and 232°C for centrifugal compressors [260]. An isentropic centrifugal compressors with 72% efficiency were used here.

5.4.2.4 Stripper

The liquid effluent from the third flash tank is sent to the stripping column after reducing its pressure from 5 bar to 3 bar and then preheated from 316.57 K to 358.15 K. The stripper works at a pressure close to atmospheric (1.4 bar) to allow for the flashing of the acid gases and to reduce the reboiler duty. The purpose of pre-heating the stripper feed is to reduce the regeneration duty of the stripper. The bottom effluent of the stripper (Lean IL) is used to preheat the stripper feed stream. The lean IL is then sent to a holding-up tank where it can be stored. From there it can be pumped and further cooled before being sent back to the absorber.

It is worth mentioning here that due to the negligible volatility of ILs, unlike MDEA, no IL make-up is required for all IL cases. However, in practice a small amount of IL makeup might be needed, although it would be negligible compared to MDEA makeup. This is one of the main advantages of using ILs instead of MDEA, as this will save in the solvent consumption, and consequently, the capital and operating

costs. Table 5.7 summarises stream conditions and flow rates for the North Caroline plant gas sweetening unit with the optimal composition (at which the energy cost is minimised) of $C_6mimNTf_2$ IL as a solvent.

Table 5.7: Stream table for the North Caroline sweetening unit with $C_6mimNTf_2$ IL as a solvent.

Stream	Acid gas	Sour gas	Recovered methane	Feed	Water make up	Solvent IL+water	Lean IL	Rich IL	Sales gas	Sweet gas
Phase	Vapour	Vapour	Mixed	Vapour	Liquid	Liquid	Liquid	Liquid	Mixed	Vapour
Temperature, K	330.25	305.37	305.37	304.93	317.04	317.04	380.42	315.99	314.51	317.76
Pressure, bar	1.4	55.16	55	55	55	55	1.41	55	45	55
Total mass flow, kg/hr	1260	27950	1586.88	29537	138	186621	186483	189609	26828	26550
H_2O, kg/hr	81.16	25.88	18.26	44.14	138	59069	58931	59031	83.08	82.20
CH_4, kg/hr	104.6	25413	1047	26461.6	0.0	0.0	1.1E-05	1398	25309	25063
CO_2, kg/hr	1071.33	2508.06	520.15	3028.21	0.0	0.0	0.0	1624	1436	1404
H_2S, kg/hr	2.9	3.1	0.7	3.8	0.0	0.0	0.038	3.63	0.20	0.17
$C_6mimNTf_2$, kg/hr	2E-37	0.0	5.4E-16	5.4E-16	0.0	127551	127551	127551	7E-13	7E-13

To summarise, by comparing the flowsheet of the base case (Figure 5.2) to that of the IL case (Figure 5.5), It is clear that three extra flash tanks with two valves and three extra compressors with three intercoolers are needed for the IL case. The main reason for that is the high solubility of methane in ILs, consequently, flashing out the dissolved methane in the IL and compress it back to the absorber for further treatment is needed. In the following section, the steps of building the IL process in the simulation environment are presented .

5.4.3 Process simulation

Once all pure component properties and binary interaction parameters are defined, we can now move to the simulation environment and start building our process. The first step in building the process is defining the feed gas stream that needs to be treated. This is done by adding a stream and defining its composition and conditions as given in Table 5.1 above. The absorber unit with 21 trays (the same MDEA case absorber) is then added where the feed gas stream enters the bottom tray of the absorber. The purpose of using the same number of trays is to check if we can make use of the existing amine absorber for IL. The solvent stream is then defined by setting up its composition

(IL+water), temperature and pressure. This stream enters the top tray of the absorber to pick up the acid gases from the sour gas. The stream withdrawn from the top tray of the absorber is named as the sweet gas, and the stream withdrawn from the bottom tray is named as the rich IL. At this stage, we can run the absorber and check the sweet gas specification. If the acid gas content of the sweet gas stream is higher than the typical limit for the sales gas specification (4 PPM/V for H_2S and 2 mole% for CO_2), the IL flow rate is adjusted until the sales gas specifications are met.

Then the process of IL regeneration starts by flashing off methane and acid gases from the rich IL stream into a three stage flash followed by a tray stripper. The bottom effluent of the stripper is referred to as the Lean IL, which is a hot stream that needs to be cooled before being pumped back to the absorber to pick up the acid gases. The gas streams from the flash tanks can either be mixed with the sweet gas, if their acid gas content is low enough to not affect the sales gas specification (first flash tank), or compressed and mixed with the sour gas stream for further treatment if their acid gas content is high (second and third flash tanks). A water makeup stream is added and mixed with the lean IL stream to compensate for the water losses during the process. In the following section, the simulation results of the base case and the different IL cases are presented and analysed.

5.4.4 Simulation results

A summary of the key simulation results and a comparison between the base MDEA case of the North Caroline plant with 33 wt% MDEA solution (equivalent to 7 mol %) and the different investigated IL cases are given in Table 5.8 for $C_6mimNTf_2$ and Table 5.9 for $C_8mimNTf_2$. For the IL cases, different IL-water solution compositions were investigated to identify the optimum composition for the solvent solution.

This comparison revealed that for both $C_6mimNTf_2$ and $C_8mimNTf_2$ ILs, there was an optimum composition for the IL solvent at which the energy cost is minimised. For $C_6mimNTf_2$ IL, the 15 mol% IL composition case has the lowest regeneration re-

Table 5.8: Base MDEA case versus different $C_6mimNTf_2$ IL cases for gas sweetening

	Base case	IL case 1	IL case 2	IL case 3	IL case 4	IL case 5	IL case 6
Model	ELECTNRTL	PC-SAFT	PC-SAFT	PC-SAFT	PC-SAFT	PC-SAFT	PC-SAFT
Solvent (MDEA/IL+water)	33 Wt% MDEA	20 mol% IL	15 mol% IL	10 mol% IL	8 mol% IL	7 mol% IL	5 mol% IL
Solvent flow rate, kg/min	622.8	3615.2	3313.2	3108.4	3110.4	3149.5	3300.0
H_2S in the sweet gas, mol frac.$\times 10^6$	3.74	3.60	3.65	3.76	3.69	3.60	3.60
CO_2 in the sweet gas, mol frac.	0.0045	0.014	0.016	0.018	0.020	0.021	0.023
Water makeup, kg/min	4.87	3.80	2.86	2.39	2.3	1.45	1.99
Solvent makeup, kg/min	0.78	0.0	0.0	0.0	0.0	0.0	0.0
CH_4 in the solvent, kg/min	0.56	35.50	31.59	26.00	23.30	21.77	18.10
CH_4 in the feed, kg/min	423.6	423.6	423.6	423.6	423.6	423.6	
CH_4 in the sales gas, kg/min	423.0	421.1	421.3	421.6	421.8	421.9	422.0
CH_4 recovery %	99.9	99.4	99.5	99.5	99.6	99.6	99.6
CH_4 in the acid gas stream, kg/min	0.56	2.50	2.28	1.92	1.74	1.64	1.42
Regeneration temperature, K	385.75	376.15	377.45	379.29	380.1	380.6	381.1
Regeneration duty, MW	6.00	2.9	2.85	2.98	3.17	3.31	3.69
Energy saving %	0.0	51.7	**52.5**	50.3	47.2	44.8	38.5

Table 5.9: Base MDEA case versus different $C_8mimNTf_2$ IL cases for gas sweetening

	Base case	IL case 7	IL case 8	IL case 9	IL case 10	IL case 11	IL case 12
Model	ELECTNRTL	PC-SAFT	PC-SAFT	PC-SAFT	PC-SAFT	PC-SAFT	PC-SAFT
Solvent (MDEA/IL+water)	33 Wt% MDEA	30 mol% IL	20 mol% IL	15 mol% IL	10 mol% IL	7 mol% IL	5 mol% IL
Solvent flow rate, kg/min	622.8	3912.4	3318.1	3056.5	2869.3	2871.0	3006.0
H_2S in the sweet gas, mol frac.$\times 10^6$	3.74	3.71	3.69	3.64	3.69	3.89	4.00
CO_2 in the sweet gas, mol frac.	0.0045	0.012	0.013	0.015	0.018	0.021	0.023
Water makeup, kg/min	4.87	4.17	3.5	3.40	3.13	3.25	1.99
Solvent makeup, kg/min	0.78	0.0	0.0	0.0	0.0	0.0	0.0
CH_4 in the solvent, kg/min	0.56	47.92	41.81	37.26	30.58	24.98	20.36
CH_4 in the feed, kg/min	423.6	423.6	423.6	423.6	423.6	423.6	423.6
CH_4 in the sales gas, kg/min	423.0	420.3	420.6	420.9	421.3	421.7	422.0
CH_4 recovery %	99.9	99.2	99.3	99.4	99.5	99.6	99.6
CH_4 in the acid gas stream, kg/min	0.56	3.23	2.92	2.67	2.25	1.88	1.56
Regeneration temperature, K	385.75	374.85	376.15	377.35	379.25	380.5	381.45
Regeneration duty, MW	6.00	3.05	2.84	2.85	2.94	3.16	3.50
Energy saving %	0.0	49.2	**52.7**	52.5	51.0	47.3	41.7

quirement (52.5% regeneration energy saving) as can be seen in IL case 2 in Table 5.8. For $C_8mimNTf_2$ IL, the 20 mol% IL composition case has the lowest regeneration requirement (52.7% regeneration energy saving) as can be seen in IL case 8 in Table 5.9. Regeneration energy saving however, is not the only factor affecting the choice of the optimal composition case for ILs. Other factors, such as solvent cost and capital or equipment cost should also be considered.

Acid gases are more soluble in MDEA than in ILs, and MDEA is more selective to acid gases over methane than ILs. Therefore, the flow rate of MDEA required to treat

the same quantity of sour gas is much less than the IL flow rate, as we can see from Table 5.8 and Table 5.9. However, because ILs have negligible volatility compared to MDEA, no IL makeup is needed, unlike the MDEA based plant (1123 kg of MDEA is lost every day). Furthermore, less water makeup is needed for IL cases than the base case due to the lower regeneration temperature, thus less water vapourisation rate.

It is also clear that the IL absorbs more methane than MDEA, as methane is more soluble in IL than in MDEA. Because of that, it was necessary to install multistage flash tanks with multistage compression for the IL based plant to recover this valuable product from the rich IL stream. To decide whether the IL cases are economically viable despite the addition of these pieces of equipment, equipment sizing and costing need to be performed. In the following section, the different process equipment are sized in preparation for the overall cost estimation of the process which will be presented in section 5.6.

5.5 Equipment sizing

Equipment sizing and cost estimation was done using the Aspen Process Economic Analyser (APEA). In order to estimate the cost of any equipment, it needs to be sized; in other words its dimensions need to be determined. The dimensions can be calculated based on the flow rates and conditions of the equipment inlet and outlet streams obtained from the simulator. Each equipment has different sizing requirements and procedures. Below are the details of the key equipment sizing procedures and assumptions used in this work. A summary of the sizes of each piece of equipment for the base case and the two optimal composition IL cases is provided in Table 5.10.

5.5.1 Compressors

The minimum input requirements for a compressor are the inlet and outlet stream information. In order to size a compressor, the inlet stream flow rate and density are used to estimate the total volumetric flow rate through the compressor. The compression ratio

Table 5.10: Summary of equipment sizes for the base case and the two optimal composition IL cases. For equipment names refer to Figure 5.2 and Figure 5.5.

Equipment sizing parameter	Equipment size		
	Base case (33 wt% MDEA)	8 mol% C_6mimNTf$_2$	7 mol% C_8mimNTf$_2$
Absorber tower diameter, m	0.91	1.07	1.07
Absorber tower height, m	22.56	22.56	22.56
Stripper tower diameter, m	1.68	1.37	1.52
Stripper tower height, m	7.32	7.32	7.32
Stripper condenser area, m^2	47.59	4.06	4.07
Condenser accumulator diameter, m	0.91	0.91	0.91
Condenser accumulator length, m	2.74	2.74	2.74
Stripper reboiler area, m^2	446.65	207.91	210.80
Cooler area, m^2	19.86	-	-
Cooler 1 area, m^2	-	1.02	1.32
Cooler 2 area, m^2	-	1.25	1.39
Cooler 3 area, m^2	-	4.05	4.23
Cooler 4 area, m^2	-	141.34	136.17
Flash tank 1 diameter,m	-	2.13	2.13
Flash tank 1 height,m	-	6.55	6.40
Flash tank 2 diameter,m	-	2.13	2.13
Flash tank 2 height,m	-	6.55	6.40
Flash tank 3 diameter,m	-	2.13	2.13
Flash tank 3 height,m	-	6.55	6.40
LP compressor driver power, kW	-	55.13	58.32
MP compressor driver power, kW	-	62.69	65.58
HP compressor driver power, kW	-	72.82	76.41
Pump power, kW	94.29	336.81	322.15
Lean solvent HEX area, m^2	7.11	107.73	105.43
Storage tank diameter, m	1.25	2.13	2.13
Storage tank height, m	4.57	6.55	6.40

(exit to inlet pressure) is obtained from the operating pressures of the inlet and outlet stream. The compressibility factor of the inlet and outlet streams is estimated based on the fluid component. Using this information, the compressor brake horsepower can be estimated. The calculated horsepower is compared against a table of available standard compressor sizes, and the proper size is selected. If the calculated horsepower does not match any size in the table, then a compressor with the next higher horsepower is selected.

The two optimal cases compressor sizes are provided in Table 5.10. The C_8mimNTf$_2$ IL case required slightly larger compressors than the C_6mimNTf$_2$ IL case due to the

larger flow rates. No compressors are required for the base case as MDEA is highly selective to acid gases over methane unlike ILs.

5.5.2 Heat exchangers

Heat exchanger sizing involves the estimation of the heat transfer area required for the given operating conditions based on user defined specifications or system defaults. The inlet and outlet heat exchanger stream information such as flow rate and temperature are required to perform the sizing. The stream information and fluid components are used to estimate the following design parameters: latent heats of vapourisation or condensation, fouling resistance, specific heat capacity of the fluid, liquid film resistance and the overall heat transfer coefficient. The required heat transfer rate and the heat transfer area can also be calculated. For details on how to model a heat exchanger in Aspen Plus, the reader is referred to Ref. [261].

The heat transfer area obtained based on the duty is then multiplied by the heat exchanger minimum overdesign factor to get the final heat transfer area. Shell and tube heat exchangers are assumed. To minimise the surface area of the heat exchanger, the actual heat transfer area is changed for the detailed design according to the number and the dimensions of tubes and shells chosen for the heat exchanger.

The following default values for the heat exchanger internals are used by the simulator:

- Tube length: 20 feet (6.096 m)

- Tube diameter: 1 inch (2.54 cm)

- Tube thickness: 0.125 inch (0.3175 cm)

- Tube pitch:1.25 inch (3.175 cm)

- Area minimum overdesign factor: 1.15

In the present work, heat exchangers include: the condenser and the reboiler of the stripper, the lean amine cooler for the base case, the compression inter-coolers for the IL cases and the lean solvent heat exchanger, see Figure 5.2 and Figure 5.5.

It is clear from Table 5.10, that both the stripper condenser and reboiler areas of the IL cases are much smaller than that for the base case. This results from the higher regeneration duty requirement of the chemical MDEA compared to the physical ILs. To cool down the lean amine pumped back to the absorber, a cooler with approximately 20 m^2 is needed. The lean IL cooler sizes are much larger due to the larger flow rates (141 m^2 for C$_6$mimNTf$_2$ and 136 m^2 for C$_8$mimNTf$_2$). The compression inter-coolers in the IL cases have comparable sizes for both IL cases ranging from 1–4 m^2. The lean solvent heat exchanger of the base case (7 m^2) is much smaller than the lean IL exchangers (108 m^2 and 105 m^2) due to the larger flow rate requirement for the IL cases.

5.5.3 Pumps

Similar to compressors and heat exchangers, the inlet and outlet stream information are required to perform pump sizing. The capacity requirements for a pump are calculated based on the flow rate of the inlet fluid stream which should be in the liquid phase as the presence of the vapour phase is not allowed in the pump. The flow rate is multiplied by the pump overdesign factor, which is either specified by user or the default value of 1.1 is used. The pump efficiency is either specified or a default value of 70% is used. For both them the default values were used in this work.

The hydraulic horsepower is then calculated based on the capacity (flow rate), density and head, and then divided by the pump efficiency to estimate the brake horsepower as follows [262]

$$P_h = \frac{Q\rho g h_p}{3.6 \times 10^6} \tag{5.2}$$

where P_h is the hydraulic horsepower in kW, Q is the volumetric flow rate in m³/hr, ρ is the fluid density in kg/m³, g is the acceleration of gravity (9.81 m/s²), h_p is the pump head in meter calculated as the difference between the discharge and the suction heads

$$h_p = h_d - h_s \tag{5.3}$$

where h_d and h_s are the discharge head and the suction head respectively in meter.

By comparing the obtained brake horsepower against the available standard motor sizes the pump driver power can be estimated. It is assumed that there are no losses due to friction at both the inlet and the outlet streams. Also, static and velocity heads were ignored on both suction and discharge sides. As expected, the pumping power of the base case is much less than that for the IL cases for two reasons; first the larger IL flow rates, second the higher IL densities compared to MDEA.

5.5.4 Towers

Both the absorption tower and the stripping tower were sized as trayed distillation columns. The minimum input requirement to size a trayed column include the number of stages, the inlet and outlet stream flow rates and conditions and tray locations. The simulator then develops stage information for the main tower and duties for the associated condenser and reboiler, if present.

Fluid properties such as surface tension, foaming tendency, deration factor are either estimated by the simulator or specified by the user. The following default values are used for trayed towers

- Foaming tendency: Moderate

- Trayed tower flooding factor: 0.8

- Tray spacing: 24 inches (0.6096 m)

To size a trayed tower, the actual number of stages required for the separation needs to be determined. The overall column tray efficiency is needed for that. If the efficiency is not specified by the user, Lockett's modification of the Óconnell correlation below is used to estimate it [263].

$$E_{OC} = 0.492(\mu\alpha)^{-0.245} \tag{5.4}$$

where E_{OC} is the Óconnell efficiency, μ is the viscosity of liquid in centipoise, and α is the relative volatility of the key component.

The actual number of stages required for the separation is normally obtained by dividing the theoretical number of stages by the efficiency. Once the actual number of stages is calculated, the height of the tower is estimated. The simulator then estimates the cross sectional area of the stages and the tray spacings and uses it to estimate the tower diameter and height. In this work, the number of actual stages for the base MDEA case absorber is already known from the Notrh Caroline example set up in Aspen Plus. The number of theoretical stages, however, is unknown. The overall column tray efficiency was calculated using Eq. (5.4) and was found to be 22%. In case of ILs, the overall column tray efficiency was estimated as 16%, that is 6% lower than the base case efficiency due to the higher viscosity of ILs.

For the studied cases, the absorber tower dimensions of the base case and the IL cases are almost identical with a slightly smaller diameter for the base case absorber (0.9 m compared to 1.1 m). The base case however, required a larger diameter stripper (1.7 m) than the IL cases (1.4 m for C_6mimNTf$_2$ and 1.5 m for C_8mimNTf$_2$) due to the larger vapour flow across the tower in the MDEA case. The small difference in the absorber diameter can be neglected; therefore, the absorbers of the base case can be used for the IL cases. Furthermore, once the stripper of the base case has a larger cross sectional area than the IL cases with the same height, the base case stripper can still be

used for the IL cases. This would eliminate the need to purchase new absorption and stripping towers for the IL-based process in case of process retrofit.

5.6 Cost estimation

5.6.1 Capital cost

Once the size of each piece of equipment is determined, it can be ordered and its price specified by the supplier. For example, to price a compressor, a table of available standard motor sizes is referenced. If the specified horsepower is not found in the table, then the price of the motor with the next higher horsepower is used. The Aspen economic evaluation engine V9 uses a 2015 pricing basis.

For heat exchangers, the purchase cost can normally be estimated either from graphs for the cost of different types of heat exchangers versus area or from equations based on the area [264], the type of heat exchanger factor (e.g. floating head, fixed head, u-tube or kettle vapouriser), material of construction, pressure factor and tube length correction factor.

Aspen Process Economic Analyzer (APEA) is a cost estimating software used by Aspen Plus V9 to provide detailed capital and operating cost estimates for process schemes. APEA uses extensive data to estimate material cost, labour and equipment installation costs based on detailed engineering design calculation for foundation, piping and instrumentation, platforms, electrical connections, insulation, painting...etc. In this work, it was assumed the the capital cost includes the equipment cost and the solvent capital cost as will be detailed later. A summary of the costs of each piece of equipment for the base case and the two optimal composition IL cases is provided in Table 5.11.

It is clear from Table 5.11 that the total equipment cost of the IL cases is much

Table 5.11: Summary of equipment costs for the base case and the two optimal composition IL cases. For equipment names refer to Figure 5.2 and Figure 5.5.

	Equipment cost (US$)		
Equipment name	Base case (33 wt% MDEA)	8 mol% C_6mimNTf$_2$	7 mol% C_8mimNTf$_2$
Absorber tower	153700	188200	188200
Stripper condenser	17200	9700	9700
Condenser accumulator	12600	12600	12600
Stripper reboiler	101000	60600	61100
Stripper reflux pump	5200	4500	4500
Stripper tower	68800	60400	64900
Cooler	15100	-	-
Cooler 1	-	8400	8500
Cooler 2	-	8500	8500
Cooler 3	-	10400	10400
Cooler 4	-	53000	50900
Flash tank 1	-	93000	92100
Flash tank 2	-	57200	56700
Flash tank 3	-	37400	37200
LP compressor	-	875000	880800
MP compressor	-	735600	738800
HP compressor	-	796100	801900
Pump	71400	152600	152200
Lean solvent HEX	10100	28100	27900
Storage tank	50700	107300	106200
Total equipment cost (M$)	0.51	3.30	3.31

higher than that of the base MDEA case. This is mainly because of the need for multistage compression with inter-coolers in IL cases to recover methane absorbed by ILs. Furthermore, the larger flow rates of the IL cases led to larger equipment sizes.

5.6.2 Utility cost

The utility cost includes the cost of electricity or power required for pumping or compression, the cost of cooling water required for cooling and the cost of low pressure steam required for solvent regeneration. The utility specifications are available in an XML file in the utility library of Aspen Plus V9 and can be configured by the user to specify their costs. In this work, the following Aspen Plus default values are used:

- The price of electricity is $ 0.0775 /kWh.

- For cooling water utility, the inlet temperature is 20°C, and the outlet temperature is 25°C. The energy price is \$ 2.24×10^{-7} /kJ, the heat transfer coefficient is 0.0135 GJ h^{-1}m^{-2}K^{-1}, the viscosity is 1.0 cP and the density is 998.0 kg m^{-3}.

- For low pressure utility steam, the inlet temperature is 125°C, and the outlet temperature is 124°C. The energy price is \$ 1.90×10^{-6} /kJ, the heat transfer coefficient is 0.0216 GJh^{-1}m^{-2}C^{-1}, the viscosity is 1.32×10^{-2} cP, the conductivity is 2.7×10^{-2} Wm^{-1}K^{-1} and the density is 558.0 kg m^{-3}.

In this work, it was assumed that the operating cost is the sum of the total utilities cost and the solvent operating cost, which is the cost of solvent make up as will be detailed later.

5.6.3 Solvent cost

The volume of solvent required to absorb the acid gases should first be calculated to estimate its cost. The first charge of solvent should be added to the capital cost, as it is loaded once a year. The makeup for losses is an operating cost as it is required for the day-to-day functioning of the process. The liquid hold up in the sumps of the absorber and regeneration columns are the main contributors to the total charge. The total charge can be estimated by knowing the sump's volume and the residence time of these units. Guidelines from the gas processors suppliers association (GPSA) engineering data-book [265] were followed to estimate the residence time in the absorber, the regenerator and the flash tank sumps.

The liquid holdup in the column trays, filters, lean/rich heat exchanger and in the piping between absorber and regenerator was ignored. There is typically a solvent storage tank in the process to hold a complete charge of the lean solvent. The total inventory or quantity of the solvent in the system (m_{total}) in kg is determined by the holdup in the sumps as:

$$m_{total} = \dot{m} \times \tau + v_s \times \rho \tag{5.5}$$

where $\dot{m}$ is the flow rate required to meet the treated gas specification in kg/h, τ is the holdup time or residence time in h, v_s is the solvent volume in the sump's hold up in m³ and ρ is the density in kg/m³ and the *Solvent capital cost* in US$ is

$$Solvent\ capital\ cost = m_{total} \times price_{solvent} \qquad (5.6)$$

where $price_{solvent}$ is the solvent price in US$/kg. This cost should be added to the capital cost of the process. The amine price in $/kg was taken from [108]. ILs have not yet been manufactured in bulk. Rather than estimating their cost, we determined the price at which they would be competitive with respect to amine price. This would give potential manufacturers a target and a reason to start producing these ILs in bulk.

The economic life time of the plant was assumed to be 10 years, which indicates the length of time over which the capital cost will be depreciated. For simplicity, we assumed that the total capital cost of the process in US$ includes the equipment purchase cost and the solvent capital cost, which is the cost of the first charge of the solvent obtained by Eq. (5.6). The total operating cost of the process was assumed to be the sum of the total utilities cost and the solvent operating cost, which is the cost of solvent make up in US$/year. The total annual cost of the plant in US$/year is the sum of the total capital cost in US$ divided by the economic life time of the plant, and the total operating cost in US$/year. This will be detailed in the following section.

A comprehensive cost analysis of all cases is needed to make a valid decision on the optimal composition cases. The details of the cost analysis are presented in section 5.6.4.

5.6.4 Cost analysis results

For more detailed capital and operating cost analysis, the solvent cost needs to be considered. The key costs considered for a valid comparison between the base case and

the IL cases are listed in Table 5.12. As the IL price is unknown, it was considered as a variable. The listed values are when the IL price is equal to the MDEA price (1.2 US\$/kg) [108]. This is the minimum IL price which corresponds to the maximum achievable total annual cost (TAC) saving.

In Table 5.12, the solvent capital cost represents the cost of the total inventory amount of the solvent in US\$ as given in section 5.6.3, while the solvent operating cost represents the solvent makeup flow rate cost in US\$/year. The total capital cost (TCC) in US\$ is the sum of the total equipment cost in US\$ and the solvent capital cost in US\$. The total operating cost (TOC) in US\$/year is the sum of the total utility cost in US\$/year and the solvent operating cost in US\$/year.

$$TCC(US\$) = Total\ equipment\ cost + Solvent\ capital\ cost \qquad (5.7)$$

$$TOC(US\$/year) = Total\ utility\ cost + Solvent\ makeup\ cost \qquad (5.8)$$

Assuming 10 years as the plant life time, the TAC would be the sum of the total capital cost in US\$ divided by the plant life time and the total operating cost in US\$/year.

$$TAC(US\$/year) = TCC/10 + TOC \qquad (5.9)$$

Based on the TAC analysis the two optimal IL cases with maximum saving in the TAC are IL case 4 (8 mol% C_6mimNTf$_2$) and IL case 11 (7 mol% C_8mimNTf$_2$) (listed in Table 5.12). It should be noted that, these cases differ from the optimal cases determined in section 5.4.4 based on the regeneration energy saving analysis.

We found that ILs would still be more competitive than MDEA up to the point

Table 5.12: Total annual cost of MDEA plant versus IL plant for gas sweetening (IL price = MDEA price)

	Base case	IL case 4	IL case 11
Solvent	33 wt% MDEA	8 mol% C_6mimNTf$_2$	7 mol% C_8mimNTf$_2$
Equipment cost, M$	0.521	3.33	3.34
Total utilities cost, M$/year	0.499	0.638	0.643
Solvent capital cost, M$	0.0051	0.0581	0.0663
Solvent makeup cost (operating), M$/year	0.493	0.00	0.00
Total capital cost, M$	0.526	3.38	3.41
Total operating cost, M$/year	0.992	0.638	0.643
Total annual cost, M$/year	1.04	0.976	0.983
Total annual cost saving,%	0.00	6.55	5.84

where its price per kg is 12 times the MDEA price for C_6mimNTf$_2$ and up to 10 times the MDEA price for C_8mimNTf$_2$. If more expensive than that, ILs would not be profitable. If the IL price were equal to the MDEA price, 6.55% and 5.84% saving in total annual cost (TAC) can be achieved for C_6mimNTf$_2$ and C_8mimNTf$_2$, respectively. Figure 5.6 explains how the IL/MDEA price ratio affects the total annual cost saving for both IL cases.

For example, we can see from Figure 5.6 that if the IL price per kg was 4 times the MDEA price, a TAC saving of 4.88% and 3.94% can be achieved for C_6mimNTf$_2$ and C_8mimNTf$_2$, respectively. More TAC saving can be achieved with C_6mimNTf$_2$ IL than C_8mimNTf$_2$ IL. This might be attributed to the fact that methane is more soluble in the longer alkyl chain length C_8mimNTf$_2$ IL than in C_6mimNTf$_2$; therefore, we need more compression for C_8mimNTf$_2$ than for C_6mimNTf$_2$ to recover methane.

As mentioned above, the IL cases have a higher capital cost compared to MDEA case due to the need for multistage flashing and compression to recover methane. On the other hand, the IL cases have a much lower operating cost mainly because of the lower regeneration energy requirements (3.17 MW for C_6mimNTf$_2$ and 3.16 MW for C_8mimNTf$_2$) compared to MDEA case energy requirement (6.00 MW). Furthermore the IL cases have no solvent losses therefore, lower solvent operating cost. The much lower energy requirement for the IL cases can be attributed to the fact that the energy
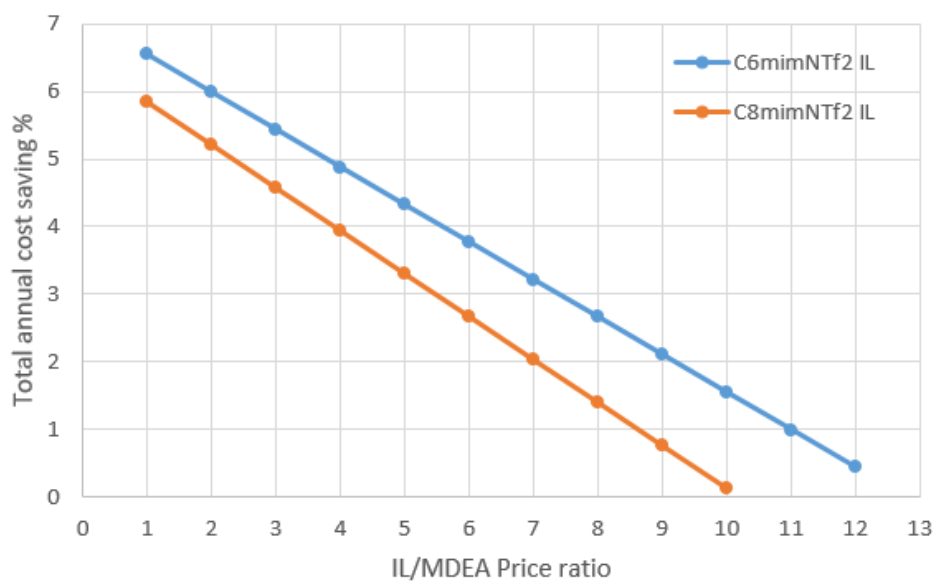
Figure 5.6: The relation between the total annual cost saving and IL/MDEA price ratio.

required to separate acid gases from ILs is much smaller, because physical absorption takes place in IL cases, whereas for the MDEA case more energy is needed to break the bonds formed by the chemical absorption between the acid gases and MDEA. The lower regeneration duty for IL cases also leads to a much lower temperatures in the stripper (380.15 K for IL cases compared to 385.75 K for MDEA case), which reduces the water losses due to evapouration. This is reflected in Table 5.8 and Table 5.9 as lower water makeup for the IL cases compared to the MDEA case. The total operating cost dominates the total annual cost therefore, lower TAC was reported for the IL cases.

5.7 Conclusions

The consequences of replacing MDEA with the two alkyl imidazolium ILs: C_6mimNTf$_2$ and C_8mimNTf$_2$ in North Caroline plant MDEA unit for gas sweetening were examined. Despite the fact that acid gases are more soluble in MDEA than in ILs and MDEA is more selective to acid gases over methane than ILs, the use of ILs is found to

be more profitable than MDEA. First, because ILs have negligible volatility compared to MDEA, no makeup is needed for the IL-based process, unlike the MDEA-based process where about 47 kg of MDEA is lost each hour. However, in reality there will be some IL losses as the vapour pressure of ILs is not zero yet, the amount of losses is much lower than MDEA losses. Second, because ILs are physical solvents, they do not react chemically with the acid gases and, therefore, are easier to regenerate requiring much less energy than MDEA.

Conversion to ILs would also help to reduce the adverse ecological impact of gas sweetening processes. The lower regeneration heat requirement implies smaller amount of generated steam needed to boil up the rich solvent or lower grade steam such as LP steam rather than MP steam or HP steam, consequently, less fuel requirement for steam generation and less gas emissions to the atmosphere. The lower regeneration duty for the IL plant also contributes to a lower temperature profile in the stripper, thereby, reducing water losses due to evapouration. It should be noted that, due to the lack of experimental data of the properties of water-IL mixtures, water and ILs were assumed as completely miscible while in reality they are not; water and the class of ILs investigated here form two liquid phases.

The price of IL was dealt with as a multiple of MDEA price as ILs have not yet been manufactured in bulk and it is difficult to know its price. The maximum TAC saving for the IL-based process (6.55% for $C_6mimNTf_2$ and 5.84% for $C_8mimNTf_2$) can be achieved when the IL price is equal to the MDEA price. As the IL price increases, the TAC saving decreases up to the point where no more saving in the TAC can be achieved for the IL process. $C_6mimNTf_2$ would still be more profitable than MDEA up to the point where its price is twelve times the MDEA price, while $C_8mimNTf_2$ would still be more profitable than MDEA up to the point where its price is ten times the MDEA price. This provides a target price for IL producers to manufacture ILs in bulk.

$C_6mimNTf_2$ was found to be more profitable than $C_8mimNTf_2$ due to its shorter

alkyl chain length and hence lower methane solubility and less compression requirement. The solvent operating cost saving was found to be the main contributor to the total annual cost saving for IL cases. Despite the capital cost penalty incurred by the need for methane recovery in IL cases (m$ 2.86 for $C_6mimNTf_2$ and m$ 2.88 for $C_8mimNTf_2$), an operating cost saving of m$ 0.35 per year for both cases, and a maximum total annual cost saving of k$ 68 per year for $C_6mimNTf_2$ and k$ 61 per year for $C_8mimNTf_2$ can still be achieved.

In an effort to further improve the IL-based process investigated in this chapter and reduce its capital cost by eliminating the need for compression, it is proposed to blend the IL with another physical solvent to reduce the solubility of methane in the IL. This will be explored in the following chapter.

Chapter 6

Improvement of the IL-based sweetening process

6.1 Introduction

The replacement of MDEA solution with alkylimidazolium ILs in an existing gas cleaning process offered many advantages, as concluded from Chapter 5. First, the required regeneration energy is reduced; second, the need for solvent and water makeup is significantly minimised, reducing the environmental impact of the process. However, due to the relatively high solubility of methane in ILs, multistage gas compression was necessary to recover methane when ILs are used. This substantially increases the capital cost of the IL plant, although, it can still be offset by the savings in the solvent operating cost.

In order to reduce the cost of the IL-based sweetening process simulated in Chapter 5, the addition of another physical solvent, methanol or dimethyl ether of polyethylene glycol (DEPG), to the IL is proposed. Methanol is selected because it is one of the physical solvents that has been commonly used for acid gas removal, especially for CO_2 capture, and it does not interact strongly with the absorbed gases, which makes the recovery process of the solvent much easier [266, 267]. Despite the high solubility of CO_2 in methanol and its low viscosity, methanol is highly volatile, which makes

136

the solvent recovery process highly energy intensive and non economically viable due to the significant loss of solvent. As ILs have negligible volatility and methanol has low viscosity, blending methanol with ILs helps to reduce the methanol volatility and reduce the IL's viscosity, consequently, reducing the operating cost associated with solvent recovery and pumping [268, 269]. DEPG, the second proposed solvent, is much less volatile than methanol, much less viscous than ILs and has a high acid gas absorption capacity with higher H_2S selectivity [266]. It has been concluded that the use of a blend of IL-DEPG solution is a more economically efficient and environmentally benign option than the use of IL alone or a blend of IL and methanol for gas sweetening.

Retrofit of an existing process can sometimes be more economically viable than the design of a new process such as, when minor structural changes are required to achieve a significant energy saving. However, retrofit study should consider advantages and limitations of both the new design and the retrofit design to make a firm decision on whether the retrofit design is more promising than the new design or not. Retrofit will be discussed later in section 6.8.

In this chapter, first a brief overview on the use of physical solvents for gas sweetening is provided in section 6.2. Two common physical solvents used commercially are discussed here, methanol and DEPG. Then a brief review of some of the previous applications of using mixture of solvents for gas cleaning is presented in section 6.3. The PC-SAFT model used earlier in Chapter 4 is then validated for pure methanol and pure DEPG and their mixtures with acid gases and with methane in section 6.4.

Aspen Plus V9 is then used to simulate IL-methanol and IL-DEPG based sweetening processes using PC-SAFT as the thermodynamic property package in sections 6.5 and 6.6. The simulation results of both processes are then compared to each other and to the simulation results of the IL based process simulated in Chapter 5. The results are then analysed and discussed in section 6.7 and the potential of retrofitting the existing North Caroline amine process with IL-DEPG as a solvent to replace MDEA is discussed in section 6.8. Finally, the main findings are presented in section 6.9.

137

6.2 Physical solvents used for acid gas removal

Physical solvents have been commonly used in industry for gas sweetening applications. Examples of commercial physical solvent based processes and their advantages over chemical solvent based processes were mentioned previously in section 2.4. Two of the most commercially used physical solvent process are the Rectisol® process developed by Lurgi and Linde companies and the Selexol™ processes developed by Allied Chemical Corporation and is now owned by the Honeywell UOP company [270]. The former uses methanol as a solvent, while the the latter uses dimethyl ether of polyethylene glycol (DEPG) as a solvent. The Rectisol® and Selexol™ processes are described below.

6.2.1 Methanol (Rectisol®)

Methanol (CH_3OH) has commonly been used since the 1950s as a physical organic solvent for the the removal of acid gases (CO_2 and H_2S) and carbonyl sulphide (COS) from sour gas streams, especially synthetic gas [266]. Rectisol® is the trade name for the methanol process. The Rectisol® process has two typical configurations: the single-stage configuration, in which the acid gases and COS are absorbed in one stage or one column, and the two-stage configuration, in which the absorption process is carried out in two columns in series [267].

In the single-stage configuration shown in Figure 6.1, the sour gas is fed to the bottom of the absorption tower T101 and the methanol is fed to the top. The purified gas is withdrawn from the top of T101, and the rich solvent streams are withdrawn from the side or the bottom of T101. The rich solvent streams flashes in the three flash vessels D101, D102 and D103. The rich solvent is then sent to the stripper column T102 to desorb CO_2 by both pressure reduction and N_2 stripping. The solvent is then fed to the distillation column T103 to separate H_2S from the solvent. The lean methanol is then dehydrated in T104. The CO_2 flashing gas is compressed and liquefied for geosequestration, and H_2S is sent to a Claus plant for sulphur production.
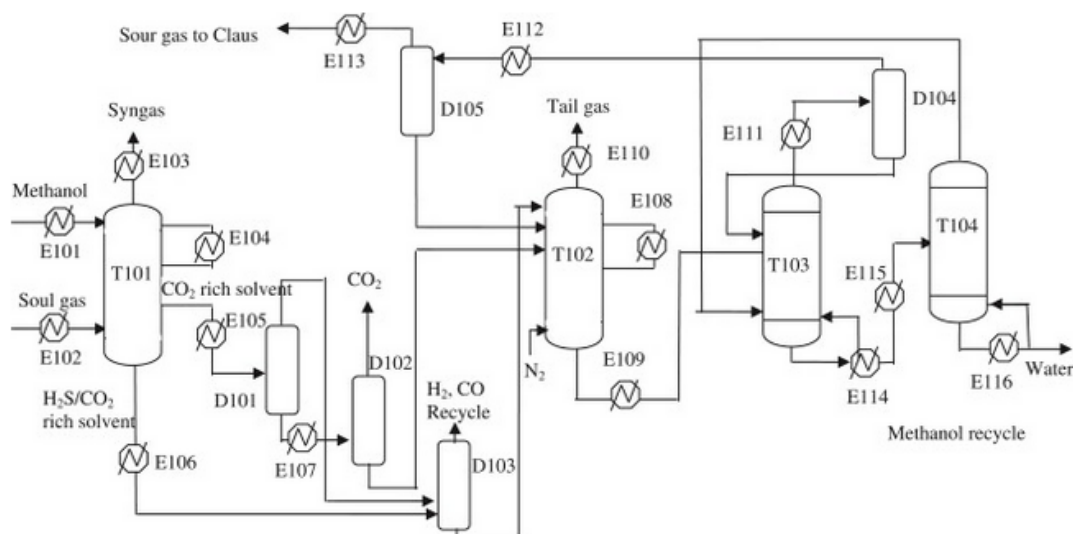
Figure 6.1: Single-stage Rectisol® wash configuration. Taken from Ref. [267].

In the two-stage configuration (Figure 6.2), the absorption is carried out in two columns in series: T101 and T103. H_2S and COS removal takes place in T101, while CO_2 removal takes place in T103. The H_2S rich methanol and CO_2 rich methanol are then regenerated independently by flashing at low pressure and stripping at high temperature.

Rectisol® has many advantages over other physical processes [267]. First, the solubility of acid gases and COS in methanol is much higher than that in other physical solvents, such as water and Purisol, which implies less solvent consumption and less regeneration requirement. Second, Rectisol® can be used for the simultaneous removal of CO_2, H_2S, COS, HCN and NH_3, unlike Purisol and Selexol™ which are selective for H_2S and Fluor which is selective for CO_2. Furthermore, high acid gas removal efficiency can be achieved using methanol due to the high selectivity of methanol towards acid gases over other gases, such as methane, nitrogen and hydrogen. Rectisol® is a low temperature process, usually operating between $-40°C$ and $-62°C$ [266] due to the volatile nature of methanol. The low temperature and high pressure conditions are favoured, as the solubility of H_2S in methanol increases at such conditions. Methanol
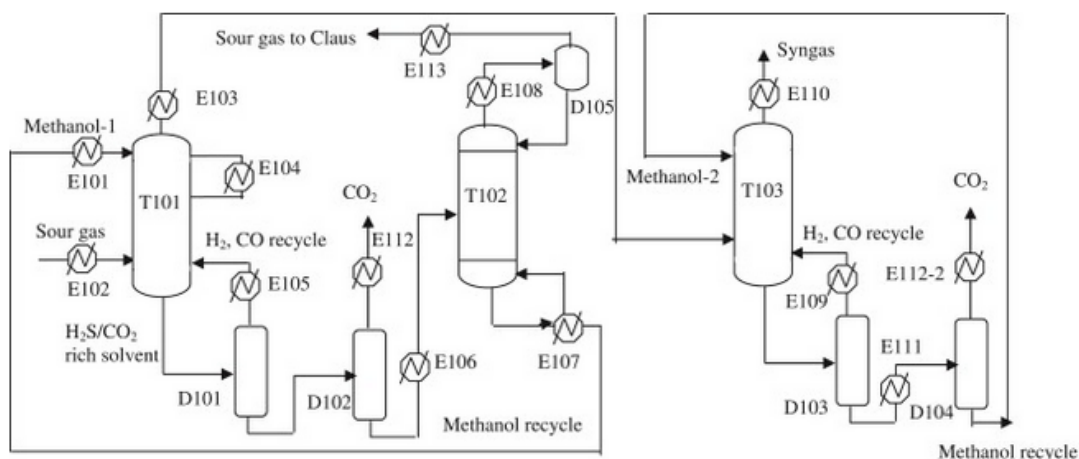
Figure 6.2: Two-stage Rectisol® wash configuration. Taken from Ref. [267].

also boils at 64.7°C, which is low enough to minimize the need for very low temperature for refrigeration during regeneration. Finally, methanol is relatively more thermally and chemically stable at low temperature, non-degradable, less corrosive and has lower viscosity than the conventional chemical amines.

6.2.2 Dimethyl ethers of polyethylene glycol (DEPG or Selexol$^{\text{TM}}$)

Mixtures of dimethyl ethers of polyethylene glycol ($CH_3O(C_2H_4O)_nCH_3$ with n between 2 and 9) or DEPG have been manufactured by different companies, such as DOW and UOP, for use as a physical solvent to absorb H_2S, CO_2, and mercaptans from natural gas. The most common commercial names of DEPG mixtures are Selexol$^{\text{TM}}$ and Genosorb [266].

Like the Rectisol® process, Selexol$^{\text{TM}}$ has two process configurations: the single-stage configuration, in which both acid gases are absorbed in one stage or one column, and the two-stage configuration, in which the absorption process is carried out in two columns.

The single-stage configuration (Figure 6.3) is similar to the amine process configu-

ration presented in Figure 2.4 in Chapter 2. Both consist of an absorber where the acid gases are captured from the raw gas with the solvent, and a stripper where the solvent is regenerated. However, in the Selexol$^{\text{TM}}$ process absorber, the acid gases dissolve in the DEPG and do not react chemically with it, as in the amine process. Therefore, it is easier to regenerate the acid gases in the Selexol$^{\text{TM}}$ process. This implies less stage requirements in the absorber and lower regeneration temperatures and pressures in the stripper for the Selexol$^{\text{TM}}$ process.

In the two-stage Selexol$^{\text{TM}}$ process configuration, hydrogen sulphide is removed from the raw gas in the first stage, and the gas is then sent to the second stage to remove most of the CO_2 in the gas. The selection of the Selexol$^{\text{TM}}$ process configuration depends on the hydrogen sulphide/carbon dioxide and sulphur removal requirement. For example, the single stage configuration can be used for selective H_2S removal. However, the H_2S content in the acid gas stream could be too low to be used in a conventional Claus plant for sulphur recovery [271]. On the other hand, the two-stage configuration can be used for the bulk removal of CO_2 in addition to H_2S [270].

In the remainder of this chapter, both methanol and DEPG and their mixtures with ILs are investigated for use as solvents in the North Caroline sweetening unit as an alternative to MDEA. Although DEPG can be used for both CO_2 and H_2S removal, it is selective to H_2S over CO_2. DEPG is much more viscous than methanol [266], which leads to higher pumping requirements. However, DEPG is much less viscous than MDEA and ILs (see table Table 6.1). This implies that the use of a mixture of DEPG and IL or DEPG and MDEA may enhance the mass transfer rates of the solvent and pumping efficiency in the acid gas removal process. DEPG is also hardly volatile compared to methanol, which reduces the solvent losses and consequently, the make up requirement in the acid gas removal process.

The following section provides a brief review of some previous efforts of using mixed solvents for gas cleaning applications.
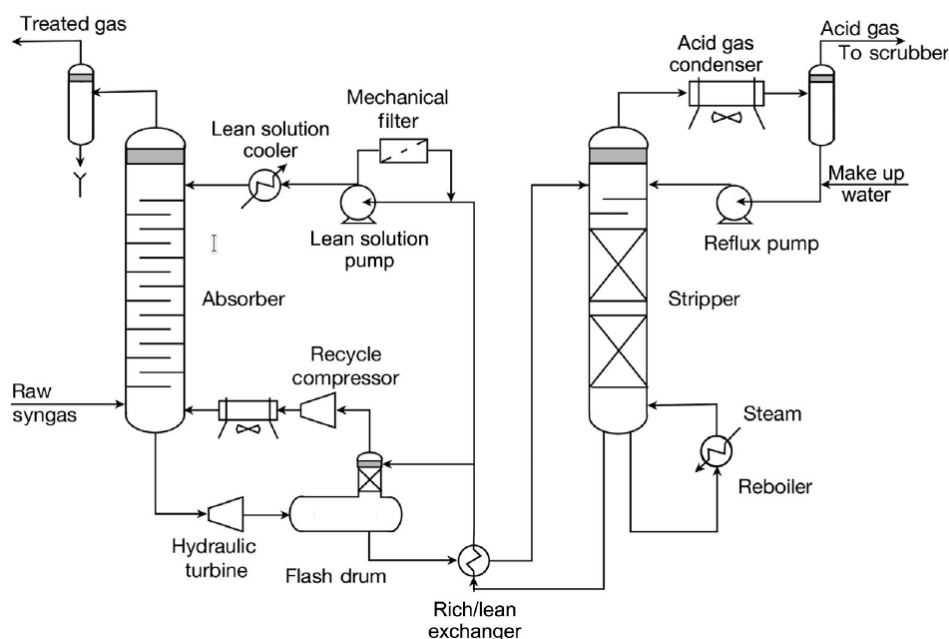
Figure 6.3: Single-stage Selexol™ process configuration. Taken from Ref. [271].

Table 6.1: Properties of different pure solvents used in this study.

Solvent	MDEA	ILs $C_6mimNTf_2$ / $C_8mimNTf_2$	Methanol	DEPG
Viscosity at 25°C (cP)	77.85 [272]	70.614 / 93.053 [259]	0.6 [266]	5.8 [266]
Molecular Weight (g mol^{-1})	119.163	447.36 / 475.48	32 [266]	280 [266]
Vapour Pressure at 25°C (mmHg)	< 0.01 [273]	neglig. [9, 10]	125 [266]	0.00073 [266]
Boiling Point at 760 mmHg (°C)	247 [273]	306 / 297 [274]	65 [266]	275 [266]
Heat capacity at 25°C (J g^{-1}K^{-1})	2.26 [275]	1.49 / 1.54 [257]	2.53 [276]	2.03 [277]

6.3 Blended solvents for acid gas removal

Blending different solvent to be used for gas cleaning applications may offer several benefits arising from combining the advantages of the mixed solvents. Several solvent mixtures have been used in the past for acid gas removal applications. Some involved mixtures of chemical solvents, others involved mixtures of chemical and physical solvents or mixtures of physical solvents.

Figure 6.4: Two-stage Selexol^{TM} process configuration. Taken from Ref. [270].

The use of mixed amines for gas sweetening has been addressed in several studies [278, 279, 280, 281]. Most mixed amine solutions used for gas sweetening use MDEA as the base amine, due to its attractive characteristics for acid gas removal [279]. MDEA possesses higher acid gas absorption capacity than other amines and is less corrosive, more stable, less volatile and requires less regeneration duty. However, due to the low reaction rate of MDEA with CO_2 and its higher cost, it is usually mixed with cheaper amines with higher CO_2 reaction rates, such as MEA or DEA. The higher the absorption rate the higher the acid gas removal performance in the sweetening process, the better the solvent.

Amines can also be mixed with physical solvents to enhance their acid gas capacity and reduce the energy requirement for their regeneration. One of the first attempts of

mixing amines with physical solvent is the Sulfinol process [282]. The solvent solution is a mixture of di-isopropanol amine (DIPA) or methyldiethanol amine (MDEA), sulfolane (tetramethylene sulfone or TMS), and water. Recently, several studies investigated mixtures of amines with ILs as a physical solvent for efficient CO_2 capture [9, 38, 283, 284, 285]. These mixtures combine the eco-friendly characteristics of ILs with the high acid gas capacity of amines. Furthermore, mixing the expensive, highly viscous ILs with the cheap and less viscous amines could improve the mass transfer efficiency and the economics of the process.

Other studies proposed the use of mixed physical solvents, such as methanol and ILs [268, 269]. Mixing a highly viscous non-volatile solvent such as ILs with a non-viscous highly volatile solvent such methanol may reduce the viscosity of the IL and the volatility of methanol. This leads to improved mass transfer and pumping efficiency and reduced solvent makeup requirement. Some research studies proposed the use of IL-methanol blend as a solvent for CO_2 capture applications [268, 269]. These studies claimed that the investigated mixtures of methanol and ILs may be used for CO_2 capture combining the advantages of conventional organic solvents and ILs [268]. In addition, Dai et. al. [269] found that the methanol loss of in the absorption column and flash tanks decreases significantly when methanol and IL mixture is used as an absorbent instead of methanol in the CO_2 removal process. The use of blends of alkyl imidazolium IL-methanol-water and alkyl imidazolium IL-DEPG-water as an alternative solvent to MDEA solution for gas sweetening in the existing North Caroline amine process is explored later in this chapter. The presence of water in these blends helps to reduce the viscosity of the solvent.

In the following sections, the PC-SAFT model used in Chapter 4 is first validated for pure methanol and DEPG and then for binary systems of both solvents with acid gases and with methane. The PC-SAFT will then be used in Aspen Plus V9 for simulation purposes in subsequent sections.

6.4 PC-SAFT validation for methanol, DEPG and their mixtures with acid gases and methane

In this section, the PC-SAFT model is parameterized and validated for pure methanol, pure DEPG and their binary mixtures with acid gases and with methanol. The model is first used to reproduce the pure experimental solvent (methanol/DEPG) properties, and then the binary experimental solubility data from literature.

6.4.1 Pure methanol and DEPG

For methanol, the PC-SAFT pure component parameters of Gross and Sadowski [286] were used with 2 association sites. The methanol parameters are listed in Table 6.2. In order to validate these parameters, we used them to represent the vapour pressure of methanol using PC-SAFT. The calculations were able to successfully reproduce the experimentally measured vapour pressure data taken from Ref. [214] with reasonable accuracy (2.7% AARD). Although Gross and Sadowski [286] already validated the model for methanol, here the PC-SAFT was validated for methanol by reproducing another set of vapour pressure experimental data just to double check its validity and confirm that. The vapour pressure curve is shown in Figure 6.5.

Table 6.2: PC-SAFT parameters for methanol and DEPG.

Component	association sites	MW g mol^{-1}	T range K	m_i	σ_i Å	ε_i/k_B K	$\varepsilon^{A_iB_i}/k_B$ K	$K^{A_iB_i}$	Ref.
Methanol	2	32.042	200–512	1.5255	3.2300	188.90	2899.5	0.035176	[286]
DEPG	0	250	293.15–323.15	11.7456	3.0951	169.76			This work

The PC-SAFT parameters of DEPG where estimated in this work by fitting to experimental density data taken from Parsa et al. [287]. The DEPG mixture used in this study is a mixture of Glymes studied by Ref. [287] and its average MW is 250 g mol^{-1}. DEPG is modelled as a non-associating component just for simplicity as it is hard to model as an associating component because as a mixture of glymes a large number of possible hydrogen bonds may form. The PC-SAFT successfully reproduced the pure density with an AARD% of 0.26%. The PC-SAFT parameters for DEPG are given
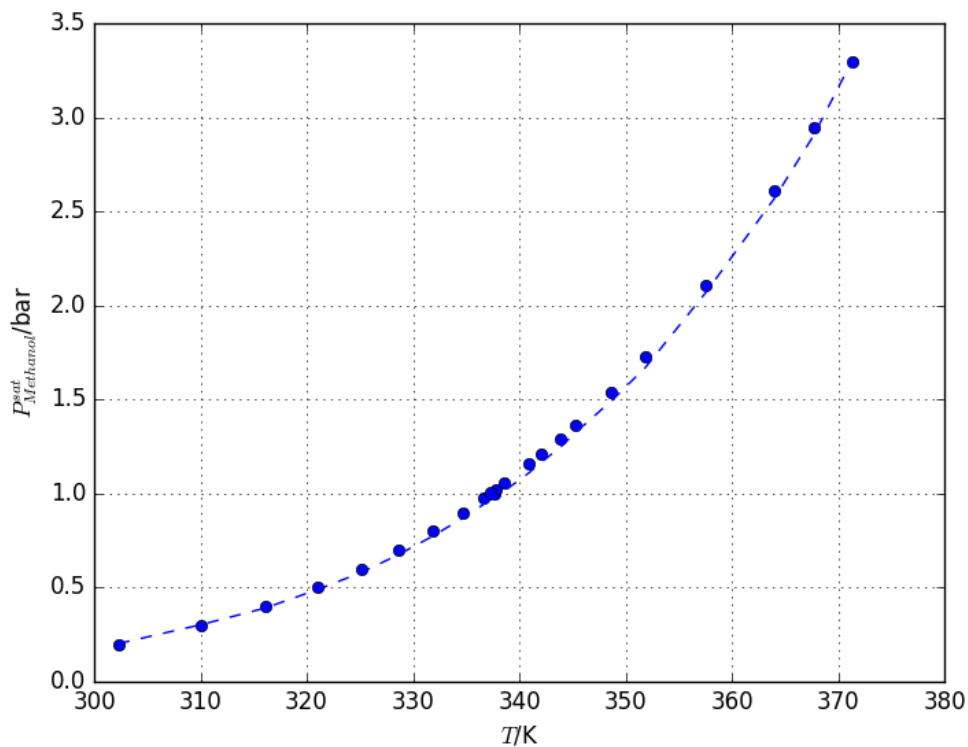
Figure 6.5: Vapour pressure of methanol. The symbols represent the experimental vapour pressure data taken from Ref. [214]. The dashed line is the vapour pressures calculated using PC-SAFT with the parameters given in Table 6.2.

in Table 6.2. The experimental and calculated densities of DEPG are shown in Figure 6.6.

Once PC-SAFT is validated for the pure solvents, the interactions between the involved gases in the sweetening process and these solvents are then considered. This can be done by investigating the binary solubility of acid gases and methane in these solvents as will be detailed in the following section.
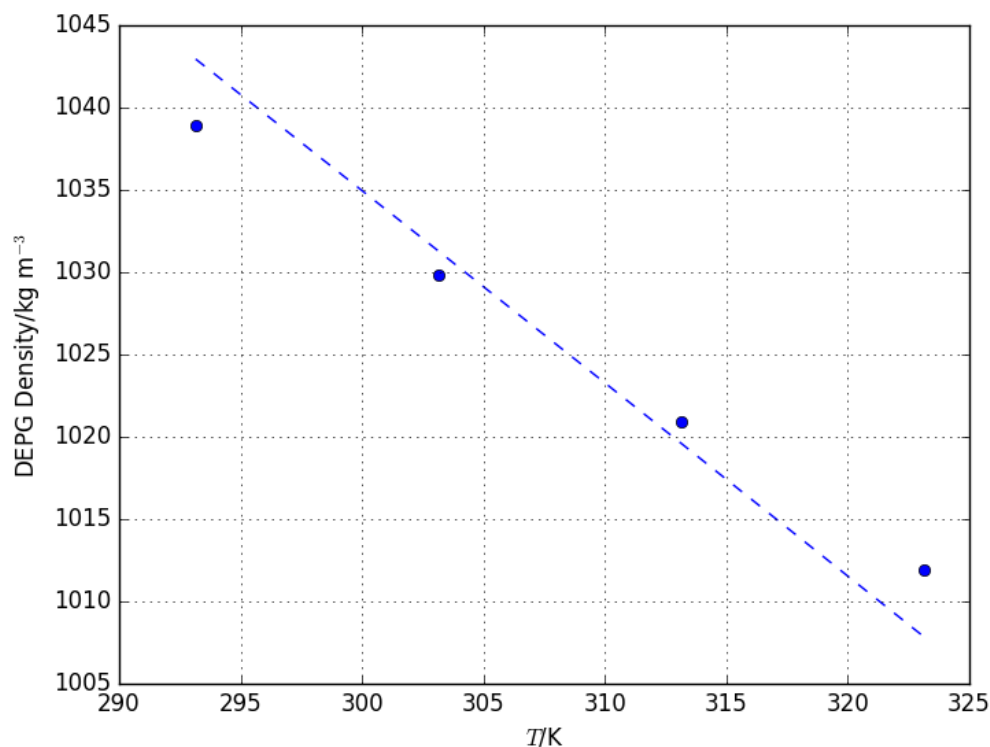
Figure 6.6: Density of DEPG. The symbols represent the experimental density data taken from Ref. [287]. The dashed line is the density calculated using PC-SAFT with the parameters given in Table 6.2.

6.4.2 Binary solubility

The solubility of acid gases in the selected solvent is the most vital factor to be considered in the solvent selection process. The more soluble the acid gases are in the solvent, the more efficient the solvent is. However, the selectivity of the solvent to acid gases over methane, the main natural gas constituent, should also be considered. The more selective the solvent to acid gases over methane, the higher the methane recovery. In this section, the solubility of acid gases and methane in both methanol and DEPG is investigated and represented using PC-SAFT.

6.4.2.1 Solubility of acid gases in methanol

Here, the experimental solubility data of both CO_2 and H_2S in methanol taken from Refs. [268] and [288], respectively are represented using PC-SAFT. The calculated solubility of CO_2 in methanol is represented by the red dashed line in Figure 6.7, and the solubility of H_2S in methanol is represented by the blue dashed line shown in Figure 6.7. Symbols represent the experimental data. Temperature dependent binary interaction parameters (k_{ij}) for CO_2-methanol and H_2S-methanol were retrieved from Aspen Plus V9 [289] and used. The binary parameters are expressed as

$$k_{ij} = A + B/T_r + C \ln T_r + DT_r + ET_r^2 \tag{6.1}$$

where k_{ij} is the temperature dependant binary interaction parameter between the acid gas and methanol. A, B, C, D and E are constant coefficients given in Table 6.3, T_r is the ratio between the system temperature T and the reference temperature $T_{ref} = 298.15K$.

$$T_r = T/T_{ref} \tag{6.2}$$

Table 6.3: PC-SAFT binary interaction parameter coefficients for acid gas-methanol systems for Eq. (6.1).

Acid gas	A	B	C	D	E	T_{ref}/K	Ref.
CO_2	0.00	0.024566	-0.014496	0.00	0.00	298.15	[289]
H_2S	0.00	-0.019155	-0.174772	0.00	0.00	298.15	[289]

Using the parameters in Table 6.3, the solubility of both CO_2 and H_2S in methanol was successfully represented using PC-SAFT with AARD of 0.19% for CO_2 and 2.05% for H_2S.

According to the experimental solubility measurements provided by [268] and [288],
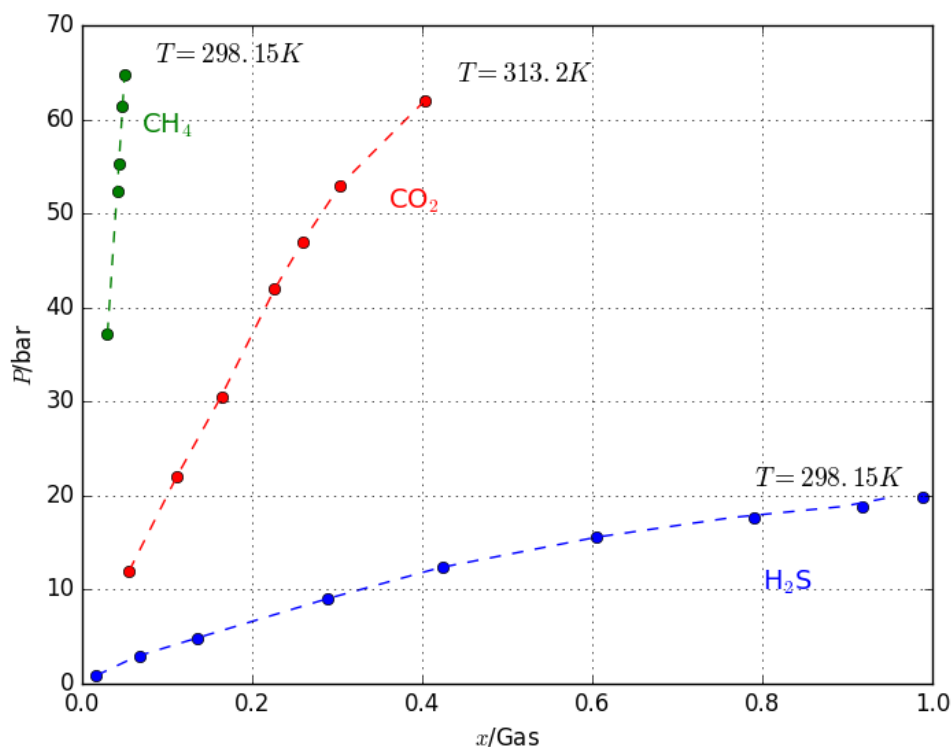
Figure 6.7: Solubility of CO_2 (red), H_2S (blue) and CH_4 (green) in methanol. Dashed lines represent the solubility calculated using PC-SAFT. Symbols represent the experimental data taken from Refs. [268, 288, 290].

and by comparing Figure 6.7 to Figure 4.7, it is obvious that acid gases are much more soluble in ILs than in methanol. For example, the mole fraction of CO_2 in C_8mimNTf$_2$ at 12 bar and 313.2 K is about 0.22, while the mole fraction of CO_2 in methanol at the same conditions is only 0.056 [268]. The mole fraction of H_2S in C_4mimNTf$_2$ at 8 bar and 298.15 K is about 0.51, while the fraction of H_2S in methanol at the same conditions is 0.21. H_2S is more soluble than CO_2 in both methanol and ILs. This suggests that the use of a blend of methanol and IL instead of pure IL for acid gas removal from methane may reduce the solvent capacity to absorb acid gases. However, methanol is more selective to acid gases over methane than ILs, as will be shown in the following

section. In fact, there is a trade-off between the solvent selectivity towards acid gases and its absorption capacity. The best solvent is the one which has the lowest methane solubility and the highest acid gas absorption capacity. A preliminary process design and simulation helps to perform this trade off to select the best solvent.

6.4.2.2   Solubility of methane in methanol

In this section, the solubility of methane, the main natural gas constituent, in methanol is represented using PC-SAFT. Methanol is modelled as an associating component with two associating sites using the parameters listed in Table 6.2. Pure methane parameters used are also given in the table. Figure 6.7 also shows the solubility of methane in methanol at 298.15K represented using PC-SAFT (green dashed line) with 0.06 binary interaction parameter used to fit the calculation to the experimental data (green symbols) taken from [290]. The PC-SAFT satisfactorily represented the experimental solubility data with AARD of 0.6%.

It can be concluded from Figure 6.7 and Figure 4.17 that methane is hardly soluble in methanol compared to its solubility in ILs. The mole fraction of methane in methanol at 55 bar and 298.15 K is only 0.04 compared to 0.16 mole fraction in C_6mimNTf$_2$ IL at the same pressure and 293.3 K [229]. This suggests that the use of a blend of IL-methanol instead of pure IL for acid gas removal from methane may reduce the amount of methane loss in the process. However, other factors such as acid gas solubility in the solvent and the whole process design can affect the solvent selection decision as will be detailed later. For example, from Figure 4.12, the CO_2 mol fraction in C_8mimNTf$_2$ IL is approximately 0.62 at 60 bar and 345 K, while Figure 6.7 shows 0.38 CO_2 mole fraction in methanol at 313 K and 60 bar. Thus, CO_2/CH$_4$ selectivity in IL (0.62/0.17 = 3.6) < CO_2/CH$_4$ selectivity in methanol (0.4/0.04 = 10). In the following section, the solubility of both acid gases (CO_2 and H$_2$S) in DEPG is considered and compared to their solubility in methanol and to that in ILs studied in Chapter 4.

6.4.2.3 Solubility of acid gases in DEPG

The experimental solubility data of both CO_2 and H_2S in DEPG is represented using PC-SAFT. The calculated solubility of CO_2 in DEPG is represented by the red dashed line in Figure 6.8 and the solubility of H_2S in DEPG is represented by the blue dashed line in Figure 6.8. Symbols represent the experimental data taken from Ref. [291]. Temperature dependent binary interaction parameters (k_{ij}) for CO_2-DEPG and H_2S-DEPG were retrieved from Aspen Plus V9 [289] and used. The binary parameters are expressed using the same formula given by Eq. (6.1). The constant coefficients A, B, C, D, E and T_{ref} are given in Table 6.4.

Table 6.4: PC-SAFT binary interaction parameter coefficients for acid gas-DEPG systems for Eq. (6.1).

Acid gas	A	B	C	D	E	T_{ref}/K	Ref.
CO_2	0.218926	-0.171017	0.00	0.00	0.00	298.15	[289]
H_2S	0.007871	-0.076734	0.00	0.00	0.00	298.15	[289]

Using the parameters in Table 6.4, the solubility of both CO_2 and H_2S in DEPG was satisfactorily represented using PC-SAFT with AARD of 11.8% for CO_2 and 17.5% for H_2S, see Figure 6.8.

According to the experimental solubility measurements provided by [291], and by comparing Figure 6.8 to Figure 6.7, it is evident that both acid gases are more soluble in DEPG than in methanol. For example, the mole fraction of H_2S in DEPG at 15 bar and 298.15 K is 0.9, while its mole fraction in methanol at the same conditions is only 0.6. As for CO_2, its mole fraction in DEPG at 15 bar and 298.15 K is 0.40, while only 0.08 mole fraction of CO_2 was measured in methanol at the same conditions.

If these solubility figures are compared to the solubility of acid gases in ILs presented earlier in Figure 4.7, It clear that acid gases are much more soluble in DEPG than in ILs. For example, the solubility of CO_2 in DEPG at 15 bar and 298.15 K is
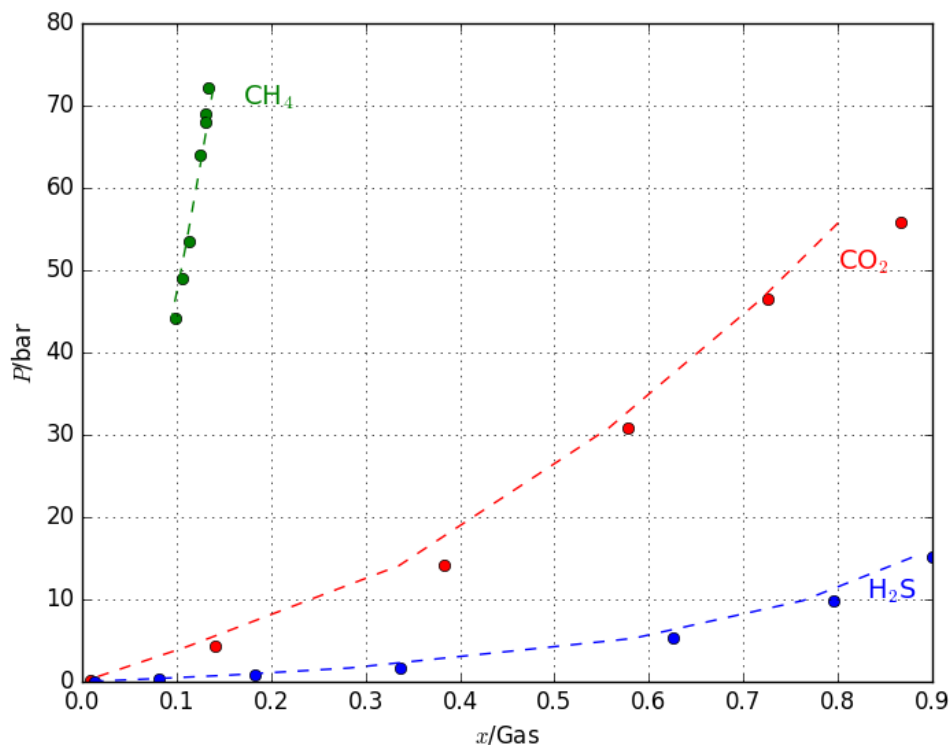
Figure 6.8: Solubility of CO_2 (red), H_2S (blue) and CH_4 (green) in DEPG at 298.15K. Dashed lines represent the solubility calculated using PC-SAFT. Symbols represent the experimental data taken from Refs. [291, 292].

about 40 mol% while the the solubility of CO_2 in $C_6mimNTf_2$ at the same conditions is 37 mol%. The solubility of H_2S in DEPG at 15 bar and 298.15 K is about 90 mol% while the the solubility of H_2S in $C_6mimNTf_2$ at the same conditions is 70 mol%. Furthermore, DEPG is more selective to H_2S over CO_2, where 90 mol% of H_2S is soluble in DEPG at 15 bar and 298.15 K and only 40 mol% of CO_2 is soluble in DEPG at the same conditions (see Figure 6.8 and Figure 4.7).

This leads to the conclusion that DEPG possesses the highest acid gas absorption capacity when compared to methanol and ILs. This suggests that blending DEPG with

IL to be used for acid gas removal could enhance the solvent performance in acid gas removal by improving its acid gas absorption capacity or its ability to capture more acid gases. In the following section, methane solubility in DEPG is considered.

6.4.2.4 Solubility of methane in DEPG

The solubility of methane in DEPG at 298.15K is also represented in Figure 6.8 using PC-SAFT (green dashed line). DEPG is modelled as a non-associating component using the parameters listed in Table 6.2 resulted from the pure experimental density fit. A binary interaction parameter of 0.13 was used to fit the calculation to the experimental data taken from [292] and represented by the green symbols in Figure 6.8. PC-SAFT satisfactorily represented the experimental solubility data with AARD of 2.6%.

By comparing the solubility of methane in DEPG to that in methanol shown in Figure 6.7 and that in ILs provided by Refs. [228] and [229], it can be concluded that the solubility of methane in the studied physical solvents follows the order IL > DEPG > methanol. The mole fraction of methane in DEPG at 63.93 bar and 298.15 K is about 0.125. This is considered lower than the mole fraction of methane in C_6mimNTf$_2$ IL at 293.3 K and the same pressure which is 0.18, and much higher than the mole fraction of methane in methanol at the same conditions (0.048). This suggests that, blending DEPG or methanol with ILs may reduce the solubility of methane in the solvent as compared to IL on its own. The high solubility of methane in DEPG and ILs is one of the disadvantages of using them for natural gas cleaning due to the loss of methane in the solvent. This creates the need for methane recovery from the solvent as discussed previously in Chapter 5 for IL cases.

In the following sections, the effect of mixing ILs with other physical solvents, such as methanol and DEPG is explored for the North Caroline plant amine unit investigated in Chapter 5.

6.5 IL-methanol based sweetening unit

In Chapter 5, the use of alkyl imidazolium ILs as an alternative solvent to MDEA in the North Caroline plant amine unit was investigated. The replacement of MDEA with IL was found to be promising and profitable. However, due to the high solubility of methane in ILs, it was necessary to install multi-stage compressors to recover methane from the ILs. This incurred a capital cost penalty. To further optimise the process and improve its economic feasibility, we propose to blend the IL with another physical solvent, such as methanol or DEPG, in which methane is less soluble and is cheaper than ILs, and at the same time, benefit from the exceptional properties of ILs. In this section, the use of an IL-methanol blend in North Caroline plant amine unit is investigated and compared to the use of IL alone. First, methanol is used as a solvent in the sweetening unit, then a blend of methanol with IL is used for the same purpose. The sweetening unit is simulated in Aspen Plus V9 using PC-SAFT as the thermodynamic model package, and the results are compared to the IL-based sweetening unit simulated in Chapter 5.

Methanol has been commonly used for acid gas removal. This is mainly due to the physical nature of the acid gas-methanol interaction, which makes the regeneration process of the solvent much easier than chemical absorption-based processes. Despite the high selectivity of acid gases over methane in methanol, the low methanol viscosity and low cost, methanol is highly volatile, which makes the solvent recovery process highly energy intensive and not economically viable due to the significant loss of solvent. Blending the non volatile viscous ILs with the volatile non-viscous methanol helps to reduce the overall solvent volatility, viscosity and cost [269], consequently, reducing the operating cost associated with solvent recovery, pumping and material cost. The complete process simulation helps to compare the performance of the IL-methanol blend solvent against pure IL solvent to make a clear decision on the best solvent option.

Table 6.5 provides a comparison of the key simulation results between the two optimal IL cases determined in Chapter 5 and the methanol cases. The regeneration

energy consumption is significantly reduced by replacing the IL solvent in the plant shown in Figure 5.5 with methanol. Up to 83% of the energy is saved in the methanol based process compared to the amine based process, and up to 68% of the energy is saved compared to the IL processes. This indicates that methanol releases acid gases much more easily than ILs. Furthermore, by using methanol as a solvent in the North Caroline plant sweetening unit, the amount of methane in the rich solvent is significantly reduced from 24.98 kg min^{-1} in the C_8mimNTf$_2$ IL case and 23.30 kg min^{-1} in the C_6mimNTf$_2$ IL case to 7.84 kg min^{-1} in the methanol case (i.e. by about 66–68%). That is because methane is much less soluble in methanol than in IL. This allows the elimination of one compression stage (LP stage) in Figure 5.5 for the methanol case. However, due to the highly volatile nature of methanol, 14.11 kg of methanol is lost each minute in the process (1069 liter hr^{-1}), which must be compensated for with a make up stream. As a result, the solvent make up cost of the methanol case rocketed to 3.2 m\$ per year. For the IL cases, no solvent make up is needed due to the negligible vapour pressure of ILs compared to methanol. This leads to the conclusion that the use of methanol as a solvent in North Caroline sweetening unit is not economically viable. For this reason, methanol is normally used under cryogenic conditions.

To benefit from the low regeneration energy requirement of methanol and its high selectivity to acid gases over methane while minimising the solvent losses, blending methanol with the non-volatile ILs is suggested. A blend of 10 mol% C_8mimNTf$_2$ IL, 5 mol% methanol and 85% water is used as a solvent in the North Caroline sweetening unit. The addition of IL helps to reduce the solvent losses due to its negligible vapour pressure. The simulation results are reported in the last column of Table 6.5.

Compared to the base MDEA case of North Caroline plant, about 70% saving in the regeneration duty is achieved in the IL-methanol process. 44% of the energy is saved compared to the IL cases, and no energy saving is achieved compared to the methanol case. However, about 800 k\$/year is saved in the solvent make up cost in the IL-methanol process compared to the methanol case. The addition of IL to methanol increased the regeneration duty by 800 KW, moreover, it increased the methane solu-

bility in the rich solvent by 17%, therefore, the LP compressor is again required in the IL-methanol case. Despite that, the total operating cost of the process is significantly reduced due to the saving in the solvent make up cost. The total annual cost of both the methanol and IL-methanol cases was significantly higher than the base case and the optimal IL cases, consequently, the option of using methanol or its blend with IL in the North Caroline sweetening unit is not recommended.

Table 6.5: Methanol and its blend with $C_8mimNTf_2$ IL cases versus $C_6mimNTf_2$ and $C_8mimNTf_2$ IL cases for gas sweetening

	Base case	$C_8mimNTf_2$ IL case	$C_6mimNTf_2$ IL case	Methanol case	$C_8mimNTf_2$ IL-methanol case
Model	ELECTNRTL	PC-SAFT	PC-SAFT	PC-SAFT	PC-SAFT
Solvent	33 wt% MDEA	7 mol% IL	8 mol% IL	15 mol% methanol	10 mol% IL, 5% methanol
Solvent flow rate exc. water, kg min^{-1}	205.47	1909.7	2125.85	759.67	1461.58/941.41
H$_2$S in the sweet gas, mol frac.$\times 10^6$	3.74	3.89	3.69	3.67	3.84
CO$_2$ in the sweet gas, mol frac.	0.0045	0.021	0.020	0.029	0.022
Water makeup, kg min^{-1}	4.87	2.25	2.30	1.63	2.54
Solvent losses, kg min^{-1}	0.78	0.0	0.0	14.11	0.0/10.48
CH$_4$ in the solvent, kg min^{-1}	0.56	24.98	23.30	7.84	21.50
CH$_4$ in the feed, kg min^{-1}	423.56	423.56	423.56	423.56	423.56
CH$_4$ in the sales gas, kg min^{-1}	423.00	421.68	421.80	421.37	421.10
CH$_4$ recovery %	99.87	99.56	99.58	99.50	99.40
CH$_4$ in the acid gas stream, kg min^{-1}	0.56	1.88	1.74	2.19	2.43
Regeneration duty, MW	6.00	3.16	3.17	1.00	1.80
Regeneration temperature, °C	112.6	107.4	107.0	86.6	97.1
Energy saving %	0.0	47.33	47.17	**83.33**	70.00

In the following section, the use of DEPG and its blend with ILs will be investigated.

6.6 IL-DEPG-based sweetening unit

As a consequence of the high solvent losses and the lower acid gas capacity of methanol compared to IL, the search for another less volatile physical solvent with higher acid gas absorption capacity than methanol is considered for further improvement of the IL cases. Dimethyl ethers of propylene glycol or DEPG is the proposed solvent; it has negligible vapour pressure (9.7×10^{-7} bar) compared to methanol (0.17 bar) at 298.15 K [266]. DEPG also has much higher acid gas absorption capacity than methanol. For example, the solubility of CO$_2$ in DEPG at 273.15 K and 5 bar is 24.5 mole% compared to only 5.9 mole% for methanol at the same conditions, about

four times higher. Moreover, the solubility of H_2S in DEPG at the same conditions is 79.2 mole%, which is about three times higher than that in methanol (the solubility of H_2S in methanol is only 25 mole% at the same conditions) [291, 293, 294].

In this section, the performance of the DEPG as a solvent for gas sweetening in North Caroline unit is first evaluated and compared to the performance of IL. DEPG is tested as a solvent at the North Caroline sweetening unit, and the process is simulated in Aspen Plus V9 using PC-SAFT as the thermodynamic model package. The results are then compared to the optimal IL case determined in Chapter 5. Different DEPG solutions of compositions 5%, 10%, 15% and 20% are tested. Table 6.6 and Table 6.7 provide a summary of the simulation results and the cost analysis of the different investigated compositions for the DEPG solvent, respectively. The optimal composition case, with both the highest energy and total annual cost saving is 10% DEPG and 90% water, for which the results are reported in the third column of each of Table 6.8 and Table 6.9. It is clear from the tables that the regeneration duty of the DEPG cases decreases as the concentration of the DEPG in the solution increase up to 15% composition at which it starts to increase again. The total operating cost and thus the total annual cost follow the same trend. The optimal composition case is that at which the total annual cost is minimum. Then the use of IL-DEPG blend in North Caroline sweetening unit is investigated and compared to the use of IL alone and DEPG alone. There was no solubility data in the literature for the investigated IL with DEPG, thus the interaction between them is ignored.

The DEPG based sweetening process performed better than the base MDEA case with 30% saving in the regeneration duty and 2.75% saving in the total annual cost. This is mainly due to the physical nature of the acid gas absorption process in the DEPG case which requires less energy for solvent regeneration (4.2 MW) compared to 6.0 MW for the chemical based MDEA process. Furthermore, DEPG is less volatile than MDEA, which reduces the solvent losses in the process from 0.78 kg min^{-1} (47 kg hr^{-1}) to 0.27 kg min^{-1} (16 kg hr^{-1}) thus, reduces the operating cost. One disadvantage of DEPG is the high methane solubility compared to that in MDEA, which

Table 6.6: Investigated compositions of DEPG

Case	Base case	DEPG case 1	DEPG case 2	DEPG case 3	DEPG case 4
Solvent	33 wt% MDEA	5 mol% DEPG	10 mol% DEPG	15 mol% DEPG	20 mol% DEPG
Solvent flow rate exc. water, kg min^{-1}	205.47	786.95	866.53	919.80	974.40
H$_2$S in the sweet gas, mol frac.$\times 10^6$	3.74	4.00	3.65	3.52	3.64
CO$_2$ in the sweet gas, mol frac.	0.0045	0.027	0.028	0.029	0.028
Water makeup, kg min^{-1}	4.87	2.62	2.18	2.59	2.66
Solvent losses, kg min^{-1}	0.78	0.27	0.27	0.28	0.29
CH$_4$ in the solvent, kg min^{-1}	0.56	5.78	6.44	6.91	7.30
CH$_4$ in the feed, kg min^{-1}	423.56	423.56	423.56	423.56	423.56
CH$_4$ in the sales gas, kg min^{-1}	423.00	421.39	421.17	421.01	420.80
CH$_4$ recovery %	99.87	99.5	99.4	99.4	99.3
CH$_4$ in the acid gas stream, kg min^{-1}	0.56	2.16	2.39	2.55	2.70
Regeneration duty, MW	6.00	4.38	4.20	4.7	4.9
Regeneration temperature, °C	112.6	103.7	98.8	96.5	95.1
Energy saving %	0.0	27.00	**30.00**	21.67	18.33

Table 6.7: Total annual cost of different investigated DEPG cases (DEPG price = 2.8 US\$.kg^{-1})

Case	Base case	DEPG case 1	DEPG case 2	DEPG case 3	DEPG case 4
Solvent	33 wt% MDEA	5 mol% DEPG	10 mol% DEPG	15 mol% DEPG	20 mol% DEPG
Equipment cost, M\$	0.52	1.44	1.45	1.46	1.54
Total utilities cost, M\$/year	0.499	0.503	0.467	0.464	0.485
Solvent capital cost, M\$	0.005	0.051	0.060	0.065	0.068
Solvent makeup operating cost, M\$/year	0.493	0.397	0.397	0.419	0.427
Total capital cost, M\$	0.526	1.49	1.511	1.527	1.614
Total operating cost, M\$/year	0.992	0.900	0.865	0.883	0.911
Total annual cost, M\$/year	1.044	1.049	1.016	1.036	1.073
Total annual cost saving,%	0.00	-0.49	**2.75**	0.82	-2.73

caused the loss of 6.44 kg min^{-1} (386 kg hr^{-1}) of methane in DEPG compared to only 0.56 kg min^{-1} (33 kg hr^{-1}) of methane in MDEA, see Table 6.8.

In comparison to the C$_6$mimNTf$_2$ IL case, DEPG requires lower solvent flow rate to achieve the same acid gas specification in the sales gas, less compression stages to recover methane, lower water make up flow rate and lower regeneration temperature. The higher acid gas absorption capacity of DEPG and the lower methane solubility in it lead to a reduced solvent flow rate requirement, lower methane loss and lower number of compression stages, therefore, lower utility and capital costs (see Table 6.8 and Table 6.9). The solvent flow rate of the DEPG case (866 kg min^{-1}) is much lower than the solvent flow rate of the C$_6$mimNTf$_2$ IL case (2125 kg min^{-1}). The amount

Table 6.8: DEPG and its blend with IL cases versus IL case for gas sweetening

Case	Base case	$C_6mimNTf_2$ IL	DEPG	$C_6mimNTf_2$-DEPG	$C_8mimNTf_2$-DEPG
Solvent	33 wt% MDEA	8 mol% IL	10 mol% DEPG	10 mol% DEPG, 5 mol% IL	10 mol% DEPG, 5 mol% IL
Solvent flow rate exc. water, kg min^{-1}	205.47	2125.85	866.53	613.00 / 767.35	470.73 / 554.40
H_2S in the sweet gas, mol frac.$\times 10^6$	3.74	3.65	3.65	3.85	3.81
CO_2 in the sweet gas, mol frac.	0.0045	0.020	0.028	0.026	0.029
Water makeup, kg min^{-1}	4.87	2.30	2.18	2.40	2.17
Solvent losses, kg min^{-1}	0.78	0.0	0.27	0.0/0.12	0.0 / 0.13
CH_4 in the solvent, kg min^{-1}	0.56	23.30	6.44	11.57	9.39
CH_4 in the feed, kg min^{-1}	423.56	423.56	423.56	423.56	423.56
CH_4 in the sales gas, kg min^{-1}	423.00	421.80	421.17	420.66	421.03
CH_4 recovery %	99.87	99.58	99.4	99.3	99.4
CH_4 in the acid gas stream, kg min^{-1}	0.56	1.74	2.39	2.90	2.54
Regeneration duty, MW	6.00	3.17	4.20	3.6	3.6
Regeneration temperature, °C	112.6	107.0	98.8	100.7	100.6
Energy saving %	0.0	47.17	30.00	40.00	40.00

of methane in the rich solvent is also significantly reduced to 6.44 kg min^{-1} by using DEPG compared to 23.3 kg min^{-1} in case of IL use. One HP compression stage is enough in the DEPG case to recover methane and reduce its amount in the acid gases stream from 6.44 kg min^{-1} to 2.39 kg min^{-1}. In case of IL, three compression stages are needed to reduce the amount of methane in the acid gases stream from 23.3 kg min^{-1} to 1.74 kg min^{-1}.

Despite of all the above advantages of using DEPG over IL, the IL case is still the winner case with 47% regeneration energy saving and 6.55% TAC saving. The lower regeneration duty of the IL case indicates that acid cases can be released much easier from ILs than from DEPG. The higher TAC of the DEPG case results from the higher solvent operating cost required to make up the solvent losses in the process.

By blending DEPG with the non volatile IL, the DEPG consumption is reduced thus, the amount of solvent losses can also be reduced. A blend of 10 mole% DEPG and 5 mole% IL solution is investigated for use in the same North Caroline sweetening unit and the solvent performance is compared to the previously investigated cases. It was found that the blends of both $C_6mimNTf_2$-DEPG and $C_8mimNTf_2$-DEPG require the same amount of energy to be regenerated (3.6 MW). 40% of the regeneration energy saving is achieved compared to the base MDEA case. The regeneration duty of the IL-DEPG blend cases lies between the regeneration duty of the pure solvent cases,

it is higher than the regeneration duty of the pure IL case (3.17 MW) but lower than that of the pure DEPG case (4.20 MW).

When both IL-DEPG cases were considered for further cost analysis, the C_8mimNTf$_2$-DEPG case is found to be the optimal case with 26.5% saving in the total annual cost compared to 20% for the C_6mimNTf$_2$-DEPG case (see Table 6.9). The higher solvent flow rate requirement of the C_6mimNTf$_2$-DEPG case can be attributed to the lower acid gas solubility in the shorter C_6mimNTf$_2$ IL, which led to a higher capital and utility cost requirement (see Table 6.9).

Table 6.9: Total annual cost comparison of different investigated solvents for gas sweetening (IL/MDEA price = 1)

Case	Base case	C_6mimNTf$_2$ IL	DEPG	C_6mimNTf$_2$-DEPG	C_8mimNTf$_2$-DEPG
Solvent	33 wt% MDEA	8 mol% IL	10 mol% DEPG	10 mol% DEPG, 5 mol% IL	10 mol% DEPG, 5 mol% IL
Equipment cost, M$	0.52	3.33	1.45	1.66	1.56
Total utilities cost, M$/year	0.499	0.637	0.467	0.488	0.416
Solvent capital cost, M$	0.005	0.058	0.060	0.046	0.038
Solvent makeup operating cost, M$/year	0.493	0.00	0.397	0.177	0.192
Total capital cost, M$	0.526	3.385	1.511	1.705	1.593
Total operating cost, M$/year	0.992	0.637	0.865	0.665	0.608
Total annual cost, M$/year	1.044	0.976	1.016	0.835	0.768
Total annual cost saving,%	0.00	6.55	2.75	20.02	**26.51**

As a result of the higher IL flow rate in the C_6mimNTf$_2$-DEPG case, higher amount of methane (11.57 kg min^{-1}) is lost in the process than in the C_8mimNTf$_2$-DEPG case (9.39 kg min^{-1}). This increased the compression requirement of the C_6mimNTf$_2$-DEPG case, which also contributed to the higher equipment and utility costs.

The slightly higher solvent losses in the C_8mimNTf$_2$-DEPG resulted from the slightly higher temperature profile across the stripper column. It is worth mentioning that, the equipment cost of the IL-DEPG blend cases is significantly reduced by about 51% compared to the IL case. This is mainly because of the lower methane loss in the rich solvent for the IL-DEPG cases (11.57 kg min^{-1} and 9.39 kg min^{-1}) compared to the IL case (23.3 kg min^{-1}), which allowed the elimination of two compression stages. In conclusion, the blend of 5mol% of C_8mimNTf$_2$ IL and 10 mol% of DEPG is the most profitable option for use as an alternative solvent to MDEA in

North Caroline sweetening unit as it achieved the highest TAC saving percentage of the investigated cases.

Figure 6.9 provides a comparison of the amount of solvent losses in kg min^{-1} for the studied cases. Methanol cases are not included in the figure due to the significantly high amount of solvent losses, ranging from 10 to 14 kg min^{-1} compared to the other studied cases. The base case is the highest in the solvent losses after methanol cases 0.78 kg min^{-1} and the DEPG case is the second highest in the solvent losses with 0.27 kg min^{-1}. Recalling that ILs have zero losses due to their negligible volatility, blending DEPG with ILs helped to further reduce the losses to less than 0.15 kg min^{-1}. Therefore, the IL-DEPG blend cases recorded the lowest amount of solvent losses in the studied cases (0.12 kg min^{-1} for the C_6mimNTf$_2$-DEPG case and 0.13 kg min^{-1} for the C_8mimNTf$_2$-DEPG case). The detailed flow sheets, conditions, simulation inputs and specifications are given in Appendix C.
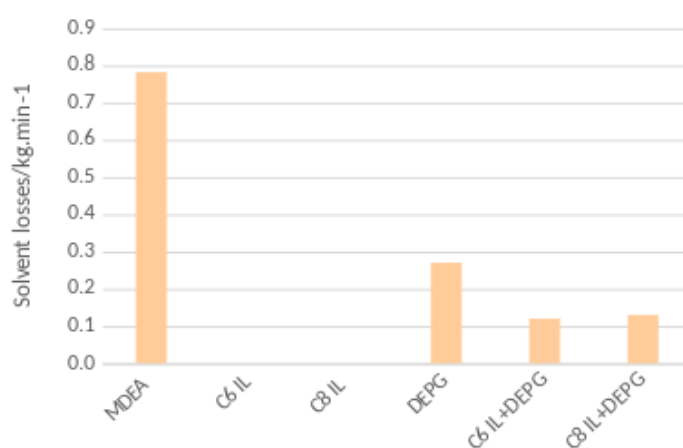
Figure 6.9: Solvent losses in kg min^{-1} for the studied cases.

In summary, blending other physical solvents such as methanol or DEPG with alkyl imidazolium ILs to be used for acid gas removal is investigated in this chapter. The use of methanol and its blend in the North Caroline sweetening unit significantly reduces the energy consumption of the unit. However, the huge amount of lost methanol in

the process considerably raised the solvent operating cost share to the TAC causing methanol cases to fail against the IL cases. Blending IL with DEPG is found to be a more promising option for use in North Caroline sweetening unit in terms of TAC saving. The following section, provides a discussion and analysis of the key simulation results of the investigated cases.

6.7 Economic analysis of results

In this section, the key simulation results considered in making a decision on the optimal case are discussed and analysed. Two main factors contribute to the final decision on the selection of the optimal case. The first is the energy requirement of the process, and the second is the total annual cost (TAC). The former is mainly governed by the solvent and water make up flow rate requirements and the regeneration energy demand, while the latter is governed by the overall cost of the process, which includes the capital and operating costs. Both factors are interconnected, as the solvent and energy costs are included in the TAC cost. However, if energy demand reduction is the main concern, only the first factor is considered in the optimal process selection, and energy analysis is enough to make the decision. On the other hand, if the overall cost of the process over the project life time is the main concern, then the TAC analysis should also be considered in the process selection.

In order to improve the IL sweetening unit presented in Chapter 5, in this chapter, the blend of ILs with other physical solvents including methanol and DEPG is examined as an alternative solvent for acid gas removal in North Caroline sweetening unit.

In an effort to reduce the amount of methane that needs to be recovered from the rich IL, the use of methanol and its blend with IL as a solvent in the in North Caroline sweetening unit is first examined. Although the use of methanol led to a significant reduction in the amount of methane in the rich solvent as well as the regeneration energy consumption, the remarkably higher volatility of methanol compared to ILs led to a substantial increase in the solvent operating cost, consequently, the total annual cost.

Therefore, methanol use did not improve the economy of the optimal IL cases decided in Chapter 5.

Next, the use of DEPG and its blend with ILs is considered. DEPG is characterised by its higher acid gas absorption capacity than ILs and methanol. It also possesses much lower vapour pressure than methanol and much lower methane solubility than ILs. This explains the lower solvent flow rate requirements for the DEPG cases compared to the IL cases to achieve the same sales gas specification. Moreover, DEPG cases require much less solvent make up compared to methanol cases and requires much less compression stages than IL cases to recover methane (HP stage only). DEPG also is much less viscous than the investigated ILs, its 16 times less viscous than C_8mimNTf$_2$ IL and 12 times less viscous than C_6mimNTf$_2$ IL (see Table 6.1). Therefore, blending DEPG with IL would also help to reduce the solvent viscosity, the pumping requirement and enhance the mass transfer efficiency of the process.

Figure 6.10 shows how the choice of solvent and its concentration affects the amount of methane that needs to be recovered from the rich solvent. The number of compression stages required for each case is also indicated in the figure. For C_6mimNTf$_2$ IL, C_8mimNTf$_2$ IL and the DEPG, where different solvent concentrations were tested, the amount of methane in the rich solvent is represented by the blue, red and green curves, respectively in Figure 6.10. The IL-DEPG blend cases (grey and brown symbols) and the base case (orange symbol) are represented by one point for each case. To reduce the amount of methane in the rich C_6mimNTf$_2$ IL solvent that otherwise would be lost with the acid gases, from 23 kg min^{-1} to below 1.74 kg min^{-1}, three stage compression (HP, MP and LP) is required. If DEPG is to be used as a solvent, only one HP compressor is required to recover methane. This was also the case when IL-DEPG blend is used. For the C_6mimNTf$_2$ IL-DEPG blend case, only one HP compressor is required to reduce the amount of methane in the rich solvent from 11.6 kg min^{-1} to 2.9 kg min^{-1}. The same applies for the C_8mimNTf$_2$ IL-DEPG blend case (see Table 6.8). For the base MDEA case represented by the orange symbol in Figure 6.10, the amount of methane in the rich MDEA is already low enough (0.56
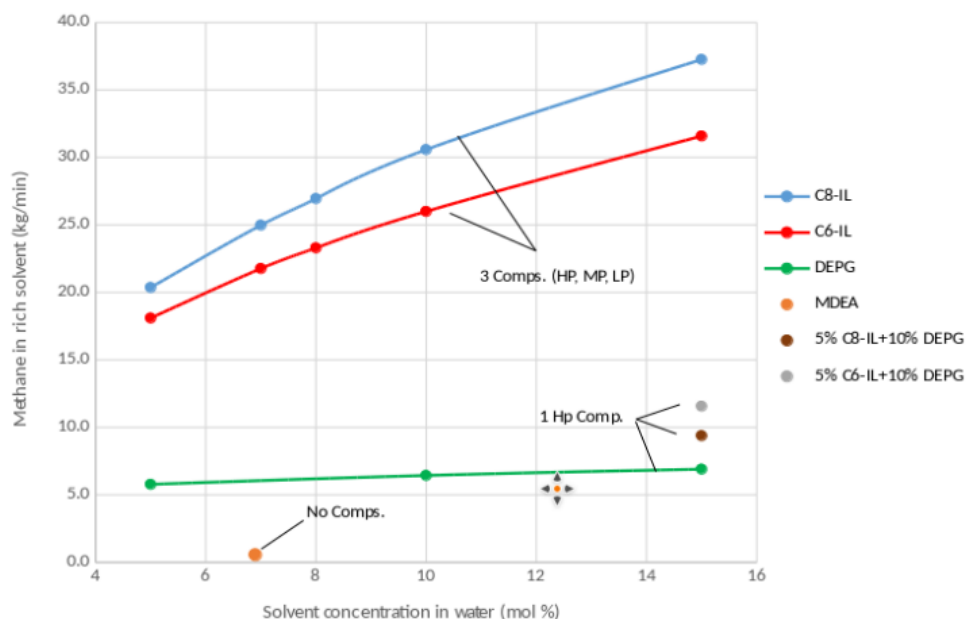
Figure 6.10: Methane in the rich solvent for the studied cases.

kg min^{-1}) due to the high selectivity of MDEA to acid gases over methane.

A summary of equipment sizes and equipment costs for the IL-DEPG blend cases along with the base case and the two optimal composition IL cases determined in Chapter 5 is provided in Table 6.10 and Table 6.11, respectively. Identical absorber and stripper towers were used for both IL-DEPG cases, however, the C_6 IL-DEPG case required larger coolers, flash tanks, compressor, pump and storage tank due to the larger flowrate requirement. In the IL-DEPG cases, two coolers, one flash tank, one pressure valve and two compressors were eliminated compared to the optimal IL cases obtained in Chapter 5. As a result, the total equipment cost is further reduced by about 50% compared to the IL cases. The complexity of the process flowsheet was also reduced in comparison to the IL cases flowsheet shown in Figure 5.5 in Chapter 5. Figure 6.11 shows the flowseet of the IL-DEPG blend cases.

Regeneration energy analysis of the investigated cases shows that methanol cases
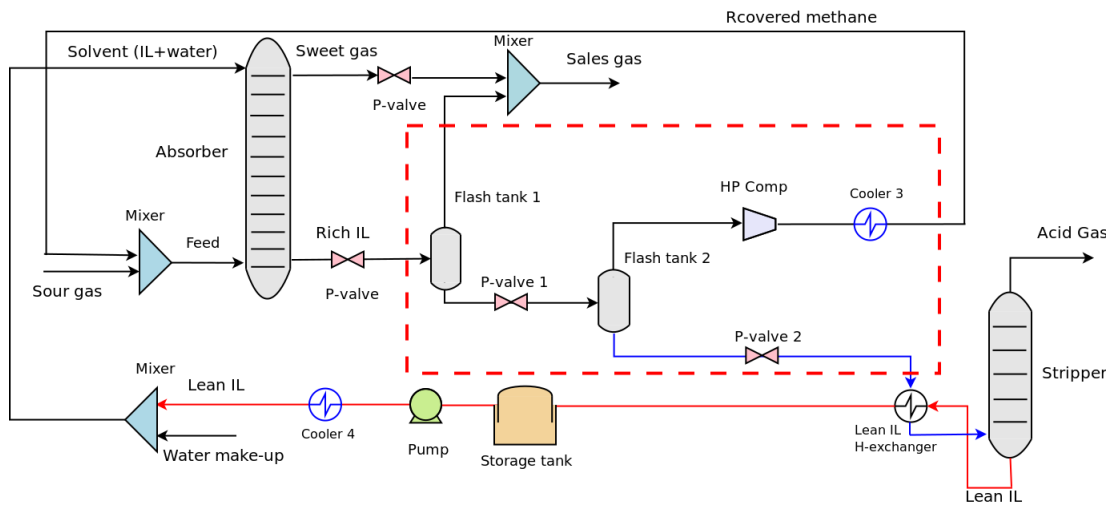
Figure 6.11: North Caroline plant gas sweetening unit with IL-DEPG blend as a solvent.

Table 6.10: Summary of equipment sizes for the base case, the two optimal composition IL cases and the IL-DEPG blend cases. For equipment names refer to Figure 5.2 and Figure 5.5.

Equipment sizing parameter	Base case (MDEA)	8 mol% C_6 IL	7 mol% C_8 IL	5 mol% C_6 IL + 10 mol% DEPG	5 mol% C_8 IL + 10 mol% DEPG
Absorber tower diameter, m	0.91	1.07	1.07	0.91	0.91
Absorber tower height, m	22.56	22.56	22.56	22.56	22.56
Stripper tower diameter, m	1.68	1.37	1.52	0.91	0.91
Stripper tower height, m	7.32	7.32	7.32	7.32	7.32
Stripper condenser area, m^2	47.59	4.06	4.07	5.79	5.63
Condenser accumulator diameter, m	0.91	0.91	0.91	0.91	0.91
Condenser accumulator length, m	2.74	2.74	2.74	2.74	2.74
Stripper reboiler area, m^2	446.65	207.91	210.80	159.63	164.51
Cooler area, m^2	19.86	-	-	-	-
Cooler 1 area, m^2	-	1.02	1.32	-	-
Cooler 2 area, m^2	-	1.25	1.39	-	-
Cooler 3 area, m^2	-	4.05	4.23	1.55	1.18
Cooler 4 area, m^2	-	141.34	136.17	273.15	172.66
Flash tank 1 diameter,m	-	2.13	2.13	1.83	1.83
Flash tank 1 height,m	-	6.55	6.40	5.79	5.33
Flash tank 2 diameter,m	-	2.13	2.13	1.83	1.83
Flash tank 2 height,m	-	6.55	6.40	5.64	5.33
Flash tank 3 diameter,m	-	2.13	2.13	-	-
Flash tank 3 height,m	-	6.55	6.40	-	-
LP compressor driver power, kW	-	55.13	58.32	-	-
MP compressor driver power, kW	-	62.69	65.58	-	-
HP compressor driver power, kW	-	72.82	76.41	46.77	33.08
Pump power, kW	94.29	336.81	322.15	217.83	167.09
Lean solvent HEX area, m^2	7.11	107.73	105.43	44.02	60.23
Storage tank diameter, m	1.25	2.13	2.13	1.83	1.83
Storage tank height, m	4.57	6.55	6.40	5.64	5.18

Table 6.11: Summary of equipment costs for the base case, the two optimal composition IL cases and the IL-DEPG blend cases. For equipment names refer to Figure 5.2 and Figure 5.5.

Equipment name	Base case (MDEA)	8 mol% C_6 IL	7 mol% C_8 IL	5 mol% C_6 IL + 10 mol% DEPG	5 mol% C_8 IL + 10 mol% DEPG
Absorber tower	153700	188200	188200	153700	153700
Stripper condenser	17200	9700	9700	9900	9900
Condenser accumulator	12600	12600	12600	12600	12600
Stripper reboiler	101000	60600	61100	51200	51700
Stripper reflux pump	5200	4500	4500	4500	4500
Stripper tower	68800	60400	64900	43400	43400
Cooler	15100	-	-	-	-
Cooler 1	-	8400	8500	-	-
Cooler 2	-	8500	8500	-	-
Cooler 3	-	10400	10400	8700	8600
Cooler 4	-	53000	50900	98600	60800
Flash tank 1	-	93000	92100	65200	63400
Flash tank 2	-	57200	56700	37700	37100
Flash tank 3	-	37400	37200	-	-
LP compressor	-	875000	880800	-	-
MP compressor	-	735600	738800	-	-
HP compressor	-	796100	801900	973700	911700
Pump	71400	152600	152200	129500	90500
Lean solvent HEX	10100	28100	27900	16900	19700
Storage tank	50700	107300	106200	80200	77700
Total equipment cost (M$)	0.51	3.30	3.31	1.69	1.55

provided the lowest energy consumption rates and the IL cases are the second lowest cases in the regeneration duty (see Figure 6.12). The DEPG case requires a higher amount of energy to be regenerated than IL cases, however, when blended with IL the regeneration duty can be slightly reduced.
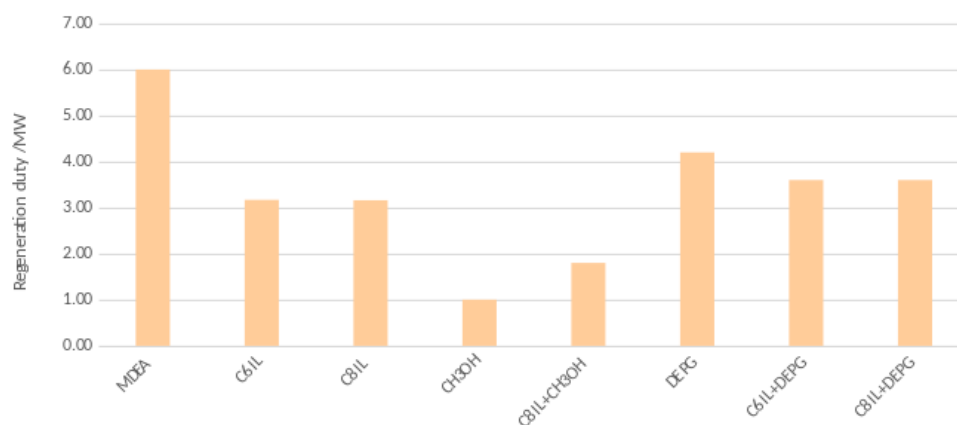
Figure 6.12: Regeneration duty for the studied cases.

Total annual cost analysis of the DEPG and its blend with IL cases revealed that blending DEPG with ILs can improve the economics of the IL sweetening unit examined in Chapter 5. Blending C_8mimNTf$_2$ IL with DEPG is found to be the most promising option for use in North Caroline sweetening unit with 26.5% TAC saving (see Table 6.8 and Table 6.9). Figure 6.13 shows the TAC saving percentage for the IL-DEPG blend cases and the IL cases examined in Chapter 5.
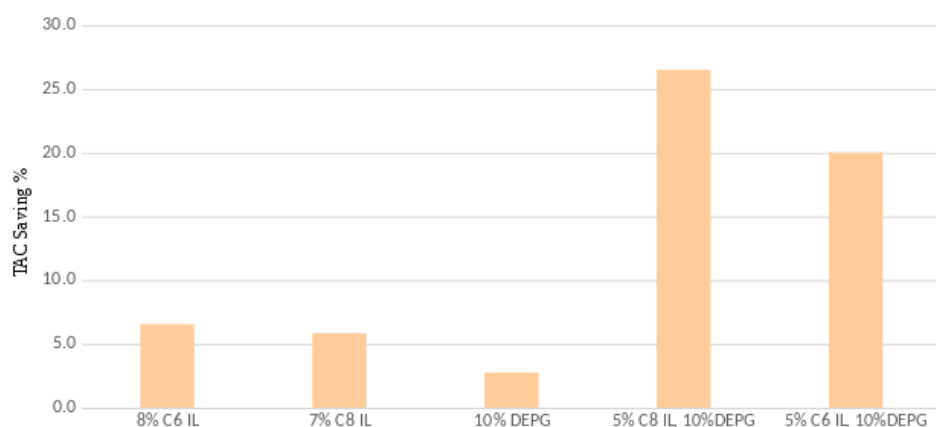
Figure 6.13: Total annual cost saving% for the studied cases.

The higher total annual cost demand of the C_6mimNTf$_2$ IL-DEPG case compared to the C_8mimNTf$_2$-DEPG IL case, can be explained by the lower acid gas solubility in the shorter C_6mimNTf$_2$ IL, which led to a higher solvent flow rate requirement, thus a higher capital and utility cost requirement. In the following section, the possibility of modifying the existing North Caroline amine process flowsheet (the base case) so that a mixture of 5 mol% IL, 10 mol% DEPG and 85% water is used instead of MDEA as a solvent is discussed.

6.8 Amine sweetening process retrofit

Retrofit is the redesign of an existing process to improve its performance, while ensuring the effective use of the existing facilities and avoiding unnecessary expenses of purchasing new equipment [295, 296]. The need for improvement arises for many reasons, such as increasing the production capacity, processing of new materials, improving the product quality, improving the process economics, safety and operability and reduce its environmental impact [295]. In this section, the possibility of retrofitting the existing North Caroline amine process with a blend of $C_6mimNTf_2$ or $C_8mimNTf_2$ ILs and DEPG as a solvent instead of MDEA, while minimising the structural modifications and the need to purchase new pieces of equipment is discussed. This can be done by comparing the process flowsheet of the North Caroline base case to that of the IL-DEPG case in terms of the required facilities and equipment sizes.

By comparing the base case flowsheet shown in Figure 5.2 to that of the IL-DEPG case shown in Figure 6.11; it is evident that some extra pieces of equipment are required for the IL-DEPG case, these are surrounded by the red dashed rectangle in Figure 6.11. The extra equipment include: two flash tanks, a high pressure compressor and a cooler. These would need to be purchased if retrofit is to be implemented to the existing North Caroline MDEA unit. The purchase cost of the extra pieces of equipment is approximately \$1.02 million. As mentioned previously, the main reason for the presence of these extra pieces of equipment is the need for the recovery of the dissolved methane in the IL.

The sizes of the equipment in common between the two flowsheets should also be compared to decide whether the existing facilities could still be utilised for the IL-DEPG process with minor internal changes or whether new pieces of equipment would need to be purchased. The equipment in common include: the absorber, the stripper, the lean solvent heat exchanger, the solvent storage tank, the lean solvent pump and the lean solvent cooler. Table 6.12 summarises the equipment sizes of the base case and the optimal IL-DEPG case along with the retrofit requirements. By comparing the sizes listed in Table 6.12 for the base case and the IL-DEPG blend cases, it is clear that

the absorbers of the base case and the IL-DEPG blend cases are identical. The same base case absorber was used for the IL-DEPG blend cases to minimize the need for retrofit, thus the existing absorber in the North Caroline unit can be left in place.

Table 6.12: Comparison of the equipment sizes of the base case and the optimal IL-DEPG blend case along with the retrofit requirement. For equipment names refer to Figure 5.2 and Figure 5.5.

Equipment sizing parameter	Base case (Existing)	C$_8$ IL-DEPG (New)	Retrofit requirement
Absorber tower diameter, m	0.91	0.91	Keep the existing
Absorber tower height, m	22.56	22.56	
Stripper tower diameter, m	1.68	0.91	Keep the existing
Stripper tower height, m	7.32	7.32	
Stripper condenser area, m^2	47.59	5.63	Keep the existing exchangers and consider plugging some tubes, use smaller bundle or swapping the exchangers
Condenser accumulator diameter, m	0.91	0.91	Keep the existing
Condenser accumulator length, m	2.74	2.74	
Stripper reboiler area, m^2	446.65	164.51	Keep the existing exchangers and consider plugging some tubes, use smaller bundle or swapping the exchangers
Cooler area, m^2	19.86	-	
Cooler 3 area, m^2	-	1.18	Install a new cooler
Cooler 4 area, m^2	-	172.66	Install an additional cooler in parallel to the existing or consider swapping
Flash tank 1 diameter,m	-	1.83	Install a new flash tank
Flash tank 1 height,m	-	5.33	
Flash tank 2 diameter,m	-	1.83	Install a new flash tank
Flash tank 2 height,m	-	5.33	
HP compressor driver power, kW	-	33.08	Install a new compressor
Pump power, kW	94.29	167.09	install a different impeller or an additional pump in parallel to the existing
Lean solvent heat exchanger area, m^2	7.11	60.23	Install an additional heat exchanger in parallel to the existing
Storage tank diameter, m	1.25	1.83	Install a small tank in parallel to the existing
Storage tank height, m	4.57	5.18	

The stripper of the IL-DEPG blend case has a slightly smaller diameter (0.91 m) than the base case (1.68 m) with the same height. This would provide a spare capacity in the stripper if the existing column is to be kept in place and used to regenerate the IL-DEPG solution instead of MDEA. However, the column should always operate above the minimum flow rate conditions. Larger cross-sectional area may lead to reduced vapour flow and reduced pressure so that the vapour force is insufficient to hold up the liquid on trays and the liquid starts to flow through the pores of the sieve tray [297]. This phenomenon is called weeping. Reducing the tray hole diameter is the

first measure to avoid weeping [298].

Due to the significant achieved saving in the regeneration energy by using IL-DEPG for gas sweetening as an alternative to MDEA (40%), both the condenser and reboiler of the IL-DEPG case have significantly smaller areas than those of the base case (see Table 6.12). The existing base case condenser and reboiler could still be utilised for the IL-DEPG process, however, plugging some of the heat exchanger tubes, replacing the tube bundle with a smaller one or swapping the heat exchanger with a smaller one in the process would need to be considered [296].

The lean solvent heat exchanger required by the IL-DEPG case (60.23 m^2) is larger than that of the base case (7.11 m^2). This also applies for the lean solvent cooler due to the larger flow rate requirement for the IL-DEPG case. The installation of an additional heat exchanger in parallel to the existing one might be needed in case of retrofit to increase the heat transfer area and accommodate the larger flow rate requirement [296].

The required pumping power for the IL-DEPG case is much larger (167.09 kW) compared to that of the base case (94.29 kW). This is because of the much higher viscosity and flow rate of the IL-DEPG solution compared to that of the MDEA solution. To increase the capacity of the existing pump, the installation of a different impeller [299] or an additional pump in parallel to the existing one would need to be considered.

The storage tank is slightly larger for the IL-DEPG case due to the larger flow rate requirement. Another small tank in parallel to the existing tank might be needed in case of retrofit if the IL-DEPG solution can not be accommodated in the existing one.

In fact, unlike the new or grass-root design, the retrofit design focuses on maximising the utilisation of the existing facilities. The estimation of the cost of a retrofit project is much more difficult than that for a grass-root project [296]. Implementation of a retrofit design requires a thorough investigation of all retrofit options and consid-

eration of the safety and operability of the process which is beyond the focus of this research.

6.9 Conclusions

To further improve the IL processes simulated in Chapter 5, blending them with other physical solvents such as methanol or DEPG is investigated in this chapter. First, the use of methanol and its blend with IL is investigated and then DEPG and its blend with IL is considered. The results of all cases are then compared to each other and to that of the IL cases of Chapter 5.

One drawback of using ILs in specific and physical solvents in general is the high methane solubility in them compared to amines. For example, the mole fraction solubility of methane in C_4mimNTf$_2$ IL at 313.15 K and 51 bar is about 0.1 [228] compared to only 0.02764 in MDEA [231]. Therefore, multistage compression is needed to recover methane from the solvent. The solubility of methane in the investigated physical solvents follows the order: IL > DEPG > methanol. This implies that blending DEPG or methanol with IL reduces the solubility of methane in the solvent blend. This was successfully achieved for both IL-methanol blend and IL-DEPG blend. However, methane solubility is not the sole factor that should be considered during the selection process of the best solvent option. Other factors, such as the solvent flow rate requirement, the solvent losses and its regeneration energy requirement need to be considered.

In this work, the total annual cost (TAC) saving of the process is used as the main criterion for the selection of the optimal process. Although methanol and its blend with IL processes showed the lowest regeneration energy requirements of the investigated cases, they have been withdrawn from the cost analysis investigation due to the remarkably high amount of solvent losses compared to IL based processes. DEPG and its blend with IL cases requires higher regeneration energy than IL cases with a slightly lower energy demand for the blend cases than the DEPG case. The IL-DEPG blend cases, however, achieved the highest TAC saving percentage with better per-

formance for the C_8mimNTf$_2$ IL-DEPG case over C_6mimNTf$_2$ IL-DEPG case. The former achieved 26% saving in the TAC while the latter achieved 20% TAC saving compared to the base MDEA case. The winner C_8mimNTf$_2$ IL-DEPG case achieved about 21% TAC saving (209 k$ per year) compared to the optimal IL case determined in Chapter 5 with much less compression and flow rate requirement than the optimal IL case therefore, lower capital and operating costs.

Finally, a brief discussion of the base case retrofit possibility with IL-DEPG as an alternative solvent to MDEA is presented. To decide whether the retrofit design is much more profitable than the grass-root design, a detailed retrofit study that takes into consideration all retrofit options, the cost penalty of lost production due to process shutdown to carry out the required structural changes and safety issues is needed.

Chapter 7

Conclusions and recommendations

Although natural gas is regarded as the cleanest type of fossil fuel, due to its relatively low carbon content, it contains impurities that need to be separated before the gas can be delivered to its end users. Acid gases, such as CO_2 and H_2S are among these impurities. These gases are corrosive, toxic, have low heating value and their presence causes several complications in the process facilities such as corrosion and pipeline blockage due to CO_2 dry ice formation. Consequently, they must be removed from natural gas before it can be delivered and used.

Several approaches have been used in industry to remove acid gases from natural gas. Chemical absorption using amines is the most popular commercial available route. Amines are characterised by their high efficiency in acid gas removal and their availability at low cost. However, amine processes have some drawbacks including, amine losses, corrosion problems and high regeneration energy consumption. Physical absorption, adsorption, membranes and cryogenic distillation are alternative industrial approaches to amine processes. The selection of the proper process depends on several factors, either operational, economic or environmental factors.

In this thesis, we focused our attention on the use of physical absorption for gas sweetening as an alternative to amines. Ionic liquids, as physical solvents and their blend with other classic physical solvents, such as methanol and DEPG, were exam-

ined. Generally, physical solvents are characterised by their higher selectivity for hydrogen sulfide over carbon dioxide, the lower regeneration requirements, as they can be simply regenerated by reducing the pressure, and finally, the higher acid gas solubility at high pressure. Ionic liquids are characterised by their negligible volatility and high thermal stability, thus by using them for gas sweetening instead of amines, the solvent losses, thermal decomposition and the consequent environmental impact can be reduced. Furthermore, using ILs for gas sweetening can lead to an overall reduction in energy consumption because physical absorption takes place, rather than chemical absorption. Thus, no chemical bonds are formed in the absorption step, which makes the regeneration step easier and reduces the regeneration energy requirement. Finally, the tunable structure of ILs can be utilised to modify the absorption selectivity and capacity of the IL.

Understanding the thermodynamic of phase equilibrium is of central importance for solving the VLE problem involved in any process for acid gas separation from natural gas. Thermodynamic models used in literature for solving VLE have been divided into two broad categories: equations of state (EOS) models and activity coefficient models. Activity coefficient models can only be used to describe liquid phase non ideality. EOSs can be used to describe both phases, however, EOS are known of their poor prediction for liquid phase properties and poor representation of VLE of highly non-ideal systems with multiple phases and associating components such as water, alcohols, amines and acids.

For systems containing ILs, besides the cubic EOSs and the activity coefficient models, both the quantum mechanics-based models and the statistical mechanics-based molecular approaches have also been used in literature to represent the phase equilibrium of different binary and ternary IL containing systems. All of the above models have been successfully used to represent the solubility of H_2S, CO_2, and other gases in some ILs and to measure the thermodynamic properties of the IL-containing mixtures. However, binary interactions parameters, found by fitting to experimental data, have been used to enhance the accuracy of the VLE results; these parameters can be depen-

dent or independent of temperature.

The statistical associating fluid theory (SAFT), one of the statistical mechanics-based molecular approaches, have been successfully used to represent complex systems with large molecules such as polymers, associating and polar compounds. In this work, the PC-SAFT EOS, one of the SAFT models, was selected to represent the VLE of the IL-containing systems as most ILs are associating compounds with a complex long chain structure.

The PC-SAFT model was used to quantitatively describe the thermodynamics of acid-gases in four methylimidazolium bis (trifluoromethylsulfonyl) imide ionic liquids. The inclusion of the electrolyte term was examined by treating the IL as separate cations and anions and compared to treating them as a system of neutral molecules. The electrolyte term improved the high pressure density of the IL and solubility of acid gases on it, whereas its effect was insignificant at low pressures. There was no need for empirical binary interaction parameters, as was required in previous studies which makes the model predictive for ternary systems. The predictive capability was enhanced by allowing the description of different ILs anion-cation combinations without the need for additional experimental data. Strategy 2 developed in this study allows the description of different anion-cation combinations in the future. The effect of using different self-association schemes for the ILs was also investigated for the first time here. By selecting the proper association scheme, the solubility of acid gases in ILs was accurately described using PC-SAFT. The accuracy of PC-SAFT was significantly improved for these systems without the need to include empirical binary interaction parameters, as was required in previous studies. Experimental data for the solubility of methane in ILs are scarce in literature, further measurements are needed for more accurate model parameterization. The effect of the inclusion of the polar term, which accounts for the dipolar interactions in systems containing polar compounds such as ILs, on the PC-SAFT model prediction capability should also be considered in future. Experimental data for the properties of mixtures of water with the investigated class of ILs are also scarce in literature, therefore, water and ILs were assumed as completely

miscible forming one phase. However, in reality they are not miscible and form two liquid phases. This assumption may have implications for the acid gas removal process from natural gas, which need to be considered in future for further investigations.

In Chapter 5, the existing North Caroline amine unit was chosen as the base case to examine the consequences of replacing MDEA with alkyl imidazolium ILs. The PC-SAFT was selected to describe the thermodynamic properties of the IL-containing systems for the sweetening process in Aspen Plus V9. Two of the ILs studied in Chapter 4 were tested: C_6mimNTf$_2$ and C_8mimNTf$_2$. Despite the fact that acid gases are more soluble in MDEA than in ILs and MDEA is more selective to acid gases over methane than ILs, the use of ILs was found to be more profitable than MDEA. First, because ILs have negligible volatility compared to MDEA, no makeup was needed for the IL process, unlike the MDEA process. Second, because ILs are physical solvents, they do not react chemically with the acid gases and, therefore, are easier to regenerate, requiring much less energy than MDEA. Up to 47% of the regeneration energy was saved by the use of ILs in replacement of MDEA. Third, because IL cases had lower temperatures in the stripper, less water was lost due to evapouration and less make up water was required.

Total annual cost analysis showed that a saving of up to 7% can be achieved when ILs were used instead of MDEA with superior performance for C_6mimNTf$_2$ over C_8mimNTf$_2$ due to its shorter alkyl chain length and hence lower methane solubility and less compression of the methane to be recycled after being recovered from the solvent is required. The solvent operating cost saving was the dominant contributor to the total annual cost saving for IL cases. Although the price of IL is unknown, it was assumed as a multiple of MDEA price to provide an estimate for the ILs price at which profit can still be achieved. This provides a target price for IL producers to manufacture ILs in bulk. The main drawback of the IL-based process is the high methane solubility in IL which led to need for compression to recover methane from the rich solvent. The capital cost penalty incurred by the need for methane recovery in IL cases can be offset by the saving in operating cost and up to 68 k$ per year of the TAC can

still be saved.

For further improvement of the IL processes simulated in Chapter 5, blending them with other physical solvents such as methanol or DEPG was investigated in Chapter 6. The high methane solubility in ILs compared to that in MDEA urged the need for multistage compression to recover methane from the ILs. By blending ILs with other solvents at which methane is less soluble, the need for multistage compression can be reduced. The solubility of methane in the investigated physical solvents follows the order: IL > DEPG > methanol. Blending DEPG or methanol with IL successfully reduced the solubility of methane in the solvent blend. Besides methane solubility, solvent flow rate requirement, solvent losses and its regeneration energy requirement were also considered in the solvent selection process.

Cases of methanol and its blend with IL failed to achieve any TAC saving despite the significantly lower regeneration duty. This is because of the highly volatile nature of methanol, DEPG and its blend with IL processes requires higher regeneration energy than IL cases with a slightly lower duty for the blend cases than the DEPG case. The IL-DEPG blend cases, however, achieved the highest TAC saving percentage with better performance for the C_8mimNTf$_2$ IL-DEPG case over C_6mimNTf$_2$ IL-DEPG case. About 209 K\$ can be saved each year in the TAC for the C_8mimNTf$_2$ IL-DEPG case compared to the optimal C_6mimNTf$_2$ IL case of Chapter 5 with much less compression and flow rate requirement, therefore, lower capital and operating costs. Compared to the base case, up to 40% and 27% of the regeneration energy consumption and the total annual cost, respectively were saved by using a blend of C_8mimNTf$_2$-IL with DEPG.

To the best of our knowledge, retrofit of the whole amine sweetening process with IL-DEPG blend as a replacement for MDEA is considered for the first time here. The extra pieces of equipment and extra size requirement to retrofit the existing amine process are determined and some retrofit options are presented. The approximate purchase cost of the extra required pieces of equipment is \$1.02 million, excluding the cost of some structural changes to increase the capacity of some existing facilities such as the

pump, tanks, and exchangers. This extra cost however can be offset by the saving achieved in the operating cost. A detailed retrofit study with a thorough investigation to all retrofit scenarios, their benefits and limitations is recommended to decide whether it is much more economically feasible than the new design of an IL-DEPG based sweetening process.

Apart from the measurements provided by the two studies of Raeissi and Peters [228] and Kumelan et al. [229] for methane solubility in ILs, experimental measurements for the solubility of methane in alkyl imidazolium ILs are scarce in literature. Further experimental measurements are recommended to allow for more accurate model parameterization.

Investigation of other IL cation-anion combinations that provide an efficient and selective acid gas removal from natural gas should be considered in future. It has been shown by [58] that the use of ILs consisting of cations and anions with appropriate functional groups, such as oxygen containing groups or amine group, could improve the interactions of ILs with the acid gases, making ILs as effective as conventional amines. Deep eutectic ILs is another class of green solvent characterised by their non-toxicity, ease of accessibility, low melting points, and low cost [300]. Their utilisation as an alternative solvent to amines for gas sweetening is another possible area of future investigations. Further experimental measurements of different IL properties such as viscosity, heat capacity, and the solubility of natural gas species and water in them is of crucial importance. This allows for more accurate thermodynamic modelling of such systems.

Blending chemical and physical solvents such as amines and ILs to be used for gas sweetening is also worth to be considered for future experimental and thermodynamic modelling investigations. Integrating the advantages of both solvents helps to improve the efficiency of the sweetening process. Finally, although several studies have addressed the toxicity and biodegradability of the most commonly used ILs [76, 77, 78], more detailed research is needed before utilising them for industrial applications.

Appendix A

Cubic equations of state and flash calculation

In the following sections, two of the most commenly known equations of state, PR and SRK, are presented. They have been widely used in literature for the calculation of pure and mixture thermodynamic properties.

A.1 Peng Robinson cubic equation of state (PR EOS)

The general form of PR EOS is given by:

$$P = \frac{RT}{V - b} - \frac{a(T)}{V(V + b) + b(V - b)} \tag{A.1}$$

Provided that;

$$A = \frac{aP}{R^2 T^2} \tag{A.2}$$

$$B = \frac{bP}{RT} \tag{A.3}$$

$$Z = \frac{PV}{RT} \tag{A.4}$$

Equation can be rewritten in terms of compressibility factor Z and in the standard cubic form as:

$$Z^3 - (1 - B)Z^2 + (A - 3B^2 - 2B)Z - (AB - B^2 - B^3) = 0 \tag{A.5}$$

where

$$a = 0.45724 \frac{R^2 T_c^2}{P_c} \tag{A.6}$$

$$b = 0.07780 \frac{RT_c}{P_c} \tag{A.7}$$

For multi-component mixtures, the following mixing rules were used [301]:

$$a_m = \sum \sum y_i y_j (\alpha a)_{ij} \qquad (\alpha a)_{ij} = \sqrt{(\alpha a)_i (\alpha a)_j} (1 - k_{ij}) \tag{A.8}$$

$$b_m = \sum_i y_i b_i \tag{A.9}$$

$$\alpha = \left[1 + (0.37464 + 1.54226\omega - 0.26992\omega^2)(1 - \sqrt{T_r}) \right]^2 \tag{A.10}$$

where

$$T_{r_i} = \frac{T}{T_{c_i}} \tag{A.11}$$

a and b are the pure component parameters given by equation A.6 and equation A.7 above.

The form for the fugacity coefficient ϕ derived from PR-CEOS is:

$$\ln \phi_i = (BB)_i(Z-1) - \ln(Z-B) - \frac{A}{2\sqrt{2}B}((AA)_i - (BB)_i) \ln \left[\frac{Z+(\sqrt{2}+1)B}{Z-(\sqrt{2}-1)B} \right] \tag{A.12}$$

where ϕ_i is the fugacity coefficient and Z is the compressibility factor calculated from equation A.5 above.

$$AA_i = \frac{2}{(a\alpha)_m} \left[\sum_j (a\alpha)_{ij} \right] \qquad BB_i = \frac{b_i}{b_m} \tag{A.13}$$

$$A = \frac{a\alpha P}{R^2 T^2} \qquad B = \frac{bP}{RT} \tag{A.14}$$

The solution of equation A.5 for the compressibility factor produces three roots. The largest root represents the vapour phase compressibility factor (Z^v), the smallest represents the liquid phase compressibility factor (Z^l) and the one in the middle is ignored as it has no physical meaning.

When Z^v is substituted in equation A.5, the vapour phase fugacity coefficient (ϕ_i^v) is obtained while the liquid phase fugacity coefficient (ϕ_i^l) is obtained when Z^l is used.

A.2 Soave Redlich Kwong (SRK EOS)

SRK EOS has a similar form to PR EOS with different constants, and is given by:

$$P = \frac{RT}{V - b} - \frac{a(T)}{V(V + b)} \tag{A.15}$$

Provided that;

$$A = \frac{aP}{R^2 T^2} \tag{A.16}$$

$$B = \frac{bP}{RT} \tag{A.17}$$

$$Z = \frac{PV}{RT} \tag{A.18}$$

Equation can be rewritten in terms of compressibility factor Z and in the standard cubic form as:

$$Z^3 - Z^2 + (A - B - B^2)Z - AB = 0 \tag{A.19}$$

where

$$a = 0.42747 \frac{R^2 T_c^2}{P_c} \tag{A.20}$$

$$b = 0.08664 \frac{RT_c}{P_c} \tag{A.21}$$

For multi-component mixtures, the following mixing rules were used [301]:

$$a_m = \sum \sum y_i y_j (\alpha a)_{ij} \qquad (\alpha a)_{ij} = \sqrt{(\alpha a)_i (\alpha a)_j} (1 - k_{ij}) \tag{A.22}$$

$$b_m = \sum_i y_i b_i \tag{A.23}$$

$$\alpha = \left[1 + (0.37464 + 1.54226\omega - 0.26992\omega^2)(1 - \sqrt{T_r})\right]^2 \qquad \text{(A.24)}$$

where

$$T_{r_i} = \frac{T}{T_{c_i}} \qquad \text{(A.25)}$$

a and b are the pure component parameters given by equation A.20 and equation A.21 above.

The form for the fugacity coefficient ϕ derived from SRK-CEOS is:

$$\ln \phi_i = (BB)_i(Z - 1) - \ln(Z - B) - \frac{A}{B}((AA)_i - (BB)_i)\ln\left[1 + \frac{B}{Z}\right] \qquad \text{(A.26)}$$

where ϕ_i is the fugacity coefficient and Z is the compressibility factor calculated from equation A.19 above.

$$AA_i = \frac{2}{(a\alpha)_m}\left[\sum_j (a\alpha)_{ij}\right] \qquad BB_i = \frac{b_i}{b_m} \qquad \text{(A.27)}$$

$$A = \frac{a\alpha P}{R^2 T^2} \qquad B = \frac{bP}{RT} \qquad \text{(A.28)}$$

Again,the solution of equation A.19 for the compressibility factor produces three roots. The largest root represents the vapour phase compressibility factor (Z^v), the smallest represents the liquid phase compressibility factor (Z^l) and the one in the middle is ignored as it has no physical meaning.

When Z^v is substituted in equation A.19, the vapour phase fugacity coefficient (ϕ_i^v)

is obtained while the liquid phase fugacity coefficient (ϕ_i^l) is obtained when Z^l is used.

Using the compressibility factor, the Helmholtz free energy can be obtained from Eq. (3.45). Once the Helmholtz free energy is obtained all other properties can be derived.

A.3   Flash calculations

Flash calculations are used to find the vapour and liquid compositions of different components in different phases for processes with vapour liquid equilibrium. Typically, for a feed stream F separated into a vapour stream V and liquid stream L, as shown in Figure A.1, flash calculations are carried out by combining the mass balances with the VLE equations as follows [301];
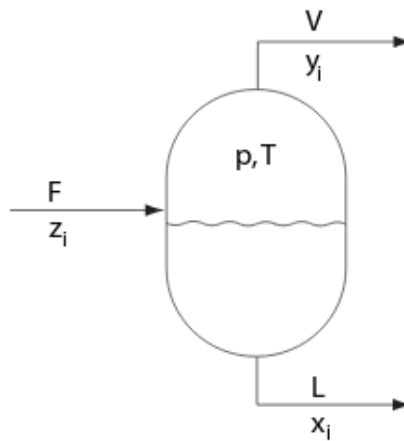
Figure A.1: Flash Tank.

$$F = L + V \tag{A.29}$$

and

$$Fz_i = Lx_i + Vy_i \tag{A.30}$$

where y_i and x_i are the component vapour and liquid phase compositions respectively.

Given that

$$y_i = K_i x_i \tag{A.31}$$

Substituting into Eq. (A.30) gives

$$Fz_i = Lx_i + VK_i x_i, \tag{A.32}$$

where K_i is the equilibrium constant and can be calculated as

$$K_i = \frac{\phi_i^l}{\phi_i^v} \tag{A.33}$$

where ϕ_i^l and ϕ_i^v are the liquid and vapour phase fugacity coefficients, respectively and can be calculated from the equations of state.

Solving Eq. (A.32) with respect to x_i and substituting for $L = F - V$ gives

$$x_i = \frac{z_i}{1 + \alpha^v(K_i - 1)} \tag{A.34}$$

where α^v is the vapour fraction of the feed ($\alpha^v = V/F$)

Substituting for $\sum_i y_i - x_i = 0$, results in Eq. (A.35), knowen as Rachford-Rice flash equation [301]

$$\sum_{i=1}^{c} \frac{z_i(K_i - 1)}{1 + \alpha^v(K_i - 1)} = 0 \tag{A.35}$$

where z_i is the mole fraction of component i in the feed stream and α^v is the vapour fraction of the feed and must be between 0 and 1. Starting from Eq. (A.35), given z_i and with initial guesses for x_i and y_i, and K_i calculated from Eq. (A.33), the value of α^v that satisfies Rachford-Rice equation can then be obtained and substituted back in Eq. (A.34) and Eq. (A.31) to find new values for the vapour and liquid phase compositions. The iterations continue until the difference between the current and the previous composition values is negligible.

Appendix B

Perturbed Chain Statistical Associating Fluid Theory (PC-SAFT) equation

This appendix summarises the PC-SAFT formulas used for the calculation of Helmholtz free energy, compressibility factor and chemical potential. The PC-SAFT pure component parameters used in this work are also presented.

B.1 Helmholtz free energy

The general form of PC-SAFT equation can be expressed in terms of Helmholtz free energy as:

$$a^{res} = a^{hc} + a^{disp} + a^{assoc} + a^{polar} + a^{elec} \qquad (B.1)$$

where a^{res} is the residual Helmholtz free energy, a^{hc} is the hard chain contribution to Helmholtz free energy, a^{disp} is the dispersion contribution to Helmholtz free energy, a^{assoc} is the association contribution to Helmholtz free energy due to hydrogen bonding, a^{polar} is the polar contribution to Helmholtz free energy, and a^{elec} is the electrolyte

contribution to Helmholtz free energy accounting for the electrostatic interactions due to the charge of molecules.

The hard-chain contribution is defined as:

$$a^{hc} = ma^{hs} - \sum_i x_i(m_i - 1) \ln g_{ii}^{hs}(\sigma_{ii}) \tag{B.2}$$

where m is the mean segment number in the mixture and is defined as

$$m = \sum_i x_i m_i \tag{B.3}$$

where: m_i is the number of segments per chain and x_i is the mole fraction of component i. g^{hs} is the radial distribution function of hard-sphere fluid and σ is the segment diameter in Å.

The hard-sphere contribution to Helmholtz free energy is:

$$a^{hs} = \frac{1}{\zeta_0} \left[\frac{3\zeta_1\zeta_2}{(1 - \zeta_3)} + \frac{\zeta_2^3}{\zeta_3(1 - \zeta_3)^2} + \left(\frac{\zeta_2^3}{\zeta_3^2} - \zeta_0 \right) \ln(1 - \zeta_3) \right] \tag{B.4}$$

With the radial distribution function given as:

$$g_{ij}^{hs} = \frac{1}{(1 - \zeta_3)} + \left(\frac{d_i d_j}{d_i + d_j} \right) \frac{3\zeta_2}{(1 - \zeta_3)^2} + \left(\frac{d_i d_j}{d_i + d_j} \right)^2 \frac{2\zeta_2^2}{(1 - \zeta_3)^3} \tag{B.5}$$

where ζ_n given as:

$$\zeta_n = \frac{\pi}{6} \rho \sum_i x_i m_i d_i^n \tag{B.6}$$

And d_i is the temperature-dependent segment diameter of component i defined as:

$$d_i = \sigma_i \left[1 - 0.12 \exp\left(-3\frac{\epsilon_i}{kT}\right) \right] \tag{B.7}$$

The dispersion contribution to the Helmholtz free energy is given by:

$$a^{disp} = -2\pi\rho I_1(\eta, m)\overline{m^2\epsilon\sigma^3} - \pi\rho m C_1 I_2(\eta, m)\overline{m^2\epsilon^2\sigma^3} \tag{B.8}$$

$$
\begin{aligned}
C_1 &= \left(1 + Z^{hc} + \rho\frac{\partial Z^{hc}}{\partial \rho}\right)^{-1} \\
&= \left(1 + m\frac{8\eta - 2\eta^2}{(1-\eta)^4} + (1-m)\frac{20\eta - 27\eta^2 + 12\eta^3 - 2\eta^4}{[(1-\eta)(2-\eta)]^2}\right)
\end{aligned}
\tag{B.9}
$$

$$\overline{m^2\epsilon\sigma^3} = \sum_i \sum_j x_i x_j m_i m_j \left(\frac{\epsilon_{ij}}{kT}\right) \sigma_{ij}^3 \tag{B.10}$$

$$\overline{m^2\epsilon^2\sigma^3} = \sum_i \sum_j x_i x_j m_i m_j \left(\frac{\epsilon_{ij}}{kT}\right)^2 \sigma_{ij}^3 \tag{B.11}$$

The commonly used Lorentz-Berthelot mixing rules were employed for the calculation of the arithmetic average segment diameter σ_{ij} and the geometric average dispersion energy ϵ_{ij} of unlike segments as

$$\sigma_{ij} = \frac{1}{2}(\sigma_i + \sigma_j) \tag{B.12}$$

$$\epsilon_{ij} = \sqrt{\epsilon_i \epsilon_j}(1 - k_{ij}) \tag{B.13}$$

$$I_1(\eta, m) = \sum_{i=0}^{6} a_i(m)\eta^i \tag{B.14}$$

$$I_2(\eta, m) = \sum_{i=0}^{6} b_i(m)\eta^i \tag{B.15}$$

$$a_i(m) = a_{0i} + \frac{m-1}{m}a_{1i} + \frac{m-1}{m}\frac{m-2}{m}a_{2i} \tag{B.16}$$

$$b_i(m) = b_{0i} + \frac{m-1}{m}b_{1i} + \frac{m-1}{m}\frac{m-2}{m}b_{2i} \tag{B.17}$$

where a_{0i}, a_{1i}, a_{2i}, b_{0i}, b_{1i} and b_{2i} are the universal PC-SAFT constants given in Table B.1 [139].

Table B.1: Universal PC-SAFT model constants

i	a_{0i}	a_{1i}	a_{2i}	b_{0i}	b_{1i}	b_{2i}
0	0.9105631445	-0.3084016918	-0.0906148351	0.7240946941	-0.5755498075	0.0976883116
1	0.6361281449	0.1860531159	0.4527842806	2.2382791861	0.6995095521	-0.2557574982
2	2.6861347891	-2.5030047259	0.5962700728	-4.0025849485	3.8925673390	-9.155856153
3	-26.547362491	21.419793629	-1.7241829131	-21.00357681	-17.215471648	20.642075974
4	97.759208784	-65.25588533	-4.1302112531	26.855641363	192.67226447	-38.804430052
5	-159.59154087	83.31868048	13.776631870	206.55133841	-161.82646165	93.626774077
6	91.297774084	-33.746922930	-8.6728470368	-355.60235612	-165.20769346	-29.666905585

The association contribution to Helmholtz free energy is given by equation B.18 below [137]

$$\frac{a^{assoc}}{RT} = \sum_i^c x_i \left[\sum_{A_i} \left(lnX^{A_i} - \frac{X^{A_i}}{2} \right) + \frac{1}{2}M_i \right] \tag{B.18}$$

where X^{A_i} is the mole fraction of molecule i not bonded at site A and M_i is the number

of sites on molecule i. X^{A_i} is defined by equation B.19

$$X^{A_i} = \left[1 + N_{Av} \sum_j \sum_{B_j} \rho_j X^{B_j} \Delta^{A_i B_J} \right]^{-1} \tag{B.19}$$

where $\sum_{B_j}$ runs over all sites on molecule j. ρ_j is the molar density of component j:

$$\rho_j = x_j \rho \tag{B.20}$$

where ρ is the molar density of the solution. $\Delta^{A_i B_J}$ is the association strength and is defined as

$$\Delta^{A_i B_J} = g_{ij}^{hs}[exp(\epsilon^{A_i B_j}/kT) - 1](\sigma_{ij}^3 \kappa^{A_i B_j}) \tag{B.21}$$

The radial distribution function g_{ij}^{hs} is given by equation 3.48 above. The combining rules for the association energy $\epsilon^{A_i B_j}$ and the effective association volume $\kappa^{A_i B_j}$ between molecule i and j are [53]:

$$\epsilon^{A_i B_j} = \frac{1}{2}(\epsilon^{A_i B_i} + \epsilon^{A_j B_j}) \tag{B.22}$$

$$\kappa^{A_i B_j} = \sqrt{\kappa^{A_i B_i} \kappa^{A_j B_j}} \left(\frac{\sqrt{\sigma_{ii} \sigma_{jj}}}{0.5(\sigma_{ii} + \sigma_{jj})} \right)^3 \tag{B.23}$$

To allow for more accurate model prediction, ionic liquids were also modelled as fully dissociated charged ions (cations and anions). The Debye Huckel theory [154] for electrolyte systems used by Cameretti et al. [302] to account for the long range Coulomb forces among ions in the systems is adopted. The electrolyte term is added to the original PC-SAFT [139] and the residual Helmholtz free energy of an electrolyte system is then calculated as:

a^{elec} is the electrostatic contribution to Helmholtz free energy and is given by Eq. (B.24) [154, 302]. Cameretti et al. treated the ions as spheres that can approach each other by a certain distance equals to the ion diameter a_i and characterized by a dielectric constant ϵ. No additional adjustable parameters are needed to represent the electrostatic contribution of the charged ions in the electrolyte system.

$$\frac{a^{elec}}{kT} = -\frac{1}{4\pi\epsilon kT} \sum_i \frac{x_i q_i^2}{3} \kappa \chi_i \qquad \text{(B.24)}$$

where

$$\chi_i = \frac{3}{(\kappa a_i)^3} \left[\frac{3}{2} + \ln(1 + \kappa a_i) - 2(1 + \kappa a_i) + \frac{1}{2}(1 + \kappa a_i)^2 \right] \qquad \text{(B.25)}$$

ϵ is the dielectric constant of the medium ($\epsilon = \epsilon_0 \epsilon_r$), where ϵ_0 is the vacuum permittivity and ϵ_r is the relative permittivity of the medium. x_i is the mole fraction of ion i, κ is the inverse Debye screening length and has units of $meter^{-1}$ and a_i is the ion diameter.

The polar contribution to Helmholtz free energy written in the Pade approximate has the following form [303]:

$$a^{polar} = \frac{a_2}{1 - a_3/a_2} \qquad \text{(B.26)}$$

where a_2 and a_3 are the second- and third-order terms in the perturbation expansion. Written for mixtures, and allowing for multiple dipolar segments, these terms have the following form:

$$a_2 = -\frac{2\pi}{9} \frac{\rho}{(kT)^2} \sum_i \sum_j x_i x_j m_i m_j x_{pi} x_{pj} \frac{\mu_i^2 \mu_j^2}{d_{ij}^2} I_{2,ij} \qquad \text{(B.27)}$$

$$a_3 = \frac{5}{162}\pi^2 \frac{\rho^2}{(kT)^3} \sum_i \sum_j \sum_k x_i x_j x_k m_i m_j m_k x_{pi} x_{pj} x_{pk} \frac{\mu_i^2 \mu_j^2 \mu_k^2}{d_{ij} d_{jk} d_{ik}} I_{3,ijk} \quad \text{(B.28)}$$

In this study, the polar contribution to the Helmholtz free energy a^{polar} is not accounted for.

The density in PC-SAFT is determined through iterative procedures. First, the reduced density η is set to 0.5 for the vapour phase and 10^{-10} for the liquid phase as starting values suggested by [139]. Then the reduced density is adjusted until the calculated pressure is equal to the system pressure.

$$\rho = \frac{6}{\pi}\eta \left(\sum_i x_i m_i d_i^3 \right)^{-1} \quad \text{(B.29)}$$

$$\hat{\rho} = \frac{\rho}{N_{AV}} \left(10^{10} \frac{\mathring{A}}{m} \right)^3 \left(10^{-3} \frac{kmol}{mol} \right) \quad \text{(B.30)}$$

B.2   The compressibility factor

The compressibility factor Z can be derived from the Helmholtz free energy a using the following relation

$$Z = \rho \left(\frac{\partial (a/RT)}{\partial \rho} \right)_{N_\alpha, T} \quad \text{(B.31)}$$

The pressure in Pascal can be calculated from the equation below

$$P = ZkT\rho \left(10^{10}\frac{\mathring{A}}{m}\right)^3 \tag{B.32}$$

$$Z = 1 + Z^{hc} + Z^{disp} + Z^{assoc} + Z^{elec} \tag{B.33}$$

The hard-chain contribution to the compressibility factor is:

$$Z^{hc} = mZ^{hs} - \sum_i x_i(m_i - 1)(g_{ii}^{hs})^{-1}\rho\frac{\partial g_{ii}^{hs}}{\partial \rho} \tag{B.34}$$

The residual contribution of the hard-sphere fluid is:

$$Z^{hs} = \frac{\zeta_3}{(1 - \zeta_3)} + \frac{3\zeta_1\zeta_2}{\zeta_0(1 - \zeta_3)^2} + \frac{3\zeta_2^3 - \zeta_3\zeta_2^3}{\zeta_0(1 - \zeta_3)^3} \tag{B.35}$$

where

$$\begin{aligned}
\rho\frac{\partial g_{ii}^{hs}}{\partial \rho} = {} & \frac{\zeta_3}{(1 - \zeta_3)^2} + \\
& \left(\frac{d_i d_j}{d_i + d_j}\right)\left(\frac{3\zeta_2}{(1 - \zeta_3)^2} + \frac{6\zeta_2\zeta_3}{(1 - \zeta_3)^3}\right) + \\
& \left(\frac{d_i d_j}{d_i + d_j}\right)^2\left(\frac{4\zeta_2^2}{(1 - \zeta_3)^3} + \frac{6\zeta_2^2\zeta_3}{(1 - \zeta_3)^4}\right)
\end{aligned} \tag{B.36}$$

The dispersion contribution to the compressibility factor is:

$$Z^{disp} = -2\pi\rho\frac{\partial(\eta I_1)}{\partial\eta}\overline{m^2\epsilon\sigma^3} - \pi\rho m\left[C_1\frac{\partial(\eta I_2)}{\partial\eta} + C_2\eta I_2\right]\overline{m^2\epsilon^2\sigma^3} \tag{B.37}$$

$$\frac{\partial(\eta I_1)}{\partial\eta} = \sum_{i=0}^{6} a_j(m)(j+1)\eta^j \tag{B.38}$$

$$\frac{\partial(\eta I_2)}{\partial\eta} = \sum_{i=0}^{6} b_j(m)(j+1)\eta^j \tag{B.39}$$

$$\begin{aligned}C_2 &= \frac{\partial C_1}{\partial\eta} \\ &= -C_1^2\left(\bar{m}\frac{-4\eta^2+20\eta+8}{(1-\eta)^5} + (1-\bar{m})\frac{2\eta^3+12\eta^2-48\eta+40}{[(1-\eta)(2-\eta)]^3}\right)\end{aligned} \tag{B.40}$$

The association contribution to the compressibility factor is defined as:

$$Z^{assoc} = \rho\left(\frac{\partial(a^{assoc}/RT)}{\partial\rho}\right) \tag{B.41}$$

where $\frac{\partial(a^{assoc}/RT)}{\partial\rho}$ is the derivative of B.18 above and is given as:

$$\frac{\partial(a^{assoc}/RT)}{\partial\rho} = \sum_i x_i\left[\sum_{A_i}\left[\frac{1}{X^{A_j}}-\frac{1}{2}\right](\frac{\partial X^{A_i}}{\partial\rho})\right] \tag{B.42}$$

and

$$\begin{aligned}\frac{\partial X^{A_i}}{\partial\rho} = -(X^{A_i})^2[\sum_j\sum_{B_j}x_j X^{B_j}\Delta^{A_iB_j} + \rho\sum_j\sum_{B_j}x_j\frac{\partial X^{B_j}}{\partial\rho}\Delta^{A_iB_j} + \\ \rho\sum_j\sum_{B_j}x_j X^{B_j}\frac{\partial\Delta^{A_iB_j}}{\partial\rho}]\end{aligned} \tag{B.43}$$

where

$$\frac{\partial \Delta^{A_i B_j}}{\partial \rho} = (\sigma_{ij})^3 \kappa^{A_i B_j} \left(\frac{\partial g_{ij}^{hs}}{\partial \rho} \right) \left[\exp(\epsilon^{A_i B_j}/kT) - 1 \right] \tag{B.44}$$

where

$$\begin{aligned}
\frac{\partial g_{ij}^{hs}}{\partial \rho} &= \left(\frac{1}{\rho} \right) \big[\frac{\zeta_3}{(1-\zeta_3)^2} + \frac{3d_i d_j}{d_i + d_j} \big[\frac{\zeta_2}{(1-\zeta_3)^2} + \\
&\frac{2\zeta_3 \zeta_2}{(1-\zeta_3)^3} \big] + 2 \big[\frac{d_i d_j}{d_i + d_j} \big]^2 \big[\frac{2\zeta_2^2}{(1-\zeta_3)^3} + \frac{3\zeta_3 \zeta_2^2}{(1-\zeta_3)^4} \big] \big]
\end{aligned} \tag{B.45}$$

The electrostatic contribution to the compressibility factor Z^{elec} is given by equation B.46 below

$$Z^{elec} = \frac{P^{elec}}{\rho_N kT} = -\left(\frac{\partial a^{elec}/kT}{\rho_N \partial \upsilon} \right)_{T,N} = \frac{\kappa}{24\pi kT\epsilon} \sum_k x_k q_k^2 \sigma_k \tag{B.46}$$

where σ_k is given by equation B.47

$$\sigma_k = \left(\frac{\partial(\kappa \chi_k)}{\partial \kappa} \right)_{T,N} = -2\chi_k + \frac{3}{1 + \kappa a_k} \tag{B.47}$$

ρ_N is the number density of the system and q_k is the ion charge.

B.3 The chemical potential

The relation between the fugacity coefficient ϕ_k and the residual chemical potential $\mu_k^{res}(T, \nu)$ is given by:

$$\ln \phi_k = \frac{\mu_k^{res}(T, \nu)}{kT} - \ln Z \tag{B.48}$$

where the chemical potential is the partial derivative of Helmholtz free energy with respect to the composition at constant temperature and volume.

$$\frac{\mu_k^{res}(T, \nu)}{kT} = a^{res} + (Z - 1) + \left(\frac{\partial a^{res}}{\partial x_k}\right)_{T,\nu,x_{i\neq k}} - \sum_{j=1}^{N} \left[x_j \left(\frac{\partial a^{res}}{\partial x_j}\right)_{T,\nu,x_{i\neq j}}\right] \tag{B.49}$$

$$\zeta_{n,xk} = \left(\frac{\partial \zeta_n}{\partial x_k}\right)_{T,\rho,x_{j\neq k}} = \frac{\pi}{6}\rho m_k (d_k)^n \qquad n \in \{0, 1, 2, 3\} \tag{B.50}$$

The partial derivative of the Hard-Chain reference contribution to Helmholtz free energy is:

$$\left(\frac{\partial a^{hc}}{\partial x_k}\right)_{T,\rho,x_{j\neq k}} = m_k a^{hs} + \bar{m} \left(\frac{\partial a^{hs}}{\partial x_k}\right)_{T,\rho,x_{j\neq k}} - \sum_i x_i (m_i - 1)(g_{ii}^{hs})^{-1} \left(\frac{\partial g_{ii}^{hs}}{\partial x_k}\right)_{T,\rho,x_{j\neq k}} \tag{B.51}$$

The partial derivative of the Hard-Sphere contribution is:

$$
\left(\frac{\partial a^{hs}}{\partial x_k}\right)_{T,\rho,x_{j\neq k}} = -\frac{\zeta_{0,xk}}{\zeta_0}a^{hs}+
$$

$$
\frac{1}{\zeta_0}\Big[\frac{3(\zeta_{1,xk}\zeta_2 + \zeta_1\zeta_{2,xk})}{(1-\zeta_3)}+
$$

$$
\frac{3\zeta_1\zeta_2\zeta_{3,xk}}{(1-\zeta_3)^2} + \frac{3\zeta_2^2\zeta_{2,xk}}{\zeta_3(1-\zeta_3)^2} + \frac{\zeta_2^3\zeta_{3,xk}(3\zeta_3-1)}{\zeta_3^2(1-\zeta_3)^3}+
$$

$$
\left(\frac{3\zeta_2^2\zeta_{2,xk}\zeta_3 - 2\zeta_2^3\zeta_{3,xk}}{\zeta_3^3} - \zeta_{0,xk}\right)\ln(1-\zeta_3)+
$$

$$
\left(\zeta_0 - \frac{\zeta_2^3}{\zeta_3^2}\right)\frac{\zeta_{3,xk}}{(1-\zeta_3)}\Big]
$$

(B.52)

$$
\left(\frac{\partial g_{ij}^{hs}}{\partial x_k}\right)_{T,\rho,x_{j\neq k}} = \frac{\zeta_{3,xk}}{(1-\zeta_3)^2}+
$$

$$
\left(\frac{d_id_j}{d_i+d_j}\right)\left(\frac{3\zeta_{2,xk}}{(1-\zeta_3)^2} + \frac{6\zeta_2\zeta_{3,xk}}{(1-\zeta_3)^3}\right)+
$$

$$
\left(\frac{d_id_j}{d_i+d_j}\right)^2\left(\frac{4\zeta_2\zeta_{2,xk}}{(1-\zeta_3)^3} + \frac{6\zeta_2^2\zeta_{3,xk}}{(1-\zeta_3)^4}\right)
$$

(B.53)

The partial derivative of the dispersion contribution to Helmholtz free energy is:

$$
\left(\frac{\partial a^{disp}}{\partial x_k}\right)_{T,\rho,x_{j\neq k}} = -2\pi\rho[I_{1,xk}\overline{m^2\epsilon\sigma^3} + I_1(\overline{m^2\epsilon\sigma^3})_{xk}]-
$$

$$
\pi\rho([m_kC_1I_2 + mC_{1,xk}I_2+
$$

$$
mC_1I_{2,xk}]\overline{m^2\epsilon^2\sigma^3} + mC_1I_2(\overline{m^2\epsilon^2\sigma^3})_{xk})
$$

(B.54)

$$(\overline{m^2\epsilon\sigma^3})_{xk} = 2m_k \sum_j x_j m_j \left(\frac{\epsilon_{kj}}{kT}\right) \sigma_{kj}^3 \tag{B.55}$$

$$(\overline{m^2\epsilon^2\sigma^3})_{xk} = 2m_k \sum_j x_j m_j \left(\frac{\epsilon_{kj}}{kT}\right)^2 \sigma_{kj}^3 \tag{B.56}$$

$$\begin{aligned} C_{1,xk} = C_2\zeta_{3,xk}- \\ C_1^2 \left[m_k\frac{8\eta - 2\eta^2}{(1-\eta)^4} - m_k\frac{20\eta - 27\eta^2 + 12\eta^3 - 2\eta^4}{[(1-\eta)(2-\eta)]^2}\right] \end{aligned} \tag{B.57}$$

$$I_{1,xk} = \sum_{i=0}^{6}[a_i(m)i\zeta_{3,xk}\eta^{i-1} + a_{i,xk}\eta^i] \tag{B.58}$$

$$I_{2,xk} = \sum_{i=0}^{6}[b_i(m)i\zeta_{3,xk}\eta^{i-1} + b_{i,xk}\eta^i] \tag{B.59}$$

$$a_{i,xk} = \frac{m_k}{m^2}a_{1i} + \frac{m_k}{m^2}\left(3 - \frac{4}{m}\right)a_{2i} \tag{B.60}$$

$$b_{i,xk} = \frac{m_k}{m^2}b_{1i} + \frac{m_k}{m^2}\left(3 - \frac{4}{m}\right)b_{2i} \tag{B.61}$$

The electrostatic contribution to the chemical potential μ_j^{elec} is given by Eq. (B.62) below

$$\left(\frac{\partial a^{elec}}{\partial x_j}\right)_{T,\rho,x_i\neq x_j} = -\frac{q_j^2\kappa}{24\pi kT\epsilon}\left[2\chi_j + \frac{\sum_k x_k q_k^2 \sigma_k}{\sum_k x_k q_k^2}\right] \tag{B.62}$$

The different contributions to the chemical potentials are added to find the overall residual contribution to the chemical potential.

B.4 PC-SAFT Pure Component Parameters Used in This Work

In this section, the PC-SAFT pure parameters for components other than ILs, used in this work are presented (see Table B.2). For ILs the parameters were estimated in Chapter 4.

Table B.2: PC-SAFT pure component parameters used in this work

Component	Association sites	T range (K)	m	σ Å	ε/k (K)	$\varepsilon^{A_iB_i}/k$ (K)	$\kappa^{A_iB_i}$	Reference
CH_4	0	97–300	1.0000	3.7039	150.03			[139]
H_2O	2	273–647	1.0656	3.0007	366.51	2500.70	0.034868	[139]
CO_2	0	216 – 304	2.0729	2.7852	169.21			[139]
H_2S	0	187 – 362	1.6686	3.0349	229.00			[53]

where m is the number of segments in a molecule, σ is the segment diameter in Å, ε is the depth of square well potential in (J), $\varepsilon^{A_iB_i}$ is the association energy between site A and B on the same molecule, $\kappa^{A_iB_i}$ is the association volume between site A and B on the same molecule and k is Boltzmann constant (1.38066×10^{-23} J/K).

B.5 Publication on the solubility of acid gases in ILs using PC-SAFT

In this section, the author's publication on the solubility of H_2S and CO_2 in Ionic liquids using the PC-SAFT model is attached. Details of this work are presented in Chapter 4 of this thesis.
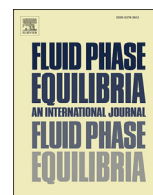
Modelling the solubility of H_2S and CO_2 in ionic liquids using PC-SAFT equation of state

Heba Al-fnaish[*], Leo Lue[**]

Department of Chemical and Process Engineering, University of Strathclyde, 75 Montrose Street, Glasgow G1 1XJ, United Kingdom

ABSTRACT

The Perturbed Chain Statistical Association Fluid Theory (PC-SAFT) is used to investigate the solubility of carbon dioxide (CO_2) and hydrogen sulfide (H_2S) in several methylimidazolium bis (tri-fluoromethylsulfonyl) imide ionic liquids (ILs) or $[C_n mim][NTf_2]$ where $n=2$, 4, 6, and 8. The pure component parameters of the ILs are estimated by fitting to experimental density data and binary solubility data of acid gases in ILs reported in literature. Two strategies are examined to model the ILs. In the first strategy, the ILs are treated as neutral molecules. In the second strategy, the ILs are modelled as two charged ions: imidazolium cation $[C_n mim]^+$ and bis (trifluoromethylsulfonyl) imide anion $[NTf_2]^-$. For each strategy, four different self association schemes are examined: non-associating, 2-site, 3-site, and 4-site schemes. The inclusion of self-association of the IL improves the calculated acid gas solubility. The 4-site association scheme with two donors and two acceptors provided the best results for almost all the investigated acid gases-IL binary systems, with an AARD of 2.76%—6.62% for H_2S-ILs systems and 1.54% —4.98% for CO_2-IL systems. Using these parameters, the solubility of ternary systems of CO_2 and H_2S in $C_8 mimNTf_2$ IL is successfully represented, with an AARD of 6.24% for CO_2 and 7.99% for H_2S, without the need for binary interaction parameters. The high pressure density of ILs and the binary solubility of CO_2-ILs at high pressure is also represented with reasonable accuracy. The inclusion of the electrolyte term in the second strategy improves the high pressure density and solubility results as well as the predictive capability of the model by allowing for the examination of the effect of using different cation-anion combinations.

© 2017 Elsevier B.V. All rights reserved.

1. Introduction

Due to its lower carbon content compared to oil and coal, natural gas is considered the most environmentally benign fossil fuel. However, raw gas still needs to be treated to remove acid gases such as carbon dioxide (CO_2) and hydrogen sulfide (H_2S) mainly because of their corrosive nature, toxicity and flammability. CO_2 may also freeze, causing blockage of pipelines [1], and has a poor heating value, which lowers the heating value of the gas [2]. Numerous technologies are available for acid gas removal from natural gas. Alkanolamine based chemical absorption is the most commercially utilized process, due to its versatility, efficiency, and low solvent cost. However, alkanolamines are volatile, corrosive, and their

regeneration process is highly energy intensive, comprising 70% of the total operating costs [3,4].

Recently, ionic liquids (ILs) have emerged as an alternative physical solvent for alkanolamines. ILs are organic salts characterized by their negligible volatility, high thermal stability, high ionic conductivity, and structural tunability. They are liquids over a wide range of temperatures; they can have melting points ranging from $-100-200°C$ [3], which is much lower than the melting points of conventional ionic compounds, such as sodium chloride.

An IL consists of two types of ions: an organic cation, such as imidazolium, pyridinium or phosphonium ions and an inorganic anion, such as Cl^-, BF_4^-, PF_6^-, $CF_3SO_3^-$, NTf_2^-, or an organic anion such as carboxylate (RCO_2^-) [5]. ILs can be used in a variety of applications, including catalysis, gas storage and separation [6]. By replacing volatile and possibly toxic organic solvents, ILs have the potential to contribute significantly to improving the safety, economy and environmental sustainability of acid gas removal processes [7]. Due to their negligible volatility and high thermal

* Corresponding author.
** Corresponding author.
E-mail addresses: heba.al-fnaish@strath.ac.uk (H. Al-fnaish), leo.lue@strath.ac.uk (L. Lue).

Appendix C

Aspen Plus simulation

C.1 Pure component properties

The following pure component parameters were used in Aspen Plus V9 for components other than ILs (CH_4, H_2S, CO_2, H_2O, MDEA), which are already defined in the Aspen Plus V9 library. The properties were retrieved from different databanks in Aspen Plus V9 as indicated below

- Molecular weight, boiling point and critical properties:
  Values used in Aspen Plus V9 for CH_4, H_2S, CO_2, H_2O and MDEA were all retrieved from the PURE35 databank [304] and recorded in Table C.1.

Table C.1: Aspen Plus V9 library components molecular weight, boiling point and critical properties. Retrieved from [304]

Component	MW g/mol	T_b K	T_c K	P_c bar	V_c cc/mol	ω
CH_4	16.0428	111.66	190.564	45.99	98.6	0.0115
H_2S	34.0819	212.8	373.53	89.6291	98.5	0.0942
CO_2	44.0098	194.7	304.21	73.83	94	0.2236
H_2O	18.0153	373.15	647.096	220.64	55.9	0.3449
MDEA	119.164	520.7	741.9	41.6	379	0.6286

- PC-SAFT EOS structural parameters:

  For the IL cases, the PC-SAFT structural parameters used for CH_4, H_2S, CO_2 and H_2O are the same parameters listed in Table B.2. The parameters can also be retrieved from the PC-SAFT databank [305] in Aspen Plus V9.

- Liquid heat capacity:

  The liquid heat capacity of CH_4, H_2S, CO_2 and H_2O was estimated using the DIPPR equation (Equation C.1).

$$C_P = C_1 + C_2T + C_3T^2 + C_4T^3 + C_5T^4 \tag{C.1}$$

where C_p is the liquid heat capacity in $\text{J mol}^{-1}\,\text{K}^{-1}$, T is the absolute temperature in kelvin and $C_1 - C_5$ are the DIPPR equation coefficients retrieved from the PURE35 databank [304] in Aspen Plus V9 and are listed in Table C.2.

Table C.2: DIPPR liquid heat capacity equation coefficients. Retrieved from [304]

Component	C_1	C_2	C_3	C_4	C_5
CH_4	2.07787	38.883	-8.1571	19.4186	0
H_2S	2.04492	49.354	0.711291	-51.3238	0
CO_2	-8304.3	104.37	-0.43333	6.0052×10^{-04}	0
H_2O	276.37	-2.0901	0.008125	-1.4116×10^{-05}	9.3701×10^{-09}

- Ideal gas heat capacity:

  The ideal gas heat capacity of CH_4, H_2S, CO_2 and H_2O was calculated using the following polynomials (Equations C.2 and C.3):

$$C_P^0 = C_1 + C_2T + C_3T^2 + C_4T^3 + C_5T^4 + C_6T^5 \quad , C_7 \leq T \leq C_8 \tag{C.2}$$

$$C_P^0 = C_9 + C_{10}T^{C_{11}} \quad , T < C_7 \tag{C.3}$$

with coefficients retrieved from the ASPENPCD databank [306] for H_2S and H_2O, and the AQUEOUS databank [307] for CH_4 and CO_2. The polynomial

coefficients are listed in Table C.3.

where C_p^0 is the ideal gas heat capacity in J mol^{-1} K^{-1}, and $C_1 - C_{11}$ are the polynomial coefficients given in Table C.3.

Table C.3: Aspen Plus ideal gas heat capacity polynomial coefficients. Retrieved from [306] and [307]

Component	C_1	C_2	$C_3 \times 10^{05}$	$C_4 \times 10^{08}$	$C_5 \times 10^{12}$	$C_6 \times 10^{16}$	C_7	C_8	C_9	C_{10}	C_{11}
CH$_4$	19.251	0.0521	1.197	-1.132	0	0	300	1641	33.256	9.951×10^{-18}	7.018
H$_2$S	31.941	0.001	2.432	-1.176	0	0	300	1407.1	33.256	2.086×10^{-10}	3.906
CO$_2$	19.795	0.073	-5.602	1.715	0	0	300	1088.6	29.099	0.001	1.637
H$_2$O	33.738	-0.007	2.730	-1.665	4.298	-4.170	200	3000	33.256	1.898×10^{-23}	9.285

- Heat of vapourisation:

  The heat of vapourisation of CH$_4$, H$_2$S, CO$_2$ and H$_2$O was calculated using the Watson equation (Equation C.4) with parameters retrieved from ASPENPCD databank [306].

$$\Delta H^{vap}(T) = H^{vap}(T_1) \left(\frac{1 - T/T_c}{1 - T_1/T_c} \right)^{a+b(1-T/T_c)} \qquad T > T_{min} \qquad \text{(C.4)}$$

where $H^{vap}(T)$ is the heat of vapourisation at temperature T, $H^{vap}(T_1)$ is the heat of vapourisation at temperature T_1, and T_c is the critical temperature. The values used for a and b, $H^{vap}(T_1)$, T_{min}, and T_1 are listed in Table C.4.

Table C.4: Watson heat of vapourisation equation parameters. Retrieved from [306]

Component	$H^{vap}(T_1)$ J mol^{-1}	T_1 K	a	b	T_{min} K
CH$_4$	8185.19	111.7	0.318	0	90.7
H$_2$S	18673.1	212.8	0.306	0	187.6
CO$_2$	17165.9	194.7	0.358	0	194.7
H$_2$O	40683.1	373.2	0.311	0	273.2

- Liquid viscosity:

  The liquid viscosity of CH_4, H_2S and CO_2 was calculated using the Andrade equation below

$$\ln \mu^l = A + \frac{B}{T} + C \ln T \quad T_l \leq T \leq T_h \tag{C.5}$$

  where μ^l is the liquid viscosity in cp, A, B, C are Andrade equation parameters, T_l and T_h are the lower and the higher temperature limits in kelvin, respectively. Andrade equation parameters used were retrieved from ASPENPCD databank and are listed in Table C.5.

Table C.5: Andrade liquid viscosity equation parameters. Retrieved from [306]

Component	A (cp)	B (cp K)	C (cp K^{-1})	T_l (K)	T_h (K)
CH_4	-4.5628	262.817	0	90.7	190.6
H_2S	-4.76805	789.303	0	187.6	373.2
CO_2	-7.8157	1331.08	0	216.6	304.2

- Vapour viscosity:

  The vapour viscosity of CH_4, H_2S, CO_2 and H_2O was calculated using the DIPPR equation below

$$\mu^v = \frac{C_1 T^{C_2}}{1 + C_3/T + C_4/T^2} \quad C_5 \leq T \leq C_6 \tag{C.6}$$

  where μ^v is the vapour viscosity in cp, T is the temperature in kelvin, $C_1 - C_4$ are the DIPPR equation parameters retrieved from the PURE35 databank [304] and listed in Table C.6. C_5 and C_6 are the lower and the upper temperature limits in kelvin, respectively.

- Vapour pressure:

  The vapour pressure of CH_4, H_2S, CO_2 and H_2O was calculated using the extended Antoine equation below

Table C.6: DIPPR vapour viscosity equation parameters. Retrieved from [304]

Component	C_1	C_2	C_3	C_4	C_5	C_6
CH_4	5.255×10^{-04}	0.590	105.670	0	90.69	1000
H_2S	3.931×10^{-05}	1.013	0	0	250	480
CO_2	2.148×10^{-03}	0.460	290	0	194.67	1500
H_2O	1.710×10^{-05}	1.115	0	0	273.16	1073.15

$$\ln P^l = C_1 + \frac{C_2}{T + C_3} + C_4 T + C_5 \ln T + C_6 T^{C_7} \quad C_8 \leq T \leq C_9 \quad (C.7)$$

where P^l is the vapour pressure in bar, T is the temperature in kelvin, $C_1 - C_7$ are the extended Antoine equation parameters retrieved from PURE35 databank [304] and listed in Table C.7. C_8 and C_9 are the lower and the upper temperature limits in kelvin, respectively .

Table C.7: Extended Antoine equation parameters. Retrieved from [304]

Component	C_1	C_2	C_3	C_4	C_5	C_6	C_7	C_8	C_9
CH_4	27.692	-1324.4	0	0	-3.437	3.102×10^{-05}	2	90.69	190.56
H_2S	74.071	-3839.9	0	0	-11.199	0.0199	1	187.68	373.53
CO_2	35.504	-2839	0	0	-3.864	2.811×10^{-16}	6	216.58	304.21
H_2O	62.136	-7258.2	0	0	-7.3037	4.165×10^{-06}	2	273.16	647.1

For ILs, which are not library components in Aspen Plus, the properties were estimated by experimental data fitting. Details were presented in Chapter 5.

C.2 Aspen Plus flowsheets and stream tables of the base case and the optimal IL and IL-DEPG blend cases

C.2.1 Base case flowsheet and stream table
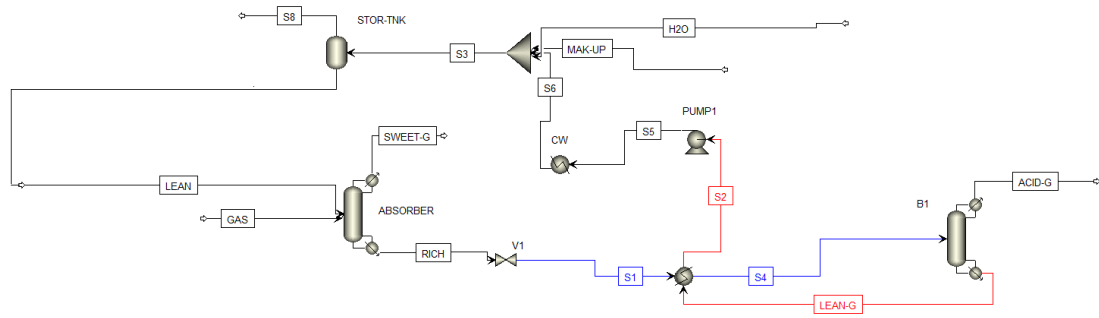
Figure C.1: Aspen Plus flowsheet for North Caroline sweetening unit with MDEA as a solvent (base case).

Stream Name	Units	Base case stream table			
		ACID-G	GAS	H2O	LEAN
Phase		Vapor	Vapor	Liquid	Liquid
Temperature	K	333.753	305.37	317	317.04
Pressure	bar	1.4	55.158	55	55
Mass Vapor Fraction		1	1	0	0
Mass Liquid Fraction		0	0	1	1
Mass Enthalpy	kJ/kg	-9144.01	-5075.15	-15782.4	-11827
Mass Entropy	kJ/kg-K	-0.0185314	-6.51386	-8.80668	-8.17103
Mass Density	kg/cum	1.98857	40.6294	993.11	1004.59
Average MW		39.1849	17.0158	18.0153	25.0374
Mass Flows	kg/min	40	465.847	87.4857	623.395
MDEA	kg/min	1.41E-13	0	0	205.466
H2O	kg/min	2.72693	0.431291	87.4857	417.283
CO2	kg/min	36.6651	41.801	0	0.379115
H2S	kg/min	0.0478374	0.0523504	0	0
H3O+	kg/min	0	0	3.14E-07	0.000185944
OH-	kg/min	0	0	2.81E-07	4.44E-08
HCO3-	kg/min	0	0	0	0.0901447
CO3-2	kg/min	0	0	0	2.26E-07
HS-	kg/min	0	0	0	0
S-2	kg/min	0	0	0	0
MDEAH+	kg/min	0	0	0	0.176362
CH4	kg/min	0.560178	423.563	0	0
Mass Fractions					
MDEA		3.54E-15	0	0	0.329592
H2O		0.0681732	0.00092582	1	0.669372
CO2		0.916626	0.0897311	0	0.000608147
H2S		0.00119593	0.000112377	0	0
H3O+		0	0	3.59E-09	2.98E-07
OH-		0	0	3.21E-09	7.11E-11
HCO3-		0	0	0	0.000144603
CO3-2		0	0	0	3.63E-10
HS-		0	0	0	0
S-2		0	0	0	0
MDEAH+		0	0	0	0.000282906
CH4		0.0140045	0.909231	0	0

Base case stream table

Stream Name	LEAN-G	MAK-UP	RICH	S1	S2
Phase	Liquid	Liquid	Liquid	Mixed	Liquid
Temperature	385.803	317.04	329.448	301.584	332.15
Pressure	1.45	55	55	2	1.2
Mass Vapor Fraction	0	0	0	0.0536704	0
Mass Liquid Fraction	1	1	1	0.94633	1
Mass Enthalpy	-11554	-3770.82	-11703.3	-11703.3	-11746.5
Mass Entropy	-7.48632	-7.09019	-7.8491	-7.88241	-8.00045
Mass Density	956.641	1028.72	1046.28	59.9648	994.391
Average MW	25.1144	119.164	26.5031	25.671	25.1097
Mass Flows	618.455	0.0001	658.455	658.455	618.455
MDEA	204.684	0.0001	108.728	205.325	205.458
H2O	412.419	0	400.718	415.225	412.519
CO2	0.000264649	0	1.37485	36.8157	0.20044
H2S	1.16E-06	0	0.00314322	0.0488199	0.0010368
H3O+	2.83E-09	0	1.15E-07	0.000479662	0.000132582
OH-	0.0167759	0	5.80E-05	6.35E-09	1.48E-07
HCO3-	0.314629	0	49.0579	0.162432	0.0934256
CO3-2	0.055401	0	0.237815	1.87E-07	2.58E-07
HS-	0.00108849	0	0.0444627	0.0001361	8.35E-05
S-2	3.60E-10	0	1.06E-10	2.06E-13	5.10E-12
MDEAH+	0.964014	0	97.7313	0.317367	0.183465
CH4	9.39E-20	0	0.560178	0.560178	0
Mass Fractions					
MDEA	0.33096	1	0.165125	0.311828	0.332211
H2O	0.666854	0	0.608573	0.630605	0.667015
CO2	4.28E-07	0	0.002088	0.0559123	0.000324097
H2S	1.88E-09	0	4.77E-06	7.41E-05	1.68E-06
H3O+	4.57E-12	0	1.75E-10	7.28E-07	2.14E-07
OH-	2.71E-05	0	8.80E-08	9.64E-12	2.39E-10
HCO3-	0.000508733	0	0.0745045	0.000246687	0.000151063
CO3-2	8.96E-05	0	0.000361172	2.84E-10	4.17E-10
HS-	1.76E-06	0	6.75E-05	2.07E-07	1.35E-07
S-2	5.82E-13	0	1.61E-13	3.13E-16	8.25E-15
MDEAH+	0.00155875	0	0.148425	0.000481988	0.00029665
CH4	1.52E-22	0	0.000850746	0.000850746	0

Stream Name	S3	S4	S5	S6	SWEET-G
Phase	Liquid	Mixed	Liquid	Liquid	Vapor
Temperature	317.029	318.683	333.864	317.04	332.959
Pressure	55	1.5	55.5	55	55
Mass Vapor Fraction	0	0.0565179	0	0	1
Mass Liquid Fraction	1	0.943482	1	1	0
Mass Enthalpy	-12291.1	-11641.4	-11737.3	-11797.2	-4714.69
Mass Entropy	-8.24354	-7.67926	-7.98425	-8.16836	-6.81955
Mass Density	1003.24	40.0648	994.964	1004.69	34.2545
Average MW	23.9409	25.6712	25.1098	25.1093	16.1798
Mass Flows	705.941	658.455	618.455	618.455	430.787
MDEA	205.516	205.304	205.451	205.507	0.00101082
H2O	500.013	415.222	412.518	412.526	2.46766
CO2	0.221974	36.8081	0.198017	0.218787	5.31226
H2S	0.00104377	0.0488752	0.00103643	0.0010363	0.00339023
H3O+	0.000140426	0.000344527	0.000131431	0.0001398	0
OH-	7.08E-08	2.81E-08	1.64E-07	5.69E-08	0
HCO3-	0.0635689	0.172943	0.0967848	0.0679879	0
CO3-2	2.57E-07	2.57E-07	2.62E-07	2.14E-07	0
HS-	7.67E-05	8.24E-05	8.38E-05	8.40E-05	0
S-2	1.87E-12	8.57E-13	5.77E-12	1.59E-12	0
MDEAH+	0.124589	0.338727	0.190089	0.133322	0
CH4	0	0.560178	0	0	423.003
Mass Fractions					
MDEA	0.291124	0.311796	0.332201	0.332292	2.35E-06
H2O	0.708293	0.6306	0.667013	0.667027	0.00572825
CO2	0.000314437	0.0559008	0.00032018	0.000353763	0.0123315
H2S	1.48E-06	7.42E-05	1.68E-06	1.68E-06	7.87E-06
H3O+	1.99E-07	5.23E-07	2.13E-07	2.26E-07	0
OH-	1.00E-10	4.27E-11	2.65E-10	9.21E-11	0
HCO3-	9.00E-05	0.00026265	0.000156494	0.000109932	0
CO3-2	3.64E-10	3.91E-10	4.24E-10	3.47E-10	0
HS-	1.09E-07	1.25E-07	1.36E-07	1.36E-07	0
S-2	2.65E-15	1.30E-15	9.34E-15	2.58E-15	0
MDEAH+	0.000176486	0.000514427	0.000307361	0.000215572	0
CH4	0	0.000850746	0	0	0.98193

Base case stream table

C.2.2 Optimal C_6mimNTf$_2$ IL case flowsheet and stream table

Figure C.2: Aspen Plus flowsheet for North Caroline sweetening unit with IL as a solvent.

Stream Name	Units	1	2	3	4	5
Phase		Mixed	Vapor	Liquid	Mixed	Mixed
Temperature	K	316.235	316.235	316.235	314.49	316.726
Pressure	bar	45	45	45	45	20
Mass Vapor Fraction		0.00146967	1	0	0.99948	0.00430086
Mass Liquid Fraction		0.99853	0	1	0.000519658	0.995699
Mass Enthalpy	kJ/kg	-5285.26	-5170.81	-5285.43	-4906.9	-5285.43
Mass Entropy	kJ/kg-K	-3.07951	-6.12127	-3.07503	-6.57277	-3.0672
Mass Density	kg/cum	1070.74	31.8325	1124.77	30.6844	848.522
Average MW		51.4397	17.3196	51.5893	16.6065	51.5893
Mass Flows	kg/min	3160.15	4.64437	3155.5	442.5	3155.5
WATER	kg/min	983.865	0.0147618	983.85	1.36992	983.85
METHA-01	kg/min	23.3003	4.09323	19.2071	417.726	19.2071
CARBO-01	kg/min	27.0684	0.535749	26.5326	23.4018	26.5326
HYDRO-01	kg/min	0.0605775	0.000624907	0.0599526	0.00276288	0.0599526
C6MIM	kg/min	2125.85	2.65E-17	2125.85	1.18E-14	2125.85
Mass Fractions						
WATER		0.311335	0.00317843	0.311788	0.00309586	0.311788
METHA-01		0.00737318	0.881332	0.00608686	0.944012	0.00608686
CARBO-01		0.00856554	0.115355	0.00840837	0.0528854	0.00840837
HYDRO-01		1.92E-05	0.000134552	1.90E-05	6.24E-06	1.90E-05
C6MIM		0.672707	5.70E-18	0.673697	2.67E-17	0.673697

C6mimNTf2 IL case stram table

C6mimNTf2 IL case stram table

Stream Name	6	7	8	9	10	11
Phase	Vapor	Liquid	Mixed	Vapor	Vapor	Liquid
Temperature	316.724	316.724	316.746	316.747	463.02	316.747
Pressure	20	20	5	5	20	5
Mass Vapor Fraction	1	0	0.00409663	1	1	0
Mass Liquid Fraction	0	1	0.995903	0	0	1
Mass Enthalpy	-5539.84	-5284.33	-5284.33	-6753.34	-6496.36	-5278.28
Mass Entropy	-5.10595	-3.0584	-3.05308	-2.88323	-2.72131	-3.05378
Mass Density	14.4561	1130.2	550.636	4.3688	11.9214	1133.79
Average MW	18.4067	51.9943	51.9943	22.7744	22.7744	52.2702
Mass Flows	13.5766	3141.93	3141.93	12.8714	12.8714	3129.06
WATER	0.0800791	983.77	983.77	0.224269	0.224269	983.546
METHA-01	10.766	8.44115	8.44115	6.69755	6.69755	1.7436
CARBO-01	2.72733	23.8053	23.8053	5.94176	5.94176	17.8635
HYDRO-01	0.00319679	0.0567558	0.0567558	0.00779348	0.00779348	0.0489623
C6MIM	6.23E-18	2125.85	2125.85	2.72E-18	2.72E-18	2125.85
Mass Fractions						
WATER	0.00589833	0.31311	0.31311	0.0174238	0.0174238	0.314327
METHA-01	0.792981	0.00268662	0.00268662	0.520345	0.520345	0.00055723
CARBO-01	0.200885	0.00757665	0.00757665	0.461626	0.461626	0.00570892
HYDRO-01	0.000235464	1.81E-05	1.81E-05	0.000605489	0.000605489	1.56E-05
C6MIM	4.59E-19	0.676608	0.676608	2.12E-19	2.12E-19	0.679392

C6mimNTf2 IL case stram table

Stream Name	12	13	14	15	16
Phase	Mixed	Mixed	Vapor	Vapor	Vapor
Temperature	316.708	358.15	383.081	343.15	417.718
Pressure	3	2.1	20	20	40
Mass Vapor Fraction	0.000775858	0.00445248	0.999997	1	1
Mass Liquid Fraction	0.999224	0.995548	2.67E-06	0	0
Mass Enthalpy	-5278.28	-5174.19	-6005.38	-6085.31	-5943.09
Mass Entropy	-3.05316	-2.74417	-3.89805	-4.11835	-4.02084
Mass Density	878.479	335.742	12.9671	14.6221	23.8849
Average MW	52.2702	52.2702	20.3016	20.3016	20.3016
Mass Flows	3129.06	3129.06	26.448	26.448	26.448
WATER	983.546	983.546	0.304352	0.304352	0.304352
METHA-01	1.7436	1.7436	17.4635	17.4635	17.4635
CARBO-01	17.8635	17.8635	8.66921	8.66921	8.66921
HYDRO-01	0.0489623	0.0489623	0.01099	0.01099	0.01099
C6MIM	2125.85	2125.85	8.95E-18	8.95E-18	8.95E-18
Mass Fractions					
WATER	0.314327	0.314327	0.0115076	0.0115076	0.0115076
METHA-01	0.00055723	0.00055723	0.660294	0.660294	0.660294
CARBO-01	0.00570892	0.00570892	0.327783	0.327783	0.327783
HYDRO-01	1.56E-05	1.56E-05	0.000415533	0.000415533	0.000415533
C6MIM	0.679392	0.679392	3.39E-19	3.39E-19	3.39E-19

Stream Name	17	18	20	ACID-G	ACID-GAS
Phase	Vapor	Vapor	Liquid	Vapor	Vapor
Temperature	348.15	434.149	342.77	330.249	305.37
Pressure	25	55	1.4	1.4	55.158
Mass Vapor Fraction	1	1	0	1	1
Mass Liquid Fraction	0	0	1	0	0
Mass Enthalpy	-6079.06	-5913.85	-5188.2	-8822.38	-5076.7
Mass Entropy	-4.18898	-4.0798	-2.87094	-0.29221	-6.51791
Mass Density	18.101	31.6294	1114.34	1.82204	40.7838
Average MW	20.3016	20.3016	52.437	35.539	17.0158
Mass Flows	26.448	26.448	3108.06	21	465.847
WATER	0.304352	0.304352	982.193	1.35264	0.431291
METHA-01	17.4635	17.4635	1.76E-07	1.7436	423.563
CARBO-01	8.66921	8.66921	0.00810744	17.8554	41.801
HYDRO-01	0.01099	0.01099	0.000629344	0.048333	0.0523504
C6MIM	8.95E-18	8.95E-18	2125.85	3.34E-39	0
Mass Fractions					
WATER	0.0115076	0.0115076	0.316015	0.0644114	0.00092582
METHA-01	0.660294	0.660294	5.67E-11	0.0830287	0.909231
CARBO-01	0.327783	0.327783	2.61E-06	0.850258	0.0897311
HYDRO-01	0.000415533	0.000415533	2.02E-07	0.00230157	0.000112377
C6MIM	3.39E-19	3.39E-19	0.683982	1.59E-40	0

C6mimNTf2 IL case stram table

Stream Name	CH4-REC	FEED	H2O-MKUP	IL	LEAN-IL	RICH-IL
			C6mimNTf2 IL case stram table			
Phase	Mixed	Mixed	Liquid	Liquid	Liquid	Liquid
Temperature	305.37	304.936	317.04	317.04	380.416	315.993
Pressure	55	55	55	55	1.41	55
Mass Vapor Fraction	0.989589	0.999846	0	0	0	0
Mass Liquid Fraction	0.010411	0.000154216	1	1	1	1
Mass Enthalpy	-6213.76	-5137.79	-15734	-5254.77	-5093.04	-5285.26
Mass Entropy	-4.90308	-6.4276	-8.6631	-3.06789	-2.60765	-3.08239
Mass Density	49.829	41.1309	912.382	1136.36	1085.09	1122.79
Average MW	20.3016	17.165	18.0153	52.3629	52.437	51.4397
Mass Flows	26.448	492.295	9.96292	3110.35	3108.06	3160.15
WATER	0.304352	0.735643	9.96292	984.499	982.193	983.865
METHA-01	17.4635	441.026	0	0	1.76E-07	23.3003
CARBO-01	8.66921	50.4702	0	0	0.00810744	27.0684
HYDRO-01	0.01099	0.0633404	0	0	0.000629344	0.0605775
C6MIM	8.95E-18	8.95E-18	0	2125.85	2125.85	2125.85
Mass Fractions						
WATER	0.0115076	0.00149431	1	0.316523	0.316015	0.311335
METHA-01	0.660294	0.895857	0	0	5.67E-11	0.00737318
CARBO-01	0.327783	0.10252	0	0	2.61E-06	0.00856554
HYDRO-01	0.000415533	0.000128663	0	0	2.02E-07	1.92E-05
C6MIM	3.39E-19	1.82E-20	0	0.683477	0.683982	0.672707

C6mimNTf2 IL case stram table

Stream Name	S1	S2	S3	SALES-G	SWEET-G
Phase	Liquid	Liquid	Liquid	Mixed	Vapor
Temperature	343.903	317.04	316.956	314.512	317.758
Pressure	55.5	55	55	45	55
Mass Vapor Fraction	0	0	0	0.999481	1
Mass Liquid Fraction	1	1	1	0.00051882	0
Mass Enthalpy	-5181.7	-5247.05	-5280.56	-4909.64	-4906.9
Mass Entropy	-2.86614	-3.06382	-3.08194	-6.56801	-6.66585
Mass Density	1115.97	1136.59	1135.65	30.6955	37.5289
Average MW	52.437	52.437	52.1188	16.6136	16.6065
Mass Flows	3108.06	3108.06	3118.02	447.145	442.5
WATER	982.193	982.193	992.156	1.38468	1.36992
METHA-01	1.76E-07	1.76E-07	1.76E-07	421.819	417.726
CARBO-01	0.00810744	0.00810744	0.00810744	23.9376	23.4018
HYDRO-01	0.000629344	0.000629344	0.000629344	0.00338779	0.00276288
C6MIM	2125.85	2125.85	2125.85	1.18E-14	1.18E-14
Mass Fractions					
WATER	0.316015	0.316015	0.318201	0.00309672	0.00309586
METHA-01	5.67E-11	5.67E-11	5.66E-11	0.943361	0.944012
CARBO-01	2.61E-06	2.61E-06	2.60E-06	0.0535343	0.0528854
HYDRO-01	2.02E-07	2.02E-07	2.02E-07	7.58E-06	6.24E-06
C6MIM	0.683982	0.683982	0.681797	2.65E-17	2.67E-17

C.2.3   IL-DEPG blend case flowsheet and stream table
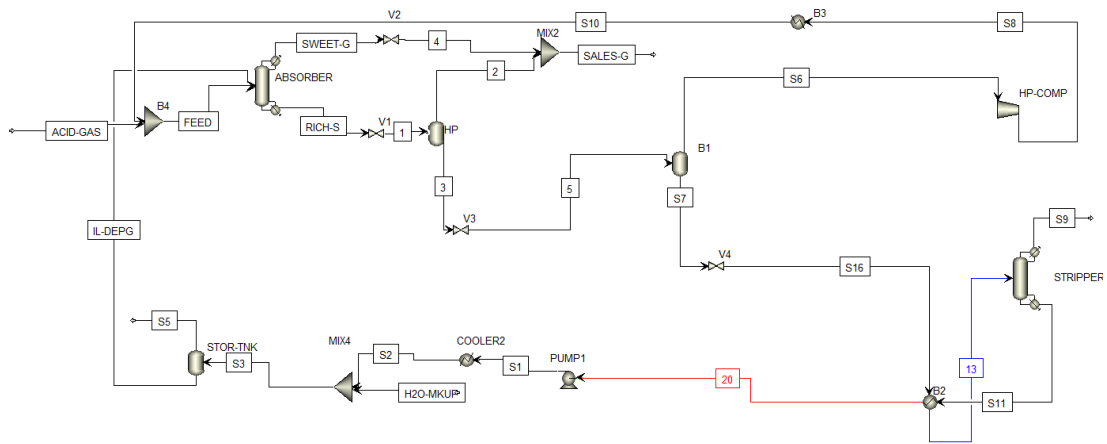
Figure C.3: Aspen Plus flowsheet for North Caroline sweetening unit with IL-DEPG blend as a solvent.

C8mimNTf2 IL-DEPG blend case stream table

Stream Name	Units	1	2	3	4	5
Phase		Mixed	Vapor	Liquid	Mixed	Mixed
Temperature	K	312.848	312.848	312.848	315.226	313.474
Pressure	bar	45	45	45	45	15
Mass Vapor Fraction		0.0013617	1	0	0.998532	0.00499622
Mass Liquid Fraction		0.998638	0	1	0.00146805	0.995004
Mass Enthalpy	kJ/kg	-3872.36	-5132.47	-3870.64	-5019.06	-3870.64
Mass Entropy	kJ/kg-K	-2.38877	-6.22563	-2.38354	-6.40118	-2.37329
Mass Density	kg/cum	1025.66	32.0109	1070.99	31.1377	725.249
Enthalpy Flow	cal/sec	-2.07E+07	-37407.2	-2.07E+07	-9.12E+06	-2.07E+07
Average MW		65.6013	17.181	65.8543	16.8743	65.8543
Mass Flows	kg/min	1344.56	1.83089	1342.73	456.324	1342.73
C8MIM	kg/min	470.725	4.56E-20	470.725	1.19E-16	470.725
WATER	kg/min	301.818	0.00676372	301.812	1.86878	301.812
METHA-01	kg/min	9.38528	1.63438	7.75089	419.392	7.75089
CARBO-01	kg/min	8.18379	0.189519	7.99427	35.0537	7.99427
HYDRO-01	kg/min	0.0507866	0.000211128	0.0505754	0.0033109	0.0505754
METHA-02	kg/min	0	0	0	0	0
DEPG	kg/min	554.394	1.40E-05	554.394	0.00643007	554.394
Mass Fractions						
C8MIM		0.350097	2.49E-20	0.350574	2.61E-19	0.350574
WATER		0.224474	0.00369422	0.224775	0.00409529	0.224775
METHA-01		0.0069802	0.892671	0.00577251	0.919066	0.00577251
CARBO-01		0.00608661	0.103512	0.00595376	0.0768175	0.00595376
HYDRO-01		3.78E-05	0.000115314	3.77E-05	7.26E-06	3.77E-05
METHA-02		0	0	0	0	0
DEPG		0.412324	7.64E-06	0.412887	1.41E-05	0.412887

C8mimNTf2 IL-DEPG blend case stream table

Stream Name	13	20	ACID-GAS	FEED	H2O-MKUP	IL
Phase	Mixed	Liquid	Vapor	Vapor	Liquid	Liquid
Temperature	319.15	333.15	305.37	305.271	317.04	317.04
Pressure	2.1	1.41	55.158	55.15	55	55
Mass Vapor Fraction	0.00457749	0	1	0.999999	0	0
Mass Liquid Fraction	0.995423	1	0	1.18E-06	1	1
Mass Enthalpy	-3847.05	-3778.6	-5076.7	-5085.49	-15734	-3834.71
Mass Entropy	-2.30854	-2.20308	-6.51791	-6.50556	-8.6631	-2.34264
Mass Density	312.978	1062.88	40.7838	40.8498	912.382	1079.83
Enthalpy Flow	-2.05E+07	-1.99E+07	-9.41E+06	-9.57E+06	-101049	-2.03E+07
Average MW	66.7061	67.383	17.0158	17.0363	18.0153	67.087
Mass Flows	1336.02	1326.02	465.847	472.559	1.61333	1328.32
C8MIM	470.725	470.725	0	5.64E-21	0	470.725
WATER	301.753	301.02	0.431291	0.489933	1.61333	303.197
METHA-01	2.53646	1.27E-05	423.563	428.777	0	0
CARBO-01	6.5587	0.00331583	41.801	43.2375	0	0
HYDRO-01	0.0488291	0.00135037	0.0523504	0.0540975	0	0
METHA-02	0	0	0	0	0	0
DEPG	554.394	554.266	0	5.26E-05	0	554.4
Mass Fractions						
C8MIM	0.352335	0.354992	0	1.19E-23	0	0.354376
WATER	0.22586	0.227011	0.00092582	0.00103677	1	0.228256
METHA-01	0.00189852	9.59E-09	0.909231	0.907352	0	0
CARBO-01	0.00490915	2.50E-06	0.0897311	0.0914965	0	0
HYDRO-01	3.65E-05	1.02E-06	0.000112377	0.000114478	0	0
METHA-02	0	0	0	0	0	0
DEPG	0.41496	0.417993	0	1.11E-07	0	0.417369

C8mimNTf2 IL-DEPG blend case stream table

Stream Name	RICH-S	S1	S2	S3	IL-DEPG	S6
Phase	Liquid	Liquid	Liquid	Liquid	Liquid	Vapor
Temperature	312.582	334.642	300	299.958	299.958	313.473
Pressure	55	55.5	55	55	55	15
Mass Vapor Fraction	0	0	0	0	0	1
Mass Liquid Fraction	1	1	1	1	1	0
Mass Enthalpy	-3872.36	-3771.04	-3857.32	-3871.76	-3871.76	-5623.36
Mass Entropy	-2.39182	-2.19566	-2.4675	-2.47531	-2.47531	-4.8907
Mass Density	1069.31	1065.15	1094.76	1094.5	1094.5	10.987
Enthalpy Flow	-2.07E+07	-1.99E+07	-2.04E+07	-2.05E+07	-2.05E+07	-150215
Average MW	65.6013	67.383	67.383	67.1594	67.1594	18.5906
Mass Flows	1344.56	1326.02	1326.02	1327.63	1327.63	6.71045
C8MIM	470.725	470.725	470.725	470.725	470.725	5.64E-21
WATER	301.818	301.02	301.02	302.633	302.633	0.0586468
METHA-01	9.38528	1.27E-05	1.27E-05	1.27E-05	1.27E-05	5.21444
CARBO-01	8.18379	0.00331583	0.00331583	0.00331583	0.00331583	1.43557
HYDRO-01	0.0507866	0.00135037	0.00135037	0.00135037	0.00135037	0.00174638
METHA-02	0	0	0	0	0	0
DEPG	554.394	554.266	554.266	554.266	554.266	5.26E-05
Mass Fractions						
C8MIM	0.350097	0.354992	0.354992	0.354561	0.354561	8.41E-22
WATER	0.224474	0.227011	0.227011	0.22795	0.22795	0.00873962
METHA-01	0.0069802	9.59E-09	9.59E-09	9.58E-09	9.58E-09	0.777062
CARBO-01	0.00608661	2.50E-06	2.50E-06	2.50E-06	2.50E-06	0.21393
HYDRO-01	3.78E-05	1.02E-06	1.02E-06	1.02E-06	1.02E-06	0.000260248
METHA-02	0	0	0	0	0	0
DEPG	0.412324	0.417993	0.417993	0.417485	0.417485	7.85E-06

C8mimNTf2 IL-DEPG blend case stream table

Stream Name	S7	S8	S9	S10	S11
Phase	Liquid	Vapor	Vapor	Mixed	Liquid
Temperature	313.473	462.403	328.362	305.37	373.736
Pressure	15	55.15	1.4	55.15	1.41
Mass Vapor Fraction	0	1	1	0.992492	0
Mass Liquid Fraction	1	0	0	0.00750838	1
Mass Enthalpy	-3861.84	-5307.71	-7988.71	-5694.83	-3669.07
Mass Entropy	-2.36066	-4.64234	-1.08698	-5.66817	-1.8931
Mass Density	1076.75	26.9874	1.4735	45.2044	1026.63
Enthalpy Flow	-2.05E+07	-141783	-318011	-152125	-1.94E+07
Average MW	66.7061	18.5906	28.6051	18.5906	67.383
Mass Flows	1336.02	6.71045	9.99998	6.71045	1326.02
C8MIM	470.725	5.64E-21	6.94E-65	5.64E-21	470.725
WATER	301.753	0.0586468	0.732874	0.0586468	301.02
METHA-01	2.53646	5.21444	2.53643	5.21444	1.27E-05
CARBO-01	6.5587	1.43557	6.55536	1.43557	0.00331583
HYDRO-01	0.0488291	0.00174638	0.0474785	0.00174638	0.00135037
METHA-02	0	0	0	0	0
DEPG	554.394	5.26E-05	0.127844	5.26E-05	554.266
Mass Fractions					
C8MIM	0.352335	8.41E-22	6.94E-66	8.41E-22	0.354992
WATER	0.22586	0.00873962	0.0732875	0.00873962	0.227011
METHA-01	0.00189852	0.777062	0.253644	0.777062	9.59E-09
CARBO-01	0.00490915	0.21393	0.655537	0.21393	2.50E-06
HYDRO-01	3.65E-05	0.000260248	0.00474785	0.000260248	1.02E-06
METHA-02	0	0	0	0	0
DEPG	0.41496	7.85E-06	0.0127844	7.85E-06	0.417993

C8mimNTf2 IL-DEPG blend case stream table

Stream Name	S16	S17	SALES-G	SWEET-G
Phase	Mixed	Vapor	Mixed	Vapor
Temperature	313.557	323.15	315.221	317.656
Pressure	10	15	45	55
Mass Vapor Fraction	0.000966898	1	0.998533	1
Mass Liquid Fraction	0.999033	0	0.00146724	0
Mass Enthalpy	-3861.84	-5603.49	-5019.51	-5019.06
Mass Entropy	-2.35909	-4.82825	-6.40047	-6.49283
Mass Density	949.507	10.6276	31.1406	38.1967
Enthalpy Flow	-2.05E+07	-149684	-9.15E+06	-9.12E+06
Average MW	66.7061	18.5906	16.8755	16.8743
Mass Flows	1336.02	6.71045	458.155	456.324
C8MIM	470.725	5.64E-21	1.19E-16	1.19E-16
WATER	301.753	0.0586468	1.87554	1.86878
METHA-01	2.53646	5.21444	421.026	419.392
CARBO-01	6.5587	1.43557	35.2432	35.0537
HYDRO-01	0.0488291	0.00174638	0.00352203	0.0033109
METHA-02	0	0	0	0
DEPG	554.394	5.26E-05	0.00644406	0.00643007
Mass Fractions				
C8MIM	0.352335	8.41E-22	2.60E-19	2.61E-19
WATER	0.22586	0.00873962	0.00409369	0.00409529
METHA-01	0.00189852	0.777062	0.91896	0.919066
CARBO-01	0.00490915	0.21393	0.0769242	0.0768175
HYDRO-01	3.65E-05	0.000260248	7.69E-06	7.26E-06
METHA-02	0	0	0	0
DEPG	0.41496	7.85E-06	1.41E-05	1.41E-05

Appendix D

Glossary

D.1 Natural gas price indicators

The following definitions are to be used with Figure 2.2 in Chapter 2

- **Henry Hub**: Is a distribution hub on the natural gas pipeline system in Louisiana Gulf coast, owned by Sabine Pipe Line LLC, a subsidiary of Chevron Corporation. Due to its importance, it lends its name to the pricing point for natural gas futures contracts traded on the New York Mercantile Exchange (NYMEX) and the IntercontinentalExchange (ICE).

- **German Import price**: Germany is considered as Europe's largest gas market, and about 92% of its gas comes from imports, mainly from Russia, Norway and Netherlands [308]. The German import price is therefore one of the important gas market price indicators.

- **UK NBP**: Stands for the UK's national balancing point which is a virtual trading location for the sale, purchase and exchange of UK's natural gas. It is equivalent to the Henry Hub in the United States.

- **Netherlands TTF index**: Stands for the Netherlands's title transfer facility which is the virtual trading point of natural gas in Netherlands.

- **Japan LNG cif price**: Price for Japanese liquefied natural gas as CIF prices, where CIF = cost + insurance + freight (average freight prices).

- **Japan Korea Marker (JKM)**: Is the spot price of the Liquefied Natural Gas delivered into Japan, South Korea, China and Taiwan. As these two countries are the world's largest LNG importers, JKM marker is thus a key reference in marking product price from supply source to the destination market.

- **Northern Natural Gas**: In business since 1930, owns and operates the largest interstate natural gas pipeline system in the United States. Northern Natural Gas' pipeline system stretches across 11 states, from the Permian Basin in Texas to Michigan's Upper Peninsula, providing access to five of the major natural gas supply regions in North America.

D.2 Concentration units conversion factors

- PPM/V = Parts Per Million by Volume

- 1 Grain/100 ft3 = 15.7 PPM/V

- 10,000 PPM/V = 1%

- 1⁄4 Grain/100 ft3 (quarter grain) = 4 PPM/V

D.3 Natural Gas Units

- 1 cubic foot (cf) = 1,027 Btu

- 1,000 cubic feet (1 Mcf) = 1,027,000 Btu (1 MMBtu)

- 1 million (1,000,000) cubic feet (1 Mmcf) = 1,027,000,000 Btu

- 1 billion (1,000,000,000 cubic feet (1 bcf) = 1.027 trillion Btu

- 1 trillion (1,000,000,000,000) cubic feet (1Tcf) = 1.027 quadrillion Btu

D.4 Commonwealth of Independent States

The Commonwealth of Independent States (CIS) was established in 1991 after the dissolution of the Soviet Union. It involves the following 12 states: Armenia, Azerbaijan, Belarus, Georgia, Kazakhstan, Kyrgyzstan, Moldova, Russia, Tajikistan, Turkmenistan, Ukraine, and Uzbekistan.

References

[1] Growing demand for natural gas, Tech. rep., International Energy Agency (2019).
URL https://www.iea.org/reports/market-report-series-gas-2019 1

[2] International Energy Outlook 2016, Tech. rep., U.S. Energy Information Administration, Office of Energy Analysis U.S. Department of Energy, Washington, DC 20585 (May 2016).
URL https://www.eia.gov/outlooks/ieo/table3-2.cfm 1

[3] V. Quaschning. Statistics: Specific Carbon Dioxide Emissions of Various Fuels [online] (2015). 1, 5

[4] D. Huo, The Global Sour Gas Problem, Tech. rep., Stanford University (November 2012).
URL https://sej.stanford.edu/global-sour-gas-problem 1, 2

[5] B. Shimekit, H. Mukhtar, Natural Gas Purification Technologies - Major Advances for CO_2 Separation and Future Directions, Advances in Natural Gas Technology, InTech, 2012. doi:10.5772/2324. 1, 9, 26, 27

[6] D. Perry, R. Fedich, L. Parks, Better Acid Gas Enrichment, Flexsorb Solvents (2010).
URL http://citeseerx.ist.psu.edu/viewdoc/download?doi=10.1.1.471.6149&rep=rep1&type=pdf 2, 12

[7] M. Stewart, K. Arnold, Part 1 - Gas Sweetening, in: Gas Sweetening and Processing Field Manual, Gulf Professional Publishing, Boston, 2011, pp. 1 – 140. `doi:10.1016/B978-1-85617-982-9.00002-8`.
URL `http://www.sciencedirect.com/science/article/pii/B9781856179829000028` 2, 12, 32

[8] Schlumberger oil field glossary, Sour gas, Schlumberger.
URL `http://www.glossary.oilfield.slb.com/Terms/s/sour_gas.aspx` 2

[9] S. Kumar, J. Cho, I. Moon, Ionic liquid-amine blends and CO_2 BOLs: Prospective solvents for natural gas sweetening and CO_2 capture technology: A review, Int. J. Greenhouse Gas Control 20 (0) (2014) 87 – 116. `doi:10.1016/j.ijggc.2013.10.019`. 3, 14, 15, 16, 20, 21, 24, 25, 26, 31, 67, 69, 114, 142, 144

[10] E. I. Alevizou, G. D. Pappa, E. C. Voutsas, Prediction of phase equilibrium in mixtures containing ionic liquids using UNIFAC, Fluid Phase Equilib. 284 (2) (2009) 99 – 105. `doi:10.1016/j.fluid.2009.06.012`. 3, 72, 74, 114, 142

[11] P. Boehm, T. Saba, Identification of Natural Gas Sources using Geochemical Forensic Tools, Exponent (2009).
URL `https://www.yumpu.com/en/document/view/19626838/identification-of-natural-gas-sources-using\-geochemical-exponent` 5, 7, 8

[12] NaturalGas.org, Natural Gas Background, NaturalGas.org (September 2013).
URL `http://naturalgas.org/overview/background/` 6

[13] Union of Concerned Scientists, Shale Gas and Other Unconventional Sources of Natural Gas. 6

[14] W. Whitman, T. Bowen, D. Boone, The Methanogenic Bacteria, in: M. Dworkin, S. Falkow, E. Rosenberg, K.-H. Schleifer, E. Stackebrandt (Eds.),

The Prokaryotes, Springer New York, 2006, pp. 165–207. `doi:10.1007/0-387-30743-5_9`.
URL `http://dx.doi.org/10.1007/0-387-30743-5_9` 6

[15] S. Mokhatab, W. A. Poe, J. G. Speight, Handbook of Natural Gas Transmission and Processing, Elsevier Inc., 2006. 7

[16] The Natural Gas Supply Association (NGSA), Natural Gas Winter Outlook 2013-2014 [online] (2014). 7

[17] A. A. Suárez, The Expansion of Unconventional Production of Natural Gas (Tight Gas, Gas Shale and Coal Bed Methane), Advances in Natural Gas Technology (2012). 7

[18] U.S. Energy Information Administration, Today in Energy: What are natural gas liquids and how are they used? (April 2012). 8

[19] A. de Angelis, Natural gas removal of hydrogen sulphide and mercaptans, Applied Catalysis B: Environmental 113-114 (2012) 37 – 42, natural Gas Conversion Symposium (NGCS 9) Special Issue. `doi:https://doi.org/10.1016/j.apcatb.2011.11.026`. 8

[20] M. F. Ezzeldin, Z. Gajdosechova, M. B. Masod, T. Zaki, J. Feldmann, E. M. Krupp, Mercury speciation and distribution in an egyptian natural gas processing plant, Energy Fuels 30 (12) (2016) 10236–10243. `doi:10.1021/acs.energyfuels.6b02035`.
URL `https://doi.org/10.1021/acs.energyfuels.6b02035` 9

[21] Gas Quality Specifications: TransCanada and other pipelines [online] (2018). 9

[22] A. J. Kidnay, W. R. Parrish, Fundamentals of Natural Gas Processing, Taylor and Francis Group, LLC, 2006. 9

[23] U.S. Energy Information Administration, Definitions, Sources and Explanatory Notes: Consumption by End Use (2014).

URL `http://www.eia.gov/dnav/ng/tbldefs/ng_cons_sum_` `tbldef2.asp` 9

[24] British Petroleum, BP Statistical Review of World Energy June, 2019 (2019).
URL `https://www.bp.com/content/dam/bp/business-sites/` `en/global/corporate/pdfs/energy-economics/` `statistical-review/bp-stats-review-2019-full-report.` `pdfhttps://www.bp.com/content/dam/bp/business-sites/` `en/global/corporate/pdfs/energy-economics/` `statistical-review/bp-stats-review-2019-full-report.` `pdf` 10, 11, 12

[25] U.S. Energy Information Administration, What are the major factors affecting natural gas prices? (June 2019). 11

[26] TOTAL Infrastructure Code of Practice (ICOP), Technical Specifications - Entry, TOTAL E&P UK LTD, [online] (2013). 13

[27] Northern Natural Gas, Informational Postings: Requirements [online] (2014). 13

[28] Hydrogen Sulfide, Occupational Safety and Health Administration, U.S. Department of Labor, OSHA Factsheet [online] (2005). 13

[29] Agency for Toxic Substances and Disease Registry, Medical Management Guidelines for Hydrogen Sulfide (H_2S), Division of Toxicology and Human Health Sciences (October 2014).
URL `https://www.atsdr.cdc.gov/MHMI/mmg114.pdf` 13

[30] K. Nalli, Corrosion and its mitigation in the oil and gas industry: An overview., Tech. rep., Tebodin & Co., Muscat, Oman (2013).
URL `https://onlinelibrary.wiley.com/doi/pdf/10.1002/` `9781118162569.app6` 13

[31] Total Materia: The world's most comprehensive materials database, Hydrogen Sulfide Corrosion (June 2014).
URL https://www.totalmateria.com/page.aspx?ID=CheckArticle&site=kts&NM=424 13

[32] D. Seddon, Gas Usage & Value: The Technology and Economics of Natural Gas Use in the Process Industries, PennWell Corporation, 2006. 13

[33] M. Bilio, S. Brown, M. Fairweather, H. Mahgerefteh, CO_2 Pipelines Material And Safety Consideration, Hazards (2009).
URL https://discovery.ucl.ac.uk/id/eprint/80288/ 14

[34] H. Kruse, M. Tekiela, Calculating the consequences of a CO_2 pipeline rupture, Energy Conversion and Management 37 (6–8) (1996) 1013 – 1018, proceedings of the International Energy Agency Greenhouse Gases: Mitigation Options Conference. doi:10.1016/0196-8904(95)00291-X. 14

[35] A. Muhammad, Y. Gadelhak, Correlating the additional amine sweetening cost to acid gases load in natural gas using aspen hysys, J. Nat. Gas Sci. Eng. 17 (0) (2014) 119 – 130. doi:10.1016/j.jngse.2014.01.008. 14

[36] R. E. Baltus, R. M. Counce, B. H. Culbertson, H. Luo, D. W. DePaoli, S. Dai, D. C. Duckworth, Examination of the potential of ionic liquids for gas separations, Sep. Sci. Technol. 40 (1-3) (2005) 525–541. doi:10.1081/SS-200042513. 14, 15

[37] L. G. Sanchez, G. Meindersma, A. de Haan, Solvent Properties of Functionalized Ionic Liquids for CO_2 Absorption, Chem. Eng. Res. Des. 85 (1) (2007) 31 – 39. doi:10.1205/cherd06124. 14, 24, 70, 74

[38] D. Camper, J. E. Bara, D. L. Gin, R. D. Noble, Room-Temperature Ionic Liquid-Amine Solutions: Tunable Solvents for Efficient and Reversible Capture of CO_2, Ind. Eng. Chem. Res (2008). doi:10.1021/ie801002m. 14, 70, 74, 144

[39] Y.-I. Park, B.-S. Kim, Y.-H. Byun, S.-H. Lee, E.-W. Lee, J.-M. Lee, Preparation of supported ionic liquid membranes (SILMs) for the removal of acidic gases from crude natural gas, Desalination 236 (1) (2009) 342 – 348. `doi:10.1016/j.desal.2007.10.085`. 14, 15

[40] D. Wappel, G. Gronald, R. Kalb, J. Draxler, Ionic liquids for post-combustion CO_2 absorption, International Journal of Greenhouse Gas Control 4 (3) (2010) 486 – 494. `doi:10.1016/j.ijggc.2009.11.012`. 14, 15

[41] O. M. Basha, M. J. Keller, D. R. Luebke, K. P. Resnik, B. I. Morsi, Development of a Conceptual Process for Selective CO_2 Capture from Fuel Gas Streams Using [hmim][Tf_2N] Ionic Liquid as a Physical Solvent, Energy and Fuels 27 (7) (6 2013). `doi:10.1021/ef400650w`. 14, 15

[42] Y. Huang, X. Zhang, X. Zhang, H. Dong, S. Zhang, Thermodynamic Modeling and Assessment of Ionic Liquid-Based CO_2 Capture Processes, Ind. Eng. Chem. Res. 53 (29) (2014) 11805–11817. `doi:10.1021/ie501538e`. 14, 15

[43] B. Zacchello, E. Oko, M. Wang, A. Fethi, Process simulation and analysis of carbon capture with an aqueous mixture of ionic liquid and monoethanolamine solvent, International Journal of Coal Science & Technology 4 (1) (2017) 25–32. `doi:10.1007/s40789-016-0150-1`. 14, 15

[44] C. F. Keen, Systematic approaches for design of ionic liquids and their mixtures for enhanced carbon capture purpose, Ph.D. thesis, University of Nottingham (2017). 14, 15

[45] P. Mahin Rameshni, Carbon capture overview, Tech. rep., WorleyParsons resources and energy (2010).
URL `http://www.worleyparsons.com/CSG/Hydrocarbons/SpecialtyCapabilities/Documents/Carbon%20Capture%20Overview%20%283%29.pdf` 16

[46] V. Shah, R. Cadours, C. Weiss, C. Benquet, Hysweet process: An improve-

ment in energy efficiency, in: Society of Petroleum Engineers, 2010. `doi:` `10.2118/137977-MS`. 16

[47] A. Acton, Carbon-Oxygen Lyases: Advances in Research and Application, ScholarlyEditions, Atlanta, Georgia, 2013. 16

[48] Huntsman Corporation, Amine Application and Properties Data, Tech. rep., Huntsman Advanced Technology Center (2008). `doi:10.1142/` `9789812814203_0013`. 17

[49] J. Polasek, J. Bullin, Selecting Amines for Sweetening Units (2006).
URL `https://www.bre.com/PDF/Selecting-Amines-for-\` `Sweetening-Units.pdf` 16

[50] A. Chakma, CO_2 capture processes: Opportunities for improved energy efficiencies, Energy Conversion and Management 38, Supplement (0) (1997) S51 – S56, proceedings of the Third International Conference on Carbon Dioxide Removal. `doi:10.1016/S0196-8904(96)00245-2`. 17, 20

[51] F. Lallemand, G. Perdu, C. Maretto, C. Weiss, J. Magne-Drisch, A.-C. Lucquin, Solutions for the treatment of highly sour gases: Process technologies for the cost-effective treatment of natural gas with high and ultra-high acid gas content, Digital Refining (2012).
URL `https://www.digitalrefining.com/article/1000356,` `Solutions_for_the_treatment_of_highly____sour_gases.` `html#.XovE98hKhPY` 18, 19, 21, 22, 27, 29, 33

[52] D. M. Austgen, G. T. Rochelle, X. Peng, C. C. Chen, Model of vapor-liquid equilibria for aqueous acid gas-alkanolamine systems using the electrolyte-NRTL equation, Ind. Eng. Chem. Res. 28 (7) (1989) 1060–1073. `doi:` `10.1021/ie00091a028`. 18, 109

[53] K. Nasrifar, A. Tafazzol, Vapor Liquid Equilibria of Acid Gas Aqueous Ethanolamine Solutions Using the PCSAFT Equation of State, Ind. Eng. Chem.

Res. 49 (16) (2010) 7620–7630. `doi:10.1021/ie901181n`. 19, 49, 77, 78, 191, 200

[54] L. Lee, Application: Amine Solutions in Acid Gas Treating, World Scientific Publishing Co. Pte. Ltd., 2008, Ch. 13, pp. 189–221. `doi:10.1142/9789812814203_0013`.
URL `http://www.worldscientific.com/doi/abs/10.1142/9789812814203_0013` 19

[55] T. R. Carey, J. E. Hermes, G. T. Rochelle, A model of acid gas absorption/stripping using methyldiethanolamine with added acid, Gas Separation & Purification 5 (2) (1991) 95 – 109. `doi:10.1016/0950-4214(91)80006-Q`. 19

[56] E. Stewart, R. Lanning, Reduce amine plant solvent losses parts 1 &2, Hydrocarbon Processing (1994).
URL `https://www.osti.gov/biblio/7024236` 20, 21

[57] S. Rennie, Corrosion and materials selection for amine service, Mater. Forum 30 (01 2006).
URL `http://citeseerx.ist.psu.edu/viewdoc/download?doi=10.1.1.585.353&rep=rep1&type=pdf` 20, 21

[58] F. Karadas, M. Atilhan, S. Aparicio, Review on the Use of Ionic Liquids (ILs) as Alternative Fluids for CO_2 Capture and Natural Gas Sweetening, Energy Fuels 24 (11) (2010) 5817–5828. `doi:10.1021/ef1011337`. 21, 67, 68, 69, 109, 110, 178

[59] J. C. Polasek, J. A. Bullin, S. T. Donnelly, Alternative flow schemes to reduce capital and operating costs of amine sweetening units, Tech. rep., Bryan Research and Engineering, Inc. (2006). 21

[60] H. R.Khakdaman, A. T.Zoghi, M. Abedinzadegan, H. A. Ghadirian, Revamping of gas refineries using amine blends, IUST International Journal of Engineering Science (2008).

URL `https://pdfs.semanticscholar.org/3ef5/50d65ea4be7e1acec30ea02f1de1f7ee26d2.pdf?_ga=2.8823029.1562955589.1586221063-401800110.158622106322`

[61] F. Lallemand, G. Perdu, C. Maretto, C. Weiss, J. Magne-Drisch, A.-C. Lucquin, Extending the treatment of highly sour gases: Part 1 the removal of acid gas components from highly or super-sour gases requires the optimum choice of process, Digital Refining (2013).
URL `s://www.digitalrefining.com/article/1000888,Extending_the_treatment_of_highly_sour_gases__part_1.html#.XovQ_8hKhPY` 23

[62] J. N. Knudsen, J. N. Jensen, P.-J. Vilhelmsen, O. Biede, Experience with CO_2 capture from coal flue gas in pilot-scale: Testing of different amine solvents, Energy Procedia 1 (1) (2009) 783 – 790, greenhouse Gas Control Technologies 9. `doi:10.1016/j.egypro.2009.01.104`. 23

[63] P. Singh, W. V. Swaaij, D. W. Brilman, Energy efficient solvents for CO_2 absorption from flue gas: vapor liquid equilibrium and pilot plant study, Energy Procedia 37 (2013) 2021 – 2046. `doi:10.1016/j.egypro.2013.06.082`. 23

[64] H. K. Abdel-Aal, M. Aggour, M. A. Fahim, Petroleum and Gas Field Processing, Marcel Dekker, Inc., 2003. 23, 31, 32

[65] J. Murphy, S. Ferguson, Assessing the Cost Reduction Potential and Competitiveness of Novel (Next Generation) UK Carbon Capture Technology, Department for Business, Energy & Industrial Strategy (2018).
URL `https://assets.publishing.service.gov.uk/government/uploads/system/uploads/attachment_data/file/800680/Literature_Review_Report_Rev_2A__1_.pdf` 23, 24

[66] Z. Zhao, H. Dong, X. Zhang, The Research Progress of CO_2 Capture with Ionic Liquids, Chin. J. Chem. Eng. (2012). `doi:10.1016/S1004-9541(12)60371-1`. 24

[67] M. Freemantle, An Introduction to Ionic Liquids, no. ISBN 978-1-84755-161-0, The Royal Society of Chemistry, 2010. 24

[68] A. Kamps, D. Tuma, J. Xia, G. Maurer, Solubility of CO_2 in the ionic liquid [bmim][PF_6], J. Chem. Eng. Data 48 (3) (2003) 746–749. `doi:10.1021/je034023f`. 24, 70, 74

[69] S. N. Aki, B. R. Mellein, E. M. Saurer, J. F. Brennecke, High-Pressure Phase Behavior of Carbon Dioxide with Imidazolium-Based Ionic Liquids, J. Phys. Chem. B 108 (52) (2004) 20355–20365. `doi:10.1021/jp046895+`. 24, 70, 74, 86, 89

[70] A. Shariati, K. Gutkowski, C. J. Peters, Comparison of the phase behavior of some selected binary systems with ionic liquids, AIChE J. 51 (5) (2005) 1532–1540. `doi:10.1002/aic.10384`. 24, 70, 74

[71] E. D. Bates, R. D. Mayton, I. Ntai, J. H. Davis, CO_2 Capture by a Task-Specific Ionic Liquid, J. Am. Chem. Soc. 124 (6) (2002) 926–927. `doi:10.1021/ja017593d`. 24, 70, 74

[72] F.-Y. Jou, A. Mather, Solubility of Hydrogen Sulfide in [bmim][PF_6], Int. J. Thermophys. 28 (2) (2007) 490–495. `doi:10.1007/s10765-007-0185-z`. 25, 68, 71, 74, 110

[73] C. S. Pomelli, C. Chiappe, A. Vidis, G. Laurenczy, P. J. Dyson, Influence of the interaction between hydrogen sulfide and ionic liquids on solubility: experimental and theoretical investigation, J. Phys. Chem. B 111 (45) (2007) 13014–13019. `doi:10.1021/jp076129d`. 25, 68, 71, 74, 110

[74] Y. J. Heintz, L. Sehabiague, B. I. Morsi, K. L. Jones, D. R. Luebke, H. W. Pennline, Hydrogen Sulfide and Carbon Dioxide Removal from Dry Fuel Gas

Streams Using an Ionic Liquid as a Physical Solvent, Energy Fuels 23 (10) (2009) 4822–4830. `doi:10.1021/ef900281v`. 25, 68, 71, 74, 110

[75] A. H. Jalili, A. Mehdizadeh, M. Shokouhi, A. N. Ahmadi, M. Hosseini-Jenab, F. Fateminassab, Solubility and diffusion of CO_2 and H_2S in the ionic liquid 1-ethyl-3-methylimidazolium ethylsulfate, J. Chem. Thermodyn. 42 (10) (2010) 1298 – 1303. `doi:10.1016/j.jct.2010.05.008`. 25, 68, 71, 74, 110

[76] A. Romero, A. Santos, J. Tojo, A. Rodríguez, Toxicity and biodegradability of imidazolium ionic liquids, J. Hazard. Mater. 151 (1) (2008) 268 – 273. `doi:10.1016/j.jhazmat.2007.10.079`. 25, 178

[77] T. P. T. Pham, C.-W. Cho, Y.-S. Yun, Environmental fate and toxicity of ionic liquids: A review, Water Res. 44 (2) (2010) 352 – 372. `doi:10.1016/j.watres.2009.09.030`. 25, 178

[78] Y. Zhao, J. Zhao, Y. Huang, Q. Zhou, X. Zhang, S. Zhang, Toxicity of ionic liquids: Database and prediction via quantitative structure–activity relationship method, J. Hazard. Mater. 278 (2014) 320 – 329. `doi:10.1016/j.jhazmat.2014.06.018`. 25, 178

[79] C. A. Grande, Advances in Pressure Swing Adsorption for Gas Separation, ISRN Chemical Engineering (2012). 25

[80] S. G. Poulopoulos, V. J. Inglezakis, Adsorption, Ion Exchange and Catalysis: Design of Operations and Environmental Applications, Elsevier, 2006. 25

[81] D. G. Pahinkar, S. Garimella, A novel temperature swing adsorption process for natural gas purification: Part I, model development, Sep. Purif. Technol. 203 (2018) 124 – 142. `doi:10.1016/j.seppur.2018.04.020`. 25, 26

[82] Y. Wang, M. D. LeVan, Adsorption Equilibrium of Carbon Dioxide and Water Vapor on Zeolites 5A and 13X and Silica Gel: Pure Components, Journal of Chemical & Engineering Data 54 (10) (2009) 2839–2844. `doi:10.1021/je800900a`. 26

[83] K. Morishige, Adsorption and Separation of CO_2/CH_4 on Amorphous Silica Molecular Sieve, The Journal of Physical Chemistry C 115 (19) (2011) 9713–9718. `doi:10.1021/jp202572w`. 26

[84] J. A. Delgado, M. A. Uguina, J. L. Sotelo, B. Ruíz, M. Rosário, Carbon Dioxide/Methane Separation by Adsorption on Sepiolite, J. Nat. Gas Chem. 16 (3) (2007) 235 – 243. `doi:10.1016/S1003-9953(07)60054-1`. 26

[85] J. A. Delgado, M. A. Uguina, J. L. Sotelo, V. I. Águeda, A. García, A. Roldán, Separation of ethanol–water liquid mixtures by adsorption on silicalite, Chemical Engineering Journal 180 (2012) 137 – 144. `doi:10.1016/j.cej.2011.11.026`. 26

[86] N. Casas, J. Schell, R. Blom, M. Mazzotti, MOF and UiO-67/MCM-41 adsorbents for pre-combustion CO_2 capture by PSA: Breakthrough experiments and process design, Sep. Purif. Technol. 112 (2013) 34 – 48. `doi:10.1016/j.seppur.2013.03.042`. 26

[87] C. Shen, J. Yu, P. Li, C. A. Grande, A. E. Rodrigues, Capture of CO_2 from flue gas by vacuum pressure swing adsorption using activated carbon beads, Adsorption 17 (1) (2011) 179–188. `doi:10.1007/s10450-010-9298-y`. 26

[88] M. Mork, J. S. Gudmundsson, Natural gas cleaning, Tech. rep., Department of Petroleum Engineering and Applied Geophysics (2005).
URL `http://www.ipt.ntnu.no/~jsg/undervisning/prosessering/gammelt/kompendium2005/11-RensingNaturgass.pdf` 26

[89] A. A. Olajire, CO_2 capture and separation technologies for end-of-pipe applications: A review, Energy 35 (6) (2010) 2610 – 2628, 7th International Conference on Sustainable Energy Technologies 7th International Conference on Sustainable Energy Technologies. `doi:10.1016/j.energy.2010.02.030`. 26, 27

[90] C. Petit, B. Mendoza, T. J. Bandosz, Hydrogen Sulfide Adsorption on MOFs and MOF/Graphite Oxide Composites, ChemPhysChem 11 (17) (2010) 3678–3684. `arXiv:https://onlinelibrary.wiley.com/doi/pdf/10.1002/cphc.201000689`, `doi:10.1002/cphc.201000689`. 26

[91] X. Xu, C. Song, J. M. Andresen, B. G. Miller, A. W. Scaroni, Novel Polyethylenimine-Modified Mesoporous Molecular Sieve of MCM-41 Type as High-Capacity Adsorbent for CO2 Capture, Energy & Fuels 16 (6) (2002) 1463–1469. `doi:10.1021/ef020058u`. 26

[92] P. D. Jadhav, R. V. Chatti, R. B. Biniwale, N. K. Labhsetwar, S. Devotta, S. S. Rayalu, Monoethanol Amine Modified Zeolite 13X for CO2 Adsorption at Different Temperatures, Energy & Fuels 21 (6) (2007) 3555–3559. `doi:10.1021/ef070038y`. 26

[93] A. Sayari, Y. Belmabkhout, R. Serna-Guerrero, Flue gas treatment via CO_2 adsorption, Chemical Engineering Journal 171 (3) (2011) 760 – 774. `doi:10.1016/j.cej.2011.02.007`. 26

[94] A. Tabe-Mohammadi, A Review of the Applications of Membrane Separation Technology in Natural Gas Treatment, Sep. Sci. Technol. 34 (10) (1999) 2095–2111. `doi:10.1081/SS-100100758`. 27

[95] H. K. Engelien, Process Integrated Membrane Separation - with Application to the Removal of CO_2 from Natural Gas, Department of Chemical Engineering, Norwegian University of Science and Technology, NTNU.
URL `https://www.slideserve.com/castor-slater/22-march-2004-department-of-chemical-engineering-\ntnu-powerpoint-ppt-presentation` 27, 28

[96] S. Mokhatab, W. A. Poe, Handbook of Natural Gas Transmission and Processing, 2nd Edition, Elsevier Inc., 2012.
URL `http://www.sciencedirect.com/science/article/pii/B9780123869142000273` 27

[97] T. Cnop, D. Dortmundt, M. Schott. Continued development of gas separation: Membranes for highly sour service [online] (2007). 27, 28

[98] W. Echt, Hybrid Systems: Combining Technologies Leads to More Efficient Gas Conditioning, 52nd Laurance Reid Gas Conditioning Conference, Norman, Oklahoma (2002). 28

[99] K. L. Pat Hale, Advances in Membrane Materials Provide New Solutions in the Gas Business, 83rd GPA Annual Convention, New Orleans, Louisiana, March (2004). 28

[100] S. Mohebi, S. Mousavi, S. Kiani, Modeling and simulation of sour gas membrane-absorption system: Influence of operational parameters on species removal, J. Nat. Gas Sci. Eng. 1 (6) (2009) 195 – 204. doi:10.1016/j.jngse.2009.12.002. 28

[101] M. Hedayat, M. Soltanieh, S. A. Mousavi, Simultaneous separation of H_2S and CO_2 from natural gas by hollow fiber membrane contactor using mixture of alkanolamines, J. Membr. Sci. 377 (1–2) (2011) 191 – 197. doi:10.1016/j.memsci.2011.04.051. 28

[102] S. Northrop, J. Valencia, The CFZ™ process: A cryogenic method for handling high CO_2 and H_2S gas reserves and facilitating geosequestration of CO_2 and acid gases, Energy Procedia 1 (1) (2009) 171 – 177, greenhouse Gas Control Technologies 9 Proceedings of the 9th International Conference on Greenhouse Gas Control Technologies (GHGT-9), 16–20 November 2008, Washington DC, USA. doi:10.1016/j.egypro.2009.01.025. 29, 30, 33

[103] A. N. A. Binti-Hamzah, Evaluation of Modified Kent Eisenberg Model to Predict Carbon Dioxide Solubility in Methyldiethanolamine (MDEA) Under Extended Operating Conditions, Master's thesis, Universiti Teknologi, PETRONAS (2013).
URL http://utpedia.utp.edu.my/10226/1/FYP_CHE_12506.pdf 29

[104] A. S. Holmes, J. M. Ryan, Cryogenic distillative separation of acid gases from methane (1982).
URL https://patents.google.com/patent/US4318723A/en 29

[105] B. Kelley, J. Valencia, P. Northrop, C. Mart, Controlled freeze zone™ for developing sour gas reserves, Energy Procedia 4 (0) (2011) 824 – 829. doi:10.1016/j.egypro.2011.01.125. 29, 30, 33

[106] T. Rufford, S. Smart, G. Watson, B. Graham, J. Boxall, J. D. da Costa, E. May, The removal of CO_2 and N_2 from natural gas: A review of conventional and emerging process technologies, Journal of Petroleum Science and Engineering 94-95 (2012) 123 – 154. doi:https://doi.org/10.1016/j.petrol.2012.06.016.
URL http://www.sciencedirect.com/science/article/pii/S0920410512001581 30

[107] A. K. Coker, Chapter 11 - petroleum, complex-mixture fractionation, gas processing, dehydration, hydrocarbon absorption and stripping: Part 2: Fractionation, in: A. K. Coker (Ed.), Ludwig's Applied Process Design for Chemical and Petrochemical Plants (Fourth Edition), fourth edition Edition, Gulf Professional Publishing, Boston, 2010, pp. 269 – 344. doi:10.1016/B978-0-7506-8366-1.10011-8. 31

[108] K. S. Fisher, G. T. Rochelle, C. Schubert, Advanced Amine Solvent Formulations and Process Integration for Near-Term CO_2 Capture Success, Tech. Rep. DE-FG02-06ER84625, U.S. Department of Energy, National Energy Technology Laboratory (2007).
URL https://www.osti.gov/servlets/purl/945367/ 31, 130, 131

[109] J. Husebye, A. L. Brunsvold, S. Roussanaly, X. Zhang, Techno Economic Evaluation of Amine based CO2 Capture: Impact of CO2 Concentration and Steam Supply, Energy Procedia 23 (2012) 381 – 390. doi:10.1016/j.egypro.2012.06.053. 31

[110] M. Tagliabue, D. Farrusseng, S. Valencia, S. Aguado, U. Ravon, C. Rizzo, A. Corma, C. Mirodatos, Natural gas treating by selective adsorption: Material science and chemical engineering interplay, Chemical Engineering Journal 155 (3) (2009) 553 – 566. `doi:10.1016/j.cej.2009.09.010`. 31

[111] F. Berg, C. Pasel, T. Eckardt, D. Bathen, Temperature Swing Adsorption in Natural Gas Processing: A Concise Overview, ChemBioEng Reviews 6 (3) (2019) 59–71. `arXiv:https://onlinelibrary.wiley.com/doi/pdf/10.1002/cben.201900005`, `doi:10.1002/cben.201900005`. 31

[112] S. A. Marzouk, M. H. Al-Marzouqi, M. Teramoto, N. Abdullatif, Z. M. Ismail, Simultaneous removal of CO2 and H2S from pressurized CO2–H2S–CH4 gas mixture using hollow fiber membrane contactors, Sep. Purif. Technol. 86 (2012) 88 – 97. `doi:10.1016/j.seppur.2011.10.024`. 31

[113] D. Berstad, P. Nekså, R. Anantharaman, Low-temperature CO2 Removal from Natural Gas, Energy Procedia 26 (2012) 41–48. `doi:10.1016/j.egypro.2012.06.008`. 31

[114] R. Khalilpour, K. Mumford, H. Zhai, A. Abbas, G. Stevens, E. S. Rubin, Membrane-based carbon capture from flue gas: a review, Journal of Cleaner Production 103 (2015) 286 – 300. `doi:10.1016/j.jclepro.2014.10.050`. 32

[115] Linde Process Plants, Inc., A member of the Linde Group, Sulfur process technology. 32

[116] J. Meyer, Summary of Carbon Dioxide Enhanced Oil Recovery (CO_2 EOR) Injection Well Technology, Tech. rep., American Petroleum Institute (2010). URL `https://www.api.org/~/media/Files/EHS/climate-change/Summary-carbon-dioxide-enhanced-oil-\recovery-well-tech.pdf` 33

[117] S. Bachu, K. Haug, K. Michael, Stress Regime at Acid-Gas Injection Operations in Western Canada, Tech. rep., Alberta Geological Survey, Alberta Energy and

Utilities Board (2008).
URL https://ags.aer.ca/publications/SPE_094.html 33

[118] Canadian Centre for Occupational Health and Safety (CCOHS). Hydrogen Sulfide Uses and Occurrences [online] (2012). 33

[119] A. S. Hirschon, R. M. Laine, Chemistry of hydrogen sulphide under coal liquefaction conditions: Synergistic effects of H_2S and the mixed solvent system tetralin and tetrahydroquinoline on liquefaction of a moderately reactive coal, Fuel 64 (7) (1985) 911 – 915. doi:10.1016/0016-2361(85)90142-5. 33

[120] Universal Industrial Gases, Inc. Carbon Dioxide (CO_2) Properties, Uses, Applications: CO_2 Gas and Liquid Carbon Dioxide [online] (2003). 33

[121] nternational Energy Agency, "Methane Tracker": Reducing the environmental impact of oil and gas supply is a pivotal element of global energy transitions , IEA, Paris (2020). 34

[122] P. M. Mathias, T. W. Copeman, Extension of the Peng-Robinson equation of state to complex mixtures: Evaluation of the various forms of the local composition concept, Fluid Phase Equilib. 13 (1983) 91 – 108. doi:10.1016/0378-3812(83)80084-3. 35

[123] M. Medeiros, P. Tellez-Arredondo, Cubic two-state equation of state for associating fluids, Ind. Eng. Chem. Res. 47 (15) (2008) 5723–5733. doi:10.1021/ie071397j. 35, 47

[124] L. Faramarzi, G. M. Kontogeorgis, K. Thomsen, E. H. Stenby, Extended UNIQUAC model for thermodynamic modeling of CO_2 absorption in aqueous alkanolamine solutions, Fluid Phase Equilib. 282 (2) (2009) 121 – 132. doi:10.1016/j.fluid.2009.05.002. 35

[125] J. Prausnitz, R. Lichtenthaler, Molecular Thermodynamics of Fluid-Phase Equilibria, Prentice Hall, Inc., 1986. 36, 42, 56, 58, 59, 60, 62, 64, 65

[126] K. Denbigh, The Principles of Chemical Equilibrium, The syndics of the Cambridge university press, 1963. 36, 37, 42, 45, 59

[127] M. Modell, R. Reid, Thermodynamics and its applications, Prentice-Hall international series in the physical and chemical engineering sciences, Prentice–Hall, 1983. 42, 59

[128] J. M. Smith, H. C. Van Ness, Introduction to chemical engineering thermodynamics, McGraw-Hill, 1975. 43, 44, 45, 57, 60, 62, 65

[129] D. Y. Peng, D. B. Robinson, A new two-constant equation of state, Ind. Eng. Chem. Fund 15 (1) (1976) 59–64. doi:10.1021/i160057a011. 45, 71

[130] S. Giorgio, Equilibrium constants from a modified Redlich-Kwong equation of state, Chem. Eng. Sci. 27 (6) (1972) 1197 – 1203. doi:10.1016/0009-2509(72)80096-4. 45, 71

[131] E. des Grades, A New Equation of State for Natural Gases and Other Mixtures for the Gas and Liquid Regions and the Phase Equilibrium, Ph.D. thesis, Ruhr-University Bochum (2006).
URL http://www-brs.ub.ruhr-uni-bochum.de/netahtml/HSS/Diss/KunzOliver/diss.pdf 47

[132] S. Poormohammadian, A. Lashanizadegan, M. K. Salooki, Modelling VLE data of CO_2 and H_2S in aqueous solutions of N-methyldiethanolamine based on non-random mixing rules, International Journal of Greenhouse Gas Control 42 (2015) 87 – 97. doi:10.1016/j.ijggc.2015.07.036. 47

[133] I. G. Economou, M. D. Donohue, Equations of state for hydrogen bonding systems, Fluid Phase Equilib. 116 (1) (1996) 518 – 529. doi:10.1016/0378-3812(95)02926-5. 47

[134] E. A. Muller, K. E. Gubbins, Molecular–Based Equations of State for Associating Fluids: A Review of SAFT and Related Approaches, Ind. Eng. Chem. Res. 40 (10) (2001) 2193–2211. doi:10.1021/ie000773w. 47

[135] A. T. Zoghi, F. Feyzi, S. Zarrinpashneh, F. Alavi, Solubility of light reservoir gases in water by the modified Peng-Robinson plus association equation of state using experimental critical properties for pure water, J. Pet. Sci. Eng. 78 (1) (2011) 109 – 118. `doi:10.1016/j.petrol.2011.05.001`. 47

[136] A. T. Zoghi, F. Feyzi, M. R. Dehghani, Modeling CO_2 Solubility in Aqueous N-methyldiethanolamine Solution by Electrolyte Modified Peng–Robinson Plus Association Equation of State, Ind. Eng. Chem. Res. 51 (29) (2012) 9875–9885. `doi:10.1021/ie2026053`. 47

[137] W. G. Chapman, K. E. Gubbins, G. Jackson, M. Radosz, New reference equation of state for associating liquids, Ind. Eng. Chem. Res. 29 (8) (1990) 1709–1721. `doi:10.1021/ie00104a021`. 47, 48, 51, 53, 73, 190

[138] S. H. Huang, M. Radosz, Equation of state for small, large, polydisperse, and associating molecules, Ind. Eng. Chem. Res. 29 (11) (1990) 2284–2294. `doi:10.1021/ie00107a014`. 47, 48, 73

[139] J. Gross, G. Sadowski, Perturbed Chain SAFT: An Equation of State Based on a Perturbation Theory for Chain Molecules, Ind. Eng. Chem. Res. 40 (4) (2001) 1244–1260. `doi:10.1021/ie0003887`. 48, 49, 51, 53, 74, 75, 77, 78, 95, 190, 191, 193, 200

[140] J. W. Gibbs, Elementary Principles in Statistical Mechanics, Charles Scribner's Sons, 1902. 48

[141] S. Beret, J. M. Prausnitz, Perturbed hard-chain theory: An equation of state for fluids containing small or large molecules, AIChE J. 21 (6) (1975) 1123–1132. `doi:10.1002/aic.690210612`. 48

[142] M. D. Donohue, J. M. Prausnitz, Perturbed hard chain theory for fluid mixtures: Thermodynamic properties for mixtures in natural gas and petroleum technology, AIChE J. 24 (5) (1978) 849–860. `doi:10.1002/aic.690240511`. 48

[143] P. Vimalchand, M. D. Donohue, Thermodynamics of quadrupolar molecules: the perturbed anisotropic chain theory, Ind. Eng. Chem. Fundam. 24 (2) (1985) 246–257. `doi:10.1021/i100018a018`. 48

[144] G. D. Ikonomou, M. D. Donohue, Thermodynamics of hydrogen-bonded molecules: The associated perturbed anisotropic chain theory, AIChE J. 32 (10) (1986) 1716–1725. `doi:10.1002/aic.690321015`. 48

[145] M. Banaszak, Y. C. Chiew, R. O'Lenick, M. Radosz, Thermodynamic perturbation theory: Lennard-jones chains, J. Chem. Phys 100 (5) (1994) 3803–3807. `doi:10.1063/1.466368`. 48

[146] J. K. Johnson, E. A. Mueller, K. E. Gubbins, Equation of state for lennard-jones chains, J. Phys. Chem. 98 (25) (1994) 6413–6419. `doi:10.1021/j100076a028`. 48, 49

[147] M. S. Wertheim, Thermodynamic perturbation theory of polymerization, J. Phys. Chem. 87 (12) (1987) 7323–7331. `doi:10.1063/1.453326`. 48

[148] D. Chandler, Introduction to Modern Statistical Mechanics, New York: Oxford University Press, 1987. 48

[149] M. Thol, G. Rutkai, A. Köster, R. Lustig, R. Span, J. Vrabec, Equation of State for the Lennard-Jones Fluid, Journal of Physical and Chemical Reference Data 45 (2) (2016) 023101. `arXiv:https://doi.org/10.1063/1.4945000`, `doi:10.1063/1.4945000`.
URL `https://doi.org/10.1063/1.4945000` 48

[150] X.-J. Li, Y. C. Chiew, Monte carlo simulation of equation of state and structure of chain fluids, Chem. Eng. Sci. 49 (17) (1994) 2805 – 2813. `doi:10.1016/0009-2509(94)E0099-C`. 49

[151] A. Gil-Villegas, A. Galindo, P. J. Whitehead, S. J. Mills, G. Jackson, A. N. Burgess, Statistical associating fluid theory for chain molecules with attractive potentials of variable range, J. Chem. Phys 106 (10) (1997) 4168–4186. `doi:10.1063/1.473101`. 49

[152] J. Gross, G. Sadowski, Modeling Polymer Systems Using the Perturbed-Chain Statistical Associating Fluid Theory Equation of State, Ind. Eng. Chem. Res 41 (5) (2002) 1084–1093. `doi:10.1021/ie010449g`. 49

[153] H. Pahlavanzadeh, S. F. Baygi, Modeling CO_2 solubility in Aqueous Methyldiethanolamine Solutions by Perturbed Chain-SAFT Equation of State, J. Chem. Thermodyn. 59 (0) (2013) 214 – 221. `doi:10.1016/j.jct.2012.12.021`. 49

[154] P. Debye, E. Hückel, On the theory of electrolytes i. freezing point depression and related phenomena, Phys. Z. 24 (9) (1923) 185–206. 50, 54, 191, 192

[155] C. Held, L. F. Cameretti, G. Sadowski, Modeling aqueous electrolyte solutions: Part 1. Fully dissociated electrolytes, Fluid Phase Equilib. 270 (1–2) (2008) 87 – 96. `doi:10.1016/j.fluid.2008.06.010`. 51, 54

[156] C. G. J. Christopher G. Gray, Keith E. Gubbins, Theory of Molecular Fluids 2: Applications. International Series of Monographs on Chemistry, Oxford University Press Inc., 2011. 55

[157] T. Welton, Ionic liquids in catalysis, Coord. Chem. Rev. 248 (21-24) (2004) 2459–2477. `doi:10.1016/j.ccr.2004.04.015`. 69

[158] A. H. Jalili, M. Safavi, C. Ghotbi, A. Mehdizadeh, M. Hosseini-Jenab, V. Taghikhani, Solubility of CO_2, H_2S, and Their Mixture in the Ionic Liquid 1-Octyl-3-methylimidazolium Bis(trifluoromethyl)sulfonylimide, J. Phys. Chem. B 116 (9) (2012) 2758–2774. `doi:10.1021/jp2075572`. 69, 86, 89, 91, 93, 94, 95, 96, 97

[159] A. Somers, P. Howlett, D. MacFarlane, M. Forsyth, A review of ionic liquid lubricants, Lubricants 1 (1) (2013) 3–21. 70

[160] E. Hawlicka, T. Dlugoborski, Molecular dynamics simulations of the aqueous solution of tetramethylammonium chloride, Chem. Phys. Lett. 268 (5–6) (1997) 325 – 330. `doi:10.1016/S0009-2614(97)00229-7`. 71, 74

[161] J. Oberbrodhage, Phase transfer catalysts between polar and non-polar media: a molecular dynamics simulation of tetrabutylammonium iodide at the formamide-hexane interface, Phys. Chem. Chem. Phys. 2 (2000) 129–135. `doi:10.1039/A907612C`. 71, 74

[162] C. G. Hanke, N. A. Atamas, R. M. Lynden-Bell, Solvation of small molecules in imidazolium ionic liquids: a simulation study, Green Chem. 4 (2002) 107–111. `doi:10.1039/B109179B`. 71, 74

[163] T. I. Morrow, , E. J. Maginn, Molecular Dynamics Study of the Ionic Liquid 1-n-Butyl-3-methylimidazolium Hexafluorophosphate, J. Phys. Chem. B 106 (49) (2002) 12807–12813. `doi:10.1021/jp0267003`. 71, 74

[164] X. Liu, S. Zhang, G. Zhou, G. Wu, X. Yuan, X. Yao, New Force Field for Molecular Simulation of Guanidinium-Based Ionic Liquids, J. Phys. Chem. B 110 (24) (2006) 12062–12071. `doi:10.1021/jp060834p`. 71, 74

[165] S. Tsuzuki, W. Shinoda, H. Saito, M. Mikami, H. Tokuda, M. Watanabe, Molecular Dynamics Simulations of Ionic Liquids: Cation and Anion Dependence of Self-Diffusion Coefficients of Ions, J. Phys. Chem. B 113 (31) (2009) 10641–10649. `doi:10.1021/jp811128b`. 71, 74

[166] S. Feng, G. A. Voth, Molecular dynamics simulations of imidazolium-based ionic liquid/water mixtures: Alkyl side chain length and anion effects, Fluid Phase Equilib. 294 (1–2) (2010) 148 – 156. `doi:10.1016/j.fluid.2010.02.034`. 71, 74

[167] G. Hantal, I. Voroshylova, M. N. D. S. Cordeiro, M. Jorge, A systematic molecular simulation study of ionic liquid surfaces using intrinsic analysis methods, Phys. Chem. Chem. Phys. 14 (2012) 5200–5213. `doi:10.1039/C2CP23967A`. 71, 74

[168] B. Yoo, J. K. Shah, Y. Zhu, E. J. Maginn, Amphiphilic interactions of ionic liquids with lipid biomembranes: a molecular simulation study, Soft Matter 10 (2014) 8641–8651. `doi:10.1039/C4SM01528B`. 71, 74

[169] L. F. Vega, O. Vilaseca, F. Llovell, J. S. Andreu, Modeling ionic liquids and the solubility of gases in them: Recent advances and perspectives, Fluid Phase Equilib. 294 (1–2) (2010) 15 – 30. `doi:10.1016/j.fluid.2010.02.006`. 71

[170] A. Shariati, C. J. Peters, High pressure phase behavior of systems with ionic liquids: measurements and modeling of the binary system fluoroform+1-ethyl-3-methylimidazolium hexafluorophosphate, J. Supercrit. Fluids 25 (2) (2003) 109 – 117. `doi:10.1016/S0896-8446(02)00160-2`. 71, 74

[171] M. B. Shiflett, A. Yokozeki, Solubilities and Diffusivities of Carbon Dioxide in Ionic Liquids: [bmim][PF_6] and [bmim][BF_4], Ind. Eng. Chem. Res. 44 (12) (2005) 4453–4464. `doi:10.1021/ie058003d`. 71, 74

[172] M. B. Shiflett, A. Yokozeki, Solubility of CO_2 in Room Temperature Ionic Liquid [hmim] [Tf_2N], J. Phys. Chem. B 111 (8) (2007) 2070–2074. `doi:10.1021/jp067627`. 71, 89

[173] M. B. Shiflett, A. Yokozeki, Separation of CO_2 and H_2S using room-temperature ionic liquid [bmim][PF6], Fluid Phase Equilib. 294 (1–2) (2010) 105 – 113. `doi:10.1016/j.fluid.2010.01.013`. 71

[174] H. Renon, J. M. Prausnitz, Local compositions in thermodynamic excess functions for liquid mixtures, AIChE J. 14 (1) (1968) 135–144. `doi:10.1002/aic.690140124`. 72

[175] D. S. Abrams, J. M. Prausnitz, Statistical thermodynamics of liquid mixtures: A new expression for the excess gibbs energy of partly or completely miscible systems., AIChE J. 21 (1) (1975) 116–128. 72

[176] U. Domanska, A. Marciniak, Phase behaviour of 1-hexyloxymethyl-3-methyl-imidazolium and 1,3-dihexyloxymethyl-imidazolium based ionic liquids with alcohols, water, ketones and hydrocarbons: The effect of cation and anion on solubility, Fluid Phase Equilib. 260 (1) (2007) 9 – 18. `doi:10.1016/j.fluid.2006.07.005`. 72, 74

[177] T. Banerjee, M. K. Singh, R. K. Sahoo, A. Khanna, Volume, surface and {UNIQUAC} interaction parameters for imidazolium based ionic liquids via Polarizable Continuum Model, Fluid Phase Equilib. 234 (1–2) (2005) 64 – 76. `doi:10.1016/j.fluid.2005.05.017`. 72, 74

[178] A. Fredenslund, R. L. Jones, J. M. Prausnitz, Group-contribution estimation of activity coefficients in nonideal liquid mixtures, AIChE J. 21 (6) (1975) 1086–1099. `doi:10.1002/aic.690210607`. 72

[179] U. Weidlich, J. Gmehling, A modified UNIFAC model. 1. Prediction of VLE, h^E and γ^∞, Ind. Eng. Chem. Res. 26 (7) (1987) 1372–1381. `doi:10.1021/ie00067a018`. 72

[180] Y. Gaston-Bonhomme, P. Petrino, J. Chevalier, UNIFAC—VISCO group contribution method for predicting kinematic viscosity: extension and temperature dependence, Chem. Eng. Sci. 49 (11) (1994) 1799 – 1806. `doi:10.1016/0009-2509(94)80065-0`. 72

[181] N. Zhao, R. Oozeerally, V. Degirmenci, Z. Wagner, M. Bendová, J. Jacquemin, New Method Based on the UNIFAC–VISCO Model for the Estimation of Ionic Liquids Viscosity Using the Experimental Data Recommended by Mathematical Gnostics, J. Chem. Eng. Data 61 (11) (2016) 3908–3921. `doi:10.1021/acs.jced.6b00689`. 72

[182] N. Zhao, J. Jacquemin, R. Oozeerally, V. Degirmenci, New Method for the Estimation of Viscosity of Pure and Mixtures of Ionic Liquids Based on the UNIFAC–VISCO Model, J. Chem. Eng. Data 61 (6) (2016) 2160–2169. `doi:10.1021/acs.jced.6b00161`. 72

[183] R. Kato, J. Gmehling, Systems with ionic liquids: Measurement of VLE and γ^∞ data and prediction of their thermodynamic behavior using original UNIFAC, mod. UNIFAC(Do) and COSMO-RS(Ol), J. Chem. Thermodyn. 37 (6) (2005) 603 – 619. `doi:10.1016/j.jct.2005.04.010`. 72, 74

[184] S. Nebig, R. Bolts, J. Gmehling, Measurement of vapor liquid equilibria (vle) and excess enthalpies (he) of binary systems with 1-alkyl-3-methylimidazolium bis(trifluoromethylsulfonyl)imide and prediction of these properties and γ^∞ using modified UNIFAC (dortmund), Fluid Phase Equilib. 258 (2) (2007) 168 – 178. doi:10.1016/j.fluid.2007.06.001. 72, 74

[185] Z. Lei, C. Dai, W. Wang, B. Chen, UNIFAC model for ionic liquid-CO_2 systems, AIChE J. 60 (2) (2014) 716–729. doi:10.1002/aic.14294. 72

[186] A. Klamt, Conductor-like Screening Model for Real Solvents: A New Approach to the Quantitative Calculation of Solvation Phenomena, J. Phys. Chem. 99 (7) (1995) 2224–2235. doi:10.1021/j100007a062. 72

[187] U. Domanska, A. Pobudkowska, F. Eckert, (Liquid + liquid) phase equilibria of 1-alkyl-3-methylimidazolium methylsulfate with alcohols, or ethers, or ketones, J. Chem. Thermodyn. 38 (6) (2006) 685–695. doi:10.1016/j.jct.2005.07.024. 72, 74

[188] T. Banerjee, M. Singh, A. Khanna, Prediction of binary VLE of imidazolium-based ionic liquids by COSMU-RS, Ind. Eng. Chem. Res. 45 (20) (2006) 6876. doi:10.1021/ie061107j. 72, 74

[189] M. Freire, L. Santos, I. Marrucho, J. Coutinho, Evaluation of COSMO-RS for the prediction of LLE and VLE of alcohols + ionic liquids, Fluid Phase Equilib. 255 (2) (2007) 167–178. doi:10.1016/j.fluid.2007.04.020. 72, 74

[190] A. Klamt, F. Eckert, W. Arlt, COSMO-RS: An Alternative to Simulation for Calculating Thermodynamic Properties of Liquid Mixtures, Annual review of chemical and biomolecular engineering 1 (2010) 101–22. doi:10.1146/annurev-chembioeng-073009-100903. 72, 73

[191] A. Gil-Villegas, A. Galindo, P. J. Whitehead, S. J. Mills, G. Jackson, A. N. Burgess, Statistical associating fluid theory for chain molecules with attractive potentials of variable range, J. Chem. Phys 106 (10) (1997) 4168–4186. doi:10.1063/1.473101. 73, 74

251

[192] F. J. Blas, L. F. Vega, Thermodynamic behaviour of homonuclear and heteronuclear Lennard-Jones chains with association sites from simulation and theory, Mol. Phys. 92 (1) (1997) 135–150. `doi:10.1080/002689797170707`. 73, 74

[193] A. Lymperiadis, C. S. Adjiman, A. Galindo, G. Jackson, A group contribution method for associating chain molecules based on the statistical associating fluid theory (SAFT-γ), J. Phys. Chem. 127 (23) (2007) 234903. `doi:10.1063/1.2813894`. 73, 74

[194] E. K. Karakatsani, I. G. Economou, Perturbed Chain-Statistical Associating Fluid Theory Extended to Dipolar and Quadrupolar Molecular Fluids, J. Phys. Chem. B 110 (18) (2006) 9252–9261. `doi:10.1021/jp056957b`. 73, 74

[195] M. Rahmati-Rostami, B. Behzadi, C. Ghotbi, Thermodynamic modeling of hydrogen sulfide solubility in ionic liquids using modified SAFT-VR and PC-SAFT equations of state, Fluid Phase Equilib. 309 (2) (2011) 179 – 189. `doi:10.1016/j.fluid.2011.07.013`. 73, 74

[196] M. C. Kroon, E. K. Karakatsani, I. G. Economou, G. J. Witkamp, C. J. Peters, Modeling of the Carbon Dioxide Solubility in Imidazolium-Based Ionic Liquids with the tPC-PSAFT Equation of State, J. Phys. Chem. B 110 (18) (2006) 9262–9269. `doi:10.1021/jp060300o`. 73, 74

[197] F. Llovell, E. Valente, O. Vilaseca, L. F. Vega, Modeling Complex Associating Mixtures with [$C_n$mim][Tf_2N] Ionic Liquids: Predictions from the Soft-SAFT Equation, J. Phys. Chem. B 115 (15) (2011) 4387–4398. `doi:10.1021/jp112315b`. 73, 74

[198] S. Ashrafmansouri, S. Raeissi, Modeling gas solubility in ionic liquids with the SAFT-γ group contribution method, J. Supercrit. Fluids 63 (2012) 81 – 91. `doi:10.1016/j.supflu.2011.12.014`. 73, 74

[199] A. H. Jalili, M. Rahmati-Rostami, C. Ghotbi, M. Hosseini-Jenab, A. N. Ahmadi, Solubility of H_2S in Ionic Liquids [bmim][PF_6], [bmim][BF_4], and

[bmim][Tf$_2$N], J. Chem. Eng. Data 54 (6) (2009) 1844–1849. `doi:10.1021/je8009495`. 74, 89

[200] B. Guo, E. Duan, Y. Zhong, L. Gao, X. Zhang, D. Zhao, Absorption and oxidation of H$_2$S in caprolactam tetrabutyl ammonium bromide ionic liquid, Energy & Fuels 25 (1) (2010) 159–161. 74

[201] C. G. Hanke, S. L. Price, R. M. Lynden-Bell, Intermolecular potentials for simulations of liquid imidazolium salts, Mol. Phys. 99 (10) (2001) 801–809. `doi:10.1080/00268970010018981`. 74

[202] Z. Liu, S. Huang, W. Wang, A refined force field for molecular simulation of imidazolium-based ionic liquids, J. Phys. Chem. B 108 (34) (2004) 12978–12989. `doi:10.1021/jp048369o`. 74

[203] J. A. C. Marta L.S. Batista, J. R. Gomes, Prediction of Ionic Liquids Properties through Molecular Dynamics Simulations, Current Physical Chemistry 4 (2) (2014) 151–172. 74

[204] R. L. Gardas, J. A. Coutinho, Extension of the Ye and Shreeve group contribution method for density estimation of ionic liquids in a wide range of temperatures and pressures, Fluid Phase Equilib. 263 (1) (2008) 26 – 32. `doi:10.1016/j.fluid.2007.09.016`. 74

[205] R. L. Gardas, J. A. Coutinho, Applying a {QSPR} correlation to the prediction of surface tensions of ionic liquids, Fluid Phase Equilib. 265 (1–2) (2008) 57 – 65. `doi:10.1016/j.fluid.2008.01.002`. 74

[206] R. L. Gardas, J. A. Coutinho, Estimation of speed of sound of ionic liquids using surface tensions and densities: A volume based approach, Fluid Phase Equilib. 267 (2) (2008) 188 – 192. `doi:10.1016/j.fluid.2008.03.008`. 74

[207] U. Domanska, A. Pobudkowska, F. Eckert, Liquid-liquid equilibria in the binary systems (1,3-dimethylimidazolium, or 1-butyl-3-methylimidazolium methylsulfate + hydrocarbons), Green Chem. 8 (2006) 268–276. `doi:10.1039/B514521J`. 74

[208] Y. Chen, F. Mutelet, J. N. Jaubert, Modeling the Solubility of Carbon Dioxide in Imidazolium Based Ionic Liquids with the PCSAFT Equation of State, J. Phys. Chem. B 116 (49) (2012) 14375–14388. `doi:10.1021/jp309944t`. 74, 84, 111

[209] M. B. Oliveira, F. Llovell, J. A. P. Coutinho, L. F. Vega, Modeling the [NTf2] Pyridinium Ionic Liquids Family and Their Mixtures with the Soft Statistical Associating Fluid Theory Equation of State, J. Phys. Chem. B 116 (30) (2012) 9089–9100, pMID: 22712755. `doi:10.1021/jp303166f`. 74

[210] P. A. Hunt, C. R. Ashworth, R. P. Matthews, Hydrogen bonding in ionic liquids, Chem. Soc. Rev. 44 (2015) 1257–1288. `doi:10.1039/C4CS00278D`. 75

[211] B. D. Mather, Non-covalent interactions in block copolymers synthesized via living polymerization techniques, Ph.D. thesis, Virginia Polytechnic Institute and State University (2007). 75

[212] K. Dong, S. Zhang, J. Wang, Understanding the hydrogen bonds in ionic liquids and their roles in properties and reactions, Chem. Commun. 52 (2016) 6744–6764. `doi:10.1039/C5CC10120D`. 75

[213] X. Ji, C. Held, G. Sadowski, Modeling imidazolium-based ionic liquids with ePC-SAFT, Fluid Phase Equilib. 335 (2012) 64 – 73. `doi:10.1016/j.fluid.2012.05.029`. 76, 84, 85

[214] E.W. Lemmon and M.O. McLinden and D.G. Friend, "Thermophysical Properties of Fluid Systems" in **NIST Chemistry WebBook, NIST Standard Reference Database Number 69**, Eds. P.J. Linstrom and W.G. Mallard, National Institute of Standards and Technology, Gaithersburg MD, 2089, retrieved October 6, 2016. `doi:10.18434/T4D303`. 78, 79, 145, 146

[215] J. Jacquemin, P. Husson, V. Mayer, I. Cibulka, High-Pressure Volumetric Properties of Imidazolium-Based Ionic Liquids: Effect of the Anion, J. Chem. Eng. Data 52 (6) (2007) 2204–2211. `doi:10.1021/je700224j`. 80, 81, 84, 85

[216] J. Kumelan, A. P. S. Kamps, D. Tuma, G. Maurer, Solubility of CO_2 in the ionic liquid [hmim][Tf$_2$N], J. Chem. Thermodyn. 38 (11) (2006) 1396 – 1401. `doi:10.1016/j.jct.2006.01.013`. 80, 81, 84, 85

[217] D. Santos, M. Santos, E. Franceschi, C. Dariva, A. Barison, S. Mattedi, Experimental Density of Ionic Liquids and Thermodynamic Modeling with Group Contribution Equation of State Based on the Lattice Fluid Theory, J. Chem. Eng. Data 61 (1) (2015) 348–353. `doi:10.1021/acs.jced.5b00592`. 80, 81, 84, 85

[218] M. Newville, T. Stensitzki, D. B. Allen, A. Ingargiola, LMFIT: Non-linear least-square minimization and curve-fitting for Python (2014). `doi:10.5281/zenodo.11813`. 80

[219] J. Safarov, W. A. El-Awady, A. Shahverdiyev, E. Hassel, Thermodynamic Properties of 1-Ethyl-3-methylimidazolium Bis(trifluoromethylsulfonyl)imide, J. Chem. Eng. Data 56 (1) (2011) 106–112. `doi:10.1021/je100945u`. 82

[220] S. V. Gadamsetty, M. H. Joshipura, P. Saxena, A Review on Property prediction of ionic liquids using Cubic equation of state, INSTITUTE OF TECHNOLOGY, NIRMA UNIVERSITY, AHMEDABAD (382 481, 08) (2011). 82

[221] K. R. Harris, M. Kanakubo, L. A. Woolf, Temperature and Pressure Dependence of the Viscosity of the Ionic Liquids 1-Hexyl-3-methylimidazolium Hexafluorophosphate and 1-Butyl-3-methylimidazolium Bis(trifluoromethylsulfonyl)imide, J. Chem Eng Data 52 (3) (2007) 1080–1085. `doi:10.1021/je700032n`. 83

[222] P. J. Carvalho, V. H. Alvarez, J. J. Machado, J. Pauly, J.-L. Daridon, I. M. Marrucho, M. Aznar, J. A. Coutinho, High pressure phase behavior of carbon dioxide in 1-alkyl-3-methylimidazolium bis(trifluoromethylsulfonyl)imide ionic liquids, J. Supercrit. Fluids 48 (2) (2009) 99 – 107. `doi:10.1016/j.supflu.2008.10.012`. 89, 91, 92

[223] A. M. Schilderman, S. Raeissi, C. J. Peters, Solubility of carbon dioxide in the ionic liquid 1-ethyl-3-methylimidazolium bis(trifluoromethylsulfonyl)imide, Fluid Phase Equilib. 260 (1) (2007) 19 – 22. `doi:10.1016/j.fluid.2007.06.003`. 89, 91, 92

[224] H. Sakhaeinia, A. H. Jalili, V. Taghikhani, A. A. Safekordi, Solubility of H_2S in Ionic Liquids 1-Ethyl-3-methylimidazolium Hexafluorophosphate ([emim][PF6]) and 1-Ethyl-3-methylimidazolium Bis(trifluoromethyl)sulfonylimide ([emim][Tf$_2$N]), J. Chem. Eng. Data 55 (12) (2010) 5839–5845. `doi:10.1021/je100794k`. 89

[225] J. L. Anthony, J. L. Anderson, E. J. Maginn, J. F. Brennecke, Anion Effects on Gas Solubility in Ionic Liquids, J. Phys. Chem. B 13 (109) (2005) 6366–6374. `doi:10.1021/jp046404l`. 89

[226] E.-K. Shin, B.-C. Lee, J. S. Lim, High-pressure solubilities of carbon dioxide in ionic liquids: 1-Alkyl-3-methylimidazolium bis(trifluoromethylsulfonyl)imide, J. Supercrit. Fluids 45 (3) (2008) 282 – 292. `doi:10.1016/j.supflu.2008.01.020`. 89, 93

[227] X. Ji, C. Held, G. Sadowski, Modeling imidazolium-based ionic liquids with ePC-SAFT. Part II. Application to H_2S and synthesis-gas components, Fluid Phase Equilib. 363 (2014) 59 – 65. `doi:10.1016/j.fluid.2013.11.019`. 84, 85

[228] S. Raeissi, C. Peters, High pressure phase behaviour of methane in 1-butyl-3-methylimidazolium bis(trifluoromethylsulfonyl)imide, Fluid Phase Equilib. 294 (1–2) (2010) 67 – 71. `doi:10.1016/j.fluid.2010.03.021`. 95, 98, 99, 153, 171, 178

[229] J. Kumełan, Á. Pérez-Salado Kamps, D. Tuma, G. Maurer, Solubility of the Single Gases Methane and Xenon in the Ionic Liquid [hmim][Tf$_2$N], Ind. Eng. Chem. Res. 46 (24) (2007) 8236–8240. `doi:10.1021/ie070848x`. 96, 98, 99, 111, 150, 153, 178

[230] P. J. Carvalho, J. A. P. Coutinho, The polarity effect upon the methane solubility in ionic liquids: a contribution for the design of ionic liquids for enhanced CO_2/CH_4 and H_2S/CH_4 selectivities, Energy & Environmental Science (2011). `doi:10.1039/C1EE01599K`. 96

[231] F.-Y. Jou, A. E. Mather, Solubility of Methane in Methyldiethanolamine, J. Chem. Eng. Data 51 (4) (2006) 1429–1430. `doi:10.1021/je060118g`. 99, 171

[232] D.-Y. Peng, D. B. Robinson, Density, Viscosity, Speed of Sound, and Electrolytic Conductivity for the Ionic Liquid 1-Hexyl-3-methylimidazolium Bis(trifluoromethylsulfonyl)imide and Its Mixtures with Water, J. Chem. Eng. Data 52 (6) (2007) 2331–2338. `doi:10.1021/je700329a`. 99

[233] S. L. I. Toh, J. McFarlane, C. Tsouris, D. W. DePaoli, H. Luo, S. Dai, Room-temperature ionic liquids in liquid–liquid extraction: Effects of solubility in aqueous solutions on surface properties, Solvent Extraction and Ion Exchange 24 (1) (2006) 33–56. `doi:10.1080/07366290500388400`. 99

[234] M. Klähn, C. Stüber, A. Seduraman, P. Wu, What determines the miscibility of ionic liquids with water? Identification of the underlying factors to enable a straightforward prediction, J. Phys. Chem. B (114) (2010) 2856–2868. `doi:10.1021/jp1000557`. 100

[235] M. G. Freire, P. J. Carvalho, R. L. Gardas, I. M. Marrucho, L. M. N. B. F. Santos, J. A. P. Coutinho, Mutual Solubilities of Water and the $[C_n mim][Tf_2N]$ Hydrophobic Ionic Liquids, J. Phys. Chem. B 112 (6) (2008) 1604–1610. `doi:10.1021/jp7097203`. 100

[236] M. G. Freire, C. M. S. S. Neves, P. J. Carvalho, R. L. Gardas, A. M. Fernandes, I. M. Marrucho, L. M. N. B. F. Santos, J. A. P. Coutinho, Mutual solubilities of water and hydrophobic ionic liquids, The Journal of Physical Chemistry B 111 (45) (2007) 13082–13089. `doi:10.1021/jp076271e`. 100

[237] D. Santos, M. GÃ, E. Franceschi, A. Santos, C. Dariva, M. Fortuny, S. Mattedi, PHASE EQUILIBRIA FOR BINARY SYSTEMS CONTAINING IONIC LIQUID WITH WATER OR HYDROCARBONS, Brazilian Journal of Chemical Engineering 32 (2015) 967 – 974. 100

[238] J. Jacquemin, P. Husson, A. A. H. Padua, V. Majer, Density and viscosity of several pure and water-saturated ionic liquids, Green Chem. 8 (2006) 172–180. doi:10.1039/B513231B. 100

[239] J. Troncoso, Isobaric heat capacity of ionic liquids in aqueous solutions. a review, Journal of Chemical & Engineering Data 64 (11) (2019) 4611–4618. doi:10.1021/acs.jced.9b00056. 101

[240] B. Davies, Z. Ali, K. E. Porter, Distillation of systems containing two liquid phases, AIChE Journal 33 (1) (1987) 161–163. doi:10.1002/aic.690330120. 101

[241] L. V. G. Cordeiro, S. Dantas, R. Brito, Effect of Two Liquid Phases on the Separation Efficiency of Distillation Columns, Advances in Chemical Engineering and Science 3 (1) (2013) 1–8. doi:10.4236/aces.2013.31001. 101

[242] K. Paduszynski, U. Domanska, Thermodynamic modeling of ionic liquid systems: Development and detailed overview of novel methodology based on the pc-saft, The Journal of Physical Chemistry B 116 (16) (2012) 5002–5018. doi:10.1021/jp3009207. 101

[243] A. Nann, C. Held, G. Sadowski, Liquid–liquid equilibria of 1-butanol/water/il systems, Industrial & Engineering Chemistry Research 52 (51) (2013) 18472–18481. doi:10.1021/ie403246e. 102

[244] M. Bulow, X. Ji, C. Held, Incorporating a concentration-dependent dielectric constant into ePC-SAFT. An application to binary mixtures containing ionic liquids, Fluid Phase Equilibria 492 (2019) 26 – 33. doi:10.1016/j.fluid.2019.03.010. 102

[245] G. R. Daviet, S. T. Donnelly, J. A. Bullin, Dome's North Caroline Plant Successful Conversion to MDEA, Tech. rep., Dome Petroleum Limited, Calgary, Canada (2006).
URL www.researchgate.net/publication/237445692_Dome's_North_Caroline_Plant_Successful_Conversion_to_MDEA 105, 106, 107

[246] J. Polasek, J. A. Bullin, Selecting Amines for Sweetening Units, Tech. rep., Bryan Research and Engineering, Inc. (1994). 106

[247] Aspen Technology Inc., Aspen Plus example, version 9 (35.0.1.271) (2016). 106, 107

[248] D. Green, Perry's Chemical Engineers' Handbook, Eighth Edition, McGraw-Hill Publishing, 2008. 108

[249] D. A. Glasscock, J. E. Critchfield, G. T. Rochelle, CO_2 absorption/desorption in mixtures of methyldiethanolamine with monoethanolamine or diethanolamine, Chem. Eng. Sci. 46 (11) (1991) 2829 – 2845. doi:10.1016/0009-2509(91)85152-N. 109

[250] P. T. Frailie, Modeling of carbon dioxide absorption/stripping by aqueous methyldiethanolamine/piperazine, Ph.D. thesis, The University of Texas at Austin (2014). 109

[251] B. J. Sherman, Thermodynamic and Mass Transfer Modeling of Aqueous Hindered Amines for Carbon Dioxide Capture, Ph.D. thesis, The University of Texas at Austin (2016). 109

[252] L. A. Blanchard, D. Hancu, E. J. Beckman, J. F. Brennecke, Green processing using ionic liquids and CO_2, Nature 399 (1999) 28. doi:10.1038/19887. 109

[253] M. Ramdin, T. W. de Loos, T. J. Vlugt, State-of-the-Art of CO_2 Capture with Ionic Liquids, Ind. Eng. Chem. Res. 51 (24) (2012) 8149–8177. doi:10.1021/ie3003705. 109

[254] D. G. Hert, J. L. Anderson, S. N. Aki, J. F. Brennecke, Enhancement of oxygen and methane solubility in 1-hexyl-3-methylimidazolium bis(trifluoromethylsulfonyl) imide using carbon dioxide, Chem. Commun. (2005) 2603–2605doi:10.1039/B419157A. 110

[255] N. Rai, E. J. Maginn, Critical behaviour and vapour-liquid coexistence of 1-alkyl-3-methylimidazolium bis(trifluoromethylsulfonyl)amide ionic liquids via monte carlo simulations, Faraday Discuss. 154 (2012) 53–69. doi:10.1039/C1FD00090J. 111

[256] J. O. Valderrama, R. E. Rojas, Critical properties of ionic liquids. revisited, Ind. Eng. Chem. Res. 48 (14) (2009) 6890–6900. doi:10.1021/ie900250g. 111

[257] R. Ge, C. Hardacre, J. Jacquemin, P. Nancarrow, D. W. Rooney, Heat capacities of ionic liquids as a function of temperature at 0.1 mpa. measurement and prediction, Journal of Chemical & Engineering Data 53 (9) (2008) 2148–2153. doi:10.1021/je800335v. 112, 113, 142

[258] M. E. Kandil, K. N. Marsh, A. R. H. Goodwin, Measurement of the Viscosity, Density, and Electrical Conductivity of 1-Hexyl-3-methylimidazolium Bis(trifluorosulfonyl)imide at Temperatures between (288 and 433) K and Pressures below 50 MPa, Journal of Chemical & Engineering Data 52 (6) (2007) 2382–2387. doi:10.1021/je7003484. 114

[259] M. Tariq, P. J. Carvalho, J. A. Coutinho, I. M. Marrucho, J. N. C. Lopes, L. P. Rebelo, Viscosity of (C_2—C_{14}) 1-alkyl-3-methylimidazolium bis(trifluoromethylsulfonyl)amide ionic liquids in an extended temperature range, Fluid Phase Equilibria 301 (1) (2011) 22 – 32. doi:10.1016/j.fluid.2010.10.018. 114, 142

[260] P. Gallick, G. Phillippi, B. F. Williams, What's correct for my application - a centrifugal or reciprocating compressor?, Texas A&M University, Turbomachinery Laboratories (2006).

URL https://oaktrust.library.tamu.edu/handle/1969.1/
163189 117

[261] R. Schefflan, Teach Yourself the Basics of Aspen Plus, 2nd Edition, American Institute of Chemical Engineers, 2016. 123

[262] Chapter 3 - pumping of liquids, in: E. E. Ludwig (Ed.), Emphasizes how to apply techniques of process design and interpret results into mechanical equipment details, Vol. 1 of Applied Process Design for Chemical & Petrochemical Plants, Gulf Professional Publishing, 1999, pp. 160 – 223. doi: 10.1016/S1874-8635(99)80004-1. 124

[263] D. B. Salunke, An Óconnell type correlation for prediction of overall efficiency of valve tray columns, Master's thesis, Pune University (2006).
URL https://shareok.org/handle/11244/9663 126

[264] M. S. Peters, K. D. Timmerhaus, Plant design and economics for chemical engineers, New York, McGraw-Hill, 1991. 127

[265] GPSA Engineering Data Book ERRATA, SI Edition, Gas Processors Suppliers Association, Tulsa, 2004. 129

[266] B. L. Burr, L. Lyddon, A Comparison of Physical Solvents for Acid Gas Removal, Bryan Research & Engineering, Inc. , Bryan, Texas, U.S.A., 2008. 136, 137, 138, 139, 140, 141, 142, 156

[267] L. Sun, R. Smith, Rectisol wash process simulation and analysis, Journal of Cleaner Production 39 (2013) 321 – 328. doi:10.1016/j.jclepro. 2012.05.049. 136, 138, 139, 140

[268] Z. Lei, B. Zhang, J. Zhu, W. Gong, J. Lü, Y. Li, Solubility of CO_2 in Methanol, 1-Octyl-3-methylimidazolium Bis(trifluoromethylsulfonyl)imide, and Their Mixtures, Chin. J. Chem. Eng. 21 (3) (2013) 310 – 317. doi: 10.1016/S1004-9541(13)60464-4. 137, 144, 148, 149

[269] C. Dai, W. Wei, Z. Lei, C. Li, B. Chen, Absorption of CO_2 with methanol and ionic liquid mixture at low temperatures, Fluid Phase Equilib. 391 (2015) 9 – 17. `doi:10.1016/j.fluid.2015.02.002`. 137, 144, 154

[270] C. Higman, Gasification processes and synthesis gas treatment technologies for carbon dioxide (CO_2) capture, in: M. M. Maroto-Valer (Ed.), Developments and Innovation in Carbon Dioxide (CO_2) Capture and Storage Technology, Vol. 1 of Woodhead Publishing Series in Energy, Woodhead Publishing, 2010, pp. 243 – 279. `doi:10.1533/9781845699574.2.243`. 138, 141, 143

[271] B. G. Miller, Clean Coal Technologies for Advanced Power Generation, in: B. G. Miller (Ed.), Clean Coal Engineering Technology (Second Edition), second edition Edition, Butterworth-Heinemann, 2017, pp. 261 – 308. `doi:10.1016/B978-0-12-811365-3.00006-5`. 141, 142

[272] A. Muhammad, M. I. A. Mutalib, C. D. Wilfred, T. Murugesan, A. Shafeeq, Viscosity, Refractive Index, Surface Tension, and Thermal Decomposition of Aqueous N−Methyldiethanolamine Solutions from (298.15 to 338.15) K, Journal of Chemical & Engineering Data 53 (9) (2008) 2226–2229. `doi:10.1021/je800282a`. 142

[273] O. Noll, A. Valtz, D. Richon, T. Getachew-Sawaya, I. Mokbel, J. Jose, Vapor pressures and liquid densities of N-methylethanolamine, diethanolamine, and N-methyldiethanolamine, Int. Electron. J. Phys.-Chem. Data 4 (1998) 105–120. 142

[274] L. P. N. Rebelo, J. N. Canongia Lopes, J. M. S. S. Esperança, E. Filipe, On the Critical Temperature, Normal Boiling Point, and Vapor Pressure of Ionic Liquids, The Journal of Physical Chemistry B 109 (13) (2005) 6040–6043. `doi:10.1021/jp050430h`. 142

[275] K. Zhang, B. Hawrylak, R. Palepu, P. R. Tremaine, Thermodynamics of aqueous amines: excess molar heat capacities, volumes, and expansibilities of water+ methyldiethanolamine (MDEA) and water + 2-amino-2-methyl-1-propanol

(AMP), The Journal of Chemical Thermodynamics 34 (5) (2002) 679 – 710. `doi:10.1006/jcht.2002.0937`. 142

[276] H. Ogawa, S. Murakami, Excess volumes, isentropic compressions, and isobaric heat capacities for methanol mixed with other alkanols at 25°C, J. Solution Chem. 16 (4) (1987) 315–326. `doi:10.1007/BF00646123`. 142

[277] A. Conesa, S. Shen, A. Coronas, Liquid Densities, Kinematic Viscosities, and Heat Capacities of Some Ethylene Glycol Dimethyl Ethers at Temperatures from 283.15 to 423.15 K, Int. J. Thermophys. 19 (5) (1998) 1343–1358. `doi:10.1023/A:1021927417610`. 142

[278] B. Mandal, M. Guha, A. Biswas, S. Bandyopadhyay, Removal of carbon dioxide by absorption in mixed amines: modelling of absorption in aqueous mdea/mea and amp/mea solutions, Chem. Eng. Sci. 56 (21) (2001) 6217 – 6224, proceedings of the 5th International Conference on Gas-Liquid and Gas-Liquid-Solid Reactor Engineering. `doi:10.1016/S0009-2509(01)00279-2`. 143

[279] O. C. Polasek, G. A. Iglesias-Silva, J. A. Bullin, Using Mixed Amine Solutions for Gas Sweetening, Tech. rep., Bryan Research & Engineering, Inc., and Texas A&M University and Bryan Research & Engineering, Inc., (2006).
URL `http://citeseerx.ist.psu.edu/viewdoc/download?doi=10.1.1.491.7061&rep=rep1&type=pdf` 143

[280] Z. Aliabadi, H. , S. Mirzaei, S. , Using mixed amine solution for gas sweetening, World Academy of Science, Engineering and Technology 58 (2009) 992–997. 143

[281] R. K. Abdulrahman, M. H. S. Zangana, K. S. Ali, J. C. Slagle, Utilizing mixed amines in gas sweetening process: A Kirkuk field case study and simulation, in: 2017 International Conference on Environmental Impacts of the Oil and Gas Industries: Kurdistan Region of Iraq as a Case Study (EIOGI), 2017, pp. 5–8. `doi:10.1109/EIOGI.2017.8267616`. 143

[282] F. Y. Jou, R. Deshmukh, F. Otto, A. Mather, Solubility of H_2S, CO_2, CH_4 and C_2H_6 in sulfolane at elevated pressures, Fluid Phase Equilib. 56 (C) (1990) 313–324, cited By 43. `doi:10.1016/0378-3812(90)85111-M`. 144

[283] S. Zhang, X. Zhang, Y. Zhao, G. Zhao, X. Yao, H. Yao, A novel ionic liquids-based scrubbing process for efficient CO_2 capture, Science China Chemistry 53 (7) (2010) 1549–1553, cited By 23. `doi:10.1007/s11426-010-4030-z`. 144

[284] Y. Zhao, X. Zhang, S. Zeng, Q. Zhou, H. Dong, X. Tian, S. Zhang, Density, Viscosity, and Performances of Carbon Dioxide Capture in 16 Absorbents of Amine + Ionic Liquid + H_2O, Ionic Liquid + H_2O, and Amine + H_2O Systems, J. Chem. Eng. Data 55 (9) (2010) 3513–3519. `doi:10.1021/je100078w`. 144

[285] S. Baj, A. Siewniak, A. Chrobok, T. Krawczyk, A. Sobolewski, Monoethanolamine and ionic liquid aqueous solutions as effective systems for CO_2 capture, Journal of Chemical Technology & Biotechnology 88 (7) (2013) 1220–1227. `doi:10.1002/jctb.3958`. 144

[286] J. Gross, G. Sadowski, Application of the Perturbed-Chain SAFT Equation of State to Associating Systems, Ind. Eng. Chem. Res. 41 (22) (2002) 5510–5515. `doi:10.1021/ie010954d`. 145

[287] J. B. Parsa, M. F. Haghro, Excess molar volume and viscosity deviation for binary mixtures of polyethylene glycol dimethyl ether 250 with 1,2-alkanediols (C_3–C_6) at T=(293.15 to 323.15)K, The Journal of Chemical Thermodynamics 40 (5) (2008) 782 – 788. `doi:10.1016/j.jct.2008.01.022`. 145, 147

[288] A. D. Leu, J. J. Carroll, D. B. Robinson, The equilibrium phase properties of the methanol-hydrogen sulfide binary system, Fluid Phase Equilib. 72 (1992) 163 – 172. `doi:10.1016/0378-3812(92)85024-3`. 148, 149

[289] Aspen Technology Inc., APV90 PC-SAFT Databank for PC-SAFT binary interaction parameters (2016). 148, 151

[290] M. Frost, Measurement and Modelling of Phase Equilibrium of Oil - Water - Polar Chemicals, Ph.D. thesis, Technical University of Denmark (DTU) (2014). 149, 150

[291] F. Otto, A. Mather, F. Jou, D. Lal, Development of gas treating technology, Tech. rep. (1985). 151, 152, 157

[292] A. V. Rayer, A. Henni, P. Tontiwachwuthikul, High-Pressure Solubility of Methane (CH_4) and Ethane (C_2H_6) in Mixed Polyethylene Glycol Dimethyl Ethers (Genosorb 1753) and Its Selectivity in Natural Gas Sweetening Operations, Journal of Chemical & Engineering Data 57 (3) (2012) 764–775. doi:10.1021/je200905z. 152, 153

[293] Y. Masahiro, Gas solubility in methanol at high pressure 30 (44) (1978) 2174–2177.
URL https://www.jstage.jst.go.jp/article/nikkashi1898/72/10/72_10_2174/_pdf/-char/en 157

[294] D. D. Zhang, H. J. Ng, R. Veldman, Modelling of acid gas treating using AGR physical solvent, in: Gas Processors Association Seventy-Eighth Annual Convention, Nashville, TN (US), DB Robinson Research Ltd., Edmonton, Alberta (CA), 1999.
URL https://www.osti.gov/biblio/20000887 157

[295] I. E. Grossmann, A. W. Westerberg, L. T., Retrofit design of processes, Biegler and Carnegie Mellon University, Engineering Design Research Center. (1987). doi:10.1184/R1/6467396.v1. 168

[296] R. Smith, Chemical Process: Design and Integration, John Wiley & Sons Ltd., 2005. 168, 170

[297] M. Tham, Distillation: An introduction, Factors affecting distillation column operation, COSTELLO Consulting Engineers (2018).
URL https://www.rccostello.com/distil/distilop.htm 169

[298] M. Kleiber, Process Engineering: Addressing the Gap between Study and Chemical Industry, Walter de Gruyter GmbH Co KG, 2016. 170

[299] D. B. Andrews, Increasing pump capacity, Run times 4 (8) (2007). 170

[300] H. Vanda, Y. Dai, E. G. Wilson, R. Verpoorte, Y. H. Choi, Green solvents from ionic liquids and deep eutectic solvents to natural deep eutectic solvents, C. R. Chim. 21 (6) (2018) 628 – 638. `doi:10.1016/j.crci.2018.04.002`. 178

[301] D.-Y. Peng, D. B. Robinson, A new two-constant equation of state, Industrial & Engineering Chemistry Fundamentals 15 (1) (1976) 59–64. `doi:10.1021/i160057a011`. 180, 182, 184, 186

[302] L. F. Cameretti, G. Sadowski, J. M. Mollerup, Modeling of Aqueous Electrolyte Solutions with Perturbed-Chain Statistical Associated Fluid Theory, Ind. Eng. Chem. Res. 44 (9) (2005) 3355–3362. `doi:10.1021/ie0488142`. 191, 192

[303] P. K. Jog, S. G. Sauer, J. Blaesing, , W. G. Chapman, Application of Dipolar Chain Theory to the Phase Behavior of Polar Fluids and Mixtures, Ind. Eng. Chem. Res. 40 (21) (2001) 4641–4648. `doi:10.1021/ie010264+`. 192

[304] Aspen Technology Inc., PURE35 Databank, pure component parameters for the Aspen Physical Property System (2015). 202, 203, 205, 206

[305] Aspen Technology Inc., PC-SAFT Databank for pure and binary parameters used with the PC-SAFT property method. 203

[306] Aspen Technology Inc., ASPENPCD Databank, the main source of pure component parameters in Aspen Plus (2016). 203, 204, 205

[307] Aspen Technology Inc., AQUEOUS Databank, ionic species parameters databank used for electrolytes applcation (1982). 203, 204

[308] Federal Statistical Office, Data on energy price trends: Long-time series from January 2005 to August 2018, Tech. rep., Statistisches Bundesamt (Destatis) (2018). 224